HAL
open science

Atmospheric chemistry of NO : reactions with a series of organic and inorganic compounds

Li Zhou

To cite this version:

Li Zhou. Atmospheric chemistry of NO : reactions with a series of organic and inorganic compounds. Other. Université d'Orléans, 2017. English. NNT : 2017ORLE2055 . tel-01967629

HAL Id: tel-01967629

https://theses.hal.science/tel-01967629v1

Submitted on 1 Jan 2019

HAL is a multi-disciplinary open access archive for the deposit and dissemination of scientific research documents, whether they are published or not. The documents may come from teaching and research institutions in France or abroad, or from public or private research centers.

L'archive ouverte pluridisciplinaire **HAL**, est destinée au dépôt et à la diffusion de documents scientifiques de niveau recherche, publiés ou non, émanant des établissements d'enseignement et de recherche français ou étrangers, des laboratoires publics ou privés.

UNIVERSITÉ D'ORLÉANS

ÉCOLE DOCTORALE
ENERGIE, MATERIAUX, SCIENCES DE LA TERRE ET DE L'UNIVERS

ICARE-CNRS ORLEANS

THÈSE présentée par :

Li ZHOU

soutenue le : **15 Décembre 2017**

pour obtenir le grade de : **Docteur de l'université d'Orléans**

Discipline/ Spécialité : Chimie et Physique de l'Environment

Atmospheric chemistry of NO_3 : reactions with a series of organic and inorganic compounds

THÈSE dirigée par :

Véronique DAËLE	Chargée de recherche (HDR) – CNRS-ICARE

RAPPORTEURS :

Bénédicte PICQUET-VARRAULT	Professeure Université Paris Est Créteil / LISA
Eric VILLENAVE	Professeur Université de Bordeaux

JURY

Bénédicte PICQUET-VARRAULT	Professeure - Université Paris Est Créteil / LISA	Rapporteur
Eric VILLENAVE	Professeur - Université de Bordeaux / EPOC	Rapporteur
A.R. RAVISHANKARA	Professeur - Colorado State University-USA	Examinateur
Coralie SCHOEMAECKER	Chargée de Recherche - PC2A - Lille	Examinatrice
Valéry CATOIRE	Professeur - Université d'Orléans/CNRS-LPC2E	Examinateur
Abdelwahid MELLOUKI	Directeur de recherche - CNRS-ICARE	Co-Encadrant
Véronique DAËLE	Chargée de recherche (HDR) - CNRS-ICARE	Directrice de thèse

Table of Contents

Abstract **5**

Chapter I Introduction **8**

1 The nitrate radical in the atmosphere 8

1.1 Atmospheric sources of NO_3 radical 12

1.2 Atmospheric sinks of NO_3 radical 14

1.3 Spectroscopy of NO_3 17

2 Measurement techniques for the nitrate radical (NO_3) in the troposphere 18

2.1 Differential Optical Absorption Spectroscopy (DOAS) 18

2.2 Matrix Isolation Electron Spin Resonance (MI-ESR) 20

2.3Laser Induced Fluorescence spectroscopy (LIF) 21

2.4 Cavity Ring Down Spectroscopy (CRDS) 22

2.5 Cavity Enhanced Absorption Spectroscopy (CEAS) 23

2.6 Chemical Ionization Mass Spectrometry (CIMS) 25

2.7 Summary 26

3 The unresolved issues in NO_3 radical chemistry 27

3.1 Kinetics and mechanisms of NO_3 chemical reactions 28

3.2 Field measurements and model estimation 29

3.3 Experimental techniques 30

4 Motivation and outline of this thesis 30

References 33

Chapter II Experimental system **43**

1 Reactor - indoor smog chamber 43

2 Instruments 47

2.1 Fourier Transform Infrared Spectroscopy (FTIR) 47

2.2 Proton Transfer Reaction-Time of Flight Mass Spectrometry (PTR-ToF-MS) 48

2.3 Cavity Ring down Spectroscopy (CRDS) 51

2.4 Nitrogen Dioxide (NO_2) monitor 55

2.5 Ozone (O_3) monitor 58
2.6 Formaldehyde (HCHO) analyzer 60
References 62

Chapter III Laboratory studies of the nitrate radical - Reaction of Methacrylate esters with NO_3 radicals 66

Abstract 66
1 Introduction 67
2 Experimental system 69
2.1 Reactors- Indoor atmospheric simulation chamber 69
2.2 Instrumentations 71
2.3 Chemicals 73
3 Rate coefficients measurement 74
3.1 Relative rate method 74
3.2 Rate coefficients via monitoring temporal profiles of NO_3/N_2O_5 loss using CRDS 80
3.3 Error estimation 85
3.4 Comparison of rate coefficients obtained from two methods 88
3.5 Comparison with the kinetic results in literature 89
4 Mechanism and Relationship between structure and reactivity of the methacrylate esters 91
5 Atmospheric implication 96
Supporting information 99
References 111

Chapter IV Kinetics of the Reactions of NO_3 Radical with alkanes 117

Abstract 117
1 Introduction 118
2 Experimental section 120
2.1 Experimental system 120
2.2 Chemicals 124

2.3 Kinetic study methods 126
3 Results and discussion 127
3.1 Accounting for impurities and subsequent reactions 127
3.2 Experimental results 129
3.3 Error estimation 135
3.4 Comparison with the kinetic results in literature 141
3.5 Relation between structure and reactivity of alkanes. 144
4 Conclusions and atmospheric implication 145
Supporting information 147
References 162

Chapter V Exploration of minor pathways for the atmospheric removal of N_2O, CO and SO_2: Reactions with NO_3 168
Abstract 168
1 Introduction 169
2 Experimental section 172
2.1 Methods for determining rate coefficients 172
2.2 Chemicals 176
3 Results and discussion 177
3.1 Experimental results 177
3.2 Comparison with literature 182
4 Conclusions and atmospheric implication 184
Supporting information 186
References 190

Chapter VI Conclusions 195

Appendix 201
1 Student's Distribution Table 201
2 Macro Codes used in the box model 202

Abstract

NO_3 is a key intermediate in the chemistry of the night-time atmosphere. It can react with a number of VOCs initiating their night-time degradation. In this thesis, the kinetics of NO_3 with different kinds of compounds was studied at room temperature (298 ± 2 K) and atmospheric pressure (1000 ± 5 hPa) in a Teflon simulation atmospheric chamber (ICARE-7300L) coupled to analytical tools including Fourier Transform Infrared Spectroscopy, Proton Transfer Reaction-Time of Flight-Mass Spectrometer and Cavity Ring Down Spectrometer etc. The rate coefficients for the reactions of NO_3 radical with seven methacrylate esters are firstly reported: methyl methacrylate; ethyl methacrylate; propyl methacrylate; isopropyl methacrylate, butyl methacrylate, isobutyl methacrylate, and deuterated methyl methacrylate. The trends in the measured rate coefficient with the length and nature of the alkyl group strongly suggest that the reaction proceeds via addition to the double bond on the methacrylate group. Then, an absolute method was used to determine the upper limits or rate coefficients for the reactions of NO_3 radicals with a series of alkanes and some important inorganic gases: methane, ethane, pentane, n-butane, iso-butane, 2,3-dimethybutane, cyclopentane, cyclohexane, nitrous oxide, carbon monoxideand and sulfur dioxide. With the obtained kinetics data, the atmospheric lifetimes of these compounds toward NO_3 radicals were calculated and compared with those due to loss via reactions with the other major atmospheric oxidants. The kinetics results also enhance the available database on NO_3 reactions.

Keywords: Atmospheric chemistry, NO_3 radicals, volatile organic compounds, rate coefficients, kinetic

Chapitre I Introduction

Le radical NO_3 est une espèce clé dans la chimie atmosphérique nocturne. Dans ce chapitre, sont premièrement décrits les sources et les puits de ce radical dans l'atmosphère, ainsi que ses propriétés physiques et chimiques.

Cette description est suivie d'un état de l'art des différentes techniques de mesure du radical NO_3 dans la troposphère parmi lesquelles : Differential Optical Absorption Spectroscopy (DOAS), Matrix Isolation Electron Spin Resonance (MI-ESR), Laser Induced Fluorescence (LIF), Cavity Ring Down Spectroscopy (CRDS), Cavity Enhanced Absorption Spectroscopy (CEAS), Chemical Ionization Mass Spectrometry (CIMS). Les avantages et les inconvénients de ces techniques sont comparés en insistant sur la précision de la mesure, les interférences éventuelles et la stabilité de fonctionnement des instruments.

Enfin, ce chapitre se termine par une discussion sur les enjeux des études impliquant le radical NO_3 en pointant sur les aspects encore mal ou peu connus et nécessitant des approfondissements, que ce soit par des mesures de laboratoire ou des mesures de terrain.

Chapter I Introduction

1 The nitrate radical in the atmosphere

The troposphere is indeed marked by strong convective over-turnings, whereby large parcels of warm air travel upwards to the tropopause, carrying water vapor and forming clouds as they cool down (the stratosphere, on the other hand is a very stable a stratified environment where heat transfer is mainly radiative). The troposphere contains the bulk of atmospheric water vapor, the majority of clouds and most of the weather, both on a global and a local scale. Most importantly, it is in contact with the Earth's surface and therefore interacts directly with other climate subsystems, such as the biosphere (the land and vegetation), the hydrosphere (the oceans), the cryosphere (the ice caps), the lithosphere (the topography), and most of all, with the human world (Peixoto and Oort, 1992). The bulk of dry air is made up of nitrogen (78% by volume) and oxygen (21% by volume). Noble gases, carbon dioxide and a large number of other minor gases constitute the remaining 1% of the atmosphere. Although they are in very small concentrations, these trace constituents play a vital role in all aspects of atmospheric physics and chemistry. They are emitted by natural or anthropogenic sources. Natural sources include volcanoes eruptions, swamps, wild animal emissions, forest fires and dust, while anthropogenic ones include industrial activities, fossil fuel burning, car usage, emissions from domestic animals and agriculture. (As shown in Figure 1-1) They heavily influence our climate system. Because of its growing importance, the latter category is very publicized and becoming common knowledge. Fortunately, thanks to a remarkable natural ability to cleanse itself, the atmosphere has up to now avoided any substantial accumulation of pollutants. There are three end removal processes. The first is chemical conversion to non-polluting constituents, such as H_2O or O_2. The second is dry deposition, whereby gases are absorbed by plants, water or soil. It is of limited

significance because it often only applies to gases in the boundary layer on a local scale. The third is wet deposition, or removal by precipitation, and is only effective for species that have enough solubility in water, which is not the case in general. There are, however, a number of tropospheric species capable of oxidizing these pollutants so that they become soluble. Although these species are only present in minute amounts, they constitute the pivot of tropospheric chemistry.

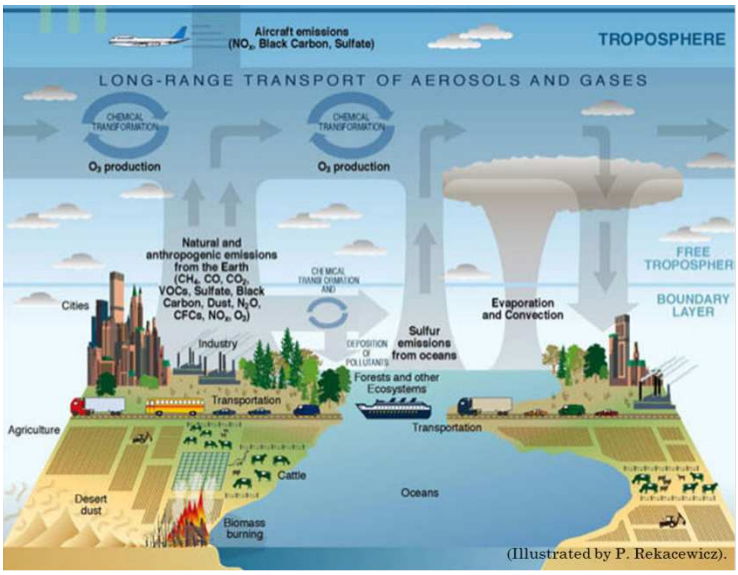

Figure 1-1 Processes related to tropospheric composition

Due to the high chemical reactivity, free radicals play a central role as intermediates in many chemical systems, such as in flames or in the atmosphere and the free radicals initiation, and carry action chains of these reactions. In the atmosphere, for instance, the first step in the degradation of most oxidizable trace gases, like hydrocarbons, carbon monoxide, or H-CFC's is the reaction with reactive species. The products degradation frequently gives rise to further radical production (chain branching) and formation of secondary oxidants like ozone and peroxides. The most important oxidant species that regulate the self-cleaning efficiency of the troposphere are the hydroxyl radical (OH), the NO_3 radical, ozone (O_3) and other oxidants.

Ozone is a powerful oxidizing agent readily reacting with other chemical compounds to make many possibly oxides. Tropospheric ozone is a greenhouse gas and initiates the chemical removal of lots of organic and inorganic compounds from

the atmosphere. Photochemical and chemical reactions involving it drive many of the chemical processes that occur in the atmosphere by day and by night.

The hydroxyl radical is a short-lived free radical and by far the most effective scavenger in the troposphere. It is the main oxidant for CO, CH_4 and higher hydrocarbons, H_2S (hydrogen sulfide) and SO_2 (sulfur dioxide). During the day, OH radical plays a decisive role in the cleaning mechanism of the atmosphere. But the formation of OH radicals needs the existence of sun light.

$$\mathbf{NO_2 + h\nu \rightarrow NO + O\,(^3P) \quad (\lambda < 420\ nm)}$$

$$\mathbf{O\,(^3P) + O_2 + M \rightarrow O_3 + M}$$

$$\mathbf{O_3 + h\nu \rightarrow O_2 + O\,(^1D) \quad (\lambda < 340\ nm)}$$

$$\mathbf{O\,(^1D) + H_2O \rightarrow 2OH}$$

While during the night, as OH radical sources are limited, its concentration becomes very low, in most situations, and it can be negligible. Thus, NO_3 radicals and O_3 are the main oxidants (Platt et al. 1984, Wayne et al. 1991) in the nighttime.

NO_3 is a key intermediate in the chemistry of the night-time atmosphere. It has been observed to be present in both stratosphere and troposphere. A detailed knowledge of its elementary reactions is required to describe adequately its behavior as a reactive free radical. It is the atmospheric source of N_2O_5, which after transport can release NO_2 and NO_3 at warmer locations.

NO_3 radical can react with a number of VOCs initiating their nighttime degradation. It also contributes to the removal of NOx mainly via nitric acid (HNO_3) and particulate nitrate formation (Allan et al. 1999, Allan et al. 2000). Schematic diagrams of the chemical behavior of NO_3 in the atmosphere are shown in Figure 1-2.

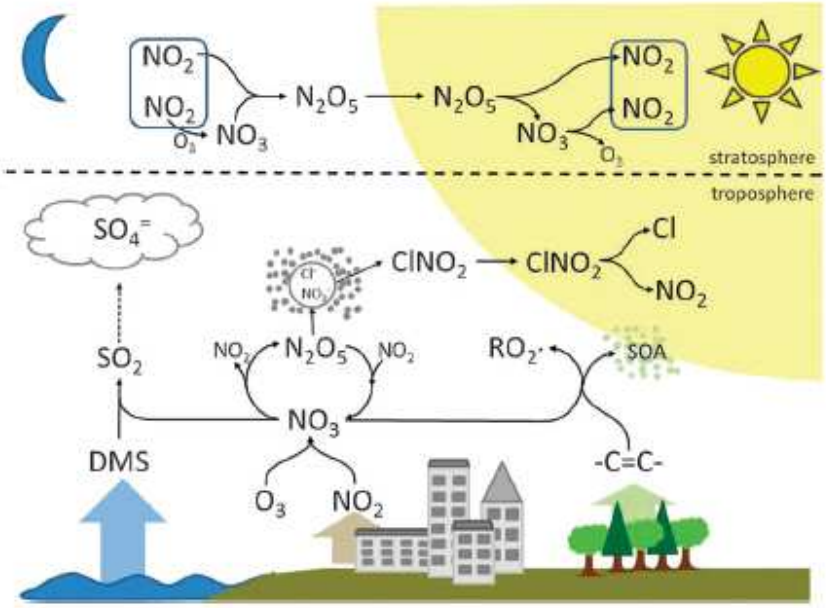

Figure 1-2 Schematic description of the atmospheric chemical processes involving NO_3 and N_2O_5. (Brown and Stutz 2012)

In conclusion, NO_3 has a number of important roles as following in the troposphere.

(1) As a source of N_2O_5, this reacts with hydrometeors (water or water vapour in the atmosphere, such as rain, snow, or cloud) to produce nitric acid.

(2) In the control of NOx (NO and NO_2) and NOy (NO, NO_2, NO_3, etc.). Reactions of NO_3 or N_2O_5, which form HNO_3, are part of a mechanism which removes NOx.

(3) Reactions of NO_3 and N_2O_5 lead to the oxidation of hydrocarbon compounds.

(4) As a potential source of atmospheric organic nitrate compounds.

In this chapter, sources and sinks of NO_3 radical in the atmosphere and its physical and chemical properties will be introduced first, and then the measurement techniques for the NO_3 radical will be summarized. At last, the research challenge of NO_3 radical chemistry study in both laboratory and field measurements will be reported.

1.1 Atmospheric sources of NO_3 radical

In the atmosphere, there are several potential atmospheric sources of the nitrate radical (NO_3).

(1) the major source of NO_3 is the oxidation of nitrogen dioxide (NO_2) by ozone (O_3):

$NO_2 + O_3 \rightarrow NO_3 + O_2$ (1-1)

The production rate of NO_3 (PNO_3) by this reaction is given by the equation

$PNO_3 = k_{NO2+O3} [NO_2][O_3]$ (I-I)

NO_3 radical can react with NO_2 to produce N_2O_5, which readily dissociates establishing equilibrium with NO_3:

$NO_3 + NO_2 + M \leftrightarrow N_2O_5 + M$ (1-2)

This equilibrium is usually achieved rapidly at ambient temperature unless the NO_2 concentrations are very low.

(2) As the equilibrium mentioned above, decomposition of dinitrogen pentoxide (N_2O_5) is another source of NO_3 radical.

$N_2O_5 + M \rightarrow NO_3 + NO_2 + M$ (1-3)

This reaction is also frequently used as a source of NO_3 in laboratory experiments.

Except these two major sources of NO_3 radical in the atmosphere, there are some other reactions which can produce NO_3 radicals, are normally used as a source of NO_3 radicals in the laboratory experiments as following:

(3) Reaction of hydroxyl radicals with nitric acid:

Husain and Norrish showed that NO_3 was produced in the photolysis of HNO_3 as a consequence of the steps (Husain and Norrish 1963)

$HNO_3 + hv \rightarrow OH + NO_2$ (1-4)

$OH + HNO_3 \rightarrow H_2O + NO_3$ (1-5)

The hydrogen abstraction process (1-5) is exothermic by 81 kJ mol^{-1}, and NO_3 formation is both fast and efficient (Ravishankara, Eisele and Wine 1982).

The photolysis of HNO_3 is thus a convenient source of NO_3 in photochemical experiments.

(4) Sources involving chlorine nitrate:

Chlorine nitrate may be treated as a source of NO_3 in two ways.

Firstly, atomic chlorine abstracts Cl from the $ClONO_2$ molecule exothermically and rapidly,

$ClONO_2 + Cl \rightarrow NO_3 + Cl_2$ (1-6)

($k = 1.2 \times 10^{-11}$ cm ^{3} molecule s^{-1})

Secondly, photolysis of chlorine nitrate can generate NO_3 directly,

$ClONO_2 + h\nu$ ($\lambda < 330$nm) $\rightarrow NO_3 + Cl$ (1-7)

Yielding to NO_3 as a primary product, and, of course, the Cl atom generated can produce a further NO_3 molecule in a secondary reaction with $ClONO_2$ (Wallington et al. 1986).

(5) Reaction of halogen atoms with nitric acid:

The reaction between atomic fluorine and nitric acid vapor is exothermic by more than 150 kJ mol^{-1}, and rapid, yielding NO_3 as one of the products

$F + HNO_3 \rightarrow NO_3 + HF$ (1-8)

The rate constant for the reaction has been determined at room temperature to be $(2.7 \pm 0.5) \times 10^{-11}$ cm ^{3} $molecule^{-1}$ s^{-1} by Mellouki et al. (Mellouki, Le Bras and Poulet 1987). During this reaction process, F atoms was produced by microwave discharge CF_4 in helium.

(6) Addition of atomic oxygen to nitrogen dioxide:

Although the bimolecular exchange reaction between O (O atom come from the photolysis of NO_2) and NO_2 is very rapid, there has long been speculation that associations channel

$O + NO_2 + M \rightarrow NO_3 + M$ (1-9)

occurred alongside it (Hippler, Schippert and Troe 1975). There is quite clear evidence for NO_3 formation by some route in the flash photolysis of NO_2, and Croce et al have also generated NO_3 by the flash photolysis (λ = 193 nm) of N_2O in the

presence of NO_2. (Croce de Cobos, Hippler and Troe 1984)

1.2 Atmospheric sinks of NO_3 radical

NO_3 absorbs strongly in the visible spectral region, hence, it is photolysed below $\lambda = 630$ nm to produce NO +O_2 or NO_2 + O; the relative and absolute yields of these reactions are dependent on the wavelength and will be introduced briefly in this part firstly (Allan et al. 2000).

In 1963, Husain and Norfish investigated the photolysis processes of NO_3 using a flash photolysis system. They have shown that photolysis of mixtures of NO_2 in N_2 produce NO_3. They have investigated the effect of light of $\lambda > 500$ nm on the photolysis of NO_3 (Husain and Norrish 1963). They concluded that the absorption of light by NO_3 from the photoflash was above $\lambda = 500$ nm, but below the estimated dissociation limit of $\lambda = 571$ nm, resulting in photolysis of the radical in accordance with the reaction:

$$NO_3 + h\nu \rightarrow NO_2 + O \qquad (1\text{-}10)$$

These authors further discovered that light of $\lambda = 624$ nm also photolysed the NO_3 radical, suggesting another reaction step

$$NO_3 + h\nu \rightarrow NO + O_2 \qquad (1\text{-}11)$$

Graham and Johnston confirmed that NO_3 is photolysed by visible light along these two reaction channels (Graham and Johnston 1978). This study employed modulated photolysis and was performed at a very coarse spectral resolution using three different broad-band fluorescent lamps with overlapping spectral distributions. In the wavelength region 470 – 610 nm, the average primary quantum yields for reactions (1-10) and (1-11), at an atmospheric pressure, were $Y_1 = 0.23$ and $Y_2 = 0.77$, respectively. The averages value of Y_1 in the 610 - 700 nm region of strong absorption was only 0.07 and Y_2 was near zero. Due to the strong absorption of NO_3 throughout the visible region of the solar spectrum, the radical is rapidly photolyzed during the day. The lifetime of NO_3 with respect to photolysis is approximately 5 s

for overhead sun and clear-sky conditions at sea level (Orlando et al. 1993).

Besides photolysis, the reactions with NO_2 and with NO also reduce the lifetime of NO_3 during the day. NO_3 reacts rapidly with NO to form NO_2: $k(NO_3+NO) = 2.8 \times 10^{-11}$ cm^3 $molecule^{-1}$ s^{-1} at T = 298 K.

$NO_3 + NO \rightarrow NO_2 + NO_2$ (1-12)

NO_2 is then photolysed back through:

$NO_2 + h\nu$ (< 400 nm) $\rightarrow NO + O$ (1-13)

The amount of NO is very variable in the troposphere. Under NO-rich conditions, reaction (1-12) competes with the photolysis of NO_3 as the dominant daytime process for the removal of NO_3.

In the nighttime, unless fresh local emissions are present, there should also be negligible levels of NO. Since NO will be rapidly titrated away by O_3 with a time constant of about 1 min, assuming 30 ppb O_3 at 283 K, therefore significant levels of NO_3 can be formed overnight via the reaction of NO_2 with O_3. Therefore, NO_3 radical concentrations are expected to build up during the early evening and nighttime hours, due to the absence of photolysis (1-10, 1-11) and the low nighttime concentrations of NO.

NO_3 has been shown to react rapidly with a variety of either man-made or biogenic emitted tropospheric trace gases. These reactions can play an important role in determining the night-time behavior of NO_3 in the troposphere. In addition, they are the starting point for an NO_3-initiated oxidation mechanism. The major direct gas phase loss mechanisms of NO_3 tend to be the reactions of the radical with a number of VOCs. The reactions of NO_3 with alkanes and aldehydes proceed via hydrogen abstraction and although both of these reactions tend to be relatively slow (Atkinson 1991), they lead to the formation of HNO_3 and peroxy radicals. Both the alkyl peroxy radicals (RO_2) and the acyl peroxy radicals (RCO_3) formed can further react with NO_3, or recombine with NO_2 to form peroxy nitrates (RO_2NO_2), which act as a reservoir for NOx. Furthermore, the HNO_3 formed via these reactions most likely provides a permanent sink for NOx. The reactions of NO_3 with alkenes (including isoprene and

various terpenes) are generally much faster than reactions with the alkanes. These reactions proceed via the addition of NO_3 to a carbon-carbon double bond, followed by recombination with O_2 to yield to a peroxy radical (Wayne et al. 1991). The peroxy radicals formed by this reaction can then react with species such as NO, NO_2, and other peroxy radicals with the probable formation of organic nitrates as reasonably stable end products (Platt and Heintz 1994). NO_3 also reacts readily with sulphur-containing compounds and a reaction of particular importance in the marine boundary layer (MBL) is the reaction with DMS. Since DMS and NOx can often have quite similar concentrations in the MBL, their concentrations can be tightly coupled as they control each other (Allan et al. 1999). The mechanism of the NO_3 + DMS reaction has received much attention (Ravishankara et al. 1997), and it is now agreed that the reaction proceeds via hydrogen abstraction followed by recombination with O_2 in the atmosphere. However, the complete reaction scheme is still not well defined and requires more work.

Due to the equilibrium between NO_3 and NO_2, any loss of N_2O_5 will result in the removal of NO_3. Hence, the behavior and fate of NO_3 and N_2O_5 in the atmosphere are linked to each other via the equilibrium reaction. The forward reaction between NO_3 and NO_2 is the only known atmospheric source of N_2O_5, and the strongly temperature-dependent decomposition of N_2O_5 produces NO_3. Thus, reactions that remove NO_3 lead to an overall removal of N_2O_5 and vice versa. A good example of such coupled behavior is the deposition of N_2O_5, which reacts heterogeneously with water on surfaces of hydrometeors to produce HNO_3.

Dry deposition in the atmosphere is the direct transfer and deposition of gases and particles to the ground, whereas wet deposition is removal via precipitation and washout. Hydrometeors are defined as the products of condensation or sublimation of atmospheric water vapor, and they include aerosols, sea spray, etc. The presence of hydrometeors at night in the troposphere can also lead to the removal of both N_2O_5 and NO_3.

1.3 Spectroscopy of NO_3

Yokelson et al. measured the temperature dependence of the NO_3 absorption cross section between 440 and 720 nm within the temperature range 200–298K in laboratory experiments (Yokelson et al. 1994). The NO_3 peak absorption cross section at 662 nm was reported to be $\sigma = (2.23\pm0.22) \times10^{-17}$ cm^2 $molecule^{-1}$ at 298K. With decreasing temperature this value was found to increase by 36% at 200 K. Orphal et al. re-measured the visible NO_3 spectrum using high-resolution Fourier transform spectroscopy (Orphal, Fellows and Flaud 2003) ($\Delta\lambda$= 0.026 nm) and derived a parametrization of the temperature dependence (200–330 K) of the peak cross section, which has been accepted into the current NASA/JPL recommendations (Burkholder et al. 2015). Excellent agreement exists between the Orphal model and the empirical relationships from Osthoff et al (Osthoff et al. 2007). This parameterization was used to calculate the respective NO_3 cross section valid for the specific temperature of different NO_3 measurement system.

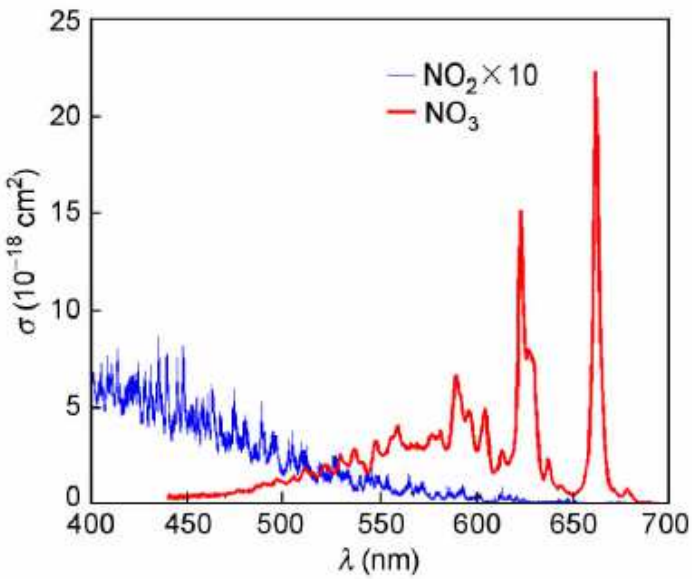

Figure 1-3 The absorption spectrum of NO_3 and NO_2 from 400 to 700nm (Yokelson et al. 1994)

2 Measurement techniques for the nitrate radical (NO_3) in the troposphere

As nitrate radical (NO_3) and dinitrogen pentoxide (N_2O_5) are key species of the tropospheric chemistry, they play a central role in the tropospheric chemical issues such as atmospheric self-cleansing capacity, secondary aerosol formations, reactive halogen chemistry, global sulfur cycles, etc. Measurements of the ambient concentrations of the NO_3 radical are of increasing importance in view of recent measurements of rate constants for the reactions of NO_3 radical with a wide range of organic compounds. Nevertheless, the accurate and precise determination of NO_3 radicals is still a challenging task due to their low ambient concentrations, high reactivity and short life time. In the following, the measurement techniques which have been used to measure the NO_3 concentrations are summarized, including Differential Optical Absorption Spectroscopy (DOAS), Cavity Ring-Down Spectroscopy (CRDS), Matrix Isolation Electron Spin Resonance Spectroscopy (MIESR), Cavity Enhance Absorption Spectroscopy (CEAS), Laser-Induced Fluorescence (LIF), and Chemical Ionization Mass Spectrometry (CIMS). The advantages and disadvantages of these techniques are also summarized insisting on the aspects of measurement accuracy, precision, time resolution, operation stability and interference in this part.

2.1 Differential Optical Absorption Spectroscopy (DOAS)

Atmospheric trace gases can be found in abundance from subppt to ppm levels. Measuring some of them requires highly sensitive and specific techniques with very low detection limits. Such techniques must not be influenced either negatively or positively by any other constituents present simultaneously with the investigated ones. Differential optical absorption spectroscopy (DOAS) can fulfil these requirements.

In the late 1970s, a detection technique of NO_3 radicals in the troposphere was pioneered by Platt and Perner (Platt and Perner 1980, Platt et al. 1980). They used long-path DOAS, which has evolved into a standard technique for the detection of atmospheric NO_3 radicals now. DOAS has been widely used in different configurations for field experiments (Platt et al. 1981, Allan et al. 2000, Geyer et al. 2001, Geyer et al. 2003, McLaren et al. 2004, Stutz et al. 2004, Vrekoussis et al. 2004, Sommariva et al. 2007, Vrekoussis et al. 2007) and chamber studies (Wangberg, Barnes and Becker 1997, Bossmeyer et al. 2006).

A typical DOAS instrument consists of a continuous light source, i.e. a Xe-arc lamp, and an optical setup to send and receive the light through the atmosphere (Platt and Hausmann 1994). It is also possible to use the sun or scattered sun light as light source. The typical length of the light path in the atmosphere ranges from several hundred meters to many kilometers. After its path through the atmosphere, the light is spectrally analyzed and the concentrations are derived.

In the atmosphere the light of the lamp ($I_0(\lambda)$), undergoes to extinction processes by air molecules ($\sigma_{Ray}(\lambda)$) and aerosols ($\sigma_{Mie}(\lambda)$), turbulence ($T(\lambda)$), and absorption by many trace gases with the concentrations C_i and absorption cross sections $\sigma_i(\lambda)$. The light intensity from a path of length L can be described by:

$$I(\lambda)=I_0(\lambda) \times \exp\left(\Sigma\sigma_i(\lambda)\times Ci\times L+ \sigma_{Ray}(\lambda)+\sigma_{Mie}(\lambda)\right)\times T(\lambda) \qquad \text{(I-II)}$$

The task of any spectroscopic method in the atmosphere is to separate these effects in order to derive the concentrations of trace gases. DOAS overcomes this problem by separating the trace gas absorption cross sections into low and high frequency parts by specific numerical filtering methods. A diagrammatic drawing of DOAS is shown in Figure 1-4.

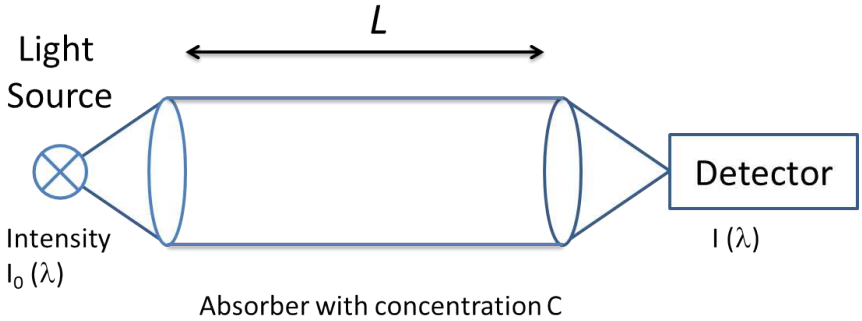

Figure 1-4 Single pass active DOAS. A beam of light passes through an air volume that contains the absorbers of interest. A well-known distance separates the detector from the light source (Platt and Stutz 2008) .

DOAS has proven its use in the past by identifying many trace gases for the first time in the atmosphere, for example OH, NO_3, HONO, BrO, IO etc. Up to now, it is still one of the most appropriate methods to measure NO_3 radicals in the open atmosphere. However, the main limitations of the DOAS method are: (1) it cannot achieve point measurement, (2) it cannot measure N_2O_5 simultaneously (3) in the haze pollution areas, DOAS method detection limit is seriously affected by the aerosol concentration.

2.2 Matrix Isolation Electron Spin Resonance (MI-ESR)

In the 1990s the Matrix Isolation Electron Spin Resonance (MI-ESR) technique was developed, enabling absolute, calibration-free detection of NO_3 radicals (Mihelcic et al. 1993). In a field inter-comparison on NO_3 detection between DOAS and MI-ESR (Geyer et al. 1999), the latter worked very successfully.

Quantitative determinations of nitrate radicals (NO_3) in the troposphere using MI-ESR technique are of high operative difficulty. The samples are collected by pumping ambient air into an evacuated dry sampler. The radicals were trapped on gold-plated copper cold fingers in polycrystalline D_2O-ice matrices at a temperature of 77 K. The use of D_2O instead of H_2O in the matrix reduces the line widths and

therefore yields a better spectral resolution of NO_2, NO_3, HO_2 and RO_2. The collection efficiency exceeded 95% (Geyer et al. 1999). Following sampling, the samples are analyzed with an ESR spectrometer in laboratory.

However, it suffered from its inferior time resolution (sampling time：about 30 min) and substantial handling difficulties which only allowed a limited number of samples to be taken per day during the measurements.

2.3Laser Induced Fluorescence spectroscopy (LIF)

Laser Induced Fluorescence spectroscopy (LIF) has been proven to be an accurate, sensitive, and selective method for measurement of trace atmospheric species throughout the troposphere and stratosphere. In this technique, a laser is used to excite the compound of interest to an excited electronic state, followed by the measurement of the subsequent spontaneous emission (fluorescence).

In the past 20 years, new spectroscopic instruments for sensitive tropospheric NO_3 detection have been developed. Their detection principle either makes use of the specific fluorescence properties of the NO_3 radical, as applied in laser induced fluorescence (LIF) spectroscopy (Matsumoto et al. 2005, Wood et al. 2003).

The NO_3 absorption spectrum is broad and diffuse, with no rotational structure evident even under high resolution (Marinelli, Swanson and Johnston 1982). Like NO_2, the excited-state lifetime of NO_3 is over 2 orders of magnitude longer than the lifetime calculated from its absorption cross section. These properties have been explained in the context of the Douglas effect (i.e., strong coupling between the ground and excited electronic states) (Douglas 1966). To confirm that the signal was indeed produced by NO_3 fluorescence, the excitation spectra of the calibration gas mixture are measured by tuning the multi-mode diode laser from 659 to 663 nm and monitoring the fluorescence. The excitation spectrum is along with the absorption cross section for reference. A LIF schematic from University of California is shown in Figure 1-5.

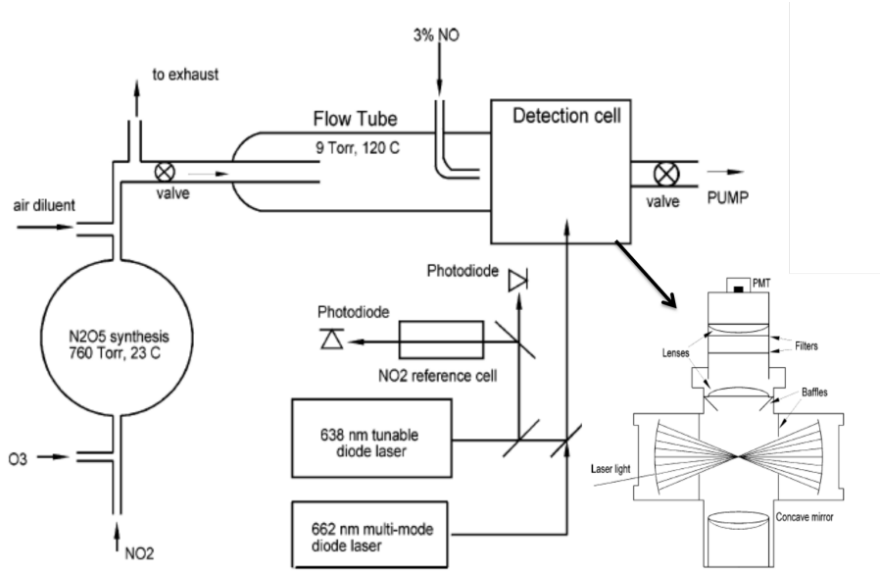

Figure 1-5 Experimental setup of LIF for calibrations (Wood et al. 2003)

However, the difficulty of measuring NO_3 with LIF technique is that the fluorescence quantum yield after NO_3 excitation is low, resulting in a low sensitivity of NO_3 measurement. In high NO_2 concentration conditions, NO_2 fluorescence signal will affect NO_3 signal to produce a strong interference. So, LIF in NO_3 actual measurement process requires the use of dual-wavelength laser light source to subtract NO_2 fluorescence signal interference. But this will reduce the instrument detection limit. In general, laser-induced fluorescence technology is not a particularly promising measurement technology for NO_3 and N_2O_5.

2.4 Cavity Ring Down Spectroscopy (CRDS)

Cavity Ring-Down Spectroscopy (CRDS) is a sensitive absorption measurement based on the time constant for the exponential decay of light intensity from an optical cavity. Since the first laboratory detection of NO_3 radicals by CRDS by King et al. (King, Dick and Simpson 2000), many cavity-based approaches have been developed (Ayers et al. 2005, Bitter et al. 2005, Brown et al. 2001, Dube et al. 2006). Some of these instruments are also capable of measuring N_2O_5 concentrations indirectly by quantitative thermal conversion into NO_3 in a heated detection cell, and the N_2O_5

concentration is obtained after subtraction of the NO_3 concentration. In this way, simultaneous measurements of NO_3 and its equilibrium partner N_2O_5 in the troposphere became feasible for the first time (Chang et al. 2011).

The optical cavity of CRDS is formed by at least two highly reflective mirrors. The laser (centered at 662 nm) is directed into the cavity, the optical intensity builds in the cavity, and then the laser is turned off quickly, compared with the decay of optical intensity in the cavity. An exponential decay of light intensity from the cavity is monitored by measuring the light transmitted through the back mirror. Light transmitted through the back mirror of the each cavity is collected by an optical fiber and detected by a photomultiplier tube (PMT). Because NO_3 radical has strong absorption bands in the red portion of the visible spectrum centered at 662nm, when it is present, the exponential decay time constant is reduced. By measuring the decay time in the absence and presence of the NO_3, its concentration, $[NO_3]$, can be given as shown by the equation (I-III)

$$[NO_3]=\frac{R_L}{c\sigma_{NO_3}}\left(\frac{1}{\tau}-\frac{1}{\tau_0}\right) \qquad \text{(I-III)}$$

In this equation, $[NO_3]$ is the concentration of NO_3, σ is the absorption cross-section of NO_3 (cm^2 $molecule^{-1}$); c is the speed of light ($c=2.9979\times10^8$ m/s), R_L is the ratio of the total cavity length to the length over which the absorber is present. τ and τ_0 are the exponential decay constants (μs) with and without the absorber in the cavity, respectively.

Therefore, measurement of the time constants in the absence and presence of an absorbing species gives its concentration directly. The detail of this kind of instrument will be described in Chapter II.

2.5 Cavity Enhanced Absorption Spectroscopy (CEAS)

The Cavity Enhanced Absorption Spectroscopy (CEAS) is a broadband multi-component absorption technique using an optical cavity to measure the total extinction of an air sample (Fiedler, Hese and Ruth 2003). Instead of observing the

temporal decay of the light intensity inside the cavity as in CRDS, the steady state intensity (I) of light leaking out of the cavity is measured and spectrally resolved. The related technique CEAS is often employed with continuous wave light sources (Engeln et al. 1998). In CEAS, a constant flow of light entering through the cavity's input mirror replenishes the light lost due to reflection inefficiencies and absorption by the sample (Ball, Langridge and Jones 2004).

The instrument consisted of transmitter and a receiver unit, each housing one of the cavity mirrors. Considering the length of the cavity the setup is very stable. Between the mirrors the wavelength range is selected with a dielectric band-pass filter. Because the light spot tended to wander on the cathode, a fraction of the light was focused onto a quadrant detector which triggered a feedback loop to correct for changes in spot position. A telescope imaged the iris aperture approximately into the center of the open-path cavity. Light transmitted by the cavity was further filtered in the receiver unit with a long-pass cut-off filter and a 700 nm short-pass interference filter to ensure that light outside the mirror reflectivity range was eliminated. The light was focused into a fiber bundle (1mm diameter) and connected to the entrance slit of a spectrometer. A spectral interval from 620 to 720 nm was normally detected by a CCD detector (as shown in Figure 1-6).

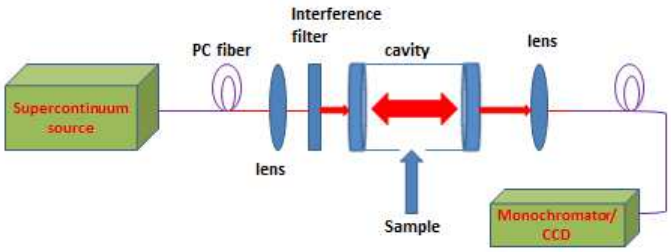

Figure 1-6 Schematic diagram of the CEAS. (Ball et al. 2004)

CEAS technology does not need to use NO titration NO_3 to obtain zero frequently like CRDS, while zero air or high purity nitrogen are used to do the background spectrum. The principle of measurements is based on collecting NO_3 strong absorption of the entire band spectral intensity signal. The spectrums can

quantify not only the gas concentration of NO_3 radicals, which can also measure a variety of trace gases from a variety of trace gas superposition of absorption simultaneously. This technique inverts the center of the spectrum to produce the absorbed medium gas concentration by fitting the spectrum calculated as following:

$$\ln\left(\frac{I_0(\lambda)}{I(\lambda)}\right)=(\Sigma\sigma_i C_i+\xi_R+\xi_M)\times L\times\frac{1}{1-R} \qquad \text{(I-IV)}$$

The samples absorbance per unit path can be calculated from measurements of the steady state intensity with and without the sample present, I (λ) and I_0 (λ), respectively. Here, σ_i is the absorption cross-section corresponding to the absorber in the units of cm^2, C_i is the mixing ratio of the absorber in the units of cm^{-3}, ξ_R and ξ_M are the absorption coefficients in the units of cm^{-1} from Rayleigh scattering and Mie scattering respectively, L is the separation between the mirrors in the units of cm, the effective cavity length, and R is the average mirror reflectivity as a function of wavelength (Venables et al. 2006, Chen and Venables 2011). Therefore, the main interference for CEAS system is aerosol.

2.6 Chemical Ionization Mass Spectrometry (CIMS)

Recently, Chemical Ionization Mass Spectrometry (CIMS) has been widely applied to the *in situ* measurements of atmospheric trace species. CIMS is based on a different principle from those of the spectroscopic and wet chemical techniques, and it has been employed for *in situ* measurement of a variety of atmospheric trace species, as recently reviewed by Huey (Huey 2007). With CIMS, the ion-molecule reactions specifically convert the atmospheric species of interest into an ionic species, which is then analyzed by a mass spectrometer with high sensitivity and high selectivity, and with an integration time of 1 min or less.

An instrument schematic of CIMS is shown in Figure 1-7. The sum of N_2O_5 and NO_3 can be measured as the nitrate anion, NO_3^- , by chemical ionization mass spectrometry (CIMS) using the iodide reagent ion (I^-).

$I^- + NO_3 \rightarrow NO_3^- + I$ (1-12)

$I^- + N_2O_5 \rightarrow NO_3^- + INO_2$ (1-13)

Indeed, this particular CIMS approach has been employed in numerous laboratory studies (Huey et al., 1995, Thornton et al., 2003) and has been demonstrated as a potential *in situ* method for N_2O_5 detection (Slusher et al. 2004, Huey 2007).

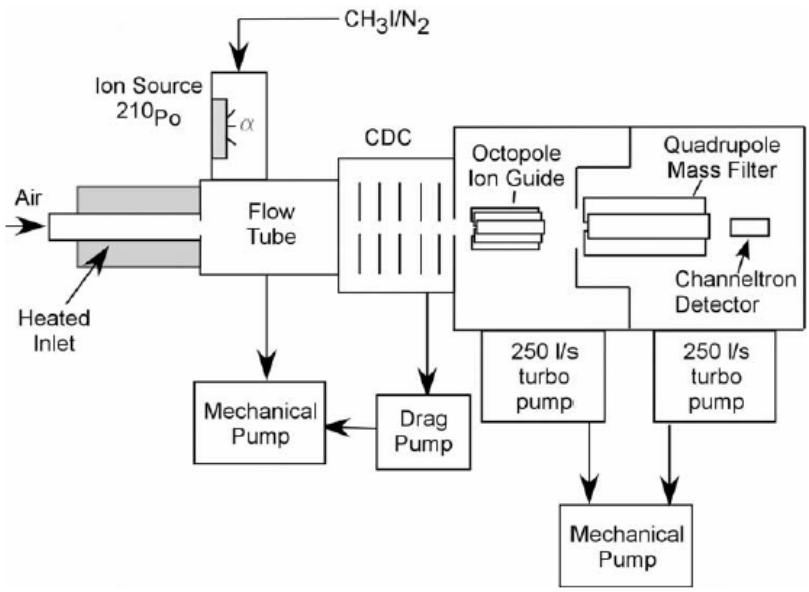

Figure 1-7 Instrument schematic of CIMS. (Slusher et al. 2004)

The disadvantage of the technology is that it could be easily disturbed by PAN, $ClONO_2$, $BrONO_2$ and other substances during the measurement of N_2O_5. When NO_2 is present, PAN can generate a large number of signals in the measurement process, and it can cause serious interferences to NO_3 and N_2O_5 measurements

2.7 Summary

The advantages and disadvantages of those techniques are summarized in Table 1-1 insisting on the aspects of measurement accuracy, precision, time resolution, interference, and operation stability.

Table 1-1 Measurement techniques for nitrate radical and dinitrogen pentoxide.

Technique	Measuring parameter	Limit of detection	Accuracy	Selection	Main interference	Ref.
DOAS	Absorption spectrum	~3ppt	~10%	low	meteorology	(Stutz et al. 2010)
MIESR	Unpaired electrons	~3ppt	~5%	low	H_2O	(Geyer et al. 1999, Mihelcic et al. 1993)
CRDS	Ring down time	~0.5-1ppt	~11%	high	Aerosol,	(Wagner et al. 2011)
CEAS	Absorption spectrum	~0.5-1ppt	~11%	low	Aerosol, H_2O	(Kennedy et al. 2011)
LIF	Fluorescence spectrum	10ppt	~8%	high	High NO_2	(Wood et al. 2003)
CIMS	Mass spectrum	12ppt	~20%	high	PAN	(Slusher et al. 2004)

In conclusion, the absorption spectroscopy seems to be the best technical approach, especially the subcategories CRDS and CEAS developed in the last decade, are the techniques with high potential of good performance in field applications. However, because high aerosol loadings are always present in the atmosphere in urbanized areas such as mega cities, the aerosol extinction could be a significant barrier to come over for the techniques based on absorption spectroscopy. Therefore, the accurate and precise determination of NO_3 radical is still a challenging task due to their low ambient concentrations, high reactivity and short life time.

3 The unresolved issues in NO_3 radical chemistry

Radical chemistry in the polluted nighttime troposphere is mostly governed by the abundance of NO_3 radicals. They are very reactive and effectively oxidized alkenes, aldehydes, and biogenic volatile organic compounds (BVOCs). Although their role as atmospheric oxidant during the day is generally negligible due to their

fast photolytic decomposition. Their importance in atmospheric nighttime chemistry is comparable to that of OH radicals during daytime (Dorn et al. 2013). In particular, since the daytime NO_3 radical concentrations may approach the daytime OH radical concentrations under certain NOx concentration condition, there are organic compounds for which the NO_3 radical reaction rate constants are comparable to, or exceed, the OH radical reaction rate constants (for example, 2,3-dimethyl-2-butene, α -phellandrene, α -terpinene, terpinolene, pyrrole, azulene, dimethyl selenide et al.). It may undergo significant reaction during daytime hours with the NO_3 radical in addition to reaction with the OH radical and/or O_3.

The main properties and reactions of the NO_3 radical important for the atmosphere have been identified and investigated and considerable progress has been made over the last decade in this field. Nevertheless, uncertainties still remain in the different areas of the NO_3 radical chemistry in our knowledge, and further work is consequently needed.

3.1 Kinetics and mechanisms of NO_3 chemical reactions

A substantial data base concerning the rate constants for the gas-phase reactions of the nitrate (NO_3) radical with organic compounds is now available, with rate constants having been determined using both absolute and relative rate methods. To date, the majority of these kinetic data have been obtained at room temperature using relative rate techniques utilizing both the reactions of the NO_3 radical with other organic compounds and the equilibrium constant for the $NO_3 + NO_2 \rightarrow N_2O_5$ reactions as the reference reaction (Atkinson 1991, Calvert et al. 2008, Calvert et al. 2011). Although rate constant data are available for many classes of compounds, often there has been only one determination for a particular substrate. In such cases, there is obviously justification for further studies. Furthermore, absolute rate data are needed, preferably as a function of temperature. Most importantly, mechanistic and product data for the reactions of the NO_3 radical with organic compounds need to be obtained (Atkinson 2000, Calvert et al. 2008, Calvert et al. 2011).

As for the reactions of the OH radical with organic compounds, there is a general lack of mechanistic and product data available for the reactions of the NO_3 radical with organic compounds. Product data for the atmospherically important reactions of VOCs need to be obtained over temperature and pressure ranges representative of tropospheric conditions. This will require advances in analytical techniques to identify and quantify compounds for which standards may not be available and which cannot presently be accurately quantified. Analytical methods should, wherever possible, minimize the potential for sample losses and/or sample reaction during any sample collection procedure (Atkinson and Arey 2003).

3.2 Field measurements and model estimation

Since the late 1970s, with the successful instrumentation development, field measurements of NO_3 and N_2O_5 have been progressively achieved and are increasingly being used in large-scale observations of tropospheric chemistry (Platt and Perner 1980, Platt et al. 1980).

Various laboratory studies have shown that NO_3 + biogenic VOC reactions efficiently form secondary organic aerosol particles (Mellouki, Le Bras and Sidebottom 2003, Fry et al. 2009, Ziemann and Atkinson 2012). These laboratory studies remain few in number compared to investigations of biogenic VOC oxidation by O_3 and OH. Some regional and global models predict large SOA formation from NO_3–biogenic VOC reactions, but there is little information to constrain the magnitude of the process from field observations. Further, focused field experiment would provide critical tests for these model predictions.

Besides, there remains a disagreement of the significance of NO_3 chemistry for the global sulphur cycle between various modelling studies. This can in part be attributed to an incomplete understanding of the DMS degradation chain, but also to the lack of observations in marine regions, in particular away from coastal locations (Brown et al. 2004, Aldener et al. 2006).

Up to now, there also remain discrepancies between models and measurements of nighttime peroxy radicals and OH, especially with respect to the peroxy radical source predicted from reactions of NO_3 with biogenic VOCs and DMS. Better measurements of this system, along with better analytical tools for peroxy radical measurements, particularly those associated with DMS are required. Finally, further study of nocturnal radical chemistry seems warranted to better assess the consequences of future changes in anthropogenic emissions on ozone, NOx, and aerosol levels on local, regional, and global scales.

3.3 Experimental techniques

Nowadays, the accurate and precise determination of NO_3 radical is still a challenging task due to their low ambient concentrations, high reactivity and short life time. Considerable progress has been achieved in applying existing kinetic methods to the studies of NO_3 reactions. Sources, titration, and analytical methods have been developed or adapted to the spectroscopic and kinetic studies of this radical. These methods should continue to be developed and also combined in specific and original experiments in order to measure with the highest precision the key spectroscopic and kinetic parameters for the NO_3 radical that are relevant to the atmosphere.

4 Motivation and outline of this thesis

The nitrate radical, NO_3, is photochemically unstable and then one of the most chemically important species in the nocturnal atmosphere. It is accompanied by the presence of dinitrogen pentoxide, N_2O_5, with which it is in rapid thermal equilibrium at lower tropospheric temperatures. These two nitrogen oxides participate in numerous atmospheric chemical systems. NO_3 reactions with VOCs are important, or in some cases even dominant, oxidation pathways, impacting the budgets of these species and their degradation products. Nowadays, the oxidation pollution by NOx is

becoming increasingly serious and it has already caused great effect to our life and ecological environment. Because of the large abundances of NO_3 radicals in the atmosphere, it makes even slower reactions important. For the long lived chemicals, even a small reaction rate coefficient can significantly alter their lifetimes. So it is important to characterize these slower reactions to determine their influence on atmospheric lifetimes and production of other species. Investigation of the kinetics and mechanisms of these atmospheric NO_3 oxidation reactions could help to extend the available database on NO_3 reactions and approach a better understanding on these gas-phase reactions.

In our laboratory, we have devised an absolute method where the temporal profiles of NO_3 and N_2O_5 can be measured for thousands of seconds by a sensitive instrument cavity ring down spectrometer (CRDS) in a very large chamber (7300 L) where wall loss rates are minimized. With this method, the reactant can be added and mixed rapidly compared to the times for reactions, affords a way to measure very small rate coefficients. In the present work, the kinetics of NO_3 with different kinds of compounds were studied at room temperature (298 ± 2 K) and atmospheric pressure (1000 ± 5 hPa) in the ICARE-7300L Teflon chamber with a series of analytical tools.

This thesis is divided in six chapters:

Chapter I outlines the sources and sinks of NO_3 radicals in the atmosphere and the technical method used to detect NO_3 and/or N_2O_5.

A brief introduction about the atmospheric simulation chamber and instruments used in this thesis is given in Chapter II.

Chapter III introduces the laboratory studies of the nitrate radical (NO_3) with methacrylate esters. In this work, we obtain the room temperature (298 ± 2K) rate coefficients for the reactions of NO_3 radical with six methacrylate esters (shown below): methyl methacrylate (MMA); ethyl methacrylate (EMA); propyl methacrylate (PMA); isopropyl methacrylate (IPMA); butyl methacrylate (BMA); and isobutyl methacrylate (IBMA) by using two different experimental methods.

Chapter IV introduces the kinetics reactions of NO_3 radical with alkanes. In this work, absolute method was used to obtain the room temperature (298 ± 2K) rate coefficients for the reactions of NO_3 radical with methane, ethane, propane, n-butane, iso-butane, cyclopentane and cyclohexane.

Chapter V introduces the kinetics reactions of NO_3 radical with N_2O, CO and SO_2, the upper limits of rate coefficients of N_2O, CO and SO_2, with NO_3 were derived by using absolute method.

Chapter VI summarizes the results about this thesis and gives an outlook into further possible research work.

References

Aldener, M., S. S. Brown, H. Stark, E. J. Williams, B. M. Lerner, W. C. Kuster, P. D. Goldan, P. K. Quinn, T. S. Bates, F. C. Fehsenfeld & A. R. Ravishankara (2006) Reactivity and loss mechanisms of NO_3 and N_2O_5 in a polluted marine environment: Results from in situ measurements during New England Air Quality Study 2002. *Journal of Geophysical Research-Atmospheres*, 111. DOI: 10.1029/2006jd007252

Allan, B. J., N. Carslaw, H. Coe, R. A. Burgess & J. M. C. Plane (1999) Observations of the nitrate radical in the marine boundary layer. *Journal of Atmospheric Chemistry,* 33**,** 129-154.

Allan, B. J., G. McFiggans, J. M. C. Plane, H. Coe & G. G. McFadyen (2000) The nitrate radical in the remote marine boundary layer. *Journal of Geophysical Research-Atmospheres,* 105**,** 24191-24204.

Atkinson, R. (1991) Kinetics and mechanisms of the gas-phase reactions of the NO_3 radical with organic-compounds. *Journal of Physical and Chemical Reference Data,* 20**,** 459-507.

Atkinson, R. (2000) Atmospheric chemistry of VOCs and NOx. *Atmospheric Environment,* 34**,** 2063-2101.

Atkinson, R. & J. Arey (2003) Atmospheric Degradation of Volatile Organic Compounds. *Chemical Reviews,* 103**,** 4605-4638.

Ayers, J. D., R. L. Apodaca, W. R. Simpson & D. S. Baer (2005) Off-axis cavity ringdown spectroscopy: application to atmospheric nitrate radical detection. *Applied Optics,* 44**,** 7239-7242.

Ball, S. M., J. M. Langridge & R. L. Jones (2004) Broadband cavity enhanced absorption spectroscopy using light emitting diodes. *Chemical Physics Letters,* 398**,** 68-74.

Bitter, M., S. M. Ball, I. M. Povey & R. L. Jones (2005) A broadband cavity ringdown spectrometer for in-situ measurements of atmospheric trace gases.

Atmospheric Chemistry and Physics, 5**,** 2547-2560.

Bossmeyer, J., T. Brauers, C. Richter, F. Rohrer, R. Wegener & A. Wahner (2006) Simulation chamber studies on the NO_3 chemistry of atmospheric aldehydes. *Geophysical Research Letters,* 33.

Brown, S. S., H. Stark, S. J. Ciciora & A. R. Ravishankara (2001) In-situ measurement of atmospheric NO_3 and N_2O_5 via cavity ring-down spectroscopy. *Geophysical Research Letters,* 28**,** 3227-3230.

Brown, S. S., J. E. Dibb, H. Stark, M. Aldener, M. Vozella, S. Whitlow, E. J. Williams, B. M. Lerner, R. Jakoubek, A. M. Middlebrook, J. A. DeGouw, C. Warneke, P. D. Goldan, W. C. Kuster, W. M. Angevine, D. T. Sueper, P. K. Quinn, T. S. Bates, J. F. Meagher, F. C. Fehsenfeld & A. R. Ravishankara (2004) Nighttime removal of NOx in the summer marine boundary layer. *Geophysical Research Letters*, 31. DOI: 10.1029/2004gl019412

Brown, S. S. & J. Stutz (2012) Nighttime radical observations and chemistry. *Chemical Society Reviews,* 41**,** 6405-6447.

Burkholder, J. B., S. P. S., J. P. D. Abbatt,J. R. Barker,R. E. Huie,C. E. Kolb,M. J. Kurylo,V. L. Orkin,D. M. Wilmouth,P. H. Wine (2015) Chemical Kinetics and Photochemical Data for Use in Atmospheric Studies.

Calvert, J. G., R. G. Derwent, J. J. Orlando, G. S. Tyndall & T. J. Wallington. 2008. Mechanisms of Atmospheric Oxidation of the Alkanes. Oxford University Press.

Calvert, J., A. Mellouki, J. Orlando, M. Pilling & T. Wallington. 2011. Mechanisms of Atmospheric Oxidation of the Oxygenates. Oxford University Press.

Chang, W. L., P. V. Bhave, S. S. Brown, N. Riemer, J. Stutz & D. Dabdub (2011) Heterogeneous Atmospheric Chemistry, Ambient Measurements, and Model Calculations of N_2O_5: A Review. *Aerosol Science and Technology,* 45**,** 665-695.

Chen, J. & D. S. Venables (2011) A broadband optical cavity spectrometer for measuring weak near-ultraviolet absorption spectra of gases. *Atmos. Meas.*

Tech., 4**,** 425-436.

Croce de Cobos, A. E., H. Hippler & J. Troe (1984) Study of the recombination reaction nitrogen dioxide + nitrogen trioxide + M .fwdarw. nitrogen pentoxide (N_2O_5) + M at high pressures. *The Journal of Physical Chemistry,* 88**,** 5083-5086.

Dorn, H. P., R. L. Apodaca, S. M. Ball, T. Brauers, S. S. Brown, J. N. Crowley, W. P. Dube, H. Fuchs, R. Haeseler, U. Heitmann, R. L. Jones, A. Kiendler-Scharr, I. Labazan, J. M. Langridge, J. Meinen, T. F. Mentel, U. Platt, D. Poehler, F. Rohrer, A. A. Ruth, E. Schlosser, G. Schuster, A. J. L. Shillings, W. R. Simpson, J. Thieser, R. Tillmann, R. Varma, D. S. Venables & A. Wahner (2013) Intercomparison of NO_3 radical detection instruments in the atmosphere simulation chamber SAPHIR. *Atmospheric Measurement Techniques,* 6**,** 1111-1140.

Douglas, A. (1966) Anomalously long radiative lifetimes of molecular excited states. *The Journal of Chemical Physics,* 45**,** 1007-1015.

Dube, W. P., S. S. Brown, H. D. Osthoff, M. R. Nunley, S. J. Ciciora, M. W. Paris, R. J. McLaughlin & A. R. Ravishankara (2006) Aircraft instrument for simultaneous, in situ measurement of NO_3 and N_2O_5 via pulsed cavity ring-down spectroscopy. *Review of Scientific Instruments,* 77.

Engeln, R., G. Berden, R. Peeters & G. Meijer (1998) Cavity enhanced absorption and cavity enhanced magnetic rotation spectroscopy. *Review of Scientific Instruments,* 69**,** 3763-3769.

Fiedler, S. E., A. Hese & A. A. Ruth (2003) Incoherent broad-band cavity-enhanced absorption spectroscopy. *Chemical Physics Letters,* 371**,** 284-294.

Fry, J. L., A. Kiendler-Scharr, A. W. Rollins, P. J. Wooldridge, S. S. Brown, H. Fuchs, W. Dube, A. Mensah, M. dal Maso, R. Tillmann, H. P. Dorn, T. Brauers & R. C. Cohen (2009) Organic nitrate and secondary organic aerosol yield from NO_3 oxidation of beta-pinene evaluated using a gas-phase kinetics/aerosol partitioning model. *Atmospheric Chemistry and Physics,* 9**,** 1431-1449.

Geyer, A., R. Ackermann, R. Dubois, B. Lohrmann, T. Muller & U. Platt (2001) Long-term observation of nitrate radicals in the continental boundary layer near Berlin. *Atmospheric Environment,* 35**,** 3619-3631.

Geyer, A., B. Alicke, R. Ackermann, M. Martinez, H. Harder, W. Brune, P. di Carlo, E. Williams, T. Jobson, S. Hall, R. Shetter & J. Stutz (2003) Direct observations of daytime NO_3: Implications for urban boundary layer chemistry. *Journal of Geophysical Research-Atmospheres,* 108.

Geyer, A., B. Alicke, D. Mihelcic, J. Stutz & U. Platt (1999) Comparison of tropospheric NO_3 radical measurements by differential optical absorption spectroscopy and matrix isolation electron spin resonance. *Journal of Geophysical Research-Atmospheres,* 104**,** 26097-26105.

Graham, R. A. & H. S. Johnston (1978) The photochemistry of the nitrate radical and the kinetics of the nitrogen pentoxide-ozone system. *The Journal of Physical Chemistry,* 82**,** 254-268.

Hippler, H., C. Schippert & J. Troe (1975) Photolysis of NO_2 and Collisional Energy Transfer in the Reactions $O + NO \rightarrow NO_2$ and $O + NO_2 \rightarrow NO_3$. *Int J. Chem. Kinet.*

Huey, L. G. (2007) Measurement of trace atmospheric species by chemical ionization mass spectrometry: Speciation of reactive nitrogen and future directions. *Mass Spectrometry Reviews,* 26**,** 166-184.

Husain, D. & R. Norrish. 1963. The Production of NO_3 in the Photolysis of Nitrogen Dioxide and of Nitric Acid Vapour Under Isothermal Conditions. In *Proceedings of the Royal Society of London A: Mathematical, Physical and Engineering Sciences*, 165-179. The Royal Society.

Kennedy, O. J., B. Ouyang, J. M. Langridge, M. J. S. Daniels, S. Bauguitte, R. Freshwater, M. W. McLeod, C. Ironmonger, J. Sendall, O. Norris, R. Nightingale, S. M. Ball & R. L. Jones (2011) An aircraft based three channel broadband cavity enhanced absorption spectrometer for simultaneous measurements of NO_3, N_2O_5 and NO_2. *Atmospheric Measurement*

Techniques., 4**,** 1759-1776.

King, M. D., E. M. Dick & W. R. Simpson (2000) A new method for the atmospheric detection of the nitrate radical (NO_3). *Atmospheric Environment,* 34**,** 685-688.

Marinelli, W., D. Swanson & H. Johnston (1982) Absorption cross sections and line shape for the NO_3 (0–0) band. *The Journal of Chemical Physics,* 76**,** 2864-2870.

Matsumoto, J., N. Kosugi, H. Imai & Y. Kajii (2005) Development of a measurement system for nitrate radical and dinitrogen pentoxide using a thermal conversion/laser-induced fluorescence technique. *Review of Scientific Instruments,* 76.

McLaren, R., R. A. Salmon, J. Liggio, K. L. Hayden, K. G. Anlauf & W. R. Leaitch (2004) Nighttime chemistry at a rural site in the Lower Fraser Valley. *Atmospheric Environment,* 38**,** 5837-5848.

Mellouki, A., G. Le Bras & G. Poulet (1987) Discharge flow kinetic study of nitrate radical reactions with free radicals: the reaction of nitrate radical with chlorine atom. *The Journal of Physical Chemistry,* 91**,** 5760-5764.

Mellouki, A., G. Le Bras & H. Sidebottom (2003) Kinetics and mechanisms of the oxidation of oxygenated organic compounds in the gas phase. *Chemical Reviews,* 103**,** 5077-5096.

Mihelcic, D., D. Klemp, P. Musgen, H. W. Patz & A. Volzthomas (1993) Simultaneous measurements of peroxy and nitrate radicals at schauinsland. *Journal of Atmospheric Chemistry,* 16**,** 313-335.

Orlando, J. J., G. S. Tyndall, G. K. Moortgat & J. G. Calvert (1993) Quantum yields for nitrate radical photolysis between 570 and 635 nm. *The Journal of Physical Chemistry,* 97**,** 10996-11000.

Orphal, J., C. E. Fellows & P. M. Flaud (2003) The visible absorption spectrum of NO_3 measured by high-resolution Fourier transform spectroscopy. *Journal of Geophysical Research-Atmospheres,* 108.

Osthoff, H. D., M. J. Pilling, A. R. Ravishankara & S. S. Brown (2007) Temperature dependence of the NO_3 absorption cross-section above 298 K and determination of the equilibrium constant for NO_3+NO_2 <-> N_2O_5 at atmospherically relevant conditions. *Physical Chemistry Chemical Physics,* 9**,** 5785-5793.

Platt, U. & M. Hausmann (1994) Spectroscopic measurement of the free-radicals NO_3, BrO, IO, and OH in the troposphere. *Research on Chemical Intermediates,* 20**,** 557-578.

Platt, U. & F. Heintz (1994) Nitrate Radicals in Tropospheric Chemistry. *Israel Journal of Chemistry,* 34**,** 289-300.

Platt, U. & D. Perner (1980) Direct measurements of atmospheric CH_2O, HNO_2, O_3, NO_2, and SO_2 by differential optical-absorption in the near UV. *Journal of Geophysical Research-Oceans and Atmospheres,* 85**,** 7453-7458.

Platt, U., D. Perner, J. Schroder, C. Kessler & A. Toennissen (1981) THE DIURNAL-VARIATION OF NO3. *Journal of Geophysical Research-Oceans and Atmospheres,* 86**,** 1965-1970.

Platt, U., D. Perner, A. M. Winer, G. W. Harris & J. N. Pitts (1980) Detection of NO_3 in the polluted troposphere by differential optical-absorption. *Geophysical Research Letters,* 7**,** 89-92.

Platt, U. & J. Stutz. 2008. The Design of DOAS Instruments. In *Differential Optical Absorption Spectroscopy: Principles and Applications*, 175-285. Berlin, Heidelberg: Springer Berlin Heidelberg.

Platt, U. F., A. M. Winer, H. W. Biermann, R. Atkinson & J. N. Pitts (1984) Measurement of nitrate radical concentrations in continental air. *Environmental Science & Technology,* 18**,** 365-369.

Peixóto, J. P. & A. H. Oort (1984) Physics of climate. *Reviews of Modern Physics,* 56**,** 365.

Ravishankara, A. R., F. L. Eisele & P. H. Wine (1982) Study of the reaction of hydroxyl with nitric acid. Kinetics and NO_3 yield. *The Journal of Physical*

Chemistry, 86**,** 1854-1858.

Ravishankara, A. R., Y. Rudich, R. Talukdar & S. B. Barone (1997) Oxidation of atmospheric reduced sulphur compounds: perspective from laboratory studies. *Philosophical Transactions of the Royal Society of London. Series B: Biological Sciences,* 352**,** 171-182.

Slusher, D. L., L. G. Huey, D. J. Tanner, F. M. Flocke & J. M. Roberts (2004) A thermal dissociation–chemical ionization mass spectrometry (TD-CIMS) technique for the simultaneous measurement of peroxyacyl nitrates and dinitrogen pentoxide. *Journal of Geophysical Research: Atmospheres,* 109**,** D19. DOI: 10.1029/2004JD004670.

Sommariva, R., M. J. Pilling, W. J. Bloss, D. E. Heard, J. D. Lee, Z. L. Fleming, P. S. Monks, J. M. C. Plane, A. Saiz-Lopez, S. M. Ball, M. Bitter, R. L. Jones, N. Brough, S. A. Penkett, J. R. Hopkins, A. C. Lewis & K. A. Read (2007) Night-time radical chemistry during the NAMBLEX campaign. *Atmospheric Chemistry and Physics,* 7**,** 587-598.

Stutz, J., B. Alicke, R. Ackermann, A. Geyer, A. White & E. Williams (2004) Vertical profiles of NO_3, N_2O_5, O_3, and NOx in the nocturnal boundary layer: 1. Observations during the Texas Air Quality Study 2000. *Journal of Geophysical Research-Atmospheres,* 109. DIO: 10.1029/2003jd004209.

Stutz, J., K. W. Wong, L. Lawrence, L. Ziemba, J. H. Flynn, B. Rappenglück & B. Lefer (2010) Nocturnal NO_3 radical chemistry in Houston, TX. *Atmospheric Environment,* 44**,** 4099-4106.

Venables, D. S., T. Gherman, J. Orphal, J. C. Wenger & A. A. Ruth (2006) High sensitivity in situ monitoring of NO_3 in an atmospheric simulation chamber using incoherent broadband cavity-enhanced absorption spectroscopy. *Environmental Science & Technology,* 40**,** 6758-6763.

Vrekoussis, M., M. Kanakidou, N. Mihalopoulos, P. J. Crutzen, J. Lelieveld, D. Perner, H. Berresheim & E. Baboukas (2004) Role of the NO_3 radicals in oxidation processes in the eastern Mediterranean troposphere during the

MINOS campaign. *Atmospheric Chemistry and Physics,* 4**,** 169-182.

Vrekoussis, M., N. Mihalopoulos, E. Gerasopoulos, M. Kanakidou, P. J. Crutzen & J. Lelieveld (2007) Two-years of NO_3 radical observations in the boundary layer over the Eastern Mediterranean. *Atmospheric Chemistry and Physics,* 7**,** 315-327.

Wagner, N. L., W. P. Dube, R. A. Washenfelder, C. J. Young, I. B. Pollack, T. B. Ryerson & S. S. Brown (2011) Diode laser-based cavity ring-down instrument for NO_3, N_2O_5, NO, NO_2 and O_3 from aircraft. *Atmospheric Measurement Techniques,* 4**,** 1227-1240.

Wallington, T. J., R. Atkinson, A. M. Winer & J. N. Pitts (1986) Absolute rate constants for the gas-phase reaction of the nitrate radical with dimethyl sulfide, nitrogen dioxide, carbon monoxide and a series of alkanes at 298 .+-. 2 K. *The Journal of Physical Chemistry,* 90**,** 4640-4644.

Wangberg, I., I. Barnes & K. H. Becker (1997) Product and mechanistic study of the reaction of NO3 radicals with alpha-pinene. *Environmental Science & Technology,* 31**,** 2130-2135.

Wayne, R. P., I. Barnes, P. Biggs, J. P. Burrows, C. E. Canosamas, J. Hjorth, G. Lebras, G. K. Moortgat, D. Perner, G. Poulet, G. Restelli & H. Sidebottom (1991) The nitrate radical - physics, chemistry, and the atmosphere. *Atmospheric Environment Part a-General Topics,* 25**,** 1-203.

Wood, E. C., P. J. Wooldridge, J. H. Freese, T. Albrecht & R. C. Cohen (2003) Prototype for in situ detection of atmospheric NO_3 and N_2O_5 via laser-induced fluorescence. *Environmental Science & Technology,* 37**,** 5732-5738.

Yokelson, R. J., J. B. Burkholder, R. W. Fox, R. K. Talukdar & A. R. Ravishankara (1994) Temperature-dependence of the NO_3 absorption-spectrum. *Journal of Physical Chemistry,* 98**,** 13144-13150.

Ziemann, P. J. & R. Atkinson (2012) Kinetics, products, and mechanisms of secondary organic aerosol formation. *Chemical Society Reviews,* 41**,**

6582-6605.

Chapitre II Système experimental

Ce chapitre présente les moyens expérimentaux utilisés dans ce travail. Il s'agit d'une chambre de simulation atmosphérique, de 7300L, avec des parois en Téflon. Ce dispositif expérimental permet d'étudier des systèmes réactionnels d'intérêt pour l'atmosphère dans des conditions réalistes et contrôlées. Il est couplé à différents instruments d'analyse tels que la spectroscopie Infra-Rouge *in situ* (FTIR), des spectromètres de masse (PTR-ToF-MS, API-ToF-MS) et des instruments spécifiques à certaines espèces (NO_2, O_3, NO_3, SO_2, HCHO). Un granulomètre (SMPS) a aussi été utilisé pour la mesure des particules.

Chapter II Experimental system

In this Chapter, I present the experimental reactor-indoor smog chamber and related instruments (FTIR, PTR-ToF-MS, API-CIMS, etc.) that have been used for the study on the present thesis work.

1 Reactor - indoor smog chamber

Smog chambers provide a controlled environment to study the formation and the evolution of specific compounds of interest by isolating the influence of emissions, meteorology and mixing effects in the real air conditions. Smog chambers were initially constructed for developing and evaluating atmospheric gas phase chemical mechanisms or models for predicting secondary pollutants.

This part describes the indoor smog chamber facility established at the ICARE-CNRS. This indoor chamber facility is designed to study the kinetic of gas phase reaction as well as the evolution of secondary aerosols, to evaluate the reaction mechanisms, particularly under different initial conditions; and to serve as a platform for evaluating the performance of newly developed gas or particle monitors. The 7300L chamber reactor is made of FEP Teflon film with dimensions of 2.1 × 2.0 × 1.8 m (Bernard et al. 2010, Chen et al. 2015, Zhou et al. 2017). It is kept dark by shrouding it in a container equipped with black curtains. A schematic diagram of this smog chamber is shown in Figure 2-1.

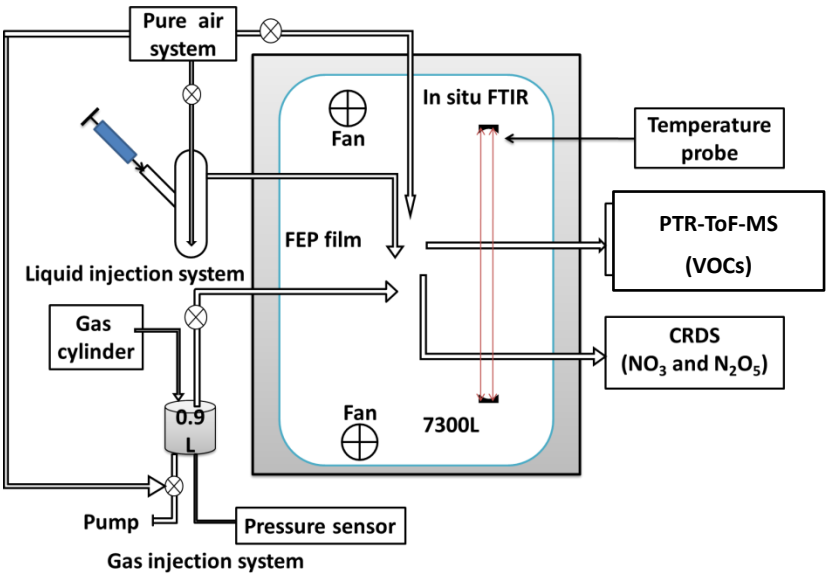

Figure 2-1: Schematic diagram of the 7300 L chamber used to study the reaction of NO_3 radicals with VOCs along with some analytical methods used to detect reactants. The gas inlet system is shown on the left. The gas outlets and the curtains to keep the chamber dark are not shown. The figure is not to scale.

As matrix gas for simulation experiments and carrier gas for reactants, we used purified dry air supplied by passing compressed air through a condenser and a zero-air supply. The maximum flow rate of purified air is about 200 L min^{-1}. The purified dry air includes less than 5 ppb of non-methane hydrocarbons (NMHCs), less than 1 ppb of NOx, O_3 and carbonyl compounds, and no detectable particles. Before each experiment the reactor is flushed with purified dry air at a flow rate of 120 L min^{-1} for at least six hours until no residual hydrocarbons, O_3, NOx or particles are detected in the reactor (lower than the detection limits of each instruments) to avoid carry-over problems from day-to-day experiments. When the reactor is not in use, it is continuously flushed with purified dry air.

The injection system for the smog chamber is designed externally to the chamber. The gas handling system is designed to inject a known volume of a gas (0.9 L) into the chamber. Pressures in the gas handling system are measured by using two

calibrated capacitance manometers (0-10 and 0-100 Torr, MKS Baratron). We could also inject a known volume of liquid (which can evaporate immediately within the chamber) into a glass tube through a gas flow that can reach to the middle of the chamber.

Two fans installed into the chamber ensure rapid mixing of reactants inside the chamber. Temperature and relative humidity data can be continuously recorded by a combined sensor placed in the chamber. To prevent contamination from outside air, a flow of purified air is added continuously during all experiments to keep the chamber slightly above atmospheric pressure and also to compensate for sampling flows of various instruments connected to the chamber. We measured the mixing time and dilution rate in the chamber by injecting a sample of SF_6 (>99.99%, Alpha Gaz) into the chamber and measuring the temporal profile of SF_6 using the *in situ* FTIR spectrometer. The mixing time (for near complete mixing, >99%) is about 30 seconds and the dilution rate could be expressed as a first-order rate coefficient depending on the sampling flow rate.

In my thesis, absolute and relative rate constants for the reactions of NO_3 with unsaturated esters, different alkanes and some other inorganic compounds were all derived and measured by using this ICARE-7300 L Teflon chamber (As shown in Figure 2-2).

The arrays of gas-phase and aerosol-phase instruments associated to the chamber are listed below and details of these instruments are described in the following sections.

Gas phase instruments:

A commercial Nicolet 5700 Magna FT-IR spectrometer coupled to a White-type multipass cell (140m) is located away from the walls and close to the center of the chamber. The FTIR is used to measure SF_6, hydrocarbons, and some other species during the course of different studies. Online monitoring of parent hydrocarbons as well as their oxidation products is also available with a Proton Transfer Reaction Time-of-Flight Mass Spectrometer (PTR-ToF-MS, Ionicon Analytic, Austria). But,

PTR-ToF-MS quantification of HCHO is highly influenced by humidity (Vlasenko et al. 2010). Therefore HCHO concentration is monitored by a HCHO analyzer (AL4021 HCHO-analyzer, Aerolaser.) based on the Hantzsch reaction. In the chamber, O_3, NO_2 and SO_2 concentrations are measured with gas phase monitors and N_2O_5 and NO_3 concentrations are monitored on line with a two-channels Cavity Ring Down Spectrometer (CRDS).

Aerosol phase instruments:

Particle number concentrations and size distributions are obtained using a scanning mobility particle sizer equipped with two differential mobility analyzers (TSI 3081 and 3085; TSI Incorporated, USA) and a condensation particle counter (TSI 3778; TSI Incorporated, USA). Flow rates of sheath and aerosol flows commonly used are 6.0 and 0.6 L min^{-1}, respectively, allowing for a size distribution scan ranging from 3 to 700 nm within 135 s. The accuracy of the particle number concentration is ±10 %.

Chemical Ionization Time-of-Flight Mass Spectrometer coupled with the FIGAERO inlet enables semi-continuous detection of both particle-phase and gas-phase compounds with the ToF-CIMS by sampling cycles between two modes: (1) Gas-phase measurement during aerosol collection (2) Thermal desorption and mass spectral analysis of collected aerosol.

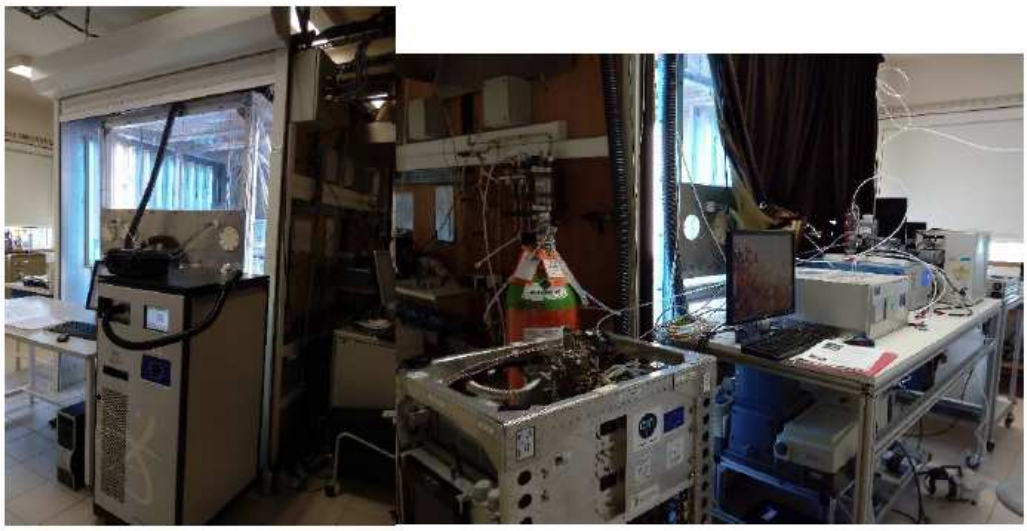

Figure 2-2 Indoor simulation chamber in ICARE, Orleans, France

2 Instruments

2.1 Fourier Transform Infrared Spectroscopy (FTIR)

FTIR is a technique where infrared (IR) radiation passes through a sample, which may absorb some of the radiation, producing a spectrum that represents the molecular absorption and transmission of the sample. A given sample analysis will have a specific IR fingerprint with absorption peaks that correspond to frequencies of vibrations between the bonds of the atoms making up the compound. The analytical method can therefore qualitatively and quantitatively identify different species from the IR absorption spectrum, exploiting the Beer-Lambert law:

$T = I / I_0 = e^{-\varepsilon bc}$

$A = -\ln(T) = -\ln(I / I_0)$

$A = \varepsilon bc$

Where T is transmittance, I_0 and I are the light intensities of the source before and after passing through atmospheric path, respectively, ε is molar absorptivity (m^2 mol^{-1}) and shows how strongly a chemical species absorbs light at a given wavelength, b is the thickness of medium through which light passes, c is molar concentration of chemical species, and A is absorbance which is the relative amount of light absorbed by a sample.

A commercial Nicolet 5700 Magna FTIR spectrometer coupled to a White-type multipass cell as already presented above. The absorption optical path length within the chamber is about 140 m. The instrument is operated with a spectral resolution of 1 cm^{-1}. The acquired spectra are analyzed using the software provided by the vendor (OMNIC Spectroscopy Software). This in-situ FT-IR spectrometer layout coupled to the simulation chamber is shown in Figure 2-3.

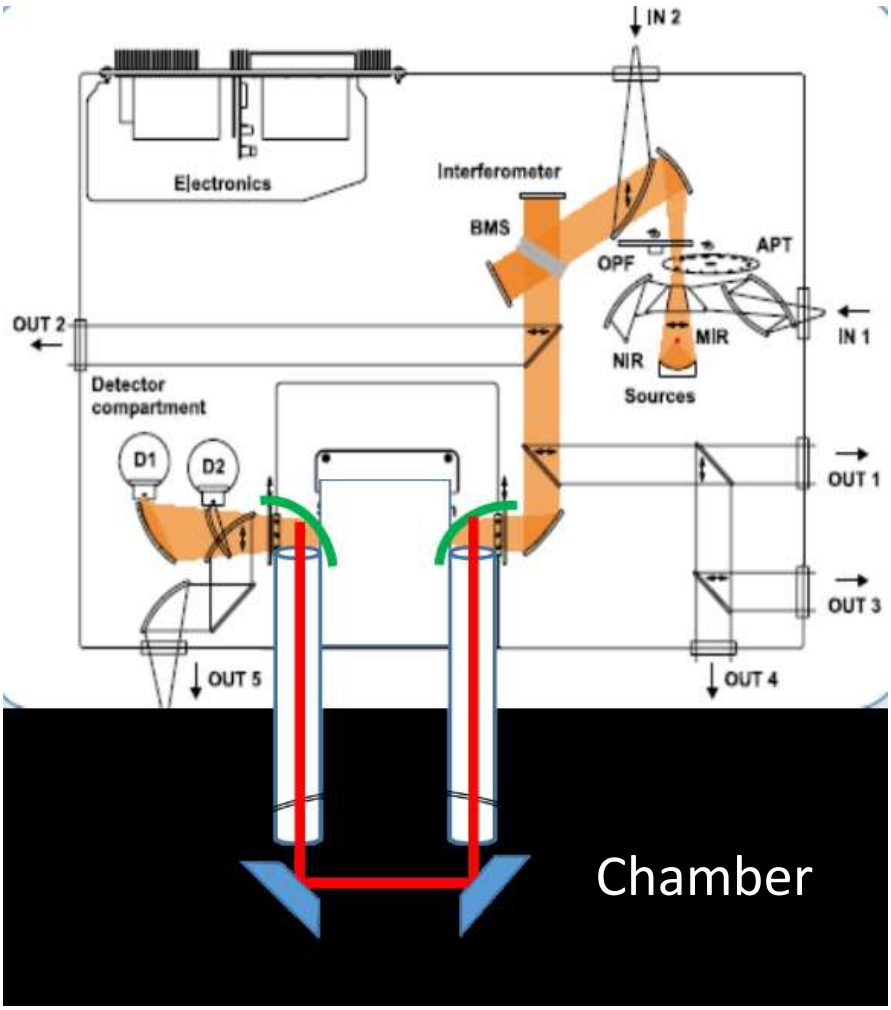

Figure 2-3 The in-situ FT-IR spectrometer layout coupled to 7.3 m^3 simulation chamber

2.2 Proton Transfer Reaction-Time of Flight Mass Spectrometry (PTR-ToF-MS)

A **P**roton **T**ransfer **R**eaction - **M**ass **S**pectrometer (**PTR-MS**) allows the simultaneous on-line monitoring of a lot of **v**olatile **o**rganic **c**ompounds (**VOC**) like acetone, acetaldehyde, methanol, ethanol, benzene, toluene, xylene and others present in concentrations down to 10pptv in ambient air. The instrument consists of three main parts (as shown in Figure 2-4):

(1) Ion source: Production of H_3O^+ ions at high purity level (up to 99%) from pure water vapor via hollow cathode discharge.

(2) Drift tube: The sampled air containing VOCs undergoes (mostly) non-dissociative proton transfer from H_3O^+ ions, which are injected into the drift tube via a Venturi-type inlet (pressure in the drift tube ~2.1mbar).

(3) Analyzing system: A high resolution Time-of-Flight (ToF) mass spectrometer separates the ions according to their mass to charge (m/z) ratio. The resolution is sufficient to distinguish between isobaric molecules and makes an unambiguous identification possible.

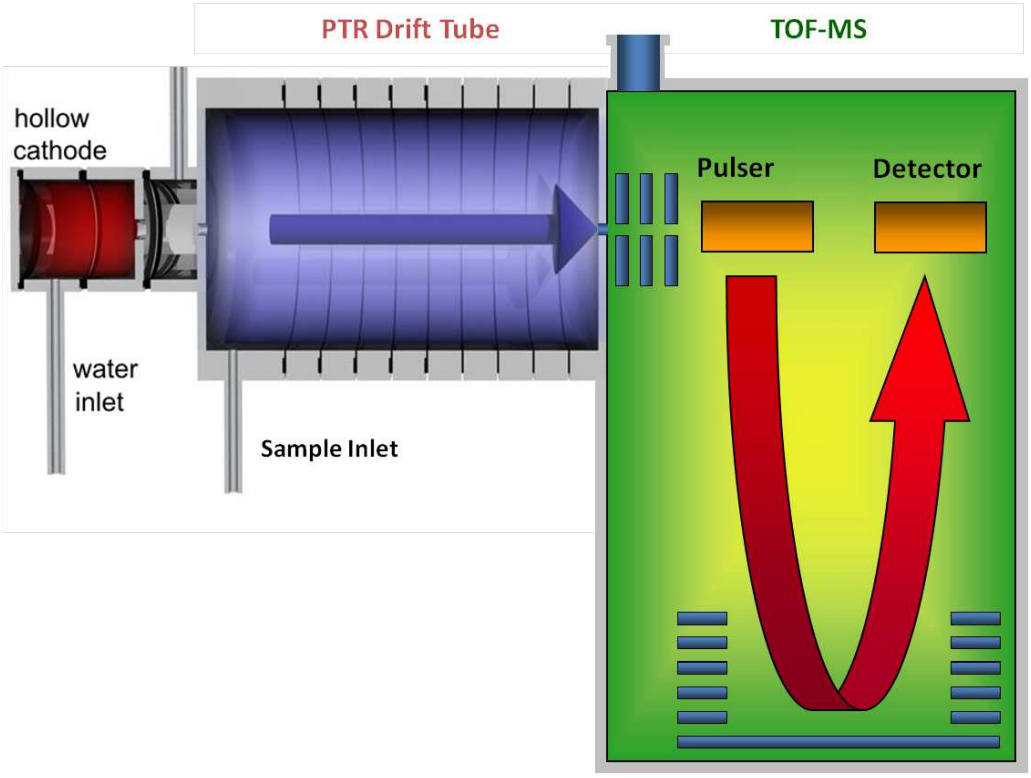

Figure 2-4 Schematic view of the PTR-ToF-MS instrument

Proton transfer reaction is a chemical process that offers a very efficient ionization for most VOCs at reaction rates of approximately 2×10^{-9} $cm^3 s^{-1}$. Since proton transfer is a soft method, the fragmentation rates can be kept very low compared to electron impact ionization. The generation of the primary H_3O^+ ions and the chemical ionization of the VOCs are individually controlled and spatially separated processes. This leads to constant and well defined conditions in the drift region and to a high purity of primary ion (H_3O^+) signal making the calculation of

absolute concentrations possible without the use of gas standards. In addition, H_3O^+ ions do not react with any of the major components present in clean air due to their low proton affinities (The proton affinities of water and other important substance are shown in appendix section). This allows, on one hand, the analyzed air to be used directly as a buffer gas and makes, on the other hand, PTR-ToF-MS very sensitive to trace gases in sample air. Another big advantage of PTR-MS is that the samples do not need to be pre-treated before measurement. In addition, the PTR-ToF-MS combines very low online detection limit with the speed and the high resolution of a time-of-flight mass spectrometer. The ToF component gives the ability to analyze a whole mass spectrum in a split second with a mass resolution of approximately 5000 m/Δm (FWHM) in V-mode. Even isobaric species can therefore be distinguished with no instrumental mass range limitation and a linearity range over six orders of magnitude.

Figure 2-5 PTR-ToF-MS instrument used in our studies

In our studies, the PTR-ToF-MS (PTR-ToF 8000, Ionicon) with hydronium ions (H_3O^+) ion source is used to measure different kinds of VOCs. The major basic

parameters of this instrument are shown in Table 2-1, in different experiments and they can be changed for adapting to different organics analysis.

Table 2-1 PTR-ToF-MS basic parameters:

Minimum inlet flow	70 sccm at 30°C
Drift pressure	2.15 mbar
Drift voltage	600 V
Reaction time	95 µsec.
Reduced mobility	2.8
Reaction length	9.2 cm
Particle of air in the drift tube	5.0×10^{16} particle/cm^3
Electric field	65 V/cm
E/N (E is electric field and N is concentration of neutral particles)	130 Td (1 Td= 10^{-17} V cm^2)
Ion velocity	96800 cm/s
ECM with air	0.162 eV

2.3 Cavity Ring down Spectroscopy (CRDS)

Cavity ring-down spectroscopy (CRDS) is a sensitive absorption measurement technique based on the light intensity exponential decay measurement attached to the residence time of a laser light pulse propagating inside an optical cavity. The optical cavity is formed by at least two separated highly reflective mirrors.

In its simplest form, CRDS is performed by measuring the 1/e decay time, also called the ring down time (τ). Extinction is determined from the measured exiting light intensity temporal decay outside one end of the cavity. Due to losses within the cavity and at the mirrors, the light intensity transmitted through the mirrors as a function of time (t) is described by $I(t) = I_0 \exp(-t/\tau)$.

Extinction due to scattering and absorption by samples reduces the lifetime of the light within the cavity. The extinction coefficient, α_{ext}, is given by:

$$\alpha_{ext} = \frac{R_L}{c}\left(\frac{1}{\tau} - \frac{1}{\tau_0}\right)$$

where R_L is the ratio of optical cavity length to optical absorption path length, c is the speed of light, τ is the ring-down time constant with sample present, and τ_0 is the ring-down time constant in the absence of absorbing species.

$$[\text{Sample}] = \frac{\alpha_{ext}}{\sigma_{ext}}$$

σ_{ext} is the absorption cross-section corresponding to the absorber in the unit of cm^2 $molecule^{-1}$.

A two channels cavity ring down spectrometer designed at NOAA (National Oceanic and Atmospheric Administration, Boulder, Colorado - USA) based on diode laser (662 nm) is used to measure NO_3 concentration (in one channel) and N_2O_5+ NO_3 (in another channel) concentration simultaneously in our experiments (as shown in Figure 2-6). The detection principle and operating characteristics of this instrument have been described in detail elsewhere (Brown et al. 2001, Brown et al. 2002a, Brown, Stark and Ravishankara 2002b, Brown 2003).

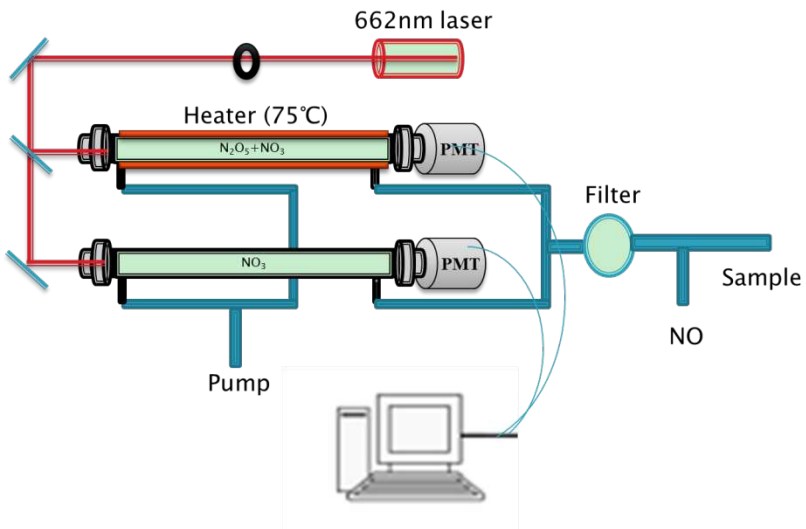

Figure 2-6 Schematic diagram of the CRDS system from NOAA

Briefly, a modulated CW diode laser beam (centered at 662 nm) is splitted in two

and directed into each cavity consisting of two identical highly concave reflective mirrors. When the laser is on, the laser beam travels back and forth inside the cavity, building up the light intensity, and the intensity of the exiting beam is measured by a detector. When the laser is quickly turned off (in less than 1 μs) an exponential decay of light intensity from the cavity is monitored by measuring the light transmitted through the exit mirror. Light transmitted through the exit mirror of each cavity is collected by an optical fiber and detected by a photomultiplier tube (PMT). Because NO_3 radical has strong absorption bands in the red portion of the visible spectrum centered at 662nm, when NO_3 radical is present, the exponential decay time constant is reduced (as shown in Figure 2-7). By measuring the decay time in the absence and presence of the NO_3, its concentration, $[NO_3]$, can be given as shown by equation (Ⅰ)

$$[NO_3]=\frac{R_L}{c\sigma_{NO_3}}\left(\frac{1}{\tau}-\frac{1}{\tau_0}\right) \qquad (Ⅰ)$$

In this equation, $[NO_3]$ is the concentration of the NO_3, σ_{NO3} is the absorption cross-section of NO_3 (cm^2 $molecule^{-1}$); c is the speed of light ($c=2.9979\times10^8$ m/s), R_L is the ratio of the total cavity length to the length over which the absorber is present (R_L=1.2). τ and τ_0 are the exponential decay constants (μs) with and without the absorber in the cavity, respectively.

The first cell is used to measure the NO_3 concentration. The second cell is heated to convert N_2O_5 to NO_3 and the sum of NO_3 and N_2O_5 concentrations is measured in this channel. The time resolution is 1 s and detection sensitivity is 0.4–2 pptv for NO_3 and N_2O_5 as described in detail by Fuchs et al (Fuchs et al. 2012). The instrument zero is determined by addition of a small quantity of NO to the air sample every 4 minutes (Brown et al. 2002a).

The flow rate on the ambient temperature cell (NO_3 detection) is 16 LPM volumetric, while on the heated cell (N_2O_5+NO_3 detection), it is 9 LPM. These flow rates allow adequate residence time for NO titration of NO_3 to zero the absorption signal and thermal conversion of N_2O_5 to NO_3 while minimizing wall loss

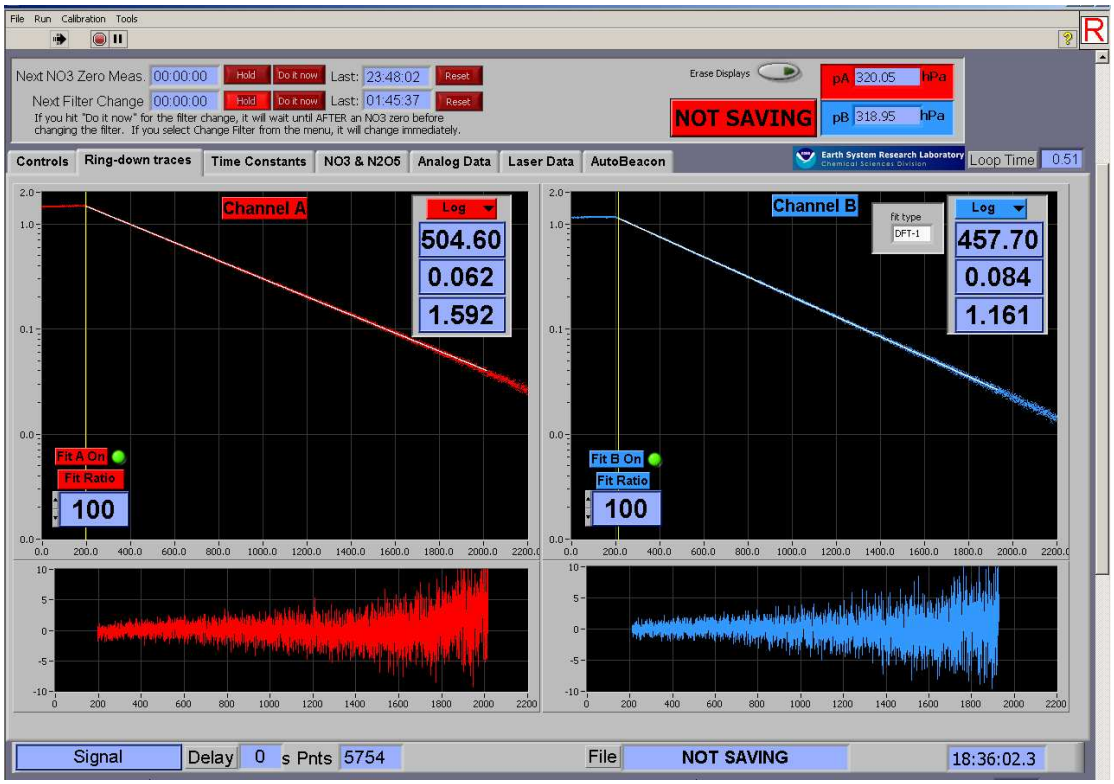

Figure 2-7 Ring-down trace with single exponential fit.

The combined loss of NO_3 and N_2O_5 to the wall and the filter have been estimated to be less than 15% and 5% (Dube et al. 2006), respectively. The uncertainties in the absorption cross section of NO_3 radical at 662 nm and the ratio of the length over which the air sample is present to the total length of the optical cavity add to the estimated uncertainties. Based on these factors, the overall (asymmetric) accuracy of the NO_3 and N_2O_5 measurement is estimated to be -8% to +11% and from −9% to +12%, respectively (Wagner et al. 2011).

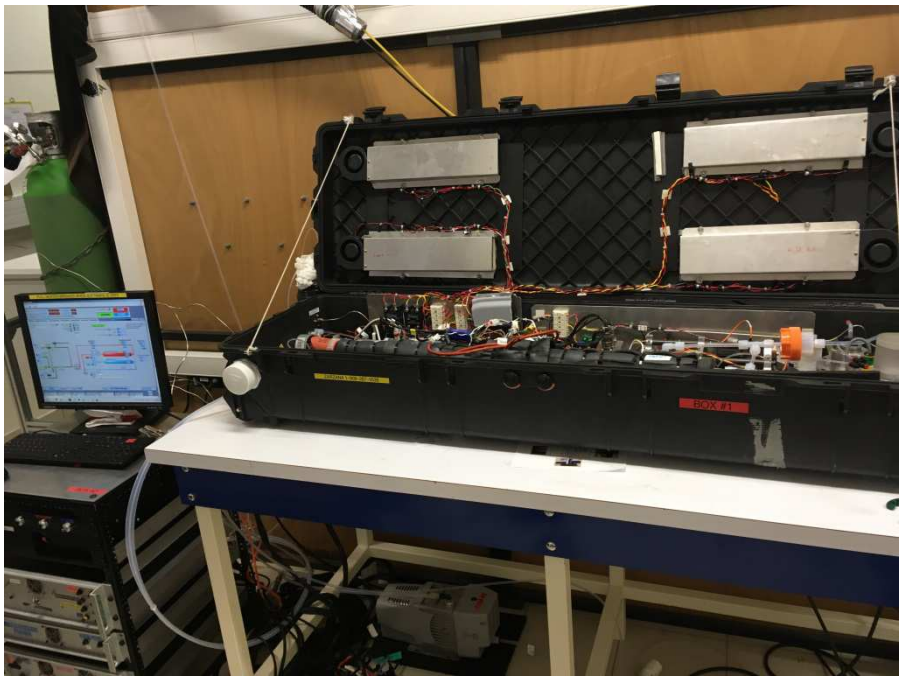

Figure 2-8 Photo of the CRDS from NOAA

2.4 Nitrogen Dioxide (NO_2) monitor

The Cavity Attenuated Phase Shift nitrogen dioxide (CAPS NO_2, Aerodyne research, Inc.) monitor operates as an optical absorption spectrometer and is used to measure the concentration of NO_2 in our work. This monitor consists of three main parts as shown in Figure 2-9: a blue light-emitting diode (LED) as a light source, a sample cell incorporating two high reflectivity mirrors centered at 450 nm and a vacuum photodiode detector. Its efficacy is based on the fact that nitrogen dioxide (NO_2) is a broadband absorber of light in the visible region of the spectrum. Figure 2-10, shown below, displays the absorption spectrum of NO_2 between 400 and 500 nm (blue to green); the specific band employed by the monitor is shown in blue.

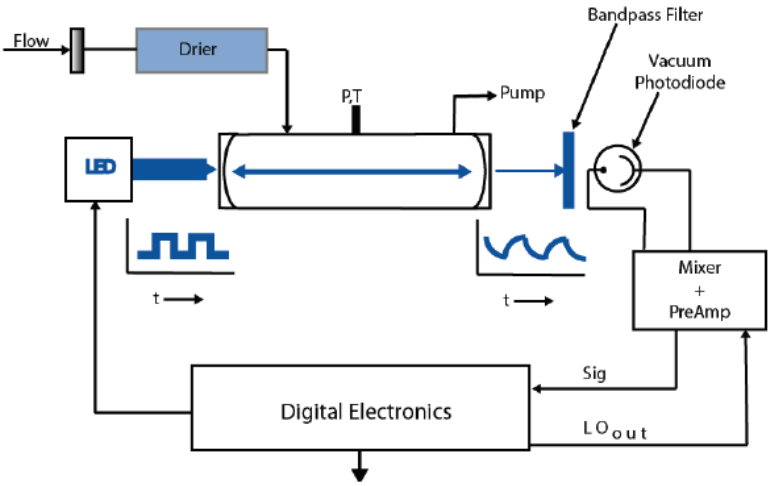

Figure 2-9 Schematic view of the CAPS NO_2 monitor

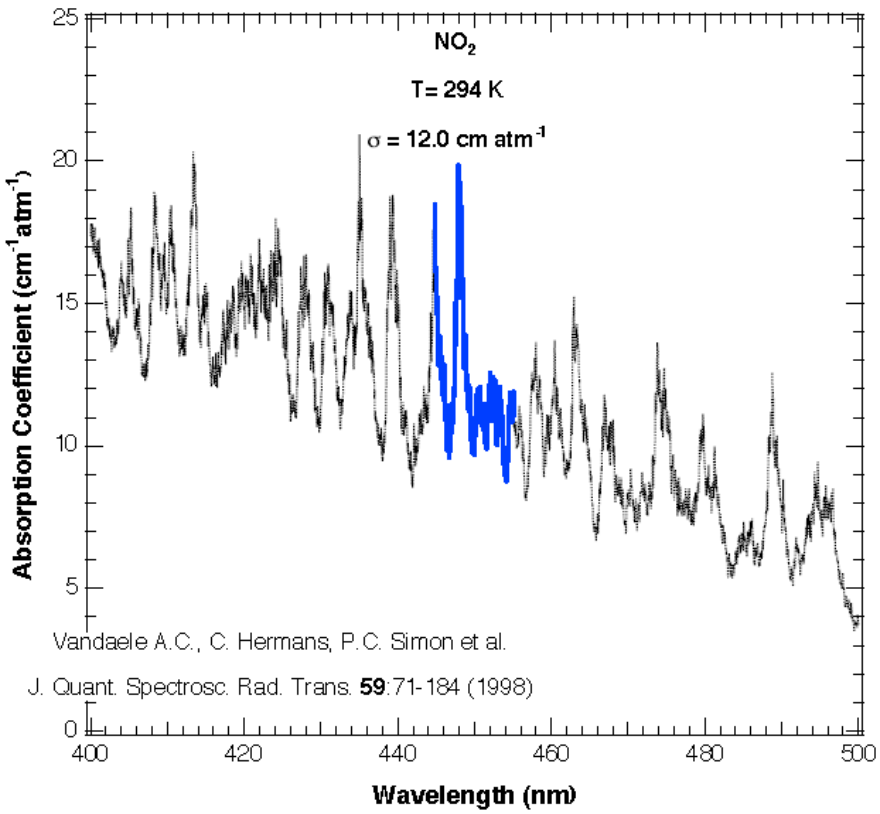

Figure 2-10 Absorption spectrum of nitrogen dioxide in the blue-green region. The pass-band of the absorption spectrometer is outlined in blue. The average absorption coefficient in this band is 12.0 cm atm^{-1}.(Vandaele et al. 1998)

The CAPS NO_2 monitor provides a direct absorption measurement of nitrogen dioxide at 450 nm in the blue region of the electromagnetic spectrum. Unlike standard chemiluminescence-based monitors, these instruments require no conversion of NO_2 to another species and thus are not sensitive to other nitro-containing species. Levels of detection of less than 100 parts per trillion with a 10 second sampling period can readily be attained; a fast response version which offers 1 second time response at reduced levels of detection (1ppb) is also available. These instruments offer completely linear response at concentrations up to several parts-per-million of NO_2. This monitor can be rack mounted and requires only a source of NO_2-free air for periodic (minutes to hours) baseline measurements. The standard gas flow is 0.85 lpm but lower flow rates with reduced time response can be chosen without loss of sensitivity.

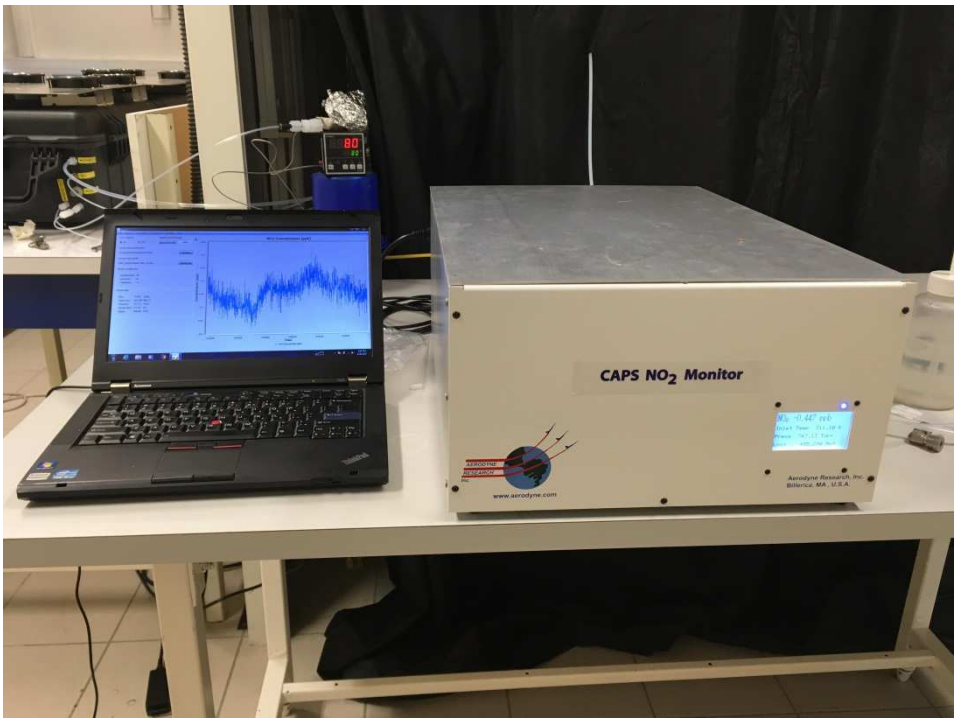

Figure 2-11 Photo view of the CAPS NO_2 monitor instrument

Table 2-2 Basic parameters of CAPS NO_2 monitor

Sensitivity (S/N =3)	Ambient Monitoring: < 0.1 pppb (10 s) Fast Response Version: < 1 pppb (1 s)
Response Time (10-90%):	Ambient Monitoring: 8 s Fast Response Monitor: 1 s
Sample Flow	0.85 lpm (ambient monitor) 2 lpm (fast response monitor)
Operating Pressure	Ambient

2.5 Ozone (O_3) monitor

The Horiba APOA-370 (Figure 2-12) is an ambient ozone (O_3) monitor using the non-dispersive ultraviolet absorption (NDUV) method as its operating principle.

Figure 2-12 Photo view of the APOA-370 O_3 monitor

The ultraviolet absorption method is based on the characteristic of absorbing ultraviolet rays of specific wavelength for ozone. In this analysis method, the sample gas which has passed through the filter is divided into two flow paths. The first one consists in the sample gas which is introduced to the de-ionizer, where ozone is eliminated, and then sent to the cell as "reference gas." In the other path, the sample gas is sent to the cell directly, as "sample gas," by switching a solenoid valve. The measurement cell is exposed to direct radiation by a low-pressure mercury lamp which generates ultraviolet rays with central wavelength of 253.7 nm, and a detector, which involving a photodiode and electric system to obtain electric signals, measures ultraviolet absorption by ozone. The "sample gas" and the "reference gas" are sent to the cell alternately, switched by frequency of 1 Hz with the solenoid valve. The difference in ozone content between the reference gas and the sample gas can be obtained from the difference in the measured ultraviolet absorption.

This means that, in principle, the APOA-370 O_3 monitor makes it possible to carry out zero-span drift free, continuous measurements.

Table 2-3 Basic parameters of APOA-370 O_3 monitor

Range Standard	0 ppm to 0.1/0.2/0.5/1.0 ppm Automatic range switching
Minimum detection sensitivity	0.5 ppb (2σ)
Reproducibility (repeating accuracy)	±1.0% of the full scale
Linearity	±1.0% of the full scale
Zero drift	±1.0% of the full scale /day ±2.0% of the full scale /week (ambient temperature change: within 5°C)
Span drift	±1.0% of the full scale /day ±2.0% of the full scale /week (ambient temperature change: within 5°C)
Response rate	120 s or shorter
Sample collection	rate approximately 0.7 L/min

2.6 Formaldehyde (HCHO) analyzer

One commercial instrument named AL4021 HCHO-analyzer is used to measure formaldehyde in my experiments. For this instrument, the detection of formaldehyde is based on the liquid phase reaction of formaldehyde with acetyl acetone (2,4-pentadione) and ammonia (Hantzsch reaction). This reaction produces 3,5-diacetly-1,4-dihydrolutidine (DDL), which is absorbing light at 410 nm and shows a strong fluorescence around 510 nm. This emitted light is measured by a photomultiplier.

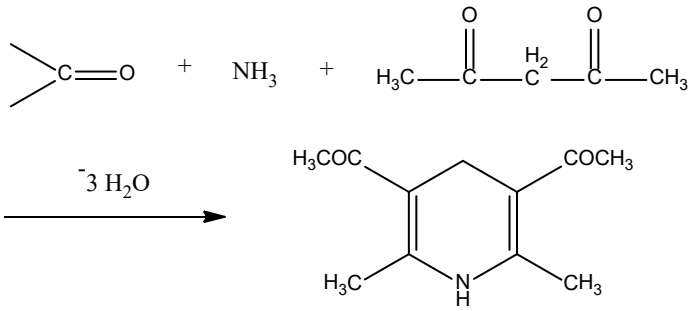

Hantzsch reaction

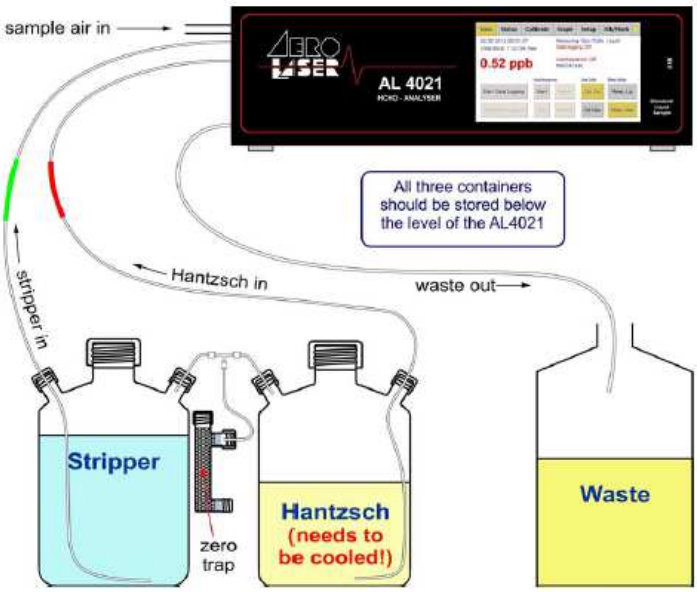

Figure 2-13 AL4021 HCHO-analyzer and related solutions.

Compared to the colorimetric measurement of DDL, the continuous fluorimetric measurement is much more sensitive, faster and, due to the short reaction time, also less cross-sensitive to other aldehydes and ketones. Since the Hantzsch reaction works in aqueous solution, gaseous formaldehyde is transferred into aqueous solution first. This is achieved in a stripping coil, where air and a stripping solution are brought into contact continuously at defined flow rates and contact surfaces. The air is then separated from the liquid stream and the solution is analyzed for formaldehyde. Size, temperature and flow rate of the stripping coil are optimized for a quantitative reaction of HCHO within short times. The scheme of this HCHO analyzer is shown in Figure 2-14. .

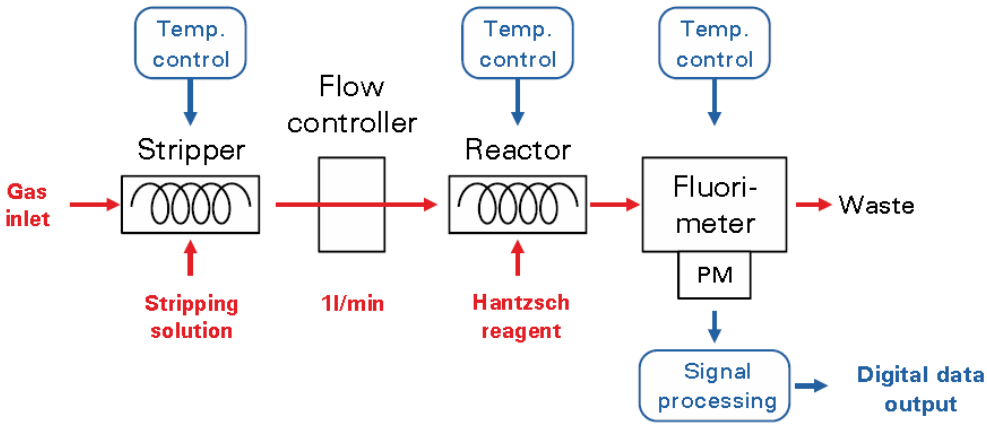

Figure 2-14 Simplified flow scheme of the AL4021 HCHO-analyzer.

Table 2-4 The AL4021 HCHO-analyzer Specifications

Linear detection range	100ppt – 3ppm (gaseous) 150ng/ L – 5mg/L (liquid)
Detection limit	100ppt (gaseous) 150ng/L (liquid)
Dynamic range	up to 50ppm (gaseous) up to 70mg/L (liquid)
Noise	2% full scale
Time resolution	~90s (10% - 90%), delay time ~300s

References

Bernard, F., G. Eyglunent, V. Daele & A. Mellouki (2010) Kinetics and Products of Gas-Phase Reactions of Ozone with Methyl Methacrylate, Methyl Acrylate, and Ethyl Acrylate. *Journal of Physical Chemistry A,* 114**,** 8376-8383.

Brown, S. S. (2003) Absorption spectroscopy in high-finesse cavities for atmospheric studies. *Chemical Reviews,* 103**,** 5219-5238.

Brown, S. S., H. Stark, S. J. Ciciora, R. J. McLaughlin & A. R. Ravishankara (2002a) Simultaneous in situ detection of atmospheric NO_3 and N_2O_5 via cavity ring-down spectroscopy. *Review of Scientific Instruments,* 73**,** 3291-3301.

Brown, S. S., H. Stark, S. J. Ciciora & A. R. Ravishankara (2001) In-situ measurement of atmospheric NO_3 and N_2O_5 via cavity ring-down spectroscopy. *Geophysical Research Letters,* 28**,** 3227-3230.

Brown, S. S., H. Stark & A. R. Ravishankara (2002b) Cavity ring-down spectroscopy for atmospheric trace gas detection: application to the nitrate radical (NO3). *Applied Physics B-Lasers and Optics,* 75**,** 173-182.

Chen, H., Y. Ren, M. Cazaunau, V. Dalele, Y. Hu, J. Chen & A. Mellouki (2015) Rate coefficients for the reaction of ozone with 2-and 3-carene. *Chemical Physics Letters,* 621**,** 71-77.

Dube, W. P., S. S. Brown, H. D. Osthoff, M. R. Nunley, S. J. Ciciora, M. W. Paris, R. J. McLaughlin & A. R. Ravishankara (2006) Aircraft instrument for simultaneous, in situ measurement of NO_3 and N_2O_5 via pulsed cavity ring-down spectroscopy. *Review of Scientific Instruments,* 77.

Fuchs, H., W. R. Simpson, R. L. Apodaca, T. Brauers, R. C. Cohen, J. N. Crowley, H. P. Dorn, W. P. Dube, J. L. Fry, R. Haeseler, Y. Kajii, A. Kiendler-Scharr, I. Labazan, J. Matsumoto, T. F. Mentel, Y. Nakashima, F. Rohrer, A. W. Rollins, G. Schuster, R. Tillmann, A. Wahner, P. J. Wooldridge & S. S. Brown (2012) Comparison of N_2O_5 mixing ratios during NO_3Comp 2007 in SAPHIR. *Atmospheric Measurement Techniques,* 5**,** 2763-2777.

Vandaele, A. C., C. Hermans, P. C. Simon, M. Carleer, R. Colin, S. Fally, M.-F. Merienne, A. Jenouvrier & B. Coquart (1998) Measurements of the NO_2 absorption cross-section from 42 000 cm− 1 to 10 000 cm− 1 (238–1000 nm) at 220 K and 294 K. *Journal of Quantitative Spectroscopy and Radiative Transfer,* 59**,** 171-184.

Vlasenko, A., A. M. Macdonald, S. J. Sjostedt & J. P. D. Abbatt (2010) Formaldehyde measurements by Proton transfer reaction – Mass Spectrometry (PTR-MS): correction for humidity effects. *Atmospheric Measurement Techniques,* 3**,** 1055-1062.

Wagner, N. L., W. P. Dube, R. A. Washenfelder, C. J. Young, I. B. Pollack, T. B. Ryerson & S. S. Brown (2011) Diode laser-based cavity ring-down instrument for NO_3, N_2O_5, NO, NO_2 and O_3 from aircraft. *Atmospheric Measurement Techniques,* 4**,** 1227-1240.

Zhou, L., A. R. Ravishankara, S. S. Brown, M. Idir, K. J. Zarzana, V. Daële & A. Mellouki (2017) Kinetics of the Reactions of NO_3 Radical with Methacrylate Esters. *The Journal of Physical Chemistry A,* 121**,** 4464-4474.

Chapitre III Etudes des réactions d'esters de méthacrylate avec des radicaux NO_3

Deux méthodes expérimentales (relative et absolue) ont été utilisées pour mesurer les constantes de vitesse des réactions de NO_3 avec six esters méthacrylates : le méthacrylate de méthyle (MMA, k1), le méthacrylate d'éthyle (EMA, k2), le méthacrylate de propyle (PMA, k3), le méthacrylate d'isopropyle (IPMA, k4), le méthacrylate de butyle (BMA, k5) et le méthacrylate d'isobutyle (IBMA, k6). Les études ont été réalisées dans une chambre de 7300 L en Téflon à 298 ± 2 K et 1000 ± 5 hPa.

Par la méthode relative, la perte des esters a été suivie en parallèle à celle d'un composé de référence Par la méthode absolue, les profils temporels de NO_3 et N_2O_5 ont été mesurés par spectroscopie CRDS (Cavity Ring Down Spectroscopy) en présence d'un excès d'ester. Les constantes de vitesse de réaction obtenues à 298K par ces deux méthodes (moyennes pondérées) sont les suivantes : k1 = 2.98 ± 0.35, k2 = 4.67 ± 0.49, k3 = 5.23 ± 0.60, k4 = 7.91 ± 1,00, k5 = 5.91 ± 0.58 et k6 = 6.24 ± 0.66 (10^{-15} cm^3 $molécule^{-1}$ s^{-1}, incertitude égale à 2σ, incluant les erreurs systématiques). Les moyennes non pondérées sont aussi reportées dans ce travail.

La constante de vitesse (k7) de la réaction de NO_3 avec le méthacrylate de méthyle deutéré (MMA-d8) a aussi été mesurée par méthode relative et été trouvée équivalente à celle de la réaction de NO_3 avec le méthacrylate de méthyle (k1).

La comparaison des constantes de vitesse obtenues en fonction des méthacrylates (longueur, nature du groupe alkyle), ainsi que le fait que les constantes k1 et k7 (méthacrylate de méthyle non deutéré et méthacrylate de méthyle deutéré), suggèrent fortement que la réaction de NO_3 avec ces esters se fait par addition sur la double liaison du groupe méthacrylate.

Ces résultats sont ensuite comparés à ceux trouvés dans la littérature. Enfin, en utilisant ces constantes de vitesse de réaction des méthacrylates avec le radical NO_3, ainsi que celles des réactions avec les radicaux OH, O_3 et les atomes de chlore, les

durées de vie atmosphériques des esters de méthacrylate ont été calculées par rapport à ces différents oxydants et comparées. Ainsi, on peut constater que les radicaux NO_3 contribuent à la perte atmosphérique de ces esters insaturés, même si c'est moins important qu'avec les radicaux OH et l'ozone.

Chapter III Laboratory studies of the nitrate radical - Reaction of Methacrylate esters with NO_3 radicals[1]

Abstract

Two different experimental methods (relative rate and absolute rate methods) were used to measure the rate coefficients for the reactions of NO_3 radical with six methacrylate esters: methyl methacrylate (MMA, k_1), ethyl methacrylate (EMA, k2), propyl methacrylate (PMA, k_3), isopropyl methacrylate (IPMA, k4), butyl methacrylate (BMA, k_5), and isobutyl methacrylate (IBMA, k_6). In the relative rate method, the loss of the esters relative to that of a reference compound was followed in a 7300 L Teflon-walled chamber at 298 ± 2 K and 1000 ± 5 hPa. In the absolute method, the temporal profiles of NO_3 and N_2O_5 were followed by using a dual channel cavity ring-down spectrometer in the presence of an excess of ester in the 7300 L chamber. The rate coefficients from these two methods (weighted averages) in the units of 10^{-15} cm^3 $molecule^{-1}$ s^{-1} at 298 K are k_1 = 2.98 ± 0.35, k_2 = 4.67 ± 0.49, k_3 = 5.23 ± 0.60, k_4 = 7.91 ± 1.00, k_5 = 5.91 ± 0.58, and k_6 = 6.24 ± 0.66. The quoted uncertainties are at the 2σ level and include estimated systematic errors. Unweighted averages are also reported. In addition, the rate coefficient k_7 for the reaction of NO_3 radical with deuterated methyl methacrylate (MMA-d8) was measured by using the relative rate method to be essentially the same as k_1. The trends in the measured rate coefficient with the length and nature of the alkyl group, along with the equivalence of k_1 and k_7, strongly suggest that the reaction of NO_3 with the methacrylate esters proceeds via addition to the double bond on the methacrylate group. The present results are compared with those from previous studies. Using the measured values of the rate coefficients, along with those for

[1] This work has been published in The Journal of Physical Chemistry A: Zhou, L., A. R. Ravishankara, S. S. Brown, M. Idir, K. J. Zarzana, V. Daële & A. Mellouki (2017) Kinetics of the Reactions of NO_3 Radical with Methacrylate Esters. The Journal of Physical Chemistry A, 121, 4464-4474. DOI: 10.1021/acs.jpca.7b02332

reactions of these esters with OH, O_3, and chlorine atoms, we calculated the atmospheric lifetimes of methacrylate esters. We suggest that NO_3 radicals do contribute to the atmospheric loss of these unsaturated esters, but to a lesser extent than their reactions with OH and O_3.

1 Introduction

Methacrylate esters are important unsaturated oxygenated volatile organic compounds (OVOCs) used in the production of polymers. They are used extensively for manufacture of many industrial products such as resins and plastics. Due to their high volatility, these unsaturated OVOCs may be released into the atmosphere, particularly in industrial areas. For example, more than 5,000 tonnes of methyl methacrylate is produced every year in the European Union. The maximum production capacities per location are estimated to be around 10,000 tonnes per year and release rates from these production and use facilities are estimated to be 0.005% and 1.1 %. If emitted, their atmospheric degradation could lead to surface ozone and aerosols formation.

Once released, these unsaturated OVOCs are degraded in the atmosphere by chemical reaction with various reactive species, which include OH and NO_3 radicals, chlorine atoms and O_3.(Mellouki, Le Bras and Sidebottom 2003) The nitrate radical, NO_3, is a photochemically unstable radical that is prevalent at night, especially in polluted areas that have large NOx emissions. NO_3 is known to be an important nighttime oxidant for OVOCs in the atmosphere.(Brown and Stutz 2012) Therefore, rate coefficients for the reactions of NO_3 radicals with methacrylate esters are needed to assess their loss rates, especially at night.

Kinetics and products of reactions of OH radical reactions with acrylates and methacrylates has been the subject of several studies.(Teruel et al. 2006, Blanco et al. 2006) Reactions of several methacrylate esters with O_3 have also been studied at room temperature.(Grosjean, Grosjean and Williams 1993, Gai, Ge and Wang 2009) Rate coefficients for the reactions of chlorine atoms with methyl methacrylate (MMA) and

ethyl methacrylate (EMA) have been reported.(Blanco et al. 2009b, Blanco et al. 2009a) Several groups(Canosa-Mas et al. 1999, Canosa-Mas et al. 2005, Wang, Ge and Wang 2010, Sagrario Salgado et al. 2011) have measured the rate constants for the reaction of NO_3 with several methacrylates near 298 K via the relative method, often using the reaction of NO_3 with propene as the reference.

In this work, we obtain the room temperature (298 ± 2K) rate coefficients for the reactions of NO_3 radical with six of the methacrylate esters (shown below): methyl methacrylate (MMA) - k_1; ethyl methacrylate (EMA) - k_2; propyl methacrylate (PMA) - k_3; isopropyl methacrylate (IPMA) - k_4; butyl methacrylate (BMA) - k_5; and isobutyl methacrylate (IBMA) - k_6.

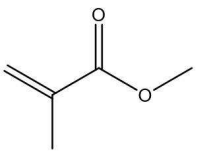

methyl methacrylate

MMA

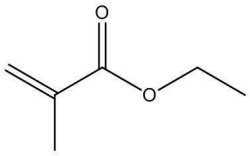

ethyl methacrylate

EMA

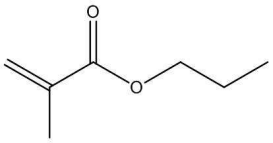

propyl methacrylate

PMA

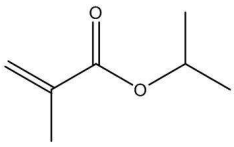

isopropyl methacrylate

IPMA

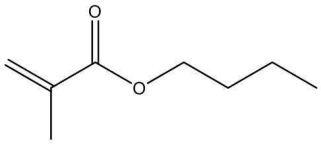

butyl methacrylate

BMA

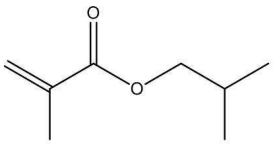

isobutyl methacrylate

IBMA

We used two different experimental methods: (1) a relative rate method where the loss of the ester was measured relative to that of a standard compound while competing for a common pool of NO_3 radicals; and (2) a direct method where the temporal profiles of NO_3 and N_2O_5 were measured using cavity ring down spectroscopy to detect NO_3 and N_2O_5 in an excess of known concentrations of esters. Both N_2O_5 and NO_3 (which are essentially in equilibrium) decay together when NO_3 is lost via its reaction with the hydrocarbon. Therefore, we used a box model consisting of 4 to 5 reactions (see later) to simulate the temporal profiles of NO_3 and N_2O_5 and compare them with the observed profiles of these species. The use of these two complementary methods enhances our confidence in the measured rate

coefficients. In addition, the rate coefficient of deuterated methyl methacrylate (MMA-D8) with NO_3 radical was also investigated to shed light on the mechanism of the reaction. Using the obtained kinetics data, the atmospheric lifetimes of methacrylate esters towards NO_3 radicals were calculated and compared with those due to loss via reactions with OH radicals, O_3 and chlorine atoms (Cl). The kinetics results also help to extend the available database on NO_3 reactions.

2 Experimental system

2.1 Reactors- Indoor atmospheric simulation chamber

The kinetic of NO_3 with esters were studied at room temperature (298±2K) in the ICARE-7300L Teflon chamber, which has been described in detail in previous work (Bernard et al. 2010, Chen et al. 2015) and also in the early part (Chapter II). Here only the features necessary to understand this study are described again. The chamber was equipped with three key analytical tools: (1) a proton transfer reaction mass spectrometer, which was fed from the center of the chamber, to measure the concentrations of hydrocarbon reactants and some of the products; (2) a Nicolet 5700 Magna FT-IR spectrometer (which sampled an axial path length along the center of the chamber) coupled to a white-type mirror system resulting in an optical path of about 143 m; and (3) a cavity ring down spectrometer fed from the center of the chamber with an inlet next to that for the PTR-MS to measure NO_3 and N_2O_5. (We could also estimate the concentration of NO_2 using this system.) All the three analytical systems sampled essentially the same part of the chamber. The contents of the chamber were mixed by two fans internal to the chamber. In addition, the chamber was equipped with multiple thermocouples to measure temperature and a set of capacitance manometers to measure pressure within the chamber, and a gas handling system to input known amounts of gases into the chamber.

In this study, this Teflon film chamber was kept dark by shrouding it in the

container equipped with black curtains. Purified dry air (relative humidity <3%) was constantly flowed into the chamber. The chamber was flushed with a large flow (about 120L/min) of dry air to clean out the chamber between experiments or to clean it overnight. However, during kinetics studies, a small flow (about 5-10L/min, depending on the sampling flow rate) of purified air was added just to make up for the continuous withdrawal of gas from the chamber for analysis; such a flow maintained a constant pressure in the chamber that was slightly above ambient. This flow arrangement resulted in a constant slow dilution of the reactants in the chamber. We measured the dilution rate and mixing time in the chamber by injecting a sample of SF_6 (>99.99%, Alpha Gaz) into the chamber and measuring the temporal profile of SF_6 using the in situ FTIR spectrometer. The mixing time (for near complete mixing, >99%) was about 30 seconds, much shorter than the times for reactions studied here, and the dilution rate could be expressed as a first order rate coefficient of $\sim 2.5 \times 10^{-5} s^{-1}$ (see below).

The gas handling system, external to the chamber, was designed to inject a known volume of a gas into the chamber. We could also inject a known volume of liquid (that evaporated immediately within the chamber) through a septum into a gas flow that reached the middle of the chamber. Pressures in the gas handling system were measured using calibrated capacitance manometers (0-10 and 0-100 Torr, MKS Baratron).

In the chamber, the organic reactants were detected in real time by using a proton-transfer-reaction time of flight mass spectrometer (PTR-ToF-MS), and the concentrations of N_2O_5 and NO_3 were monitored on line by a two-channel cavity ring down spectrometer (CRDS). The details of these instruments are described in the following sections.

2.2 Instrumentations

2.2.1 PTR-ToF-MS

The high resolution proton-transfer-reaction time-of-flight mass spectrometer (PTR-ToF-MS) (Jordan et al. 2009) (Ionicon Analytik, PTR-ToF-MS 8000) with hydronium ions (H_3O^+) ion source was used to measure methacrylates and some of the products of their reactions with NO_3. The pressure and temperature in the PTR-ToF-MS drift tube was maintained at 2.1 mbar and 333 K. A drift voltage of 400 V was used such that the reduced electric field, E/N, value was 98 Td (E is the field strength in V cm^{-1} and N is the number density of gas in molecules cm^{-3}). The flow rate of air from the chamber into the drift tube was approximately 150 mL min^{-1}. The mass resolution of the mass spectrometer, m/Δm, typically ranged from 3500 to 4500 in this study. The mass spectral data were analyzed by a PTR-ToF Data Analyzer software(Mueller et al. 2013) and the normalized peak intensities (in counts per second, ncps) were used for calibration and monitoring. The measured signals varied linearly with the concentrations of the hydrocarbon. The detection sensitivities for the hydrocarbons were derived from the slopes of the calibrations plots of the measured signal (ncps) versus the partial pressure of the hydrocarbon (ppbv) (See Figure 3S-1, in the supporting information). The detection sensitivities (in units of ncps/ppbv, 1ppbv = 2.46×10^{10} molecule cm^{-3} at 298K and 101.3kpa) at their monitored mass for propene, propanal, MMA, d8-MMA, EMA, PMA, IPMA, BMA and IBMA, respectively, were shown in the following in Table 3-1.

Table 3-1. List of specific masses monitored to detect various VOCs using the proton transfer mass spectrometry along with detection sensitivities.

	Mass charge ratio (m/z)	Detection sensitivity （ncps/ppbv）
Propene	43.05	5.22±0.09
Propanal	59.5	7.13±0.09
MMA	101.06	38.9±0.5
d8-MMA	109.09	40.0±0.6
EMA	115.07	5.95±0.47
	87.05	39.2±1.7
PMA	87.05	51.4±0.5
IPMA	87.05	46.8±1.4
BMA	87.05	53.8±2.1
IBMA	87.05	26.1±0.5

2.2.2 CRDS

A two-channel cavity ring down spectrometer operating at 662 nm was used to simultaneously measure the concentrations of NO_3 (in one channel) and N_2O_5 + NO_3 (in another channel). The detection principle and operating characteristics of this instrument has been described in detail in the previous chapter (Chapter II) and elsewhere. (Brown et al. 2002a, Brown, Stark and Ravishankara 2002b, Brown 2003)

The first channel measured the concentration of NO_3. The second, parallel, channel was heated to convert N_2O_5 to NO_3; total NO_3 (which upon quantitative conversion of N_2O_5 to NO_3) was measured and it represents the sum of NO_3 and N_2O_5. The time resolution of the instrument was 1s with detection sensitivities of between 0.4 and 2 ppt for NO_3 and N_2O_5 for 1 second integration, as described in detail by Fuchs et al (Fuchs et al. 2008). The air sample entering the CRDS system was passed

through a filter to remove aerosols, which scatter the 662 nm light and degrade the instrument sensitivity for gas phase measurement. The combined loss of NO_3 and N_2O_5 to the walls of the instrument and the filter located upstream of the device have been estimated (Fuchs et al. 2008, Dube et al. 2006, Fuchs et al. 2012, Dorn et al. 2013) to be less than 20% and 4%, respectively, for NO_3 and N_2O_5; these losses are accounted for in calculating the concentrations. The uncertainties in the absorption cross section of NO_3 radical at 662 nm and the ratio of the cavity length to the length over which NO_3 and N_2O_5 are present add to the estimated uncertainties. Based on these factors, the overall (asymmetric) accuracy of the NO_3 and N_2O_5 measurements, respectively, are estimated (Wagner et al. 2011) to be -8% to +11% and from −9% to +12%. Note that the precision of the measurements of NO_3 and N_2O_5 are used in the present study (with initial mixing ratios of NO_3 between 500 and 2,500 pptv and initial mixing ratios of N_2O_5 between 8,000 and 25,000 pptv)..

2.2.3 Fourier Transform Spectrometer

The commercial Nicolet 5700 Magna FT-IR spectrometer was coupled to a white-type mirror system located away from the walls and close to the center of the chamber. The optical path length within the chamber was about 140 m. The instrument was operated at a resolution of 1 cm^{-1}. The spectra from the instrument were analyzed using the software provided by the vendor. All the details of the instrument and data analyses are also given previously. The FTS was used to measure SF_6 (934 cm^{-1}-954 cm^{-1}), hydrocarbons, and some other species during the course of this study.

2.3 Chemicals

The purities of chemicals used in the experiments as given by the manufacturer were: methyl methacrylate (MMA, > 99%, TCI), ethyl methacrylate (EMA, >99%, TCI), propyl methacrylate (PMA, >97%, Aldrich), isopropyl methacrylate

(IPMA, >98%, TCI), butyl methacrylate (BMA, >99%, TCI), isobutyl methacrylate (IBMA, >98%, TCI), propene (>99%, Air Liquid), and propanal (>98%, Aldrich). The isotopic purity of methyl methacrylate-D8 (MMA-D8 from Apollo Scientific Limited) was quoted to be 99.50 Atom % D. The levels of stabilizers in the samples of esters are noted later. In this study, the NO_3 radicals were produced by the thermal decomposition of N_2O_5 injected into the chamber. Pure N_2O_5 was synthesized by mixing NO with O_3 in a slow flow and collecting N_2O_5 at dry ice temperature, followed by purification, as described by Davidson et al.(Davidson et al. 1978)

3 Rate coefficients measurement

In this section, I describe the results from the two methods that were used. Because the experimental methods were somewhat different, we will first describe the chamber that was used for both methods followed by the analytical methods that were employed. Subsequently, the obtained data are presented.

As noted earlier, we measured the rate coefficients, using two different methods: (a) a relative rate method by following the decay of the VOCs and a reference compound, and (b) an absolute method where the temporal profiles of NO_3 and N_2O_5 in an excess of VOC. For ease of presentation, these two experiments and the obtained results will be presented separately below.

3.1 Relative rate method

The experiments were conducted in the chamber (7300L) at atmospheric pressure (1000±5hPa) and at temperature of 298±2K. The depletion of reactant (each methacrylate esters; hereinafter VOC) and reference (propene, propanal and MMA) in the presence and in the absence of NO_3 (and N_2O_5 in equilibrium with NO_3 and NO_2) were monitored by PTR-ToF-MS. To account for dilution, as noted earlier, the losses of VOCs in the absence of NO_3 were measured along with the depletion of SF_6 added simultaneously with the VOCs to the chamber. This small decay was essentially first

order in the concentrations of VOC and SF_6. The first order rate coefficient for the loss of each reactant in the absence of NO_3 was essentially the same as that for the loss of SF_6; this decay is attributed to dilution caused by the continual injection of air into the chamber. The first-order rate coefficient for the removal of SF_6 and the VOCs, k_d, was $(2.5\pm0.2)\times10^{-5}s^{-1}$. This rate coefficient is essentially what we calculate from the volume flow rates of pure air added to the known volume of the chamber to maintain a constant pressure. The related Figure 3-1 is given as below.

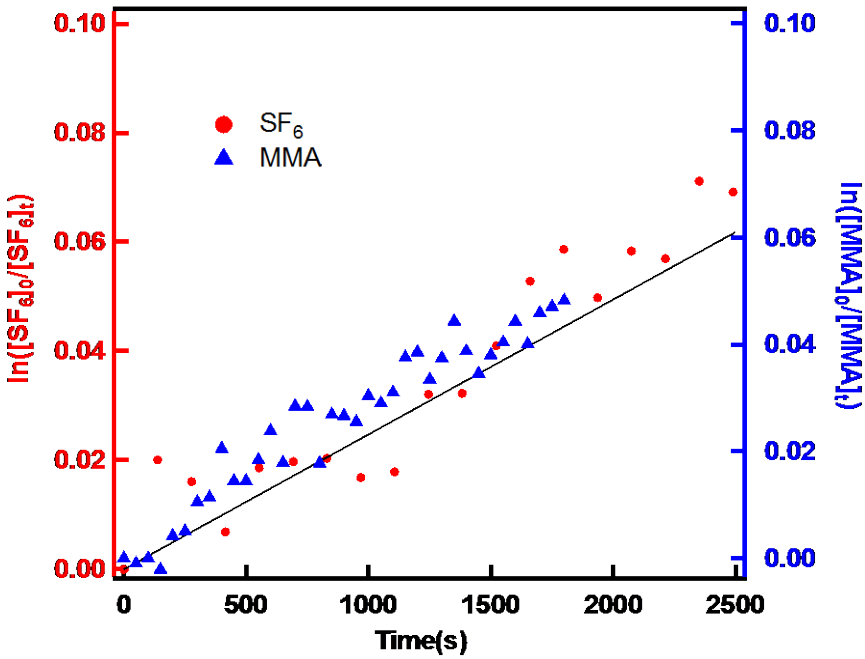

Figure 3-1 The first-order decay rate of SF_6 and MMA in the absence of NO_3.

Subsequent to these measurements, a sample of N_2O_5 was introduced into the chamber where it dissociated to give NO_3. The rates of depletion of VOCs and reference compound were monitored using the PTR-ToF-MS. The VOCs and reference compound are competing for the same pool of NO_3 radicals and are represented by the reactions:

$$\text{VOC}+\text{NO}_3 \xrightarrow{k_{voc}} \text{Products} \qquad \text{(A)}$$

$$\text{Reference}+\text{NO}_3 \xrightarrow{k_r} \text{Products} \qquad \text{(R)}$$

Under these conditions, their relative losses of the VOC and reference compound are

given by:

$$\ln\frac{[VOC]_0}{[VOC]_t} - k_d t = \frac{k_{VOC}}{k_r}(\ln\frac{[Reference]_0}{[Reference]_t} - k_d t) \qquad (I)$$

where $[VOC]_0$ and $[VOC]_t$ are the concentration of reactant at initial time t_0 and at time t, $[Reference]_0$ and [Reference] are the concentration of reactant at t_0 and t, k_{voc} and k_r were the rate coefficients for reaction (A) and (R), k_d is the first order rate constant for dilution in the chamber. A plot of $\ln([VOC]_0/[VOC]_t) - k_d t$ versus $\ln([Reference]_0/[Reference]_t) - k_d t$ would be a straight line with a zero intercept and a slope of k_{voc}/k_r. In our experiments, the rate constants of the reactions of the reference compounds with NO_3 radicals were taken to be k_r(propene) = $(9.5\pm5.5)\times10^{-15}$ $cm^3 molecule^{-1} s^{-1}$ (Atkinson et al. 2006), k_r(propanal) = $(6.3\pm2.6)\times10^{-15} cm^3$ $molecule^{-1} s^{-1}$ (Atkinson et al. 2006) k_r (MMA) = $(2.98\pm0.35)\times10^{-15}$ cm^3 $molecule^{-1} s^{-1}$ (weighted average of the absolute and relative methods from this work; see below). The initial concentration of each reactant used in this work is shown in Table 3-2. A complete summary of the initial concentrations and experimental conditions are given as Table3S-1 in the supporting information section.

Figures 3-2 and 3-3 show the loss of the esters relative to propene and MMA, respectively, according to Equation I. For measurement of each rate constant, several mixtures of the reactant and standard were used and they are all included in the same plots. Clearly, the plots show good linearity for all reactions. These plots were analyzed via linear least squares analyses to obtain the slope of k_{voc}/k_r. The obtained values (average of multiple measurements) of the rate constants are summarized in Table 3-3.

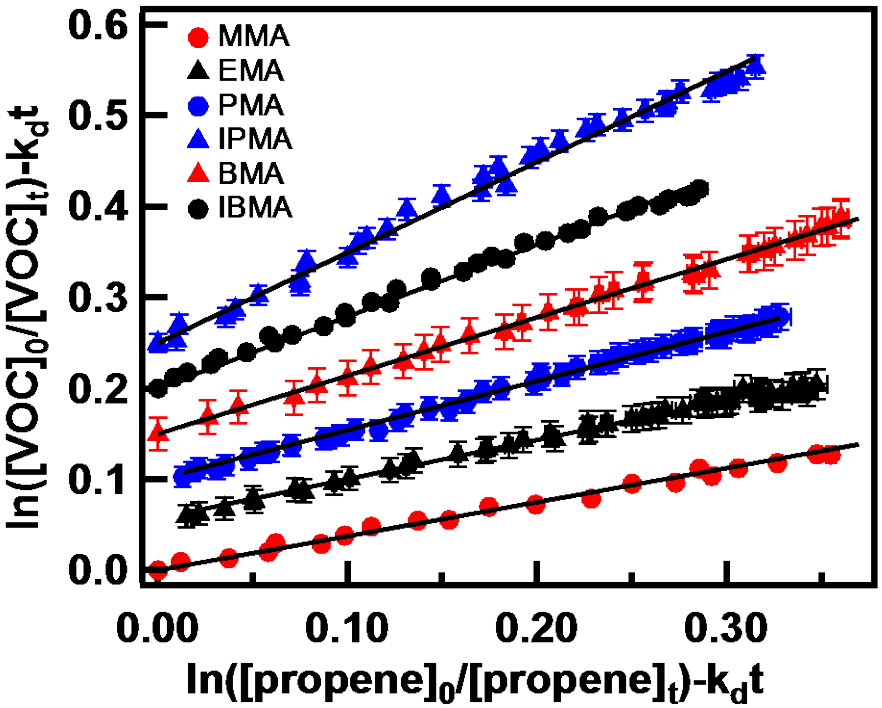

Figure 3-2 Plots of the losses of esters relative to those of propene used as reference. The specific esters are noted in the legend within the figure (EMA, Y axis offset by 0.05; PMA, Y axis offset by 0.1; IPMA, Y axis offset by 0.25; BMA, Y axis offset by 0.15; IBMA, Y axis offset by 0.2).

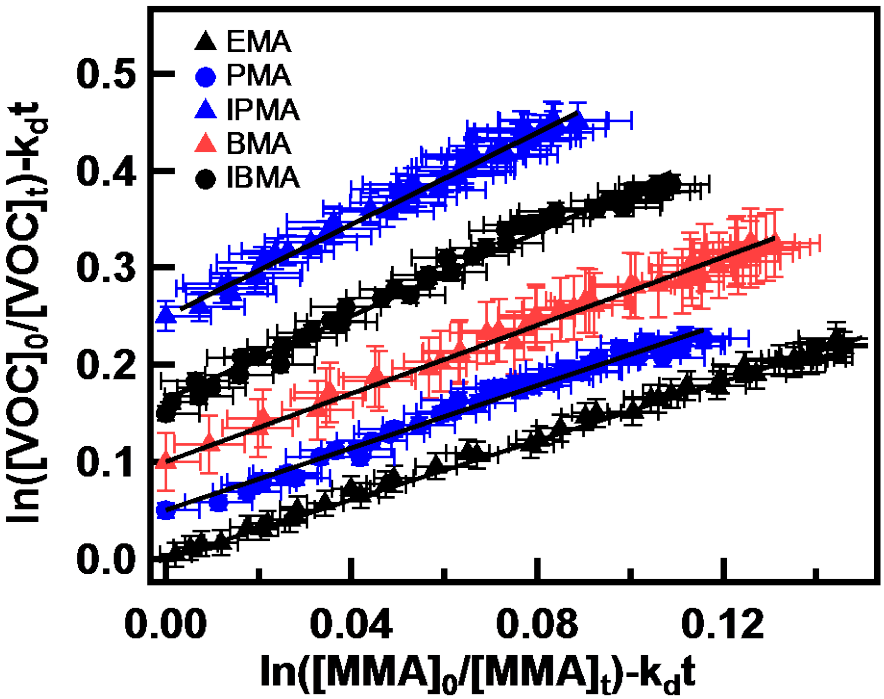

Figure 3-3 Plots of the losses of esters relative to those of MMA used as reference. The specific esters are noted in the legend within the figure (PMA, Y axis offset by 0.05; IPMA, Y axis offset by 0.25; BMA, Y axis offset by 0.1; IBMA, Y axis offset by 0.15).

The quoted errors in the rate constant ratios (k_{voc}/k_r) are twice the standard deviation ($2\sigma_{kvoc/kr}$) in the linear least-squares fit of the measured losses to Equation I. In addition to the precision of this ratio, we have included the estimated uncertainty (as given by the IUPAC evaluations) in the rate coefficient ($k_r \pm \sigma_{kr}$) for the reaction of NO_3 with the reference compound.

Table 3-2 Summary of the results from the relative rate study for reaction of NO_3 with methacrylate esters at 298±2K.

VOCs	$[VOC]_0$ 10^{12} (molecule cm^{-3})	Ref. Compound	Number of experiments	$\frac{k_{voc}}{k_r} \pm 2\sigma_{(\frac{k_{voc}}{k_r})}$	$k_{voc} \pm 2\sigma_{voc}$ 10^{-15} (cm^3 $molecule^{-1}s^{-1}$)
Methyl methacrylate (MMA)	1.13 to 3.40	propene	6	0.37±0.04	(3.52±2.07)
		propanal	2	0.58±0.06	(3.77±1.56)
				Mean average	(3.65±1.30)
				Weighted average	(3.68±1.24)
Ethyl methacrylate (EMA)	1.28 to 2.56	propene	3	0.53±0.05	(5.04±2.95)
		MMA	2	1.55±0.07	(4.62±0.58)
				Mean average	(4.83±1.50)
				Weighted average	(4.63±0.57)
Propyl methacrylate (PMA)	1.10 to1.66	propene	3	0.56±0.04	(5.32±3.10)
		MMA	3	1.70±0.16	(5.07±0.76)
				Mean average	(5.20±1.60)
				Weighted average	(5.08±0.74)
Isopropyl methacrylate (IPMA)	1.10 to1.65	propene	3	0.91±0.30	(8.65±5.76)
		MMA	3	2.71±0.61	(8.08±2.05)
				Mean average	(8.37±3.06)
				Weighted average	(8.14±1.93)
Butyl methacrylate (BMA)	1.01 to 2.53	propene	3	0.70±0.08	(6.65±3.87)
		MMA	3	1.92±0.12	(5.81±0.77)
				Mean average	(6.23±1.97)
				Weighted average	(5.84±0.76)
Isobutyl methacrylate (IBMA)	0.99 to 2.48	propene	3	0.75±0.02	(7.13±4.13)
		MMA	3	1.95±0.23	(5.81±0.96)
				Mean average	(6.47±2.12)
				Weighted average	(5.88±0.94)

Weighted average= $(w_1x_1+w_2x_2+w_3x_3\ldots w_nx_n)/n$; wn=sqrt$(\sigma_1^2+\sigma_2^2+\sigma_3^2\ldots\sigma_n^2)/n$

3.2 Rate coefficients via monitoring temporal profiles of NO_3/N_2O_5 loss using CRDS

The rate coefficients for the reactions of NO_3 radicals with methacrylate esters were also measured by following the temporal profiles of NO_3 and N_2O_5 in an excess of esters. During this process, NO_3 and N_2O_5 were nearly in equilibrium such that one could simply attempt to fit the temporal profiles to obtain the rate coefficients. However, we fitted the observed profiles to the following set of reactions that occur in the chamber:

$$N_2O_5 \xrightarrow{k_{dc}} NO_3 + NO_2 \qquad (R1)$$

$$NO_3 + NO_2 \xrightarrow{k_f} N_2O_5 \qquad (R1')$$

$$NO_3 \xrightarrow{k_{wall1}} \text{loss} \qquad (R2)$$

$$N_2O_5 \xrightarrow{k_{wall\,2}} \text{loss} \qquad (R3)$$

$$VOC + NO_3 \xrightarrow{k_{voc}} \text{loss} \qquad (R4)$$

First, N_2O_5 was injected into the middle of the chamber. N_2O_5 decomposed immediately in the chamber to give NO_3 and NO_2 and set up an equilibrium with remaining N_2O_5. The temporal variation of NO_3 and N_2O_5 in the chamber were continuously measured using CRDS. The concentrations of NO_3 and N_2O_5 decreased with time as N_2O_5 and NO_3 were lost in the chamber due to wall loss and reaction with impurities.

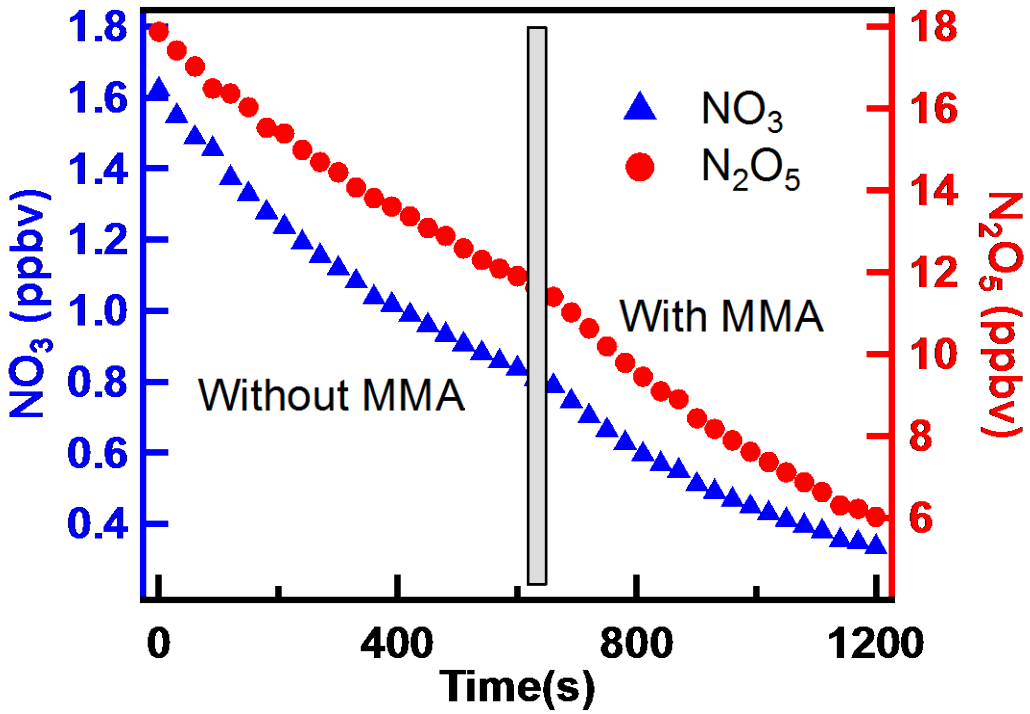

Figure 3-4 Measured temporal profiles of NO_3 and N_2O_5 mixing ratios in the chamber in the absence (up to the vertical gray bar) and presence of MMA (after the gray bar). The gray bar indicates the time at which VOCs were injected into the chamber and the time it took for complete mixing. k_{wall1}=0.0065 s^{-1}, k_{wall2}=0.00032 s^{-1}.

Typical observed temporal profiles of NO_3 and N_2O_5 in such experiments after injection of N_2O_5 into the chamber are shown in Figure 3-4. The measured temporal profiles were fit using a box model that integrated the set of reactions shown above to derive the time dependence of NO_3 and N_2O_5. The fitting was done by minimizing the sum of least squares for both NO_3 and N_2O_5 profiles, by changing the input parameters that included wall loss rates, the equilibrium constant, the rate coefficient for the reaction of NO_3 with VOC as well as the initial NO_2 concentration. First, the data in the absence of VOC was fit to the reaction scheme with VOC concentration set to zero. Using the known values of the rate coefficients for Reactions R1 and R1', the values of k_{wall1}, k_{wall2}, and the initial concentration of NO_2 were derived from the fit. The equilibrium constant was slightly varied to improve

the fit, if necessary. k_{wall1} (s^{-1}) and k_{wall2} (s^{-1}) were the first-order wall loss rate constants of NO_3 and N_2O_5, respectively. Note that we did not have an accurate independent measure of NO_2 in the chamber since the NO_2 detector (which converted NO_2 to NO by passing it over a hot molybdenum catalyst) also detected N_2O_5. Occasionally, we needed to change the N_2O_5 dissociation rate constant by at most 10% to improve the fit, which reflected the uncertainty in the temperature in the chamber of about 1 K. The equilibrium constant, $k_{eq} = [N_2O_5]/[NO_3][NO_2] = k_f/k_{dc}$, and value of k_{dc}, k_{eq} and k_f at different temperature were taken from NASA/JPL recommendation. (Burkholder et al. 2015)

After about 10 minutes, a sufficient time for NO_3 and N_2O_5 observations that enabled an accurate calculation of the equilibrium constant, a known concentration of the VOC was introduced into the chamber and its concentration was measured using PTR-MS and/or FTIR instruments. The concentration of the ester was always much greater than those of N_2O_5 or NO_3 in the chamber. The temporal profile of N_2O_5 and NO_3 measured after 60 s of VOC injection were again fit to minimize the sum of least squares for NO_3 and N_2O_5 decays in the above reaction scheme with only the rate coefficient for the reaction of VOC with NO_3 being the variable As noted earlier, the time for complete mixing was 30 s. The initial concentration of NO_2 was taken to be equal to that calculated just prior to adding the VOC assuming equilibrium between NO_3 and N_2O_5, i.e.,

$$[NO_2]_0 = \frac{[N_2O_5]_0}{[NO_3]_0 k_{eq}} \qquad \text{(II)}$$

Figure 3-5 shows a fit of the observed temporal profiles of NO_3 and N_2O_5 and the fit of the profiles to the above reaction scheme (MMA+NO_3/N_2O_5).

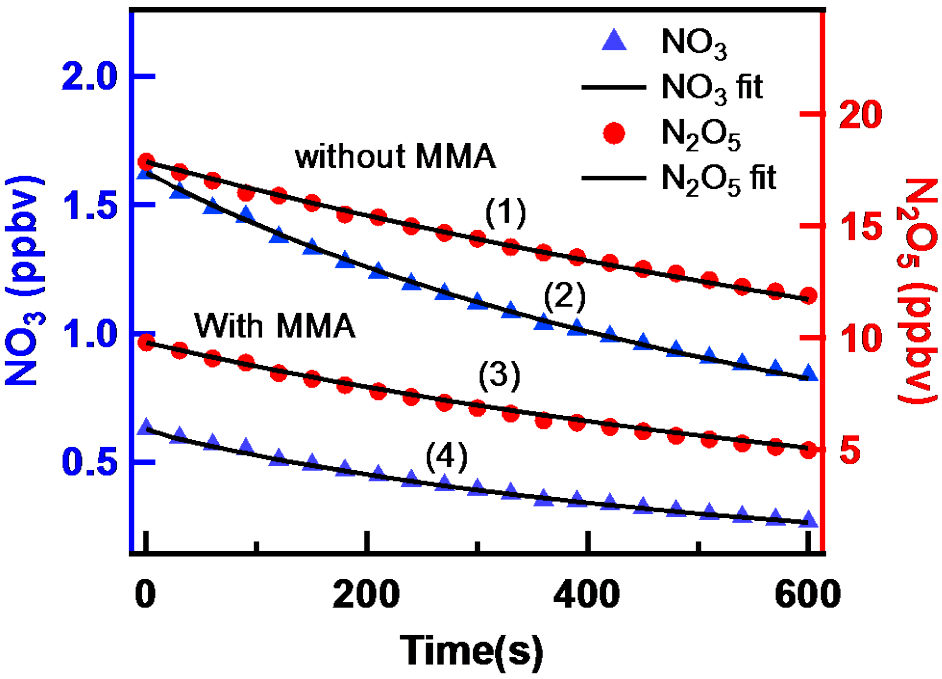

Figure 3-5 Observed NO_3 and N_2O_5 mixing ratios (circles and triangles) and their simulated temporal profiles (lines) after the injection of VOC into the chamber where NO_3 and N_2O_5 were present at equilibrium. Profile (1) - loss of N_2O_5 without MMA; Profile (2) - loss of NO_3 without MMA; Profile (3) - loss of N_2O_5 with MMA; Profile (4) - loss of NO_3 with MMA. The concentration of MMA was 3.06×10^{12} molecule cm^{-3}. The fits yield a value of $k_{voc} = 2.98 \times 10^{-15}$ $molecule^{-1}$ cm^3 s^{-1}.

Multiple experiments were carried out by varying VOC and initial N_2O_5 concentrations. In some cases, we included additional NO_2 in the chamber before the addition of N_2O_5 (to shift the equilibrium). The uncertainty in obtained value of k(VOC) due to fitting was very small, often much less than 3 %. However, the fits alone do not determine the uncertainty in the precision of our measured rate coefficient. They were obtained the standard deviation of the mean of multiple measurements and including the Student t value for the limited number of measurements. A complete summary of the initial concentrations and experimental conditions for the absolute rate method experiments are given in Table 3S-2 (In the supporting information part, at the end of this chapter) and the results of our measurements are given in Table 3-3.

Table 3-3 Summary of the experimental conditions and the results from the absolute rate study for reaction of NO_3 with VOCs at 298±2K. The k_{VOC} values shown are from the best fit to the observed profiles of NO_3 and N_2O_5.

Compound	T	Initial mixing ratio (ppbv)			k_{VOC} measured[a]	k_{VOC} incl. systematic errors[b]
	(K)	VOC	NO_3	N_2O_5	10^{-15}(cm^3 $molecule^{-1}s^{-1}$)	
Propene	296	156.6	0.54	10.16	9.15	9.15
	296	70.0	0.45	9.77	9.97	9.97
					(9.56±1.36)	(9.56±1.80)
MMA	295	121.9	0.68	11.05	2.90	2.90
	296	124.3	0.63	9.79	2.98	2.98
	298	363.7	0.78	11.46	2.89	2.89
					(2.92±0.12)	(2.92±0.37)
EMA	298	126.1	0.81	10.85	4.56	4.56
	300	130.1	0.59	6.79	5.09	5.09
	298	333.3	1.13	16.58	4.69	4.69
					(4.78±0.65)	(4.78±0.93)
PMA	297	113.5	0.79	11.15	5.14	5.14
	300	279.7	1.11	10.13	5.77	5.77
	296	113.6	0.83	8.33	5.59	5.59
					(5.50±0.76)	(5.50±1.00)
IPMA	297	101.6	0.81	10.28	7.94	7.94
	296	86.2	0.91	13.01	7.56	7.56
	300	209.3	0.84	13.69	8.00	8.00
					(7.83±0.56)	(7.83±1.15)
BMA	299	264.2	1.00	8.80	6.16	6.16

	299	199.2	1.25	11.42	5.86	5.86
	300	251.8	1.10	12.92	6.00	6.00
					(6.00±0.35)	(6.00±0.89)
IBMA	296	142.3	0.77	10.90	6.52	6.52
	297	154.5	1.09	13.00	6.46	6.46
	297	162.6	0.99	9.44	6.82	6.82
					(6.60±0.45)	(6.60±0.94)

a. Quoted error is at the 95% confidence level and is a measure of the precision of our measurements. It includes Student t-distribution contribution due to the limited number of measurements.

b. The quoted errors include estimated systematic errors as described in the text.

3.3 Error estimation

3.3.1 Relative rate measurements

One of the advantages of relative rate measurements is that uncertainties in absolute concentrations of either reactant do not lead to an error in the measured values since we depend on the relative concentrations changes as the reaction proceeds. The concentrations of the reactant, in our case esters, and the reference compound (propene, propanal, or MMA) were measured using the same PTR-ToF-MS system. The calibration plots of the concentration of VOC versus their signals were linear. The precision of the measured signal contributes to the precision of the measured rate constants. The slopes of the plots shown in Figures 3-3 and 3-4 yielded the precision of the measurement. The errors in the values of rate constant ratios (k_{voc}/k_r) are twice the standard deviation ($2\sigma_{kvoc/kr}$) in the least-squares fit of the measured losses to Equation. In addition to the precision, the main contributor to the accuracy of the measured rate constant is the accuracy of the rate coefficients for the reference reactions. The rate coefficient for the reactions of

NO_3 with propene and propanal have been evaluated and we assume the accuracy to be those assessed by the evaluation panels, k_r(propene) = $(9.5\pm5.5)\times10^{-15}$ $cm^3 molecule^{-1}s^{-1}$, k_r(propanal) = $(6.3\pm2.6)\times10^{-15}$ cm^3 $molecule^{-1}s^{-1}$. (As noted later, we believe that the uncertainty for the reaction of NO_3 with propene is less than that noted by the evaluation.) We combined the precision of our measured values with the quoted uncertainties in the rate coefficient for the reference reaction to estimate the overall accuracy of the measured rate coefficients.

$$\sigma_{voc}=k_{voc}\sqrt{\left[\frac{2\sigma_{(\frac{k_{voc}}{k_r})}}{\frac{k_{voc}}{k_r}}\right]^2+\left[\frac{\sigma_{k_r}}{k_r}\right]^2} \qquad \text{(III)}$$

3.3.2 Absolute rate constant measurements

The errors in determining the rate coefficients by monitoring the temporal profiles of NO_3 and N_2O_5 arise from the precision in the measurements of NO_3 and N_2O_5, the absolute values of N_2O_5 and NO_3 and the uncertainty in the concentration of the excess reagent, the esters in our measurements. Ordinarily, the absolute values of the NO_3 reactant would not be needed in an absolute method where NO_3 temporal profile is monitored in an excess of esters. However, in the present study, NO_3 is in equilibrium (or almost in equilibrium) with N_2O_5 and this situation requires absolute concentrations of the NO_3 and N_2O_5. The systematic errors in measurements of NO_3 and N_2O_5 using the CRDS system employed here have been assessed to be -8/+11% for NO_3 and -9/+12% for N_2O_5, as noted earlier. The uncertainty in the fitting, as noted above, is better than 3%. Systematic errors in the measured concentration of the esters are estimated for each compound using the uncertainty of the slope in the calibration plots (<4%) and the uncertainty in measuring ester concentration for the calibration (5%); all at 95% confidence level. We just added these two errors to get the estimated uncertainty in the concentration of esters in the chamber since they could be correlated. Then, the overall estimated

error was calculated by adding in quadrature the fitting error, estimated contribution of absolute concentrations of NO_3 and N_2O_5, the precision of the measurements of k_{VOC}, and the estimated uncertainty in the concentration of the esters. Table 3-3 lists the uncertainties in the measured values of the rate constants along with the estimated systematic errors.

We measured the rate coefficient for the reaction of NO_3 with propene using the absolute method. Our obtained results are in very good agreement with the literature value (see Table 3-5). This adds further confidence in our measured values of the rate coefficients using the absolute method. We note that most of the reported values for the rate coefficient for the NO_3 reaction with propene in the IUPAC assessment appear to agree reasonably well. We suggest that the error bars given for the reaction of NO_3 with propene in the IUPAC is excessively conservative.

Another potential source of error in the rate coefficient measured using the absolute method is presence of reactive impurities in the sample of the esters. The methacrylates used in the study were the purest we could obtain from commercial vendors (see materials section for purity levels). However, they contained some stabilizers, which could potentially react more rapidly with NO_3 than the esters. The stabilizers used in the methacrylates were normally around 10-20 ppmv, the maximum was about 200 ppmv of 4-Methoxyphenol (MEHQ) in isopropyl methacrylate (IPMA). Stabilizers used with these esters are aromatic compounds with a large side chain containing a saturated group. If MEHQ reacted very rapidly with NO_3, we could indeed overestimate this rate coefficient. Indeed, if the rate coefficient for the reaction of MEHQ with NO_3 were 1×10^{-10} cm^3 $molecule^{-1}$ s^{-1} as quoted for other methoxyphenols by Lauraguais et al.(Lauraguais et al. 2016) We should have measured a value of roughly 2×10^{-14} cm^3 $molecule^{-1}$ s^{-1} for IPMA. However, our measured values using the direct and relative methods agree well (see Table 3-4). Therefore, we do not believe that our reported values were greatly affected by the presence of MEHQ. In case of the other esters, the presence of stabilizers at the quoted levels would contribute at most 20% to the measured value

using the direct method. Again, the agreement between the relative and direct method suggests that the contributions of the stabilizer to the measured rate coefficients were not large. We note that the PTR-ToF-MS spectra of each of the esters did not show any measurable hydrocarbons other than the ester. Based on these observations, we conclude that our measured absolute rate coefficients were not significantly influenced by the presence of impurities.

Lastly, we note that the rate coefficients measured here reflect that for the reaction of NO_3 with esters and there is no significant contribution from any possible reaction of N_2O_5 with esters. First, we varied the ratio of NO_3 to N_2O_5 by changing NO_2 and the measured rate coefficients were insensitive to this ratio. Second, the rate coefficients measured using the absolute method agrees with that from the relative method, where some of the reference molecules are known to be non-reactive towards N_2O_5. Again, in these experiments, the ratios of NO_3 to N_2O_5 were very different and it also varied with the extent of reaction, with no effect on the derived rate coefficients.

3.4 Comparison of rate coefficients obtained from two methods

We used two different methods to measure the rate coefficients for the reactions of NO_3 with methacrylate esters; they are summarized in Table 3-4. The rate constants values we measured using the two methods are in good agreement with each other, given the estimated uncertainties in the rate constants. The largest difference is for the reaction of NO_3 with MMA, where the rate coefficients from the two methods differ by about 25%.

We have used weighted average of the two methods, i.e., the absolute and the relate rate methods, to derive the best possible values for the rate coefficients for the reactions of NO_3 with methacrylate esters studies here. They are also shown in Table 3-4.

Table 3-4 Rate constants values obtained in two methods for the reactions of NO_3 with methacrylate esters.

	Rate constants k_{voc}(10^{-15} molecule^{-1}cm^{3}s^{-1})		Ratio (k_{rm}/k_{ab})	k_{voc} (10^{-15} molecule^{-1}cm^{3}s^{-1})	
	Relative method (k_{rm})	Absolute method (k_{ab})		Mean average	Weighted average
MMA(k_1)	(3.68±1.24)	(2.92±0.37)	1.26	(3.30±0.65)	(2.98±0.35)
EMA(k_2)	(4.63±0.57)	(4.78±0.93)	0.97	(4.70±0.55)	(4.67±0.49)
PMA(k_3)	(5.08±0.74)	(5.50±1.00)	0.92	(5.29±0.62)	(5.23±0.60)
IPMA(k_4)	(8.14±1.93)	(7.83±1.15)	1.04	(7.99±1.12)	(7.91±1.00)
BMA(k_5)	(5.84±0.76)	(6.00±0.89)	0.97	(5.92±0.59)	(5.91±0.58)
IBMA(k_6)	(5.88±0.94)	(6.60±0.94)	0.89	(6.24±0.66)	(6.24±0.66)

3.5 Comparison with the kinetic results in literature

Several groups have measured the rate constants of NO_3 radical reactions with MMA, EMA and BMA using relative methods in small chambers (<150L) at room temperature and atmospheric pressure. In their experiments, the initial mixing ratios of the methacrylate esters were in a range of 5-20ppmv. A comparison of rate coefficients determined in this study with the literature data is shown in Table 3-5. As can be seen in the table, our values are in good agreement with previously reported values given the reported uncertainties.

Given the reasonably good agreement between various reported studies and a lack of obvious reasons to prefer one study over the other, we suggest that an un-weighted average of all the results be used as recommended values for the rate coefficient. Such average values are reported in the Table 3-5. Clearly, there are no previous reports for the rate coefficients for the reactions of NO_3 with PMA, IPMA,

and IBMA. However, given the similarities of those compounds with the other methacrylates studied here, it appears that our rate coefficients are also accurate to about 20% and could be used with confidence.

Table 3-5 Summary of the rate coefficients of NO_3 with MMA, EMA and BMA obtained from literatures and this work.

Reactant	Reference Chemical	k_{VOC} reported $10^{-15}cm^3$ $molecule^{-1}s^{-1}$	Reference
MMA	propene	(3.71±2.22)[a]	Canosa-Mas et al. 1999
	propene	(3.51±2.04)[a]	Wang et al. 2010
	propene	(3.61±2.10)[a]	Sagrario Salgado et al. 2011
	propene	(3.52±2.07)	This work
	methacrolein	(3.51±1.08)	Sagrario Salgado et al. 2011
	1-butene	(3.72±1.15)	Wang et al. 2010
	propanal	(3.77±1.56)	This work
	AM[b]	(2.92±0.37)	This work
		(3.12±0.31)	Weighted average of all work
		(3.53±0.60)	Mean average of all work
EMA	propene	(4.81±2.80)[a]	Wang et al. 2010
	propene	(5.70±3.31)[a]	Sagrario Salgado et al. 2011
	propene	(5.04±2.95)	This work
	1-butene	(5.09±1.61)	Wang et al. 2010
	methacrolein	(5.16±1.59)	Sagrario Salgado et al. 2011
	MMA	(4.62±0.58)	This work
	AM[b]	(4.78±0.93)	This work
		(4.76±0.44)	Weighted average of all work
		(5.03±0.83)	Mean average of all work
BMA	propene	(8.27±4.83)[a]	Sagrario Salgado et al. 2011
	propene	(6.65±3.87)	This work

	1-butene	(7.58±4.36)	Sagrario Salgado et al. 2011
	MMA	(5.81±0.77)	This work
	AM[b]	(6.00±0.89)	This work
		(5.97±0.57)	Weighted average of all work
		(6.86±1.53)	Mean average of all work
PMA		(5.23 ± 0.60)	This work
IPMA		(7.91±1.00)	This work
IBMA		(6.24±0.66)	This work

[a] The values from the literatures were recalculated by using the rate constant of propene with NO_3 (9.5 ± 5.5) $\times 10^{-15}$ cm^3 $molecule^{-1}s^{-1}$, which was used in our study. Note that these uncertainties are likely to be overestimated because of the large uncertainty quoted by IUPAC.

[b] Measured from the temporal profiles of NO_3 and N_2O_5, referred to as the absolute method.

4 Mechanism and Relationship between structure and reactivity of the methacrylate esters

The rate coefficients for all the methacrylate measured here are roughly in the same range, with the rate coefficient slightly increasing with extent of substitution going from methyl to ethyl to propyl to butyl methacrylate. We observe an increase in the reactivity with the chain length of the alkyl group. k_{voc}(MMA)<k_{voc}(EMA)<k_{voc}(PMA)<k_{voc}(BMA). Further, the isoalkyl methacrylates react a little faster than their normal analogs. This is consistent with the electron donating inductive effect of the substituents (−C(O)OR), indicative of an electrophilic addition mechanism.(Atkinson 1997). Such variations are consistent with NO_3 reaction proceeding via electrophilic addition to the double bond in the methacrylate group. These rate constants that have been measured for unsaturated esters, are conducive to understand the structure activity relationship (SAR) and complete the parameterization of this family of compounds. Curiously, however, the isopropyl

methacrylate reacts faster than the normal analog while the isobutyl methacrylate reacts with almost the same rate coefficient as the butyl methacrylate. It would be interesting to see if there is enhanced H abstraction in IPMA reaction and leads to HNO_3 as a product.

To further examine this mechanism for the reaction, we studied the reaction of NO_3 with deuterated MMA. In the reactions of MMA and MMA-D8 with NO_3 radicals are essentially identical, with k_H/k_D =0.98, as shown in Figure 3-6. The isotopic purity of the MMA-D8 was sufficiently high (>99%) so that this equality is not due to the deuteration being insufficient. This observation of the equality of the rate coefficients for the deuterated and non-deuterated MMA further strengthens the expectation that H atom abstraction is insignificant in the reaction of NO_3 with methacrylates.

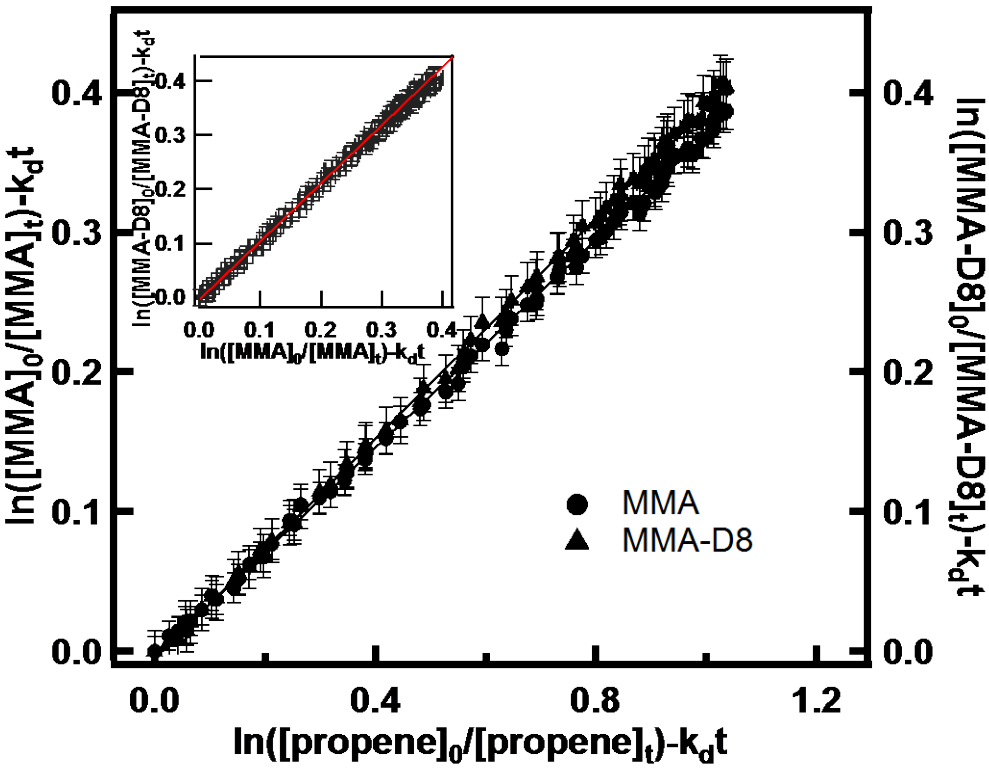

Figure 3-6: The rates of losses of MMA-D8 relative to those for propene while competing for the same pool of NO_3 radicals. The inset shows a similar plot for the loss of MMA relative that for MMA-D8, with a slope of

essentially unity showing the both deuterated and non-deuterated MMA react with NO_3 with the same rate coefficient, i.e., $k_1 \approx k_7$.

Furthermore, in our experiments, we deduced NO_2 was not produced after NO_3 was removed. Figure 3-7 shows the observed NO_3 and N_2O_5 profiles in the presence of MMA. Simulation of these profiles where we include a yield of NO_2 of unity is shown as the dashed line. Clearly, we cannot fit the data to a scheme where NO_2 is produced from the reaction with a large yield. If NO_2 were the product of the reaction, we would expect a production of one NO_2 for each NO_3 lost, unless there is stoichiometric removal of NO_2 by a peroxy radical formed by the NO_3 reaction with the methacrylate ester that reacts very rapidly with NO_2 to form a stable nitrate. Since, we cannot rule out the formation of such a nitrate, we cannot unequivocally rule out the formation of NO_2 as a product of the reaction. Future studies in a chamber that were constrained by an accurate measurements of NO_2 and total NO_y would be useful in constraining the branching ratio toward NO_2 or organic nitrate production, even if the former were small. Similarly, a simulation of the all the subsequent reactions would be useful when the majority of the stable products are identified and quantified.

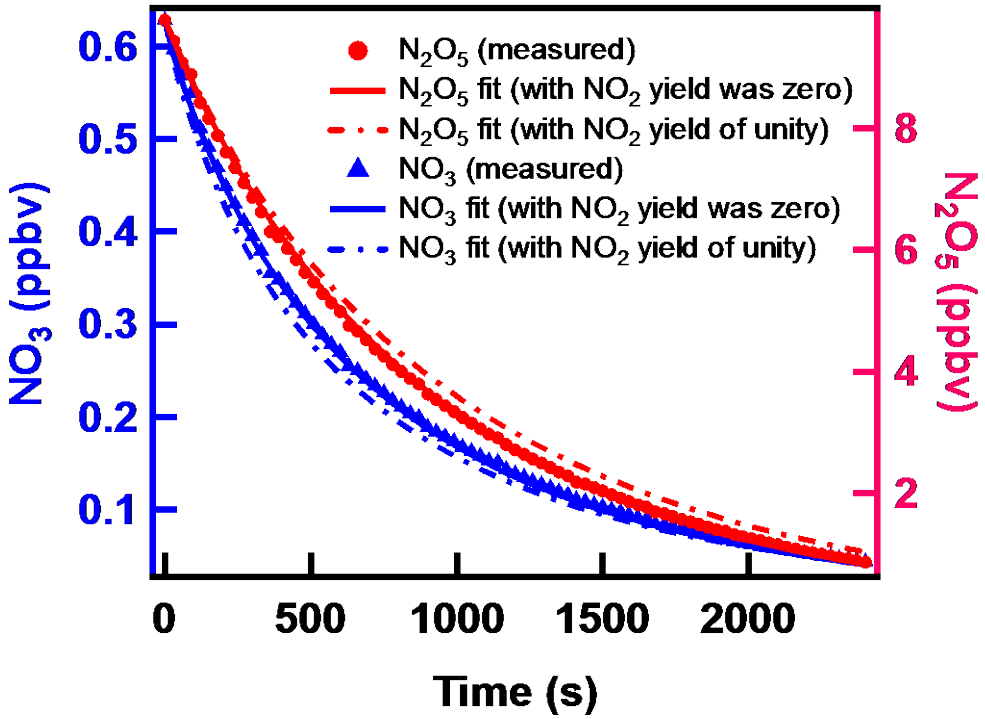

Figure 3-7 Experimental and simulated results for NO_3 and N_2O_5 profiles from chamber experiment (MMA+NO_3) when NO_2 was set as a product of unit yield in the modeled reaction scheme.

Based on these observation we suggest that, the atmospheric oxidation mechanism of NO_3 reactions with unsaturated carbonyl group compounds proceeds mostly via electrophilic addition to the C=C double bond.

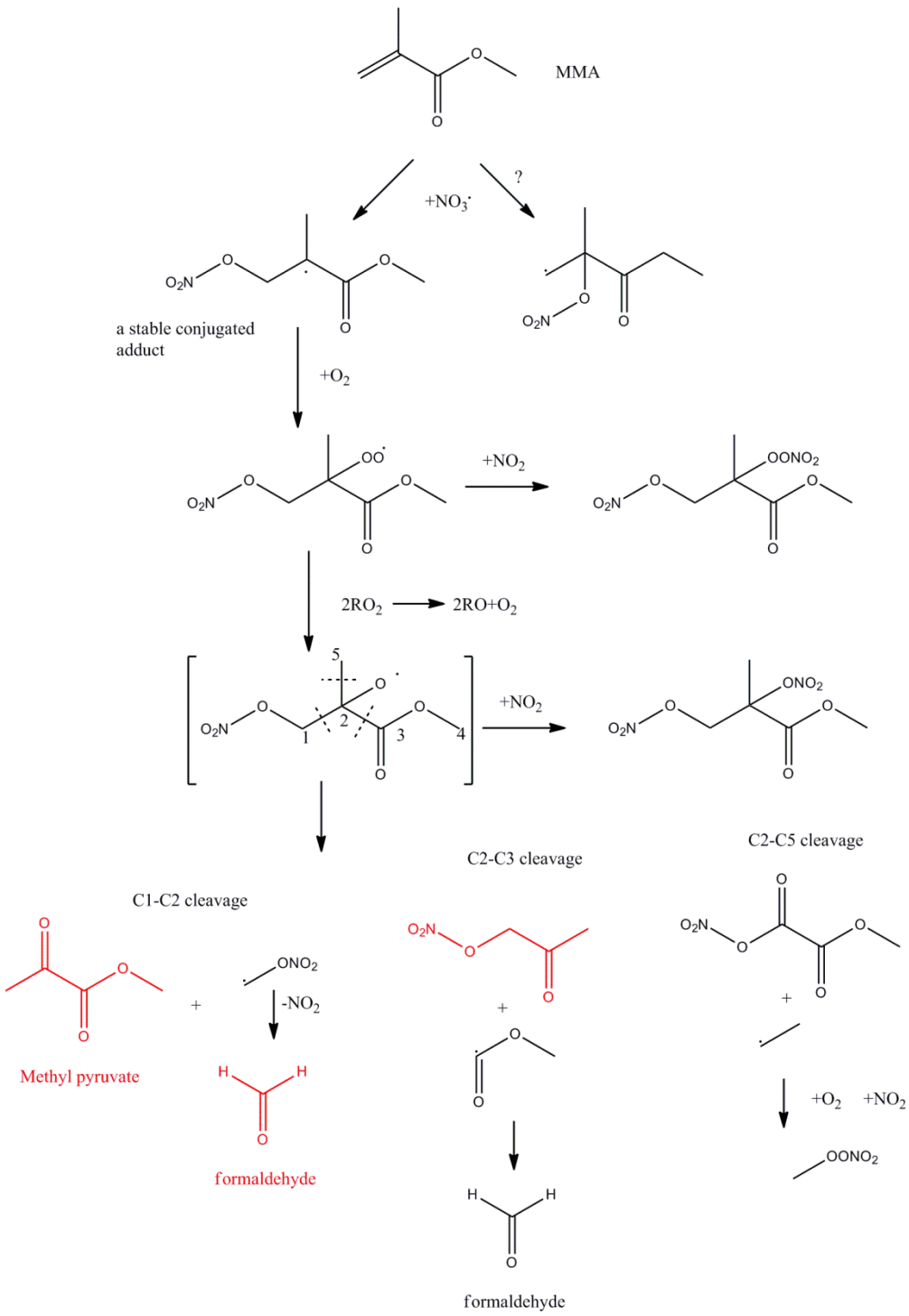

Figure 3-8 Scheme of oxidation of MMA by NO_3 radicals (compounds written in red are the stable products which can be measured by PTR-MS or HCHO analyzer)

5 Atmospheric implication

Once emitted into the atmosphere, the studied methacrylate esters are removed mainly through their reactions with reactive species such as OH, NO_3, O_3 and chlorine atoms. The lifetimes for the removal of the esters were calculated using nominal concentrations of the reactive radicals and ozone in the lower troposphere. Note that these lifetimes are nominal values and are expected to be location and time dependent. The lifetimes were calculated using the equation:

$$\tau = \frac{1}{k_{voc+x}[x]} \qquad \textbf{(IV)}$$

where k_{voc+x} is the rate coefficient for the reaction of the oxidant with the methacrylate ester and [x] is the nominal representative atmospheric concentration of the oxidants. Tropospheric concentrations of OH, NO_3, O_3 and chlorine atoms that could be expected were used in the calculations to approximate the loss of esters in the troposphere. Here we have used the concentration to be: [Cl]=1×10^4 molecule cm^{-3}(Wingenter et al. 1996) , [OH] = 1×10^6 molecule cm^{-3} (Spivakovsky et al. 2000), [NO_3] = 5×10^8 molecule cm^{-3} (Atkinson 1991), [O_3] = 1×10^{12} molecule cm^{-3} (~40 ppbv). Note that NO_3 concentration in locations where esters are emitted (such as urban plumes) can be much larger(Brown and Stutz 2012). However, the lifetimes would still be many days such that the esters would be dispersed. Therefore, the calculated atmospheric lifetimes of the methacrylate esters summarized in Table 3-6 would be reasonably representative of the removal processes for these esters.

The atmospheric lifetimes for methacrylate esters due to reaction with OH radicals are roughly a few hours, followed by that due to loss via reaction with ozone of ~40 hours. Clearly, the reaction of NO_3 would contribute only about 5% to the overall lifetime. However, in dark areas with large NOx emissions, the loss via reaction with NO_3 could be significant compared to that via reaction with OH. However, the abundances of NO_3 are closely related to those of O_3 since it is formed by the reaction of NO_2 with O_3. Therefore, clearly, both the reaction of O_3 and NO_3

will contribute significantly at night when the NOx emissions are high.

Table 3-6. Summary of rate constants and estimated atmospheric lifetimes of methacrylate esters with respect to their reactions with OH, NO_3, O_3 and Cl at (298±2)K and atmospheric pressure.

	Rate constants (cm^3 $molecule^{-1}s^{-1}$)				Lifetime (hours)			
	k_{OH}	k_{NO3}	k_{O3}	k_{Cl}	τ_{OH}	τ_{NO3}	τ_{O3}[i]	τ_{Cl}
MMA	$(4.2)\times10^{-11}$ [b,c,d]	$(2.98)\times10^{-15}$ [a]	$(7.51)\times10^{-18}$ [d]	$(2.17)\times10^{-10}$ [f]	6.6	186	37	128
EMA	$(4.58)\times10^{-11}$ [c]	$(4.67)\times10^{-15}$ [a]	$(7.68)\times10^{-18}$ [e]	$(2.71)\times10^{-10}$ [f]	6.1	119	36	103
PMA		$(5.23)\times10^{-15}$ [a]				106	~40	
IPMA		$(7.91)\times10^{-15}$ [a]				70	~40	
BMA	$(7.08)\times10^{-11}$ [c]	$(5.71)\times10^{-15}$ [a]		$(3.72)\times10^{-10}$ [f,g]	3.3	97	~40	75
IBMA		$(6.24)\times10^{-15}$ [a]				89	~40	

Assuming [OH] = 1×10^{6} molecule cm^{-3} (Spivakovsky et al. 2000), [NO_3] =5×10^{8} molecule cm^{-3} (Atkinson 1991) , [O_3] = 1×10^{12} molecule cm^{-3} (40 ppb), and [Cl] =1×10^{4}molecule cm^{-3} (Wingenter et al. 1996).

a This work. b,c,d are from references (Teruel et al. 2006), (Blanco et al.2006), and (Grosjean et al. 1993): Value reported by ref. d is roughly a factor of 2 lower than that reported by ref. b and c. We used the average value from ref. b and c.

e from reference (Blanco et al.2009), f from reference(Martín Porrero et al. 2010), and g from reference(Canosa-Mas et al.1999).

i. When the rate coefficients for the reactions of esters with ozone were not available, we have assumed it to be roughly the same as that for MMA

Supporting information

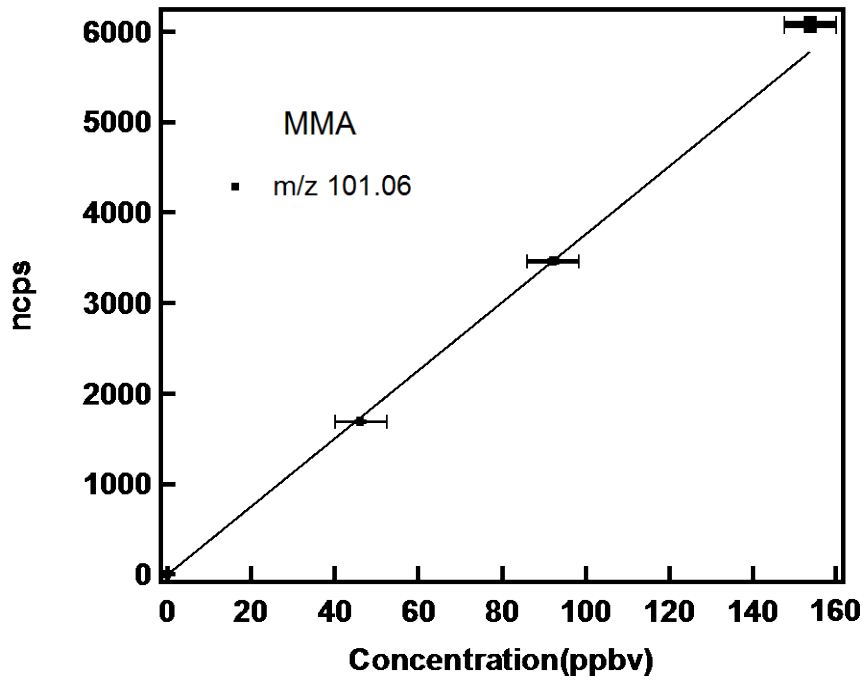

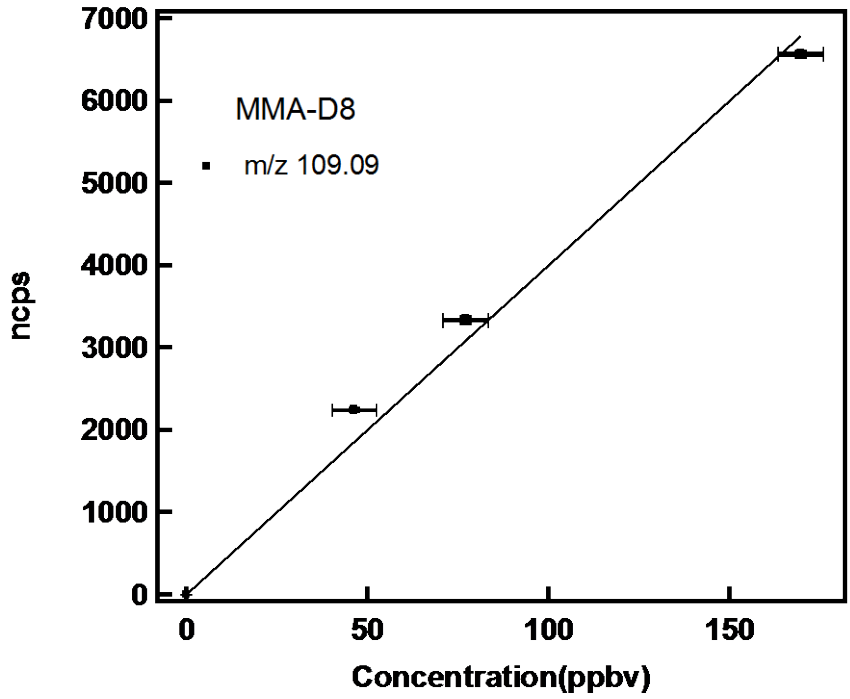

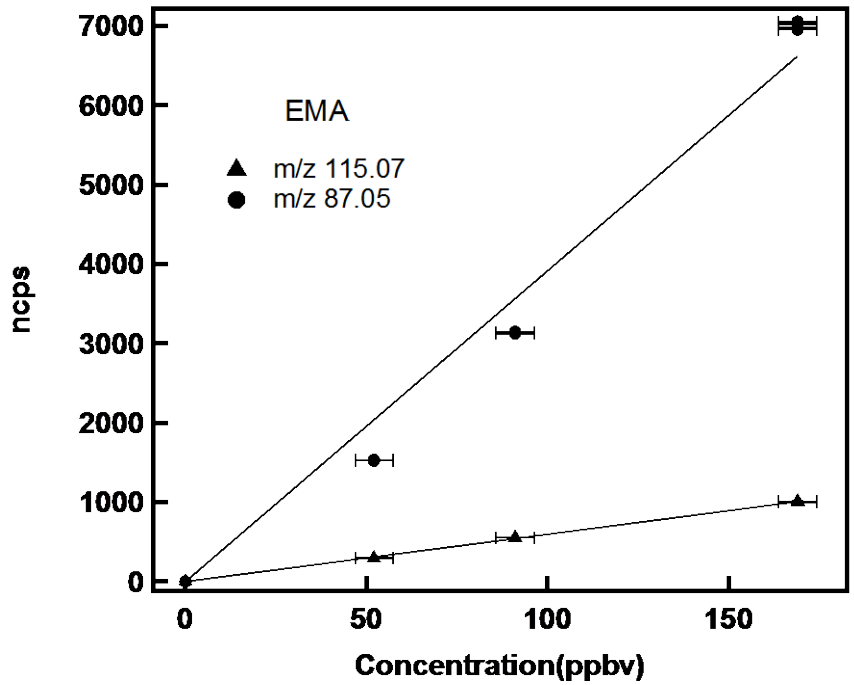
EMA
m/z 115.07
m/z 87.05
ncps
Concentration(ppbv)
0
1000
2000
3000
4000
5000
6000
7000
0
50
100
150

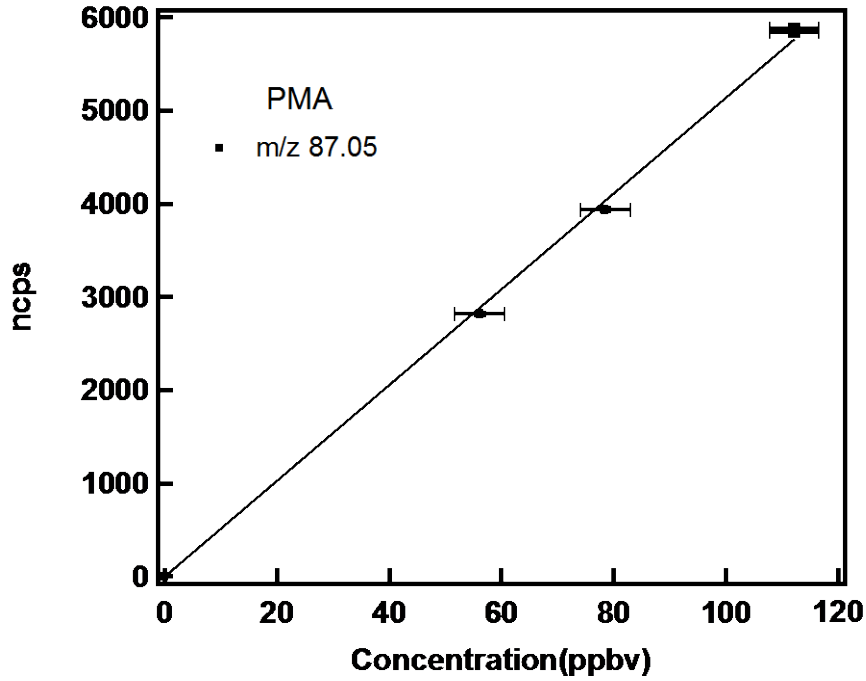
PMA
m/z 87.05
ncps
Concentration(ppbv)
0
1000
2000
3000
4000
5000
6000
0
20
40
60
80
100
120

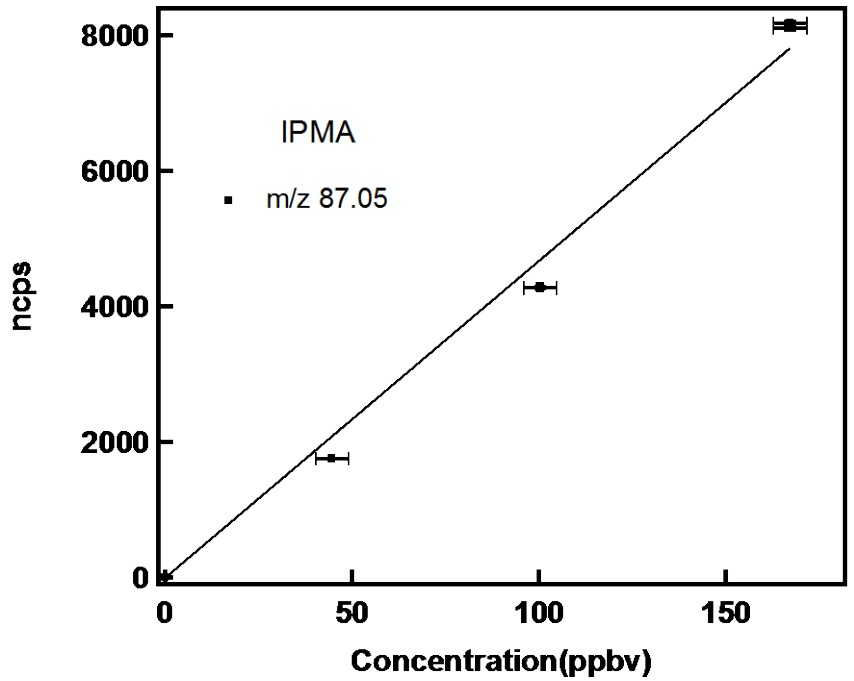
IPMA
m/z 87.05
ncps
8000
6000
4000
2000
0
0
50
100
150
Concentration(ppbv)

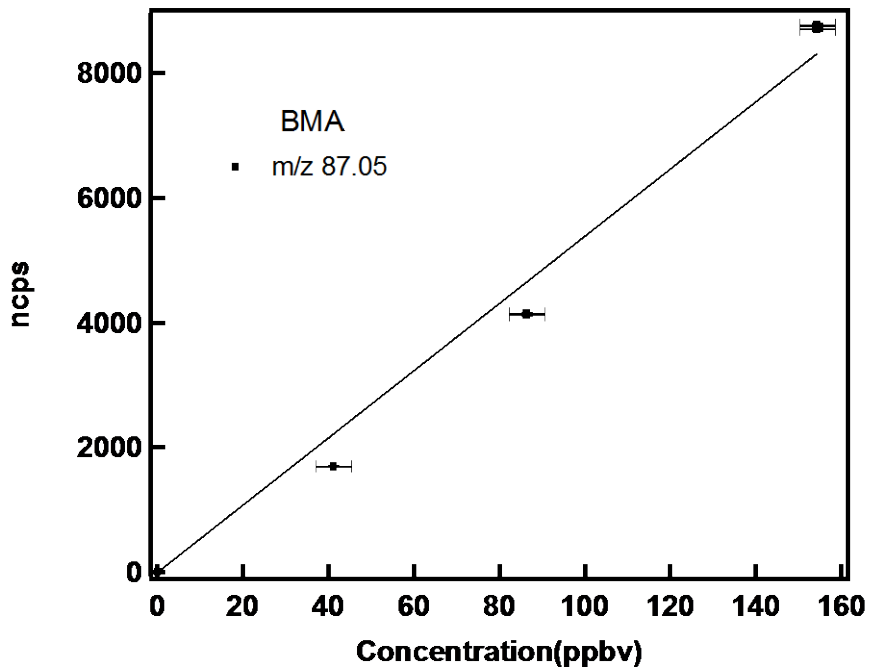
BMA
m/z 87.05
ncps
8000
6000
4000
2000
0
0
20
40
60
80
100
120
140
160
Concentration(ppbv)

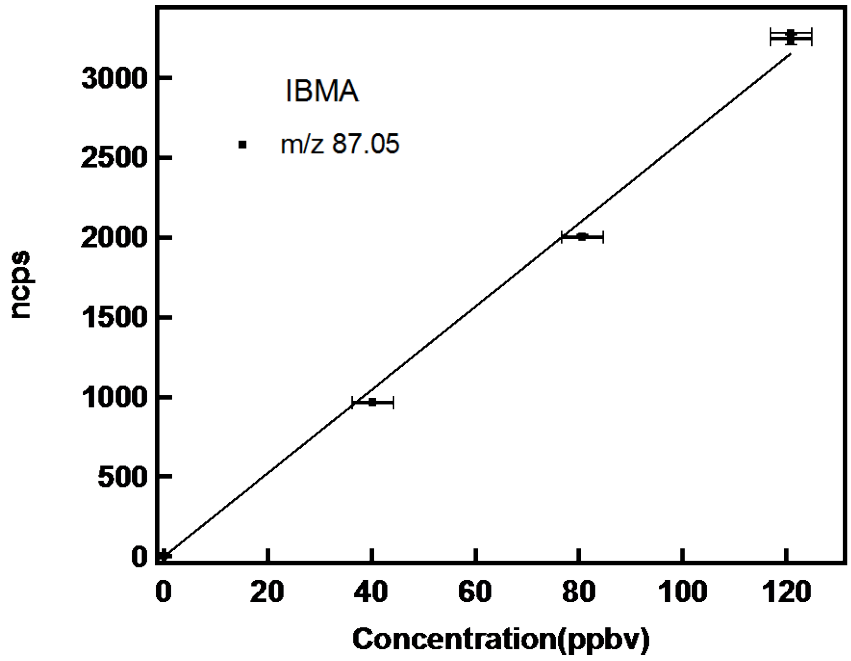
IBMA
m/z 87.05
ncps
3000
2500
2000
1500
1000
500
0
0
20
40
60
80
100
120
Concentration(ppbv)

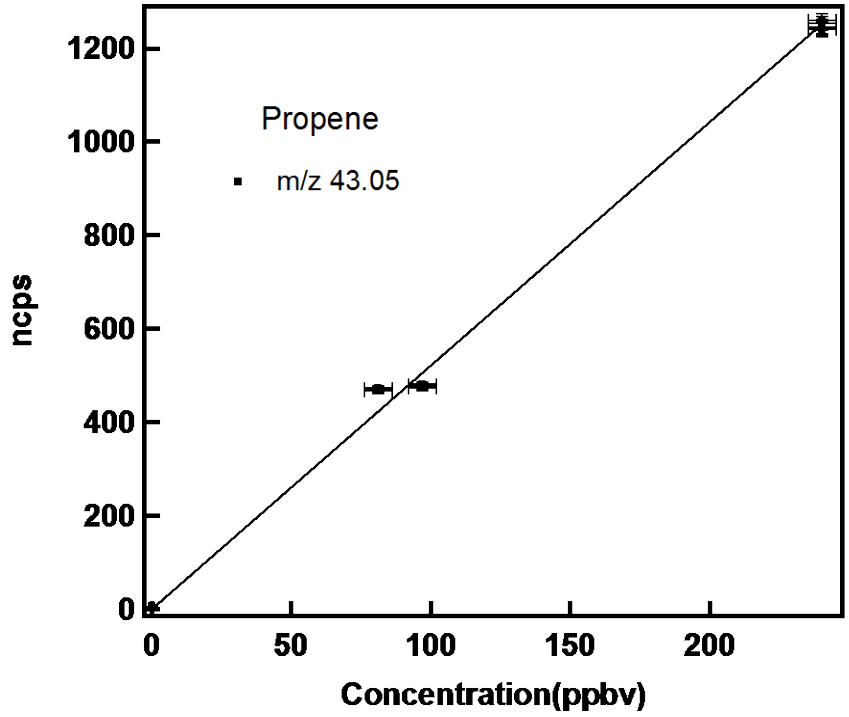
Propene
m/z 43.05
ncps
1200
1000
800
600
400
200
0
0
50
100
150
200
Concentration(ppbv)

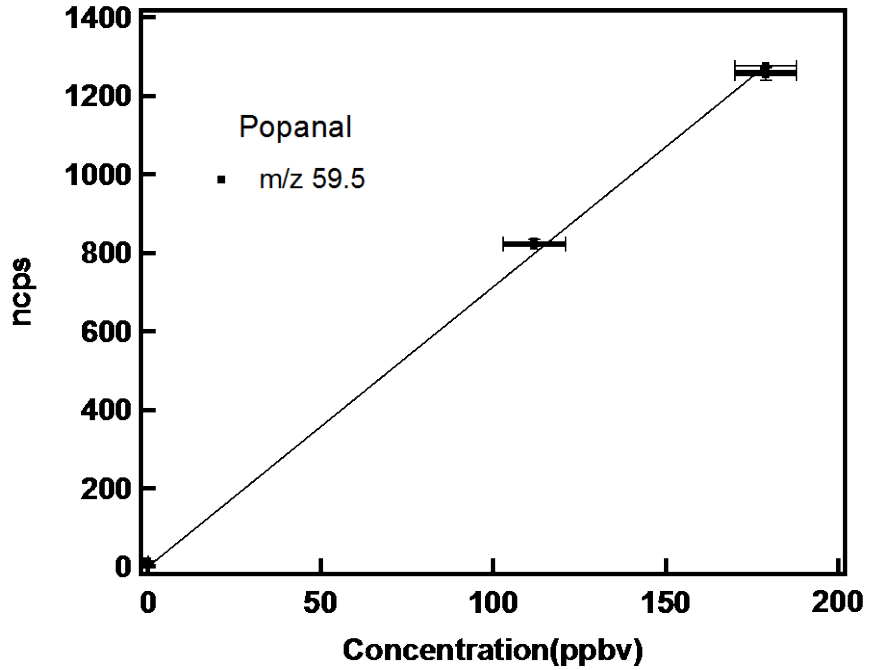

Figure 3S-1 Calibrations of each reactant and reference done with PTR-ToF-MS. Each point shown is an average of roughly 30 points. Therefore, there are close to 180 individual measurements per calibration plot.

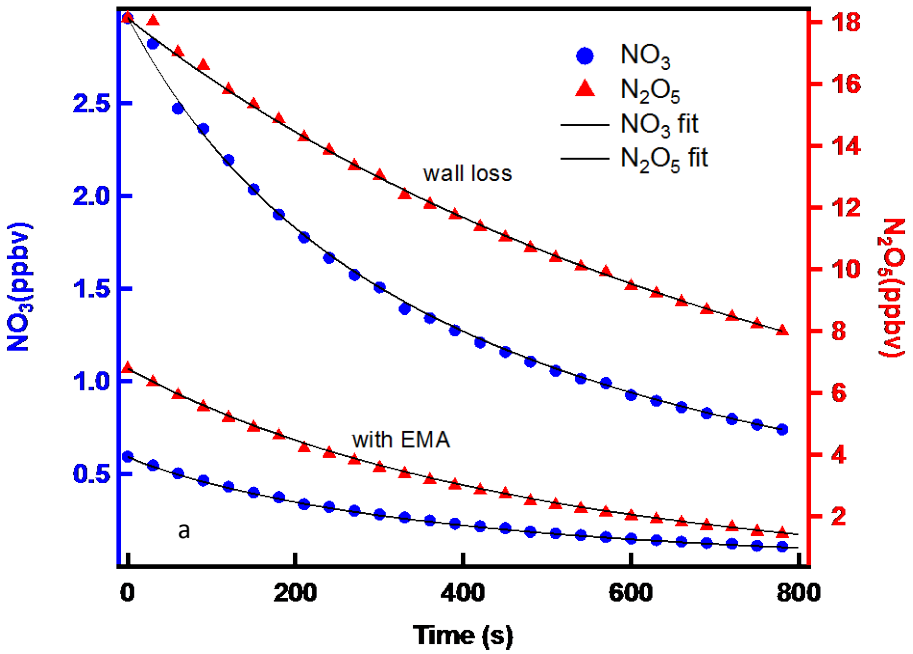
NO3
N2O5
NO3 fit
N2O5 fit
wall loss
with EMA
a
NO3(ppbv)
N2O5(ppbv)
Time (s)
0
200
400
600
800
0.5
1.0
1.5
2.0
2.5
2
4
6
8
10
12
14
16
18

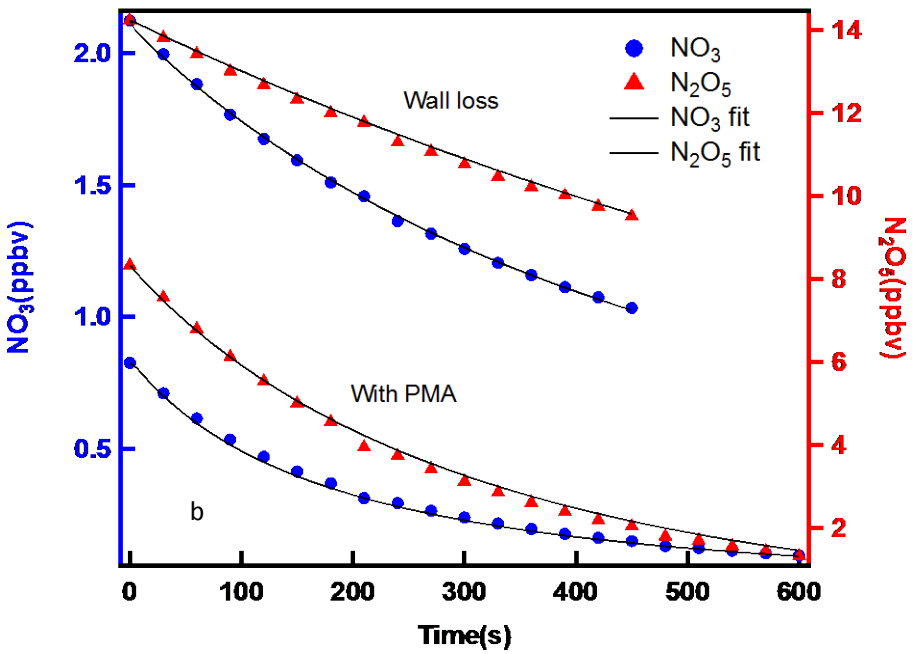
NO3
N2O5
NO3 fit
N2O5 fit
Wall loss
With PMA
b
NO3(ppbv)
N2O5(ppbv)
Time(s)
0
100
200
300
400
500
600
0.5
1.0
1.5
2.0
2
4
6
8
10
12
14

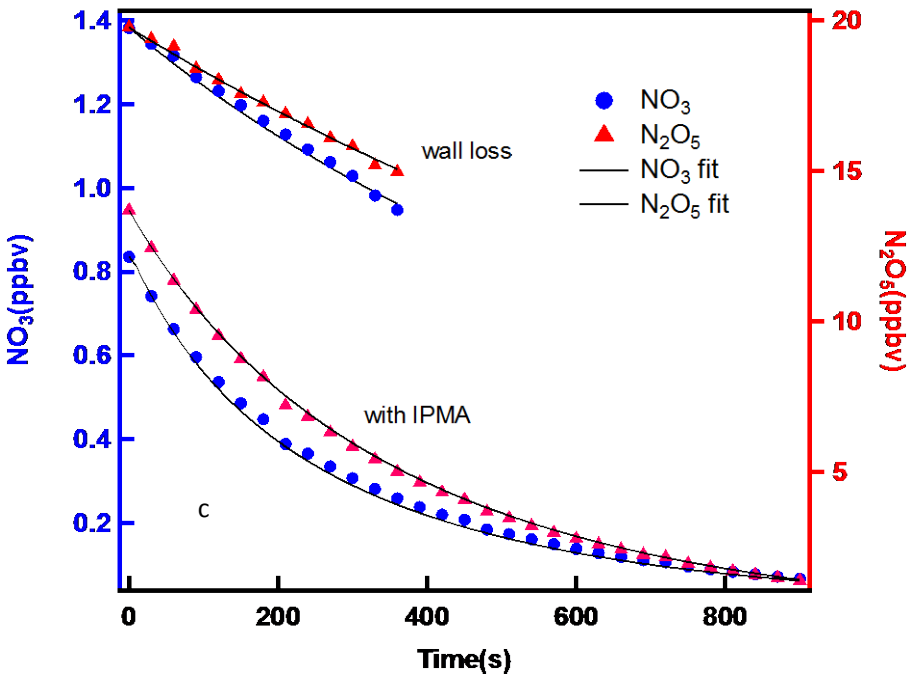
NO3
N2O5
NO3 fit
N2O5 fit
wall loss
with IPMA
c
NO3(ppbv)
N2O5(ppbv)
Time(s)

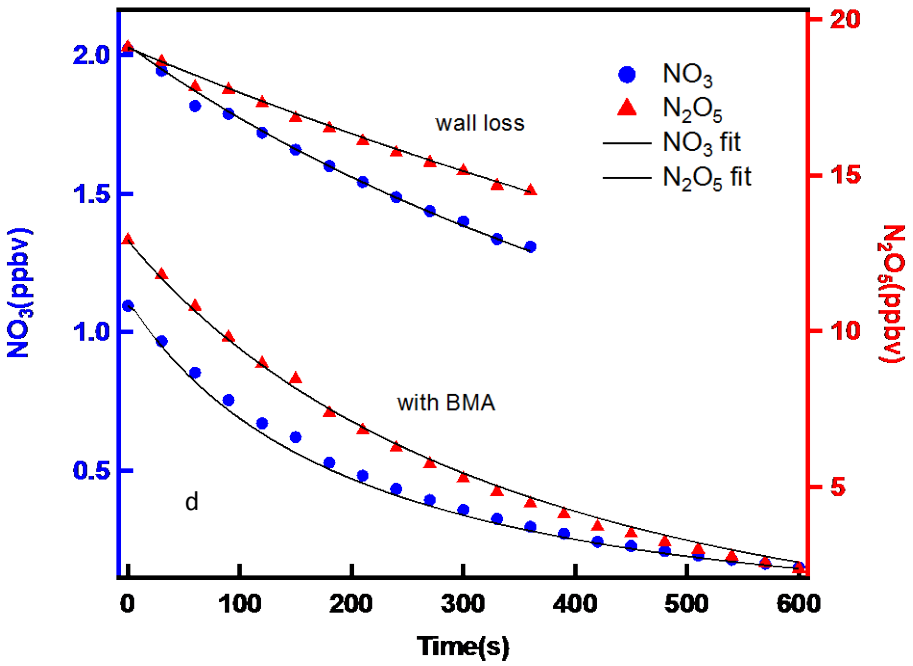
NO3
N2O5
NO3 fit
N2O5 fit
wall loss
with BMA
d
NO3(ppbv)
N2O5(ppbv)
Time(s)

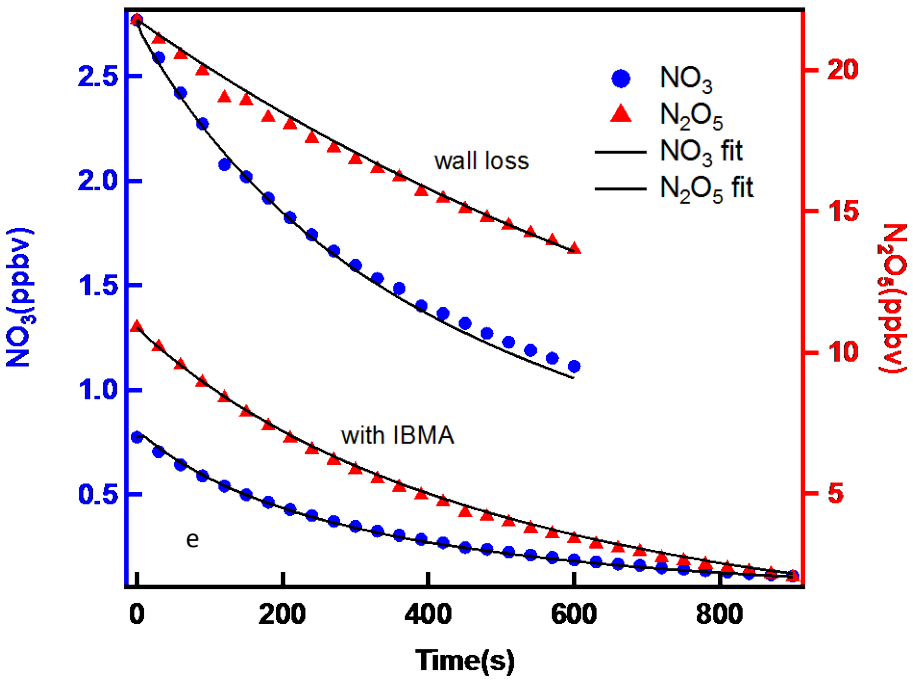

Figure 3S-2 (a-e) show other fits of the observed temporal profiles of NO_3 and N_2O_5 and the fit of the profiles to the above reaction scheme (a. EMA+NO_3/N_2O_5, b. PMA+NO_3/N_2O_5, c. IPMA+NO_3/N_2O_5, d. BMA+NO_3/N_2O_5, e. IBMA+NO_3/N_2O_5).

Table 3S-1 A complete summaries of the initial concentrations and experimental conditions for the relative rate method experiments

Subject	Reference compound	Initial mixing ratio VOC (ppbv)	Initial mixing ratio Reference (ppbv)
Methyl methacrylate (MMA)	propene	307.1	324.0
	propene	153.5	324.0
	propene	76.8	324.0
	propene	61.4	243.0
	propene	46.1	97.0
	propene	46.1	81.0
	propanal	76.8	112.0
	propanal	76.8	179.1
Ethyl methacrylate (EMA)	propene	104.0	357.0
	propene	104.0	324.0
	propene	52.0	324.0
	MMA	52.0	76.8
	MMA	52.0	61.4
Propyl methacrylate (PMA)	propene	44.9	357.0
	propene	44.9	341.0
	propene	67.3	324.0
	MMA	67.3	61.4
	MMA	44.9	61.4

	MMA	44.9	61.4
Isopropyl methacrylate (IPMA)	propene	66.9	341.0
	propene	66.9	341.0
	propene	55.7	341.0
	MMA	66.9	61.4
	MMA	44.6	76.8
	MMA	44.6	61.4
Butyl methacrylate (BMA)	propene	70.5	357.0
	propene	102.9	487.0
	propene	61.7	341.0
	MMA	102.9	123.0
	MMA	60.4	61.4
	MMA	102.9	123.0
Isobutyl methacrylate (IBMA)	propene	60.4	341.0
	propene	100.7	487.0
	propene	70.5	357.0
	MMA	60.4	61.4
	MMA	100.70	122.80
	MMA	40.30	61.40

Table 3S-2 A complete summary of the initial concentrations and experimental conditions for the absolute rate method experiments

		Without VOC					With VOC			
Experiment	T(℃)	Initial mixing ratio(ppbv)			k_{NO3} (Wallloss s^{-1})	k_{N2O5} (Wallloss s^{-1})	Initial mixing ratio(ppbv)			
		(NO_3)	(N_2O_5)	$(NO_2)_{eq}$			(VOC)	(NO_3)	(N_2O_5)	$(NO_2)_{fit}$
Propene	23	2.70	25.07	8.29	0.0065	0.00038				
	23	1.73	22.37	12.75	0.015	0.0003	70.00	0.45	9.77	20.50
MMA	22	2.53	22.16	6.74	0.0065	0.00032	121.95	0.68	11.05	11.79
	23	1.62	17.87	9.84	0.0054	0.00034	124.30	0.63	9.79	13.41
	25	3.86	26.08	7.54	0.0055	0.0003	363.70	0.78	11.46	13.40
EMA	25	2.24	20.22	10.35	0.0062	0.0003	126.10	0.81	10.85	14.23
	27	2.96	18.15	8.94	0.008	0.00032	130.10	0.59	6.79	16.30
	25	3.03	28.78	10.62	0.0065	0.00042	333.30	1.13	16.58	15.85
PMA	24	2.82	22.93	8.02	0.0065	0.00041	113.47	0.79	11.15	13.41
	27	3.13	19.00	8.64	0.0062	0.00063	279.67	1.11	10.13	11.79
	23	2.13	14.22	5.84	0.0051	0.00043	113.58	0.83	8.33	8.54

IPMA	24	2.77	20.56	7.34	0.0065	0.00035	101.60	0.81	10.28	11.38
	23	3.27	25.00	6.68	0.006	0.00035	86.17	0.91	13.01	11.79
	27	1.38	19.77	20.35	0.006	0.0004	209.34	0.84	13.69	21.54
BMA	26	3.09	16.85	6.89	0.006	0.0005	264.20	1.00	8.80	10.16
	26	2.86	17.84	7.87	0.006	0.0004	199.19	1.25	11.42	10.57
	27	2.02	19.10	11.92	0.0052	0.00039	251.80	1.10	12.92	14.63
IBMA	23	2.77	21.77	6.87	0.006	0.00035	142.30	0.77	10.90	11.79
	24	3.34	22.50	6.65	0.006	0.0004	154.50	1.09	13.00	10.57
	24	2.41	15.15	6.21	0.006	0.00039	162.60	0.99	9.44	8.33

References

Atkinson, R. (1991) Kinetics and mechanisms of the gas-phase reactions of the no3 radical with organic-compounds. *Journal of Physical and Chemical Reference Data,* 20**,** 459-507.

Atkinson, R. (1997) Gas-phase tropospheric chemistry of volatile organic compounds .1. Alkanes and alkenes. *Journal of Physical and Chemical Reference Data,* 26**,** 215-290.

Atkinson, R., D. L. Baulch, R. A. Cox, J. N. Crowley, R. F. Hampson, R. G. Hynes, M. E. Jenkin, M. J. Rossi, J. Troe & I. Subcommittee (2006) Evaluated kinetic and photochemical data for atmospheric chemistry: Volume II – gas phase reactions of organic species. *Atmospheric Chemistry and Physics,* 6**,** 3625-4055.

Bernard, F., G. Eyglunent, V. Daele & A. Mellouki (2010) Kinetics and Products of Gas-Phase Reactions of Ozone with Methyl Methacrylate, Methyl Acrylate, and Ethyl Acrylate. *Journal of Physical Chemistry A,* 114**,** 8376-8383.

Blanco, M. B., I. Bejan, I. Barnes, P. Wiesen & M. A. Teruel (2009a) The Cl-initiated oxidation of $CH_3C(O)OCH{=}CH_2$, $CH_3C(O)OCH_2CH{=}CH_2$, and $CH_2{=}CHC(O)O(CH_2)(3)CH_3$ in the troposphere. *Environmental Science and Pollution Research,* 16**,** 641-648.

Blanco, M. B., I. Bejan, I. Barnes, P. Wiesen & M. A. Teruel (2009b) Temperature-dependent rate coefficients for the reactions of Cl atoms with methyl methacrylate, methyl acrylate and butyl methacrylate at atmospheric pressure. *Atmospheric Environment,* 43**,** 5996-6002.

Blanco, M. B., R. A. Taccone, S. I. Lane & M. A. Teruel (2006) On the OH-initiated degradation of methacrylates in the troposphere: Gas-phase kinetics and formation of pyruvates. *Chemical Physics Letters,* 429**,** 389-394.

Brown, S. S. (2003) Absorption spectroscopy in high-finesse cavities for atmospheric studies. *Chemical Reviews,* 103**,** 5219-5238.

Brown, S. S., H. Stark, S. J. Ciciora, R. J. McLaughlin & A. R. Ravishankara (2002a) Simultaneous in situ detection of atmospheric NO_3 and N_2O_5 via cavity ring-down spectroscopy. *Review of Scientific Instruments,* 73**,** 3291-3301.

Brown, S. S., H. Stark & A. R. Ravishankara (2002b) Cavity ring-down spectroscopy for atmospheric trace gas detection: application to the nitrate radical (NO_3). *Applied Physics B-Lasers and Optics,* 75**,** 173-182.

Brown, S. S. & J. Stutz (2012) Nighttime radical observations and chemistry. *Chemical Society Reviews,* 41**,** 6405-6447.

Burkholder, J. B., S. P. S., J. P. D. Abbatt,J. R. Barker,R. E. Huie,C. E. Kolb,M. J. Kurylo,V. L. Orkin,D. M. Wilmouth,P. H. Wine (2015) Chemical Kinetics and Photochemical Data for Use in Atmospheric Studies.

Canosa-Mas, C. E., S. Carr, M. D. King, D. E. Shallcross, K. C. Thompson & R. P. Wayne (1999) A kinetic study of the reactions of NO_3 with methyl vinyl ketone, methacrolein, acrolein, methyl acrylate and methyl methacrylate. *Physical Chemistry Chemical Physics,* 1**,** 4195-4202.

Canosa-Mas, C. E., M. L. Flugge, M. D. King & R. P. Wayne (2005) An experimental study of the gas-phase reaction of the NO3 radical with alpha,beta-unsaturated carbonyl compounds. *Physical Chemistry Chemical Physics,* 7**,** 643-650.

Chen, H., Y. Ren, M. Cazaunau, V. Dalele, Y. Hu, J. Chen & A. Mellouki (2015) Rate coefficients for the reaction of ozone with 2-and 3-carene. *Chemical Physics Letters,* 621**,** 71-77.

Davidson, J. A., A. A. Viggiano, C. J. Howard, I. Dotan, F. C. Fehsenfeld, D. L. Albritton & E. E. Ferguson (1978) Rate constants for reactions of O_2+, NO_2+, NO+, H_3O+, CO_3-, NO_2-, and halide ions with N_2O_5 at 300 K. *Journal of Chemical Physics,* 68**,** 2085-2087.

Dorn, H. P., R. L. Apodaca, S. M. Ball, T. Brauers, S. S. Brown, J. N. Crowley, W. P. Dube, H. Fuchs, R. Haeseler, U. Heitmann, R. L. Jones, A. Kiendler-Scharr, I. Labazan, J. M. Langridge, J. Meinen, T. F. Mentel, U. Platt, D. Poehler, F.

Rohrer, A. A. Ruth, E. Schlosser, G. Schuster, A. J. L. Shillings, W. R. Simpson, J. Thieser, R. Tillmann, R. Varma, D. S. Venables & A. Wahner (2013) Intercomparison of NO_3 radical detection instruments in the atmosphere simulation chamber SAPHIR. *Atmospheric Measurement Techniques,* 6**,** 1111-1140.

Dube, W. P., S. S. Brown, H. D. Osthoff, M. R. Nunley, S. J. Ciciora, M. W. Paris, R. J. McLaughlin & A. R. Ravishankara (2006) Aircraft instrument for simultaneous, in situ measurement of NO_3 and N_2O_5 via pulsed cavity ring-down spectroscopy. *Review of Scientific Instruments,* 77.

Fuchs, H., W. P. Dube, S. J. Cicioira & S. S. Brown (2008) Determination of inlet transmission and conversion efficiencies for in situ measurements of the nocturnal nitrogen oxides, NO_3, N_2O_5 and NO_2, via pulsed cavity ring-down spectroscopy. *Analytical Chemistry,* 80**,** 6010-6017.

Fuchs, H., W. R. Simpson, R. L. Apodaca, T. Brauers, R. C. Cohen, J. N. Crowley, H. P. Dorn, W. P. Dubé, J. L. Fry, R. Häseler, Y. Kajii, A. Kiendler-Scharr, I. Labazan, J. Matsumoto, T. F. Mentel, Y. Nakashima, F. Rohrer, A. W. Rollins, G. Schuster, R. Tillmann, A. Wahner, P. J. Wooldridge & S. S. Brown (2012) Comparison of N_2O_5 mixing ratios during NO3Comp 2007 in SAPHIR. *Atmospheric Measurement Techniques,* 5**,** 2763-2777.

Gai, Y., M. Ge & W. Wang (2009) Rate constants for the gas phase reaction of ozone with n-butyl acrylate and ethyl methacrylate. *Chemical Physics Letters,* 473**,** 57-60.

Grosjean, D., E. Grosjean & E. L. Williams (1993) Rate constants for the gas-phase reactions of ozone with unsaturated alcohols, esters, and carbonyls. *International Journal of Chemical Kinetics,* 25**,** 783-794.

Jordan, A., S. Haidacher, G. Hanel, E. Hartungen, L. Maerk, H. Seehauser, R. Schottkowsky, P. Sulzer & T. D. Maerk (2009) A high resolution and high sensitivity proton-transfer-reaction time-of-flight mass spectrometer (PTR-TOF-MS). *International Journal of Mass Spectrometry,* 286**,** 122-128.

Lauraguais, A., A. El Zein, C. Coeur, E. Obeid, A. Cassez, M. T. Rayez & J. C. Rayez (2016) Kinetic Study of the Gas-Phase Reactions of Nitrate Radicals with Methoxyphenol Compounds: Experimental and Theoretical Approaches. *Journal of Physical Chemistry A,* 120**,** 2691-2699.

Martín Porrero, M. P., M. P. Gallego-Iniesta García, J. L. Espinosa Ruiz, A. Tapia Valle, B. Cabañas Galán & M. S. Salgado Muñoz (2010) Gas phase reactions of unsaturated esters with Cl atoms. *Environmental Science and Pollution Research,* 17**,** 539-546.

Mellouki, A., G. Le Bras & H. Sidebottom (2003) Kinetics and mechanisms of the oxidation of oxygenated organic compounds in the gas phase. *Chemical Reviews,* 103**,** 5077-5096.

Mueller, M., T. Mikoviny, W. Jud, B. D'Anna & A. Wisthaler (2013) A new software tool for the analysis of high resolution PTR-TOF mass spectra. *Chemometrics and Intelligent Laboratory Systems,* 127**,** 158-165.

Sagrario Salgado, M., M. Paz Gallego-Iniesta, M. Pilar Martin, A. Tapia & B. Cabanas (2011) Night-time atmospheric chemistry of methacrylates. *Environmental Science and Pollution Research,* 18**,** 940-948.

Spivakovsky, C. M., J. A. Logan, S. A. Montzka, Y. J. Balkanski, M. Foreman-Fowler, D. B. A. Jones, L. W. Horowitz, A. C. Fusco, C. A. M. Brenninkmeijer, M. J. Prather, S. C. Wofsy & M. B. McElroy (2000) Three-dimensional climatological distribution of tropospheric OH: Update and evaluation. *Journal of Geophysical Research-Atmospheres,* 105**,** 8931-8980.

Teruel, M. A., S. I. Lane, A. Mellouki, G. Solignac & G. Le Bras (2006) OH reaction rate constants and UV absorption cross-sections of unsaturated esters. *Atmospheric Environment,* 40**,** 3764-3772.

Wagner, N. L., W. P. Dube, R. A. Washenfelder, C. J. Young, I. B. Pollack, T. B. Ryerson & S. S. Brown (2011) Diode laser-based cavity ring-down instrument for NO_3, N_2O_5, NO, NO_2 and O_3 from aircraft. *Atmospheric*

Measurement Techniques, 4**,** 1227-1240.

Wang, K., M. Ge & W. Wang (2010) Kinetics of the gas-phase reactions of NO_3 radicals with ethyl acrylate, n-butyl acrylate, methyl methacrylate and ethyl methacrylate. *Atmospheric Environment,* 44**,** 1847-1850.

Wingenter, O. W., M. K. Kubo, N. J. Blake, T. W. Smith, D. R. Blake & F. S. Rowland (1996) Hydrocarbon and halocarbon measurements as photochemical and dynamical indicators of atmospheric hydroxyl, atomic chlorine, and vertical mixing obtained during Lagrangian flights. *Journal of Geophysical Research-Atmospheres,* 101**,** 4331-4340.

Chapitre IV Cinétique des réactions des radicaux NO_3 avec des alcanes

Une méthode absolue a été utilisée pour déterminer les constantes de vitesse de réaction des radicaux NO_3 avec une série d'alcanes : le méthane (CH_4), l'éthane (C_2H_6), le propane (C_3H_8), le n-butane (C_4H_10), l'iso-butane (C_4H_{10}), le 2,3-diméthylbutane (C_6H_{14}), le cyclopentane (C_5H_{10}) et le cyclohexane (C_6H_{12}). Les études ont été réalisées dans une chambre de 7300 L en Téflon à 298 ± 1,5 K et 1000 ± 5 hPa.

Pour le méthane (CH_4) et l'éthane (C_2H_6), des limites supérieures des constantes de vitesse ont été obtenues à 298K : 4×10^{-20} et 8×10^{-19} (cm^3 molécule^{-1} s^{-1}). Pour le propane (C_3H_8), le n-butane (C_4H_{10}), l'iso-butane (C_4H_{10}), le 2,3-diméthybutane (C_6H_{14}), le cyclopentane (C_5H_{10}) et cyclohexane (C_6H_{12}), les constantes de vitesse déterminées à 298 K, exprimées en cm^3 molécule^{-1} s^{-1}, sont : $(9.67 \pm 5.80) \times 10^{-18}$, $(1.57 \pm 0.94) \times 10^{-17}$, $(8.23 \pm 4.94) \times 10^{-17}$, $(6.33 \pm 3.80) \times 10^{-16}$, $(1.27 \pm 0.76) \times 10^{-16}$, $(1.24 \pm 0.74) \times 10^{-16}$, respectivement. L'estimation des erreurs dans la détermination de ces constantes est largement discutée dans un paragraphe dédié.

Ces résultats sont ensuite comparés à ceux trouvés dans la littérature et discutés. Puis, puisqu'il s'agit d'une série d'alcanes, la relation entre la structure et la réactivité de ces derniers est étudiée. Enfin, l'impact atmosphérique de ces études conclue ce chapitre.

Chapter IV Kinetics of the Reactions of NO_3 Radical with alkanes[2]

Abstract

Since many urban areas contain relatively high concentrations of a wide variety of alkanes and the huge difference in NO_3 reactivity towards alkanes in field measurements, the reaction rate coefficients of different kinds of alkanes with NO_3 radicals deserve more attention. Therefore, an absolute method was used to determine the rate coefficients for the reactions of NO_3 radicals with methane (CH_4), ethane (C_2H_6), propane (C_3H_8), n-butane (C_4H_{10}), iso-butane (C_4H_{10}), 2,3-dimethybutane (C_6H_{14}), cyclopentane (C_5H_{10}) and cyclohexane (C_6H_{12}) at atmosphere pressure (1000±5 hPa) and room temperature (298±1.5 K). The upper limits of rate coefficients in the units of cm^3 $molecule^{-1}$ s^{-1} at 298 K are 4×10^{-20} and 5×10^{-19} for methane (CH_4) and ethane (C_2H_6). The rate coefficients in the units of cm^3 $molecule^{-1}$ s^{-1} at 298 K for propane (C_3H_8), n-butane (C_4H_{10}), iso-butane (C_4H_{10}), 2,3-dimethybutane (C_6H_{14}), cyclopentane (C_5H_{10}) and cyclohexane (C_6H_{12}) are, $(9.2\pm5.5) \times 10^{-18}$, $(1.5\pm0.9) \times 10^{-17}$, $(8.2\pm4.9) \times 10^{-17}$, $(5.8\pm3.5) \times 10^{-16}$, $(1.4\pm0.8) \times 10^{-16}$, $(1.3\pm0.9) \times 10^{-16}$, respectively. Depending on the relationship between rate coefficients we measured and the enthalpies of each reaction, we suggest the reaction of alkane with NO3 radicals is through H abstraction reaction where the activation energy for the reaction is directly related to the dissociation energy for the bond being broken.

[2] This work is to be submitted to Physical Chemistry Chemical Physics: Zhou, L., A. R. Ravishankara, S. S. Brown, M. Idir, V. Daële & A. Mellouki: Kinetics of the Reactions of NO_3 Radical with alkanes.

1 Introduction

Alkanes are ubiquitous in the Earth's atmosphere and arise from both natural and anthropogenic sources. They play major roles in the atmosphere are fuels for tropospheric ozone and aerosol formation, and as source of stratospheric water vapor when transported to that region, and in some cases as greenhouse gases. Indeed, methane is the second most important anthropogenic greenhouse gas. There is often a great deal of attention paid to methane since its rather short atmospheric lifetime makes it a good target for action and some quick relief.

Alkanes are a key set of the hydrocarbons of interest in the atmosphere. Often, they are of anthropogenic origin. Most of these hydrocarbons are removed from the atmosphere via their reactions with the ubiquitous OH radical with minor contributions via their much faster reactions with Cl atoms. (Their reactions with ozone are too slow to be of significance). However, under some special conditions, their loss via reaction with the NO_3 radicals may also be important and the contributions of such reactions need to be assessed; this is especially true for larger hydrocarbons with weaker C-H bonds. For example, (Wild et al. 2016) showed that alkanes contributed roughly 45%-50% of the gas phase NO_3 loss rates in a region rich with alkanes due to oil and gas excavation activities. In contrast, Brown et al. (Brown et al. 2011) estimated that alkanes contributed less than 2% of the NO_3 loss rates in Houston, Texas, and along the U.S. Gulf Coast region, where there are other highly reactive hydrocarbons that can remove NO_3.

The rate coefficients for the reactions of alkane with NO_3 radicals are relative small and they have not been subject to extensive examinations. For example, only large upper limits at room temperature are known for the reactions of NO_3 with methane, ethane, and propane. Furthermore, these measurements have been derived from relative rate measurements methods may not be best suited for very slow reactions (As shown in Table 4-4). The rate coefficients for the reactions of NO_3 with larger alkanes are reported but they are usually limited to a few studies; for example, the rate coefficients for the reactions of NO_3 with iso-butane, 2, 3-dismethy

butane and cyclohexane have been reported (Atkinson et al. 1984, Atkinson, Aschmann and Pitts Jr 1988, Bagley et al. 1990, Boyd et al. 1991). Therefore, it is clear that further investigations of the rate coefficients for the reactions of NO_3 with simple alkanes are useful.

We have devised a direct method to measure NO_3 reaction rate coefficients that is well-suited for slow reactions. We have employed this method here to measure the rate coefficients for the following reactions at (298±1.5) K:

$NO_3 + CH_4$ (methane) $\rightarrow CH_3 + HNO_3$; $\Delta_r H^o(298\ K) = +15.12$ kJ mol^{-1} (R4-1)

(Methyl radical)

$NO_3 + C_2H_6$ (ethane) $\rightarrow C_2H_5 + HNO_3$; $\Delta_r H^o(298\ K) = -2.44$ kJ mol^{-1} (R4-2)

(Ethyl radical)

$NO_3 + C_3H_8$ (propane) $\rightarrow$ n-$C_3H_7 + HNO_3$; $\Delta_r H^o(298\ K) = -0.74$ kJ mol^{-1}

(n-Propyl radical) (R4-3-1)

$NO_3 + C_3H_8$ (propane) $\rightarrow$ iso-$C_3H_7 + HNO_3$; $\Delta_r H^o(298\ K) = -10.74$ kJ mol^{-1}

(Isopropyl radical) (R4-3-2)

NO_3 + n-C_4H_{10} (n-butane) $\rightarrow C_4H_9 + HNO_3$; $\Delta_r H^o(298\ K) = +0.65$ kJ mol^{-1} (R4-4-1)

(1-Butyl radical)

NO_3 + n-C_4H_{10} (n-butane) $\rightarrow C_4H_9 + HNO_3$; $\Delta_r H^o(298\ K) = -10.84$ kJ mol^{-1} (R4-4-2)

(2-Butyl radical)

NO_3 + iso-C_4H_{10} (iso-butane) $\rightarrow C_4H_9 + HNO_3$; $\Delta_r H^o(298\ K) = -1.24$ kJ mol^{-1}

(Isobutyl radical) (R4-5-1)

NO_3 + iso-C_4H_{10} (iso-butane) $\rightarrow C_4H_9 + HNO_3$; $\Delta_r H^o(298\ K) = -23.24$ kJ mol^{-1}

(Tert-butyl radical) (R4-5-2)

$NO_3 + C_6H_{14}$ (2,3-dimethybutane) $\rightarrow C_6H_{13} + HNO_3$; $\Delta_r H^o(298\ K) \approx 12$ kJ mol^{-1}

(2,3-dimethyl -1-Butyl radical) (R4-6-1)

$NO_3 + C_6H_{14}$ (2,3-dimethybutane) $\rightarrow C_6H_{13} + HNO_3$; $\Delta_r H^o(298\ K) = -34.64$ kJ mol^{-1}

(2,3-dimethyl -2-Butyl radical) (R4-6-2)

$NO_3 + C_5H_{10}$ (cyclopentane) $\rightarrow C_5H_9 + HNO_3$; $\Delta_r H^o(298\ K) = -23.98$ kJ mol^{-1} (R4-7)

(Cyclopentyl radical)

$NO_3 + C_6H_{12}$ (cyclohexane) $\rightarrow C_{12}H_{11} + HNO_3$; $\Delta_r H^o(298\ K) = -26.84$ kJ mol^{-1} (R4-8)

(Cyclohexanyl radical)

We have estimated the enthalpies of Reactions R4-6-1 assuming the C-H bond strengths to be similar to those in Reactions 4-5-1. Enthalpy of reaction R4-6-2 was obtained using data from Baldwin, Drewery and Walker (1984)

In these measurements, we monitored the temporal profiles on NO_3 (and N_2O_5 that is in equilibrium with NO_3) using cavity ring down spectroscopy for periods extending to many minutes in an excess the alkanes at a total pressure of 1000±5 hPa in the Orleans chamber to directly determine the rate coefficients.

2 Experimental section

The rate coefficients for reactions R4-1--R4-8 were measured by following the temporal profiles of NO_3 and N_2O_5 in an excess of alkanes in a large chamber. The temporal profiles of NO_3 and N_2O_5 were both measured via cavity ring down spectroscopy; the reasons for measuring the temporal profiles of N_2O_5 along with that of NO_3 is in the previous chapter. The reactions were carried out in a large chamber so that very slow loss of the radical reactant could be measured. The experimental set up and the procedure used has been described in details in previous chapters. However, for ease of understanding this study, we will briefly describe the experimental set up, the analytical instruments used, and the data acquisition procedure in this section. We will first describe the overall experimental system followed by the experimental and analytical methods employed to quantify alkanes, NO_3/N_2O_5, and NO_2.

2.1 Experimental system

The measurements were carried out at room temperature (298.0±1.5K) in the ICARE-7300L Teflon chamber at slightly above the ambient pressure (1000±5hPa). A detailed description of this reactor has been described in previous chapters; hence, we provide here a very cursory description. The chamber was housed in an enclosure with

black curtains to keep the contents in the dark. Before each set of experiment with a given alkane, the chamber was flushed with dry zero air (relative humidity <3%) overnight to make sure the background concentrations of alkanes and nitrogen oxides were below the detection limits of each instruments (see below). The gaseous reactants were flushed into the chamber by using a gas handling system where pressures were measured using calibrated capacitance manometers (0-10, 0-100 and 0-1000 Torr, MKS Baratron). The larger alkanes that were obtained as liquids were evaporated into the chamber through a glass tube containing dry zero air at a known pressure in a known calibrated volume. The contents of the chamber were mixed by two fans inside the chamber. All the analytical instruments sampled essentially the same part of the chamber. The temperature in the chamber was measured using two thermocouples located in different parts of the chamber; the temperature measured by these thermocouples were the same to within 0.5 K and remained constant during the rate coefficient measurements. The pressure in the chamber was measured using capacitance manometers.

A small flow (about 10 L/min) of purified air was added to keep the chamber pressure constant by making up for the loss of gases from it due to continuous withdrawal for analysis. This resulted in a slow dilution of the chamber contents. We measured the dilution rate and mixing time in the chamber by injecting a sample of SF_6 (>99.99%, Alpha Gaz) into the chamber and following its temporal profile using a FTIR spectrometer (see below). And the dilution process could be expressed as a first order loss with a rate coefficient of around 2.3×10^{-5} s^{-1} (as shown in Figure 4S-1, in the supporting information section) and the mixing time following injection of a sample into the middle of the chamber (for near complete mixing, >99%) was about 30 seconds.

The contents of the chamber were sampled using three analytical instruments: (a) an FT-IR spectrometer; (b) a Cavity Attenuated Phase Shift (CAPS) spectroscopy instrument that used a 450 nm diode laser as a light source to measure NO_2; and (c) a cavity ring down spectrometer to simultaneously measure NO_3 and N_2O_5. These instruments are described briefly below.

(1) *FT-IR spectrometer*: A commercial Nicolet 5700 Magna FT-IR spectrometer with a liquid nitrogen cooled mercury–cadmium–telluride (MCT) detector was coupled to a white-type multiple-reflection mirror system located away from the walls and close to the center of the chamber. The multipass system had a base length of 2 m and, with 70 traverses, a total optical path length of 140 m. The spectra, measured between 4000–700 cm^{-1}, were analyzed using the software provided by the vendor (OMNIC 9). The IR spectra were recorded by co-adding 16 scans at a spectral resolution of 1 cm^{-1}. The reactants and SF_6 were monitored at the following infrared absorption wavenumbers: ethane (940 cm^{-1}-734 cm^{-1}), pentane (1576 cm^{-1}-1298 cm^{-1}), n-butane (3083 cm^{-1}-2798 cm^{-1}), iso-butane (3053 cm^{-1}-2808 cm^{-1}), cyclopentane (3100 cm^{-1}-2800 cm^{-1}), cyclohexane (2970 cm^{-1} -2830 cm^{-1}), 2,3-dimethy butane (3035 cm^{-1}-2821 cm^{-1}) and SF_6 (934 cm^{-1} - 954 cm^{-1}). As noted below we did not use IR measurements to quantify methane.

The areas under the absorption bands were calculated and used for determining concentrations. Calibration plots for quantifying hydrocarbon concentrations were generated by plotting the peak areas against known mixing ratio of the hydrocarbon (ppmv); an example of such a calibration plot for ethane is shown in Figure 4-1; similar plots for other reactants are shown in the supporting information of this chapter (Figure 4S-2 ~ Figure 4S-7). Because the concentrations of methane used in our study were very large, the absorption bands were partially saturated. Therefore, methane concentrations were calculated by manometric measurements; this was a very accurate method since we could directly measure the pressure of methane that was introduced into the chamber.

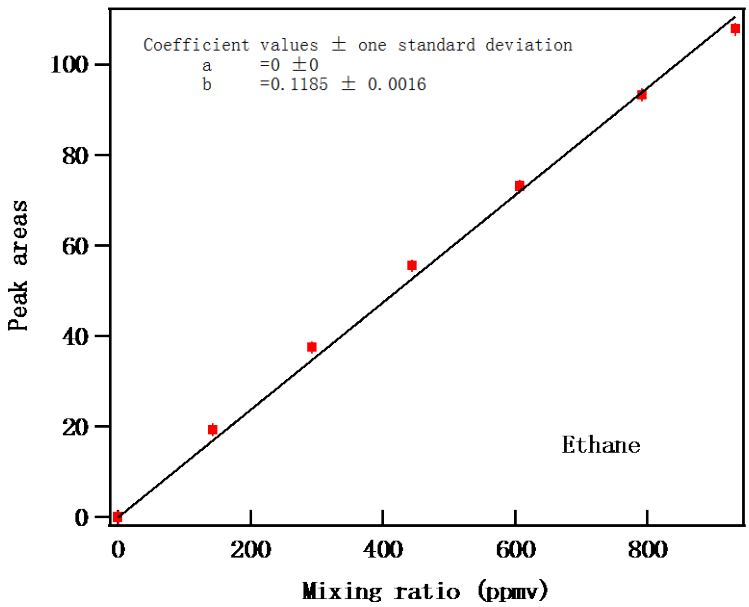

Figure 4-1 Calibration of ethane in FTIR. A plot of the measured area for ethane centered at 837 cm^{-1} as a function of the mixing ratio of ethane in the chamber as determined by manometric measurements. The data was fit to a line passing through zero using a linear least-squares analysis; the obtained slope is shown in the figure. The uncertainties in each point, derived from multiple measurements, are shown as vertical error bars.

(2) *The CAPS instrument*: A commercial NO_2 monitor form Aerodyne Research Inc. was used to measure the NO_2 concentrations during the experiments. This monitor provides a direct absorption measurement of nitrogen dioxide at 450 nm. The instrument is based on cavity attenuation detected by phase shift measurements. Unlike standard chemiluminescence-based monitors, this instrument does not require conversion of NO_2 to NO and, thus, is not sensitive to other nitrogen-containing species. Levels of detection (3σ noise levels), as specified by the vendor, was less than 100 ppt for a 10 second averaging period (Kebabian et al. 2008).

(3) *Cavity Ring Down Spectrometer*: A two-channel cavity ring down spectrometer operating at 662 nm was used to simultaneously measure the concentrations of NO_3 (in one channel) and N_2O_5 + NO_3 (in another channel). The detection principle and operating characteristics of this instrument have been described in detail in the previous chapter (Chapter II) and elsewhere (Brown, Stark and Ravishankara 2002b, Brown et al.

2002a, Brown 2003). The time resolution of the instrument was 1s with detection sensitivities of 0.4 and 2 ppt, respectively, for NO_3 and N_2O_5 for 1 second integration, as described in detail by Fuchs et al (Fuchs et al. 2008). The sample from the chamber entering the CRDS system was passed through a filter to remove aerosols, which scatter the 662 nm light and thus degrade the sensitivity for NO_3 detection. The combined loss of NO_3 and N_2O_5 to the walls of the instrument and the filter located upstream of the device have been estimated (Fuchs et al. 2008, Dube et al. 2006, Fuchs et al. 2012, Dorn et al. 2013) to be less than 20% and 4%, respectively, for NO_3 and N_2O_5; these losses were accounted for in calculating the concentrations. The overall accuracy of the NO_3 and N_2O_5 measurements, respectively, are estimated to be from -8% to +11% and from −9% to +12% (Wagner et al. 2011). In this study, the initial NO_3 and N_2O_5 mixing ratios were, respectively, between 350 and 2,500 pptv and between 4,000 and 25,000 pptv. The precision of their measurements are much better than the quoted absolute uncertainties under the concentration conditions used in the present study. However, we need the absolute concentrations of NO_3 and N_2O_5 to obtain the rate constants, as explained previously.

The absorption cell in the CAPS instrument where NO_2 is monitored was maintained at 38 ℃. Under the flow conditions employed here, a fraction of the N_2O_5 decomposed to generate NO_2 within this cell. This transformation efficiency was estimated by injecting known concentrations of pure N_2O_5 and measuring the NO_2 produced; this N_2O_5 to NO_2 conversion efficiency is determined to be (17±3)%. Therefore, the measured NO_2 signal was corrected for N_2O_5 interference using the N_2O_5 abundance measured using cavity ring down spectroscopy. This correction adds an additional level of uncertainty in the measured values of NO_2 and was taken into account.

2.2 Chemicals

The following chemicals, with purities as stated by the supplier, were used without further purification: methane (> 99.995%, Air Liquid), ethane (> 99.995%, Air Liquid),

propane (> 99.95%, Air Liquid), iso-butane (> 99.95%, Air Liquid), n-butane (> 99.95%, Air Liquid), cyclopentane (> 99.5%, Aldrich), cyclohexane (>99.5%, Aldrich), and 2,3-dimethy butane (>99.5%, Aldrich). The vendor supplied specifications of these alkane are listed in Table 4-1.

In this study, the NO_3 radicals were produced by the thermal decomposition of N_2O_5 injected into the chamber. Pure N_2O_5 was synthesized by mixing NO with O_3 in a slow flow and collecting produced N_2O_5 in a trap at -80℃, followed by purification via trap-to-trap distillation, as described by Davidson et al (Davidson et al. 1978).

Table 4-1 The specification of each alkane

	N_2 (ppm)	O_2 (ppm)	H_2O (ppm)	H_2 (ppm)	CO_2 (ppm)	C_nH_{m*} (ppm)
Methane (≥99.995%)	≤15	≤5	≤5	≤1	≤1	≤20 (C_2H_6≤15)
Ethane (≥99.995%)	≤15	≤3	≤3	≤5	≤1	≤20 (C_2H_4≤15)
Propane (≥99.95%)	≤40	≤10	≤5	≤40	≤5	≤200 (C_3H_6≤200)
n-butane (≥99.95%)	≤40	≤10	≤5	≤40	≤5	≤400
iso-butane (≥99.95%)	≤40	≤10	≤5	≤40	≤5	≤400
2,3-dimethy butane** (≥99.5%)						
Cyclopentane** (≥99%)						cyclopentene
Cyclohexane** (≥99.5%)			≤200			

* This is the quoted levels of total hydrocarbon impurities in the sample. We assumed that the hydrocarbons could be olefins in assessing some of our measured rate coefficients. They are discussed in the text.

** The impurities in these samples are unknown at this time. They will be quantified using a GC/MS as soon as the analytical capability is available.

2.3 Kinetic study method

The rate coefficients for the reactions of NO_3 radicals with alkanes were measured by following the temporal profiles of NO_3, N_2O_5 and NO_2 in an excess of alkanes. During this process, NO_3, N_2O_5 and NO_2 are in equilibrium; therefore, the rate coefficients can be obtained by fitting the temporal profiles of either NO_3 or N_2O_5. We fitted the temporal profiles of both NO_3 and N_2O_5 simultaneously (minimized the sum of least squares in the sum of deviations in NO_3 and N_2O_5) to derive the rate coefficients.

When N_2O_5 was injected into the middle of the chamber, it is immediately decomposed to give NO_3 and NO_2 and set up an equilibrium amongst these species.

$$N_2O_5 \xrightarrow{k_1} NO_3 + NO_2 \qquad \text{(R1)}$$

$$NO_3 + NO_2 \xrightarrow{k_2} N_2O_5 \qquad \text{(R2)}$$

The concentrations of NO_3 and N_2O_5 decreased with time as N_2O_5 and NO_3 were lost in the chamber due to wall loss and reaction of NO_3 with reactants. The temporal variations of NO_3, N_2O_5 and NO_2 in the chamber were continuously measured by CRDS and NO_2 monitor. The measured temporal profiles were fit by using a simple box model that integrated the set of reactions occurring in the chamber to derive the time dependence of NO_3, N_2O_5 and NO_2 concentrations. The fitting was done by minimizing the sum of least-squares for both NO_3 and N_2O_5 profiles by changing the input parameters. The input parameters include the initial concentrations of each reactant and reaction rate coefficients of each reaction. First, the data in the absence of alkane (the first 10 mins after N_2O_5 injection and before the injection of alkanes) were fit to the reaction scheme with alkane concentration set to zero. The known values of

the rate coefficients for the equilibrium reactions among NO_3, N_2O_5 and NO_2 were used. The equilibrium constant, keq = $[N_2O_5]/[NO_3][NO_2] = k_2/k_1$, and value of k_1 and k_2 at different temperatures were taken from NASA/JPL recommendation (J. B. Burkholder 2015). The values of the first order wall loss rate coefficients for loss of NO_3 and N_2O_5 (k_1 s^{-1} and k_2 s^{-1}) were derived from the fit of the reaction scheme shown below:

$$N_2O_5 \xrightarrow{k_1} NO_3 + NO_2 \qquad \text{(R1)}$$

$$NO_3 + NO_2 \xrightarrow{k_2} N_2O_5 \qquad \text{(R2)}$$

$$NO_3 \xrightarrow{k_3} \text{loss} \qquad \text{(R3)}$$

$$N_2O_5 \xrightarrow{k_4} \text{loss} \qquad \text{(R4)}$$

Subsequently (roughly 10 mins after N_2O_5 injection), a known concentration of the alkane was introduced into the chamber and its concentration was measured by FTIR. The concentration of the alkane was always much greater than those of N_2O_5 and NO_3 in the chamber. The temporal profiles of N_2O_5, NO_3 and NO_2 measured after 60 s of VOC injection were again fit to minimize the sum of least-squares for NO_3 and N_2O_5 decays in the reaction scheme with only the rate coefficient for the reaction of VOC with NO_3 being the variable with k_3, and k_4 set to the values derived from the first (~10 mins) of the observation in the absence of alkanes. K_{eq} would, of course, vary with the production of NO_2 and would be automatically incorporated. The appropriate values of the initial NO_2 concentrations were sometimes altered slightly to reproduce the known equilibrium constant.

3 Results and discussion

3.1 Accounting for impurities and subsequent reactions

We studied Reactions R4-1 through R4-8 under pseudo-first order conditions in NO_3 in the presence of an excess of alkanes. The temporal profiles of NO_3 (and N_2O_5

that is in equilibrium with NO_3) should be controlled by the reaction under study, along with the addition losses due to dilution and wall losses (which are quantified). However, the very small rate coefficients for the reactions in this study added three difficulties that need to be accounted for: (1) The temporal profiles of NO3 (and N_2O_5) could be influenced by reactions with the products of the reactions and their subsequent reaction products. (2) We need to quantify the contribution of the reactive impurities (mostly alkenes, if present) in the excess reagent to the measured loss rates of NO_3. To examine these two key issues and to account for these interferences, we carried out a series of model calculations using a box model that contained the following reactions (shown here with alkene as the main impurity):

$N_2O_5 \xrightarrow{k_1} NO_3 + NO_2$ (R1)

$NO_3 + NO_2 \xrightarrow{k_2} N_2O_5$ (R2)

$NO_3 \xrightarrow{k_3}$ loss (R3)

$N_2O_5 \xrightarrow{k_4}$ loss (R4)

alkane $+ NO_3 \xrightarrow{k_5} R_1O_2$ (R5)

alkene $+ NO_3 \xrightarrow{k_6} R_2O_2$ (R6)

$R_1O_2 + NO_3 \xrightarrow{k_7} R_1O + NO_2$ (R7)

$R_1O_2 + R_1O_2 \xrightarrow{k_8} 2R_1O$ (R8)

$R_1O_2 + R_1O_2 \xrightarrow{k_9} 2R_1OH$ (R9)

$R_1O_2 + R_1O_2 \xrightarrow{k_{10}} 2R_3CHO$ (R10)

$R_1O_2 + NO_2 \xrightarrow{k_{11}} R_1O_2NO_2$ (R11)

$R_1O_2NO_2 \xrightarrow{k_{12}} R_1O_2 + NO_2$ (R12)

$R_1O + O_2 \xrightarrow{k_{13}} R_3CHO + HO_2$ (R13)

$R_1O_2 + HO_2 \xrightarrow{k_{14}} R_1OOH + O_2$ (R14)

$R_3CHO + NO_3 \xrightarrow{k_{15}} R_3COOO + HNO_3$ (R15)

$HO_2 + NO_3 \xrightarrow{k_{16}} OH + NO_2 + O_2$ (R16)

$OH + NO_3 \xrightarrow{k_{17}} HO_2 + NO_2$ (R17)

$NO_2 + OH \xrightarrow{k_{18}} HONO_2 / HOONO$ (R18)

$R_2O_2 + NO_3 \xrightarrow{k_{19}} R_2O + NO_2$ (R19)

$R_2O_2 + R_1O_2 \xrightarrow{k_{20}} 2R_2O$ (R20)

$R_2O_2 + R_2O_2 \xrightarrow{k_{21}} 2R_2OH$ (R21)

$R_2O_2 + R_2O_2 \xrightarrow{k_{22}} 2R_4CHO$ (R22)

$R_2O_2 + NO_2 \xrightarrow{k_{23}} R_4O_2NO_2$ (R23)

$R_4O_2NO_2 \xrightarrow{k_{24}} R_2O_2 + NO_2$ (R24)

$R_2O + O_2 \xrightarrow{k_{25}} R_4CHO + HO_2$ (R25)

$R_2O_2 + HO_2 \xrightarrow{k_{26}} R_2OOH + O_2$ (R26)

$R_4CHO + NO_3 \xrightarrow{k_{27}} R_4COOO + HNO_3$ (R27)

The detailed set of secondary reactions that would take place in the chamber due to the production of the alkyl radicals is given in Table S4-1. However, we could simplify this reaction scheme by choosing only the ones that contribute to the measured NO_3 and N_2O_5 temporal profiles.

3.2 Experimental results

Figure 4-2 and 4-3 show the fits of the observed temporal profiles of NO_3, N_2O_5, NO_2 for methane and ethane. Panel (1) shows the loss of NO_3 and N_2O_5 without methane and ethane, the reactions used in the box model are R1, R2, R3, R4; Panel (2) shows the loss of NO_3 and N_2O_5 with methane and ethane, the reactions used in the box model are R1, R2, R3, R4 and R5 (i.e., without including the reactions with impurities and the subsequent reactions); Panel (3) shows the loss of NO_3 and N_2O_5 with methane and ethane as well as all the possible interfering reactions (i.e., R1-

R18).

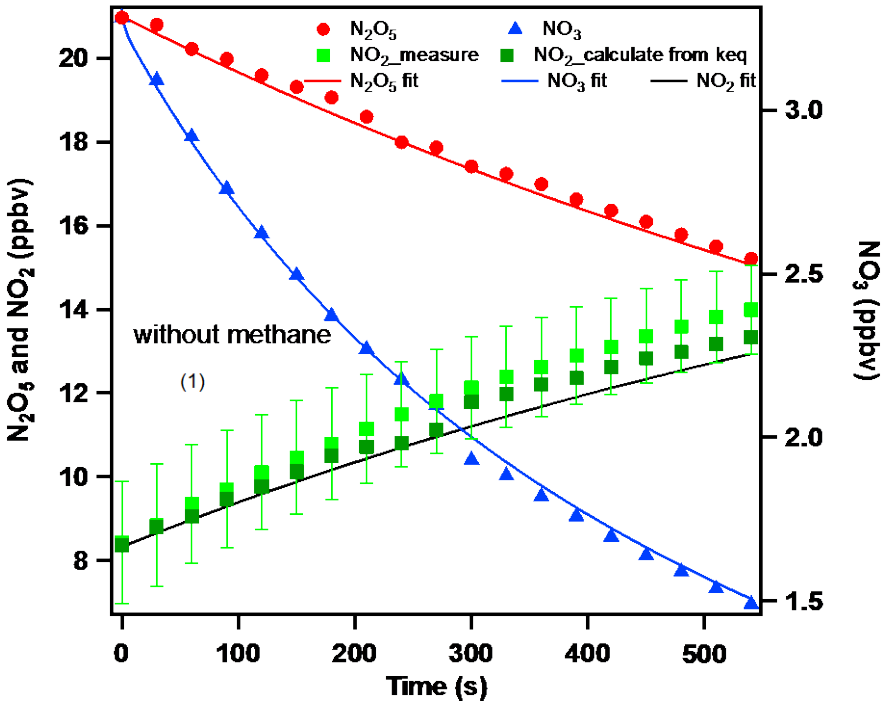
N2O5
NO3
NO2_measure
NO2_calculate from keq
N2O5 fit
NO3 fit
NO2 fit
without methane
(1)
N2O5 and NO2 (ppbv)
NO3 (ppbv)
Time (s)

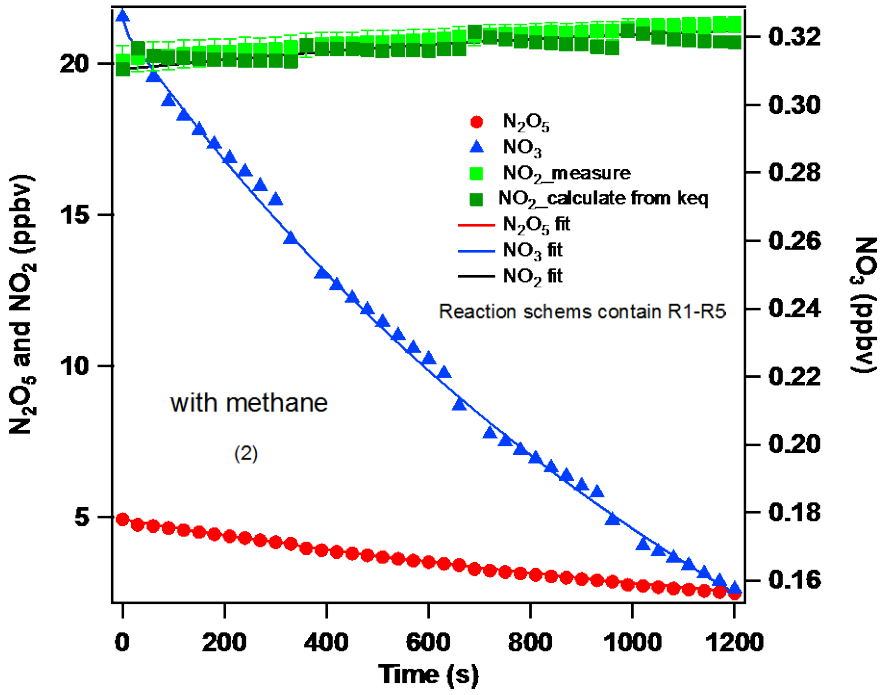
N2O5
NO3
NO2_measure
NO2_calculate from keq
N2O5 fit
NO3 fit
NO2 fit
Reaction schems contain R1-R5
with methane
(2)
N2O5 and NO2 (ppbv)
NO3 (ppbv)
Time (s)

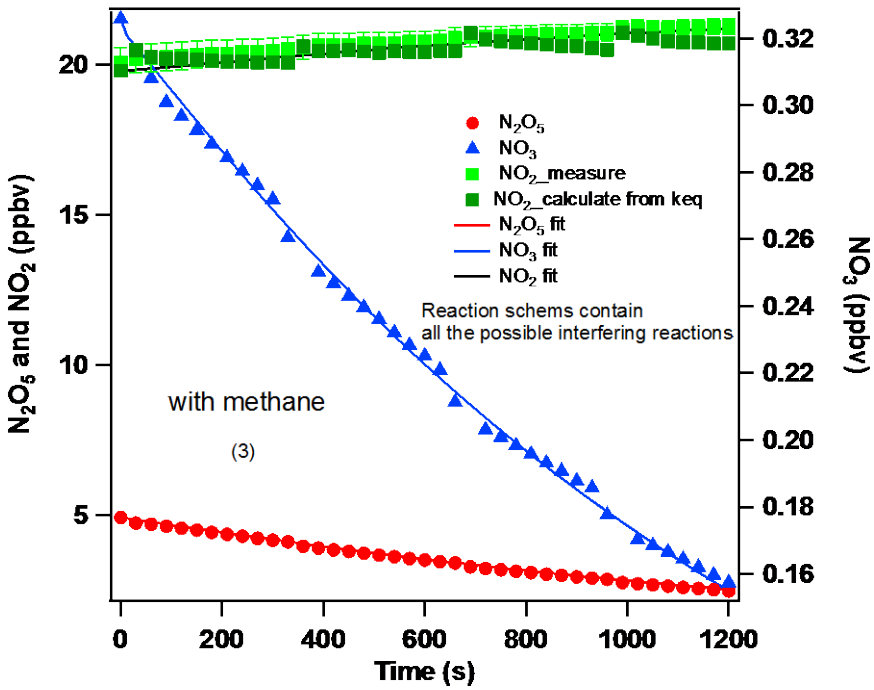

Figure 4-2 Experimental and simulated results for NO_3, N_2O_5 and NO_2 profiles from chamber experiments. The observed NO_3, N_2O_5 and NO_2 mixing ratios (circles and triangles) and their simulated temporal profiles (lines) are fit in three conditions (1) without methane (2) the mixing ratios of methane was 2624 ppmv. Reaction schemes were R1, R2, R3, R4 and R5. The fits yield a value of k_{VOC} = 2.98 × 10^{-20} molecule^{-1} cm^3 s^{-1} (3) the mixing ratios of methane was 2624 ppmv. Reaction schemes were R1-R5 and R6-R18. The fits yield a value of k_{VOC} = 1.34 × 10^{-20} molecule^{-1} cm^3 s^{-1}.

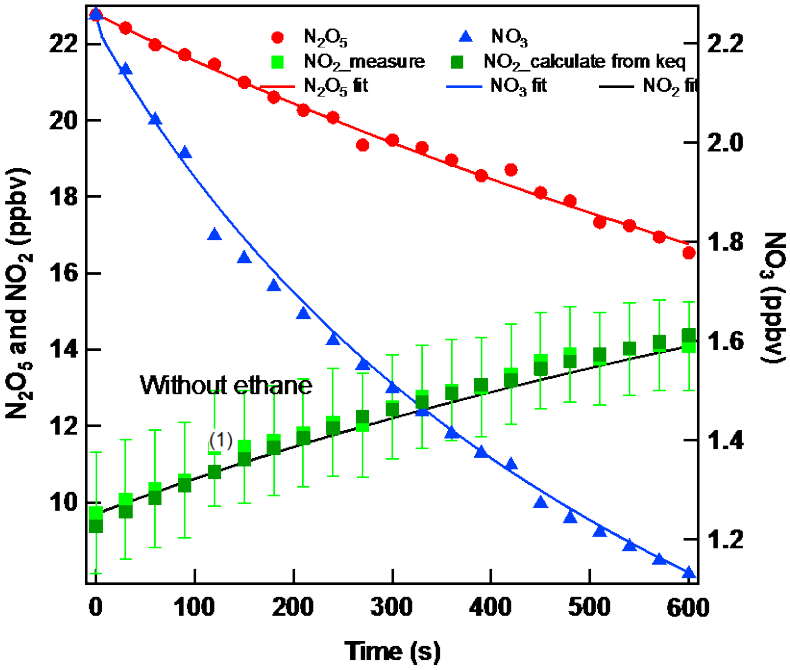
N2O5
NO3
NO2_measure
NO2_calculate from keq
N2O5 fit
NO3 fit
NO2 fit
Without ethane
(1)
N2O5 and NO2 (ppbv)
NO3 (ppbv)
Time (s)

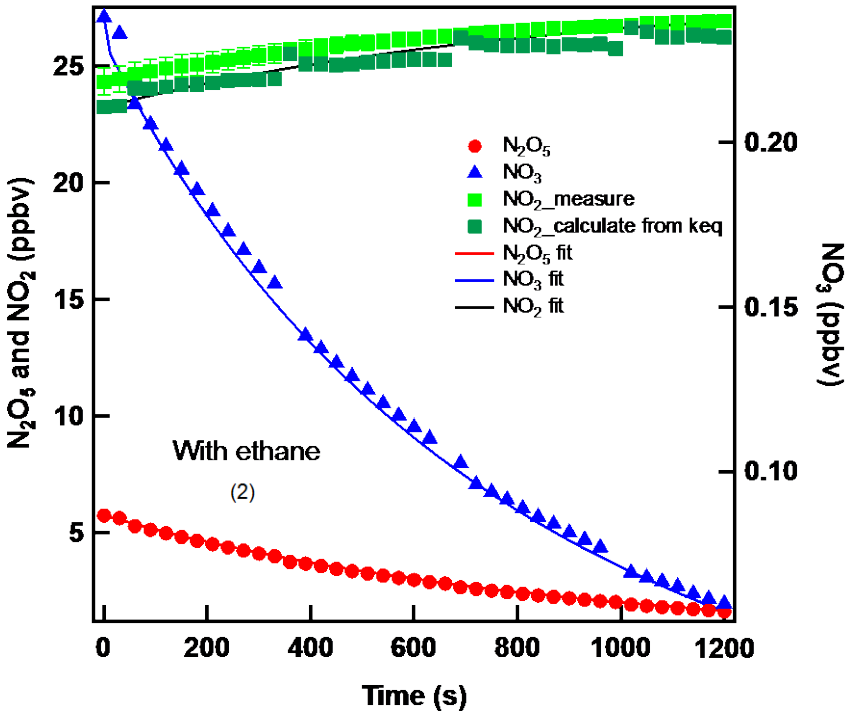
N2O5
NO3
NO2_measure
NO2_calculate from keq
N2O5 fit
NO3 fit
NO2 fit
With ethane
(2)
N2O5 and NO2 (ppbv)
NO3 (ppbv)
Time (s)

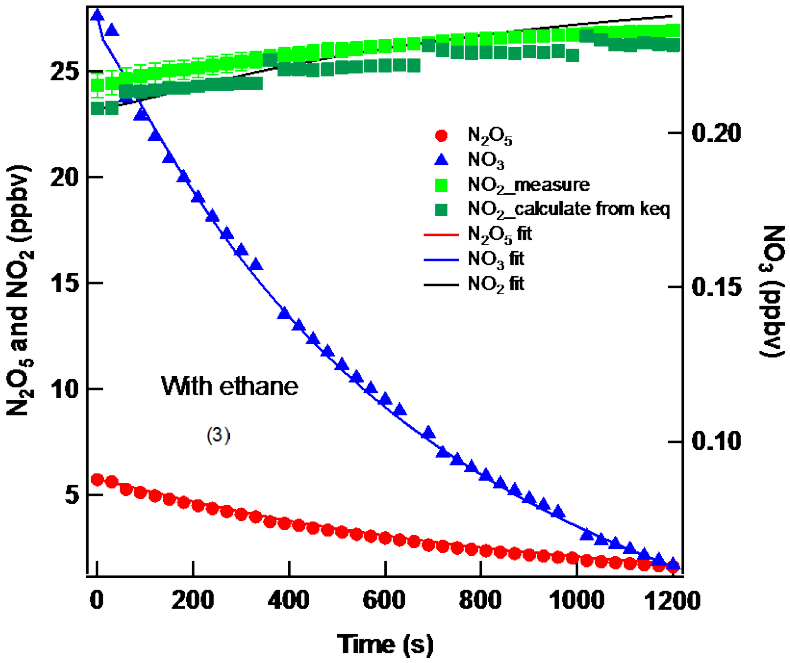

Figure 4-3 Experimental and simulated results for NO_3, N_2O_5 and NO_2 profiles from chamber experiments. The observed NO_3, N_2O_5 and NO_2 mixing ratios (circles and triangles) and their simulated temporal profiles (lines) are fit in three conditions (1) without methane (2) the mixing ratios of methane was 1106 ppmv. Reaction schemes were R1, R2, R3, R4 and R5. The fits yield a value of k_{VOC} = 7.60 × 10^{-19} molecule^{-1} cm^3 s^{-1} (3) the mixing ratios of methane was 1106 ppmv. Reaction schemes were R1-R5 and R7-R18. The fits yield a value of k_{VOC} = 4.23 × 10^{-19} molecule^{-1} cm^3 s^{-1}.

Multiple experiments were carried out by varying alkanes and initial concentrations of each reactant. The uncertainty in the obtained value of k_{VOC} due to fitting was very small, often much less than 5%. The uncertainty in the precision of our measured rate coefficient were obtained by the standard deviation of the mean of multiple measurements and including the Student t value for the limited number of measurements. The results of our measurements for methane and ethane are given in Table 4-2.

Table 4-2. Summary of the experimental conditions and upper limits for reaction of NO_3 with methane and ethane at 298.0±1.5K. The k_{VOC} measured values shown are those derived from fitting the observed profiles of NO_3 and N_2O_5 to a

least squares algorithm.

Compound	Initial mixing ratio				k_{VOC1} [a]	k_{VOC2} [b]
	VOC (ppmv)	NO_3 (ppbv)	N_2O_5 (ppbv)	NO_2 (ppbv)	(cm^3 $molecule^{-1}s^{-1}$)	
Methane	2624	0.33	4.93	19.80	2.98×10^{-20}	1.34×10^{-20}
	2520	0.84	14.49	22.49	2.48×10^{-20}	1.12×10^{-20}
	2598	0.14	2.22	20.93	3.68×10^{-20}	2.65×10^{-20}
	3440	0.28	5.14	19.11	1.55×10^{-20}	8.04×10^{-21}
	3276	0.52	10.38	20.59	1.90×10^{-20}	6.90×10^{-21}
	3389	0.14	2.64	19.33	2.80×10^{-20}	2.05×10^{-20}
				Mean average	$(2.5\pm1.7)\times10^{-20}$	$(1.7\pm1.5)\times10^{-20}$
Ethane	958	0.22	4.84	26.63	7.50×10^{-19}	4.50×10^{-19}
	1106	0.24	5.74	23.25	7.60×10^{-19}	4.23×10^{-19}
	1095	0.09	2.46	25.88	6.01×10^{-19}	4.30×10^{-19}
	1101	0.26	6.57	23.60	7.37×10^{-19}	4.05×10^{-19}
	1000	0.36	10.24	26.41	7.13×10^{-19}	3.94×10^{-19}
	1055	0.10	2.84	26.05	6.37×10^{-19}	5.02×10^{-19}
				Mean average	$(7.1\pm1.3)\times10^{-19}$	$(4.2\pm0.4)\times10^{-19}$

[a] The measurements were only based on the first step reaction (R1, R2, R3, R4 and R5). Quoted error is at the 95% confidence level and is a measure of the precision of our measurements. It includes Student t-distribution contribution due to the limited number of measurements.

[b] The measurements were based on the first step reaction and secondary reactions (R1- R5 and R7-R18). Quoted error is at the 95% confidence level and is a measure of the precision of our measurements. It includes Student t-distribution contribution due to the limited number of measurements.

Clearly, the inclusion of subsequent reactions shows that they do contribute to the measured temporal profiles. One possible way to look for their influence is to examine how these values changes with the initial concentrations of NO_3 relative to that of the alkane. Clearly, for example in the case of methane, the correction decreased significantly as the ratio of the methane to NO_3 increased. In an ideal case, increasing the ratio of methane to NO_3 by an additional factor of 10 would have almost completely suppressed the secondary reactions, but would lead to imprecision due to the very low concentrations of NO_3 to be used. The presence of a reactive impurity whose concentration does not change with reaction will not be sensitive to

this analysis. We will note this influence later.

3.3 Error estimation

The errors in determining the rate coefficients by monitoring the temporal profiles of NO_3 and N_2O_5 arise from (1) the precision in the measurements of NO_3, N_2O_5 and NO_2; (2) the uncertainty in the concentration of the alkanes in our study; (3) the uncertainty of the rate coefficients used in the reaction scheme of the box model; (4) the precision of the measurements of k_{VOC} by curve fitting.

In the present study, the systematic errors in measurements of NO_3 and N_2O_5 using the CRDS system employed here have been assessed to be −8/+11% for NO_3 and −9/+12% for N_2O_5, as noted earlier. The error in measurement of NO_2 (after correcting for the interference due to N_2O_5 detection) using CAPS monitor has been assessed to be around 10 %. Systematic errors in the measured concentration of the alkanes are estimated for each compound by using the uncertainty of the slope in the calibration plots (<2%) and the uncertainty in measuring alkane concentration for the calibration (3%); all at 95% confidence level. The uncertainty in the fitting, as noted above, is better than 5%. But the uncertainty of the rate coefficients used in the reaction scheme of the box model to fit the curves (k_7, k_8) can reach 58% (Atkinson et al. 2006) and we estimate this uncertainty includes those arising from not simulating the entire reaction sequence. When we decreased k_7 by factor 3 (k_7=k(RO_2+NO_3)/3), the final calculated rate constant increased around 26%. Therefore, we estimated that the uncertainty in our simulated correction is about 7% for the uncertainty in this rate coefficient.

The overall estimated error in the rate coefficient took the fitting error, estimated uncertainty of absolute concentrations of each reactant, the precision of the measurements of k_{VOC}, and the uncertainty due to potential errors in the rate coefficients used from the literatures into account. In total, we gave a 60% uncertainty to the final result.

Another potential source of error in the rate coefficient measured by using the

absolute method is the presence of reactive impurities in the sample of the alkanes. The alkanes used in the study were the purest we could obtain from commercial vendors. For methane and ethane, the impurities are less than 0.005% (50 ppmv) and the main impurities are nonreactive towards NO_3 such as, N_2, O_2, and CO_2. However, we cannot rule out small amounts of reactive impurities (<20 ppm). If such an impurity that reacts with a rate coefficient of 1×10^{-13} cm^3 $molecule^{-1}$ s^{-1} were present, its concentration cannot be more than about 0.5 ppmv. That is the value one would estimate even if we attributed the entire measure rate coefficient to the impurity reaction. However, such small impurity would have reacted with NO_3 and the measured NO_3 temporal profile would not be similar to the one calculated, as shown for other reactions later. Furthermore, it would vary with the reaction time as the impurities are consumed. We did not see such variations.

From these results, it is clear that the reaction of NO_3 with methane and ethane could be slower than the values noted above. Since we cannot rule out the presence of small concentrations of highly reactive impurities, we prefer to quote the rate coefficients for the reactions of NO_3 with methane and ethane to be, respectively, $<4\times10^{-20}$ and $<5\times10^{-19}$ cm^3 $molecule^{-1}$ s^{-1}.

For propane, n-butane and iso-butane, they could contain small abundances alkenes (< 200 ppmv), which could react much more rapidly with NO3 than the alkanes. (Note that the rate coefficient for reaction of NO3 with these hydrocarbons are three orders of magnitude larger than that for reaction with methane.) If alkenes were not taken in to account, we could indeed overestimate this rate coefficients. GC-MS was used to meaure the mixing radio of the impurities. For propane, less than 50 ppm propene was detected as a main reactive impurity. The rate coefficients of propane react with NO3 radicals got by fitting the observed temporal profiles of NO_3, N_2O_5, NO_2 in different conditions are shown Figure 4-4.

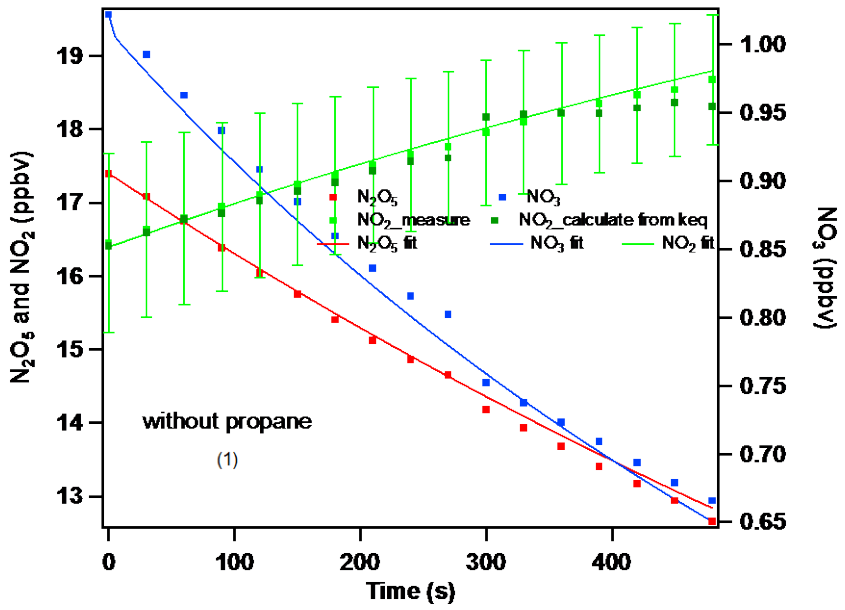
N2O5 and NO2 (ppbv)
NO3 (ppbv)
Time (s)
N2O5
NO3
NO2_measure
NO2_calculate from keq
N2O5 fit
NO3 fit
NO2 fit
without propane
(1)

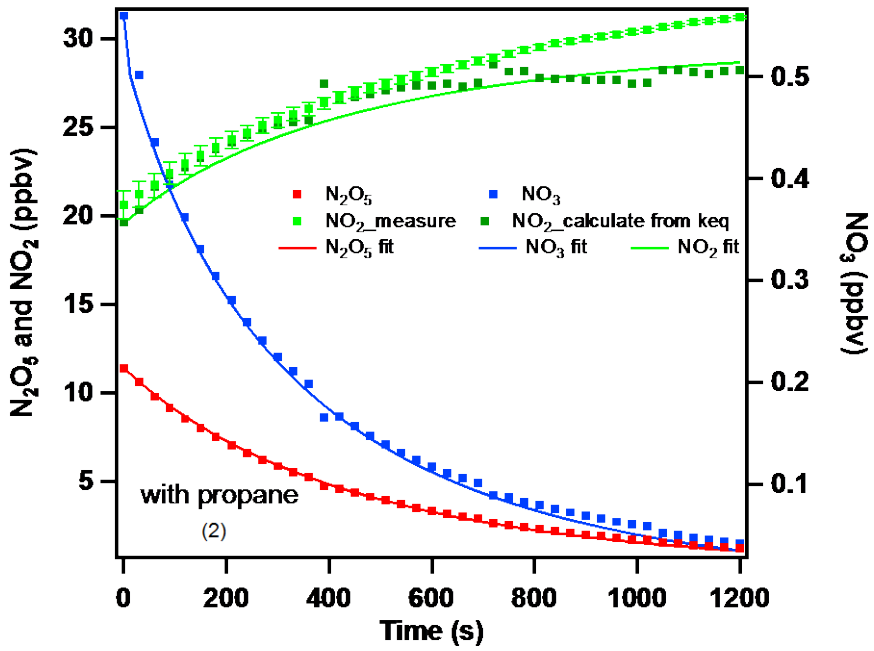
N2O5 and NO2 (ppbv)
NO3 (ppbv)
Time (s)
N2O5
NO3
NO2_measure
NO2_calculate from keq
N2O5 fit
NO3 fit
NO2 fit
with propane
(2)

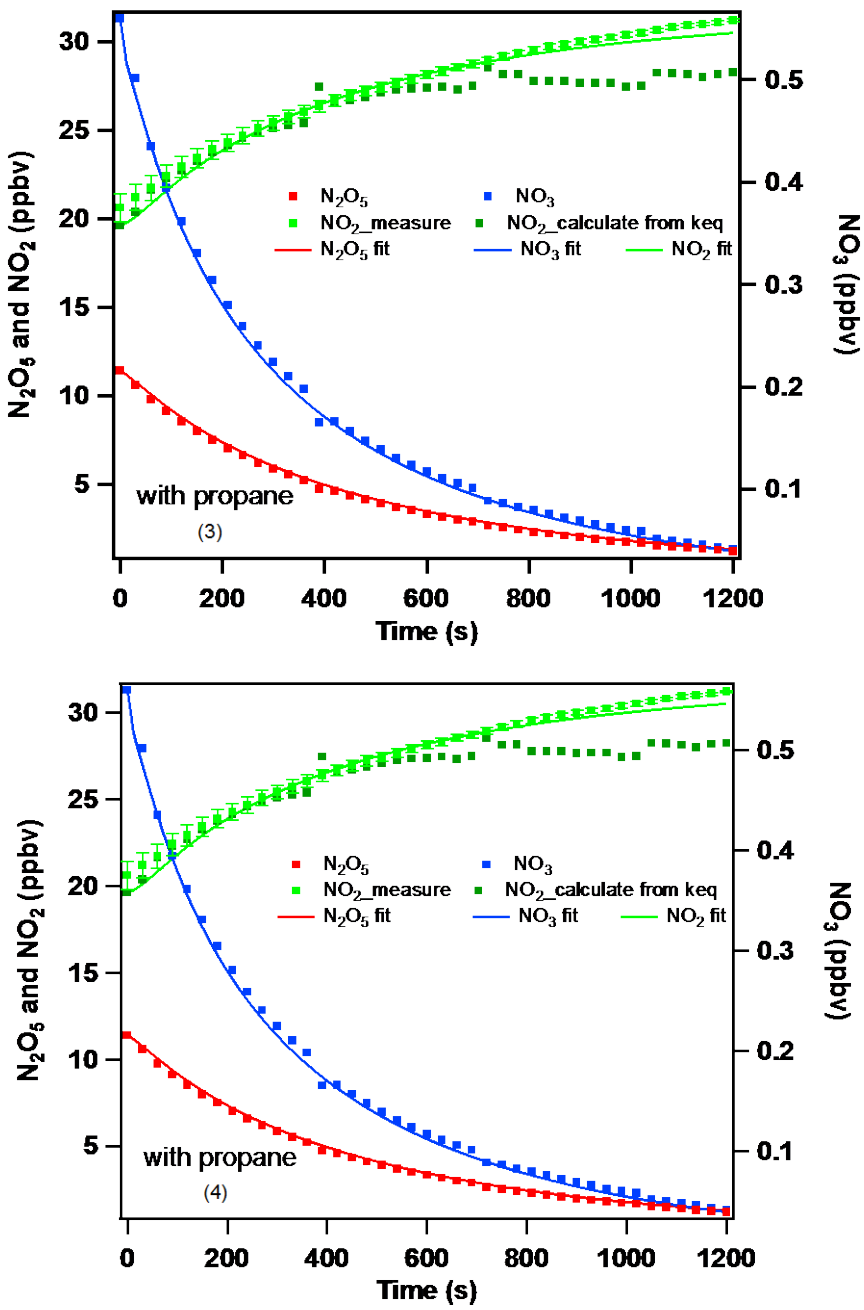

Figure 4-4 Experimental and simulated results for NO_3, N_2O_5 and NO_2 profiles from chamber experiments. The observed NO_3, N_2O_5 and NO_2 mixing ratios (circles and triangles) and their simulated temporal profiles (lines) are fit in two conditions (1) without propane (2) the mixing ratios of propane was 99.86 ppmv. Reaction schemes were R1, R2, R3, R4 and R5. The fits yield a value of $k_{VOC} = 1.71 \times 10^{-17}$ molecule^{-1} cm^3 s^{-1} (3) the mixing ratios of propane was 99.86 ppmv. Reaction schemes were R1-R5 and R7-R18. The fits yield a value of $k_{VOC} = 9.81 \times 10^{-17}$ molecule^{-1} cm^3 s^{-1} (4) the mixing ratios of propane was 99.86 ppmv,

and contain 5 ppb propene as impurity. Reaction schemes were R1-R27. The fits yield a value of $k_{VOC} = 9.75 \times 10^{-18}$ molecule^{-1} cm^3 s^{-1}

Simulation of these profiles where we assumed 0.005% propene impurity in propane is shown as the line in Figure 4-4(4). Based on such simulations, we estimate that the lower limit of the reaction rate coefficient for NO_3 reaction with propane to be 30% lower, but with a slightly higher uncertainty. Furthermore, when we fit the data from different reaction time periods, i.e., when some of the propene should be depleted due to reaction with NO_3, we got the same rate coefficients. Therefore, we suggest that the level of olefinic impurities in propane is not very large.

Simulation of these profiles where we assumed 0.005% propene (50 ppm) impurity in propane is shown as the line in Figure 4(4). Based on such simulations, we estimate that effect of reactive impurity to the reaction rate coefficient for NO_3 reaction with propane is less than 1%. Furthermore, we also tried to fit the data from different reaction time periods, i.e., when some of the alkenes should be depleted due to reaction with NO_3, we got the similar rate coefficients. Therefore, we suggest that the level of olefinic impurities in the alkane is not very large.

The rate coefficients of n-butane , iso-butane, 2,3-dimethylbutane cyclopentane and cyclohexane were also studies in this work, and the typical observed temporal profiles of NO_3 and N_2O_5 in such experiments are similar to those alkanes mentioned before. The experimental conditions and rate constants for reaction of NO_3 with these reactants are summarized in Table 4-3. The related figures are shown in the Supporting Information section

Table 4-3. Summary of the experimental conditions and upper limits for reaction of NO3 with propane, n-butane, iso-butane, 2,3-dimethylbutane cyclopentane and cyclohexane at 298.0±1.5K. The kVOC measured values shown are those derived from fitting the observed profiles of NO3 and N2O5 to a least squares algorithm.

Compound	Initial mixing ratio of reactants in the chamber	k_{VOC1} [a]	k_{VOC2} [b]	k_{VOC} [c] incl. systematic errors

	VOC (ppmv)	NO_3 (ppbv)	N_2O_5 (ppbv)	NO_2 (ppbv)	(cm^3 $molecule^{-1}s^{-1}$)		
propane	99.86	0.56	11.38	19.61	1.73×10^{-17}	9.40×10^{-18}	
	60.81	0.72	12.10	20.43	1.80×10^{-17}	1.02×10^{-17}	
	51.08	0.85	15.56	16.27	1.68×10^{-17}	9.38×10^{-18}	
	98.39	0.10	2.88	27.49	1.27×10^{-17}	1.01×10^{-17}	
	59.62	0.10	2.40	29.07	1.23×10^{-17}	9.12×10^{-18}	
				Mean average	$(1.5\pm0.6)\times10^{-17}$	$(9.2\pm2.1)\times10^{-18}$	$(9.2\pm5.5)\times10^{-18}$
n-butane	19.72	1.03	18.26	18.13	3.10×10^{-17}	1.35×10^{-17}	
	18.70	0.14	3.80	28.22	2.42×10^{-17}	1.59×10^{-17}	
	30.78	1.06	18.10	15.16	3.10×10^{-17}	1.65×10^{-17}	
	29.68	0.12	3.33	25.55	2.24×10^{-17}	1.56×10^{-17}	
	24.26	0.79	11.05	14.24	3.60×10^{-17}	1.56×10^{-17}	
				Mean average	$(2.9\pm1.1)\times10^{-17}$	$(1.5\pm0.2)\times10^{-17}$	$(1.5\pm0.9)\times10^{-17}$
iso-butane	13.90	0.83	9.40	12.99	1.35×10^{-16}	8.57×10^{-17}	
	13.73	0.10	1.86	21.23	8.93×10^{-17}	7.43×10^{-17}	
	10.26	1.10	14.64	13.84	1.40×10^{-16}	8.21×10^{-17}	
	10.04	0.10	2.42	25.26	9.52×10^{-17}	7.67×10^{-17}	
	5.22	1.30	14.04	12.07	1.65×10^{-16}	9.00×10^{-17}	
				Mean average	$(1.3\pm0.6)\times10^{-16}$	$(8.2\pm1.3)\times10^{-17}$	$(8.2\pm4.9)\times10^{-17}$
2,3-dimethyl butane	1.02	0.25	3.90	19.41	1.55×10^{-15}	6.80×10^{-16}	
	0.51	0.23	5.50	24.05	1.00×10^{-15}	5.50×10^{-16}	
	0.38	0.58	9.57	18.17	1.25×10^{-15}	6.32×10^{-16}	
	0.38	0.12	2.56	23.80	7.84×10^{-16}	5.44×10^{-16}	
	0.26	0.64	9.20	14.47	1.25×10^{-15}	6.02×10^{-16}	
	0.24	0.10	2.09	20.27	7.03×10^{-16}	4.82×10^{-16}	
				Mean average	$(1.1\pm0.6)\times10^{-15}$	$(5.8\pm1.4)\times10^{-16}$	$(5.8\pm3.5)\times10^{-16}$
cyclopentane	1.76	0.72	8.59	13.33	3.50×10^{-16}	1.80×10^{-16}	
	1.41	0.24	3.91	17.98	3.20×10^{-16}	1.68×10^{-16}	
	2.04	0.57	10.66	19.67	2.70×10^{-16}	1.31×10^{-16}	
	1.71	0.19	4.26	23.97	2.60×10^{-16}	1.38×10^{-16}	
	2.04	0.11	2.49	24.61	1.99×10^{-16}	1.41×10^{-16}	
	1.78	0.63	9.39	17.14	2.60×10^{-16}	1.29×10^{-16}	
	1.71	0.10	2.10	23.84	1.96×10^{-16}	1.41×10^{-16}	
	1.42	1.10	14.85	10.64	2.00×10^{-16}	7.78×10^{-16}	
				Mean average	$(2.6\pm1.1)\times10^{-16}$	$(1.4\pm0.6)\times10^{-16}$	$(1.4\pm0.8)\times10^{-16}$

cyclohexane	2.51	0.39	7.73	22.05	2.30×10^{-16}	1.20×10^{-16}	
	1.88	0.45	7.89	19.40	2.35×10^{-16}	1.34×10^{-16}	
	1.82	0.10	2.16	24.09	1.98×10^{-16}	1.41×10^{-16}	
	1.54	0.46	6.85	16.70	2.50×10^{-16}	1.27×10^{-16}	
	1.50	0.11	2.04	20.55	1.92×10^{-16}	1.39×10^{-16}	
	1.98	0.50	10.42	21.08	2.30×10^{-16}	1.12×10^{-16}	
				Mean average	$(2.2\pm0.5)\times10^{-16}$	$(1.3\pm0.3)\times10^{-16}$	$(1.3\pm0.8)\times10^{-16}$

[a] The measurements were only based on the first step reaction (R1, R2, R3, R4 and R5).

[b] The measurements were based on the first step reaction and secondary reactions (R1- R5, R7- R18).

[c]The quoted errors include estimated systematic errors as described in the text.

The results in the table clearly shows that a major contributor to the uncertainty in our measured rate coefficients is the secondary reactions noted earlier. This error could be greatly suppressed by increasing the ratio of alkane to NO_3 in our experiments. However, addition of too much more alkane pushes the time scale for measurement of NO_3 profiles to shorter regimes while decreasing NO_3 much further reduces the signal to noise in NO_3 signal that leads to good fits of its profiles.

3.4 Comparison with the kinetic results in literature

The upper limits and rate coefficients of NO_3 radicals with alkanes measured by different groups are summarized in Table 4-4. A comparison of rate coefficients determined in this study with the literature data are also shown in this table. Only upper limits to the room temperature rate coefficients have been determined before for methane, ethane and propane. The upper limits of methane with NO_3 radicals were all derived based on no observable reaction occurring in their systems (Burrows, Tyndall and Moortgat 1985, Wallington et al. 1986, Cantrell et al. 1987, Boyd et al. 1991). The rate coefficient of ethane with NO_3 has been measured at 453K and above (Bagley et al. 1990). The rate coefficient at room temperature, kvoc(ethane) = 3.3×10^{-19} cm^3 $molecule^{-1}s^{-1,}$ was obtained via an extrapolation. Interestingly, our value is in good agreement with this extrapolated value, given the reported uncertainties by

Bagley et al and us. Previous studies have obtained rate coefficients for reactions with n-butane, iso-butane and 2,3-dimethybutane at room temperature, mainly using relative rate techniques and ethene as the reference compound. There are no previous reports for the rate coefficients for the reactions of NO_3 with cyclepentane. As can be seen in the table, most of our values are in good agreement with previously reported values, given the reported uncertainties, whenever such comparisons are possible.

Table 4-4 Summary of the upper limits and rate coefficients of NO_3 radicals with alkanes measured by different groups.

Reactant	k_{VOC} reported $10^{-17}cm^3$ $molecule^{-1}s^{-1}$	Technique	Reference
Methane	≤40	Absolute method	Burrows et al. 1985
	≤2	Absolute method	Wallington et al. 1986
	≤0.0004	Absolute method	Cantrell et al. 1987
	≤0.08	stopped-flow apparatus	Boyd et al. 1991
	≤0.004	Absolute method	This work(kvoc)
Ethane	≤0.4	Absolute method flash photolysis-visible absorption	Wallington et al. 1986
	0.033	Absolute method	Bagley et al. 1990
	≤(2.7±0.2)	stopped-flow apparatus	Boyd et al. 1991
	<0.05	Absolute method	This work(kvoc)
Propane	≤(4.8±1.7)	stopped-flow apparatus	Boyd et al. 1991
	0.92±0.55	Absolute method	This work(kvoc2)
n-butane	2.0±1.0	RR(ethene)[a]	Atkinson et al. 1984
	6.6±3.8	RR(ethene)[b]	Atkinson et al. 1984
	≤2	Absolute method	Wallington et al. 1986
	4.5	Absolute method	Bagley et al. 1990

	1.9±0.9	Absolute method	This work(kvoc)
iso-butene	2.9±1.4	RR(ethene)[a]	Atkinson et al. 1984
	9.8±5.6	RR(ethene)[b]	Atkinson et al. 1984
	11	Absolute method	Bagley et al. 1990
	≤(60±10)	Absolute method	Boyd et al. 1991
	8.2±4.9	Absolute method	This work(kvoc)
2,3-dimethylbutane	12.1±5.4	RR(ethene)[a]	Atkinson et al. 1984
	40.4±23.2	RR(ethene)[b]	Atkinson et al. 1984
	40.6±5.7	RR(trans-2-butene)[c]	Atkinson et al. 1988
	58±35	Absolute method	This work(kvoc)
cyclopentane	14±8	Absolute method	This work(kvoc)
cyclohexane	4.0±1.9	RR(2,3-dimethylbutane)	Atkinson et al. 1984
	13.3±7.7	RR(2,3-dimethylbutane)[d]	Atkinson et al. 1984
	20.7±12.4	RR(2,3-dimethylbutane)[e]	Atkinson et al. 1984
	13±8	Absolute method	This work(kvoc)

[a] The rate constant of ethene with NO_3 radicals was $(6.1\pm2.6)\times10^{-17}$ cm^3 $molecule^{-1}s^{-1}$, when used as a reference.

[b] The values from the literatures were recalculated by using the rate constant of ethene with NO_3 $(2.1 \pm 1.2) \times 10^{-16}$ cm^3 $molecule^{-1}$ s^{-1}, which was recommended by IUPAC.

[c] The rate constant of trans-2-butene with NO_3 radicals was $(3.87 \pm0.45)\times10^{-13}cm^3$ $molecule^{-1}s^{-1}$, when used as a reference.

[d] The values from the literatures were recalculated by using the rate constant of 2,3-dimethylbutane with NO_3 $(40.4 \pm 23.2) \times 10^{-16}$ cm^3 $molecule^{-1}$ s^{-1}.

[e] The values from the literatures were recalculated by using the rate constant of 2,3-dimethylbutane with NO_3 $(63 \pm 38) \times 10^{-16}$ cm^3 $molecule^{-1}$ s^{-1} got from this work.

Clearly, we have been able to show that the upper limit for the reactions of NO_3

with methane is lower than previously reported. The slow reaction with methane is not surprising since this reaction is slightly endothermic, making the potential barrier for the reaction large. We also report an upper limit for the reaction of NO_3 with ethane that is consistent with that reported by Bagley et al. However, we feel we can quote this only as an upper limit given that it is very slow and very small levels of impurities can lead to errors. For other reaction, our data is in reasonable agreement with available values.

3.5 Relation between structure and reactivity of alkanes.

A summary of the upper limits and rate coefficients obtained in this work are given in previous Table 4-2 and 4-3. The rate coefficients for all the straight-chain alkanes-NO_3 radical reactions measured here increase with the chain length going from methane to n-butane. We observe an increase in the reactivity with the chain length k_{VOC}(methane) < k_{VOC}(Ethane) < k_{VOC}(Propane) < k_{VOC}(n-butane). Further, the iso-butane and 2,3-dimethybutane react faster than their normal analogs. This is consistent with the activity of H atom on primary, secondary, and tertiary C-H bonds, respectively.

For simple alkanes, the C-H bond dissociation energies are: primary C-H, -418.6 kcal mol^{-1}; secondary C-H, -401.8 kcal mol^{-1} and tertiary C-H -393.5 kcal mol^{-1}, respectively (Castelhano and Griller 1982). So, we expect the reaction to be faster for molecules with lower C-H bond energy, since we expect the reaction to proceed via H atom abstraction from the weakest C-H bonds in the molecule.

The enthalpies of each reaction at standard conditions are shown in the introductions section. From the enthalpies of these reactions, we find R4-1 and R4-4-1 to be endothermic reactions and all the other reactions are exothermic.

We have plotted the rate coefficient for the measured alkanes and cycloalkanes as a function of the reaction exothermicity. Clearly, the log of the rate coefficient at 298 K correlates with the exothermicity or the bond dissociation energy. This is to be expected for an abstraction reaction where the activation energy for the reaction is

directly related to the dissociation energy for the bond being broken, i.e., the C-H bond in the reactions studied here. The correlation is surprisingly robust.

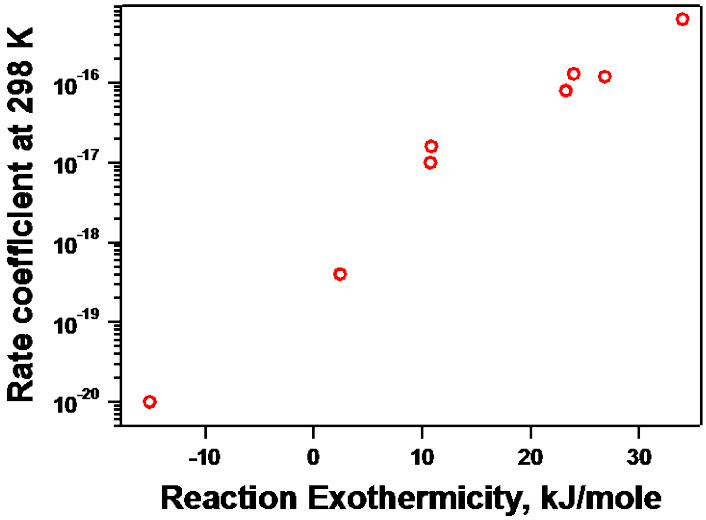

Figure 4-6 Rate coefficients (on a log scale) versus the exothermicity for each reaction of alkanes with NO_3 radicals studied here.

4 Conclusions and atmospheric implication

Note that we cannot calculate the atmospheric lifetimes of alkanes due to their reaction with NO_3 since NO_3 and alkanes are not well-mixed in the atmosphere (except for methane). However, to get an estimate of the contributions to the loss rates of the alkanes, we can estimate the contribution of NO_3 reaction by using the rate coefficients measured here.

$$\tau = \frac{1}{k_{voc}[X]}$$

In this calculation, [X] represents the concentration of typical atmospheric oxidants (OH, Cl, NO_3 and O_3) and k is the rate constant of the reactions between the oxidants at 298 K. The relative contribution of NO_3 radicals reactions, compared to those from OH radical and atomic Cl are shown in Table 4-5. Clearly, their reaction with NO_3 contributes negligibly to the lifetimes of alkanes. However, these reactions could indeed contribute to the removal of NO_3 in regions with high alkane concentrations, such as in the regions affected by oil/gas extraction activities.

Table 4-5 Rate constants and estimated the rough contribution of NO_3 reactions to the loss of alkanes in the atmosphere relative to those via their reactions with OH radicals and Cl atoms.

	Rate constants (cm^3 $molecule^{-1}s^{-1}$)			Rough Chemical Lifetime (hours) at 298 K*		
	k_{OH}	k_{Cl}	k_{NO3}	τ_{OH}	□ $_{Cl}$	□ $_{NO3}$
methane	6.4×10^{-15} [a]	1.0×10^{-15} [a]	$<4\times10^{-20}$	43403	2.78E+07	4.03E+07
ethane	2.4×10^{-13} [a]	5.8×10^{-11} [a]	$<5\times10^{-19}$	1157	479	1.33E+06
propane	1.1×10^{-12} [a]	1.4×10^{-10} [a]	9.2×10^{-18}	253	198	5.75E+04
n-butane	2.35×10^{-12} [a]	1.91×10^{-10} [b]	1.9×10^{-17}	118	145	3.54E+04
iso-butane	2.1×10^{-12} [a]	1.4×10^{-10} [c]	8.2×10^{-17}	132	198	6.75E+03
2,3-dimethybutane	2.42×10^{-12} [e]	2.31×10^{-10} [d]	5.8×10^{-16}	115	120	8.78E+02
cyclopentane	6.97×10^{-12} [e]	2.41×10^{-10} [d]	1.4×10^{-16}	40	115	4.37E+03
cyclohexane	5.78×10^{-12} [e]	2.01×10^{-10} [f]	1.3×10^{-16}	48	138	4.48E+03

a (Atkinson et al. 2006) b (Qian et al. 2001)

c (Beichert et al. 1995) d (Rowley et al. 1992)

e (Atkinson 2003) f (Hooshiyar and Niki 1995)

Supporting information

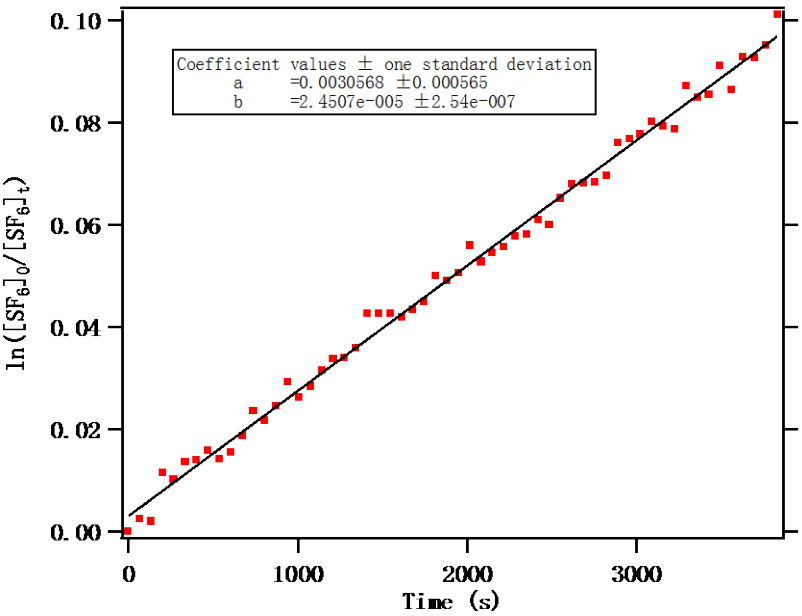

Figure 4-1S The first order decay rate of SF_6 in the chamber

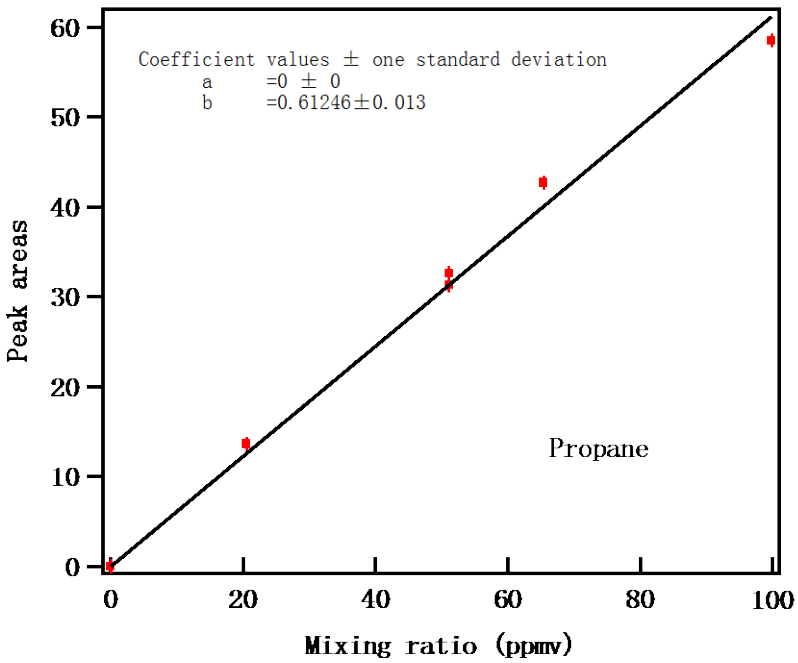

Figure 4S-2 Calibration of propane in FTIR.

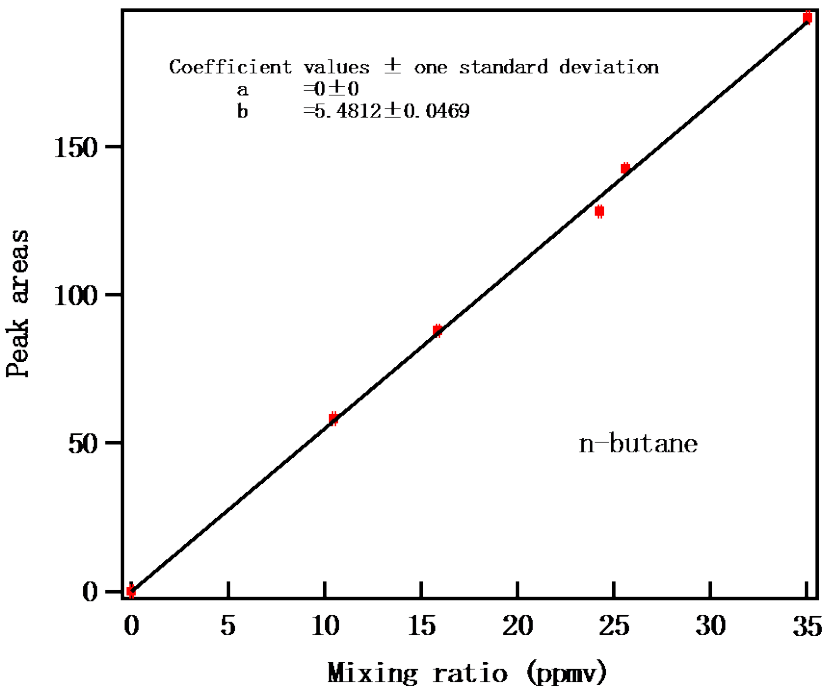

Figure 4S-3 Calibration of n-butane in FTIR.

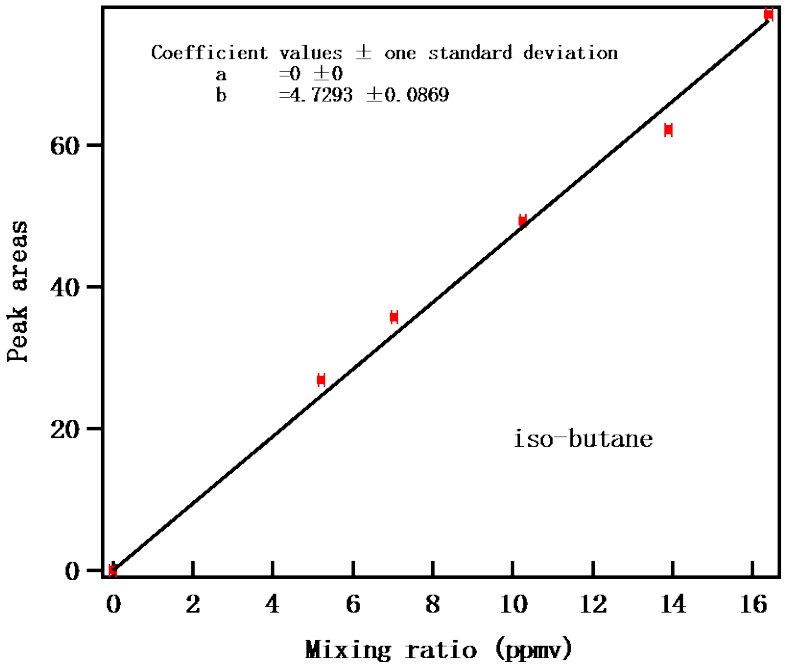

Figure 4S-4 Calibration of iso-butane in FTIR.

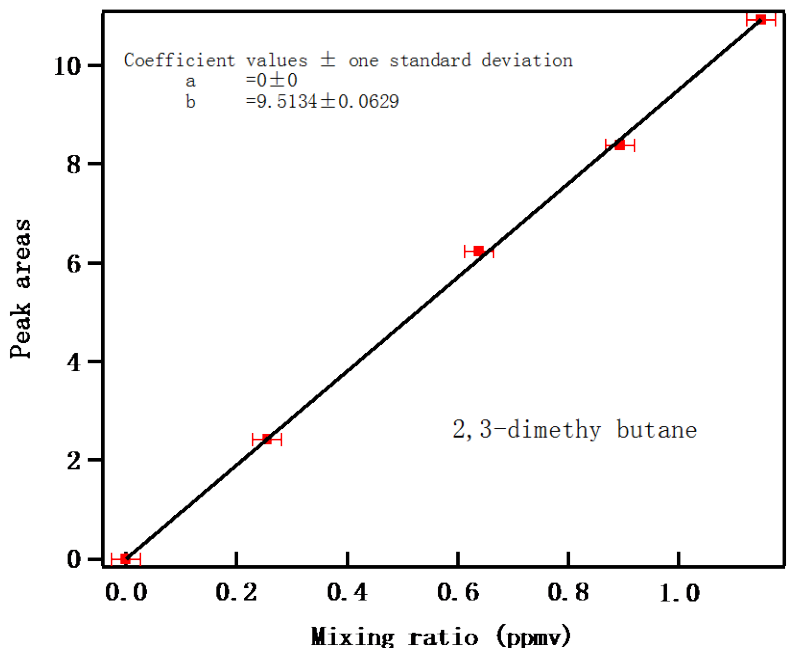

Figure 4S-5 Calibration of 2,3-dimethy-butane in FTIR.

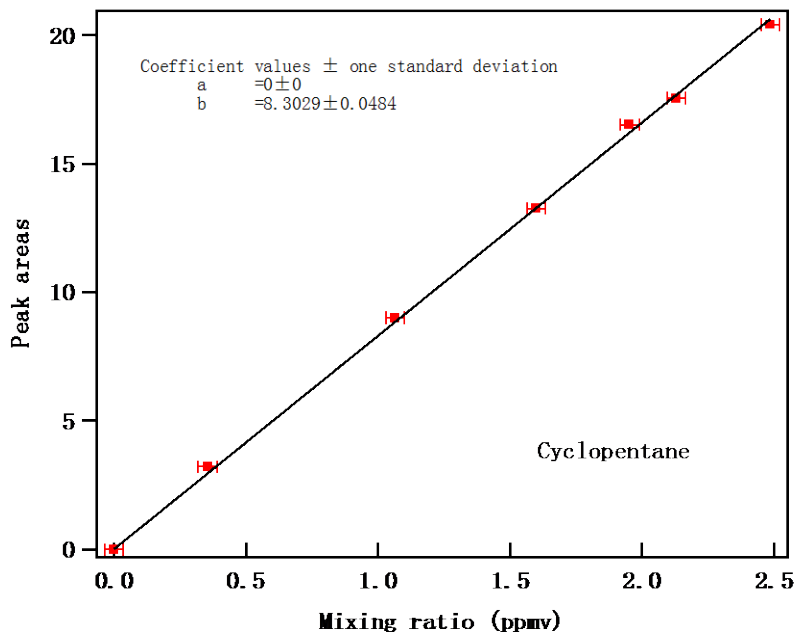

Figure 4S-6 Calibration of cyclopentane in FTIR.

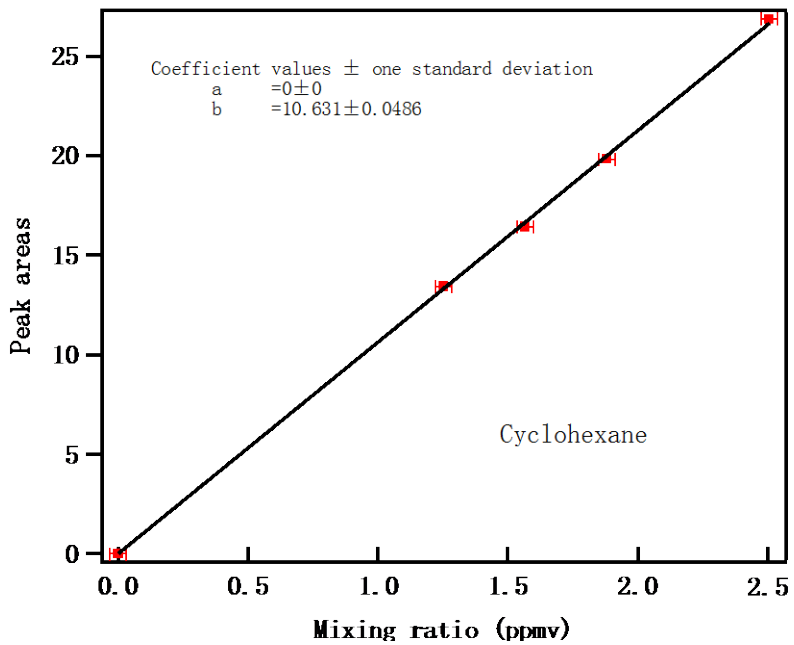

Figure 4S-7 Calibrations of each cyclohexane in FTIR

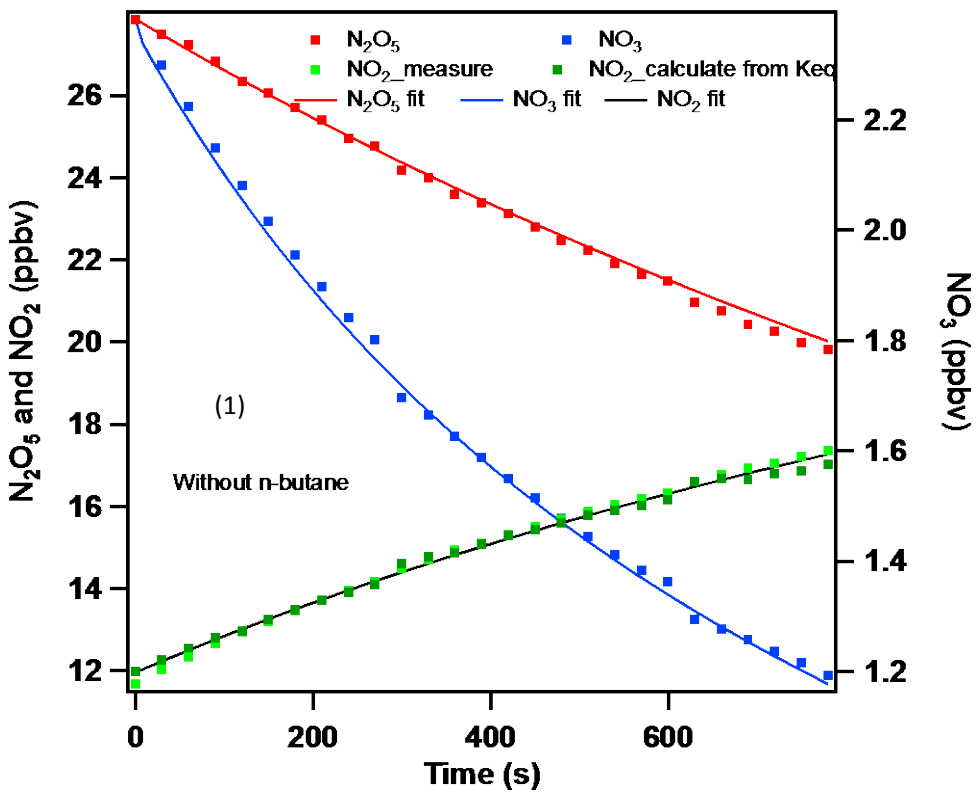

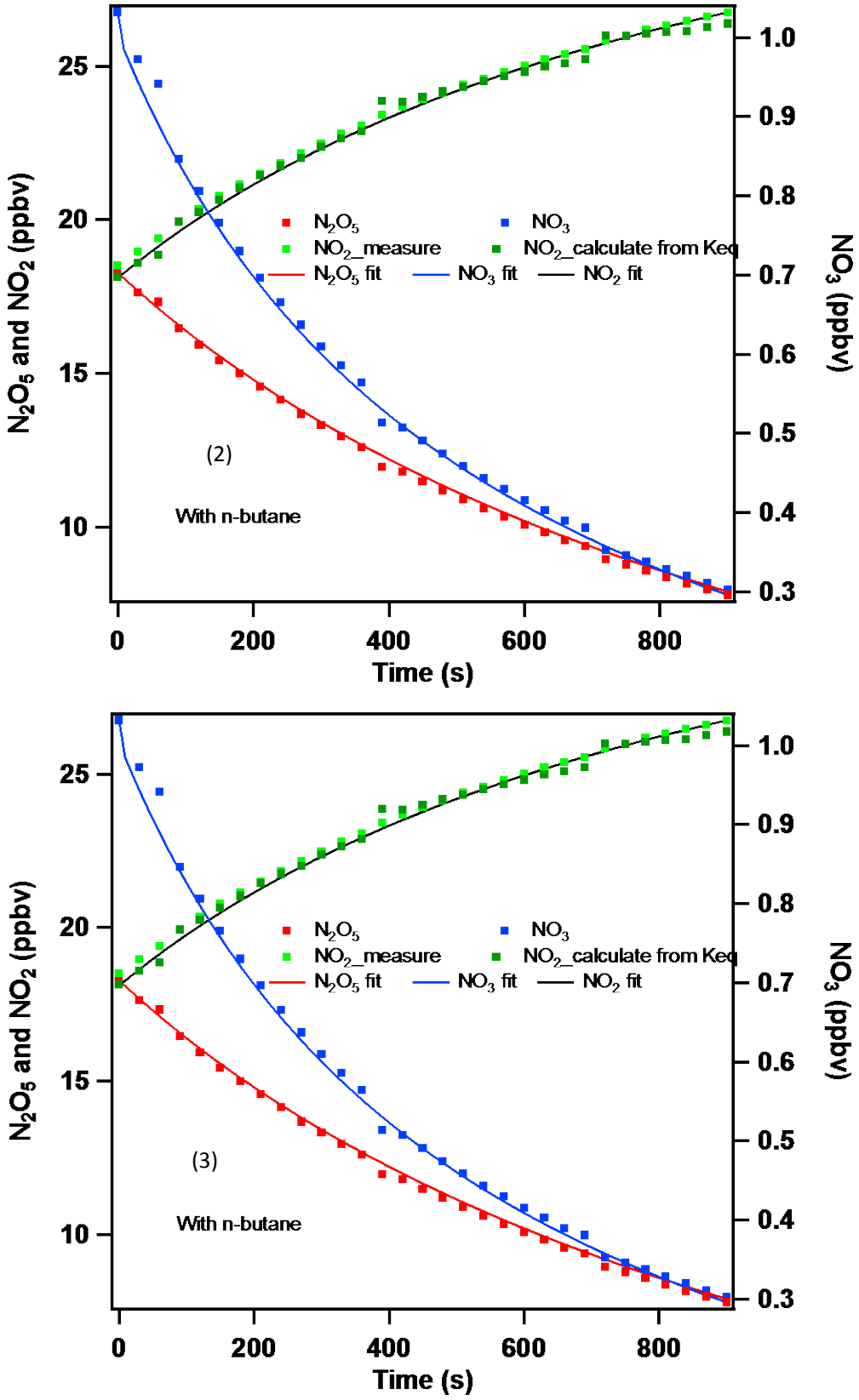

Figure 4S-8 Experimental and simulated results for NO_3, N_2O_5 and NO_2 profiles from chamber experiments. The observed NO_3, N_2O_5 and NO_2 mixing ratios (circles

and triangles) and their simulated temporal profiles (lines) are fit in two conditions (1) without n-butane (2) the mixing ratios of n-butane was 19.72 ppmv. Reaction schemes were R1, R2, R3, R4 and R5. The fits yield a value of $k_{VOC} = 3.10 \times 10^{-17}$ molecule^{-1} cm^3 s^{-1} (3) the mixing ratios of n-butane was 19.72 ppmv. Reaction schemes were R1, R2, R3, R4, R5, R7, R8, R9 and R10.The fits yield a value of $k_{VOC} = 1.50 \times 10^{-17}$

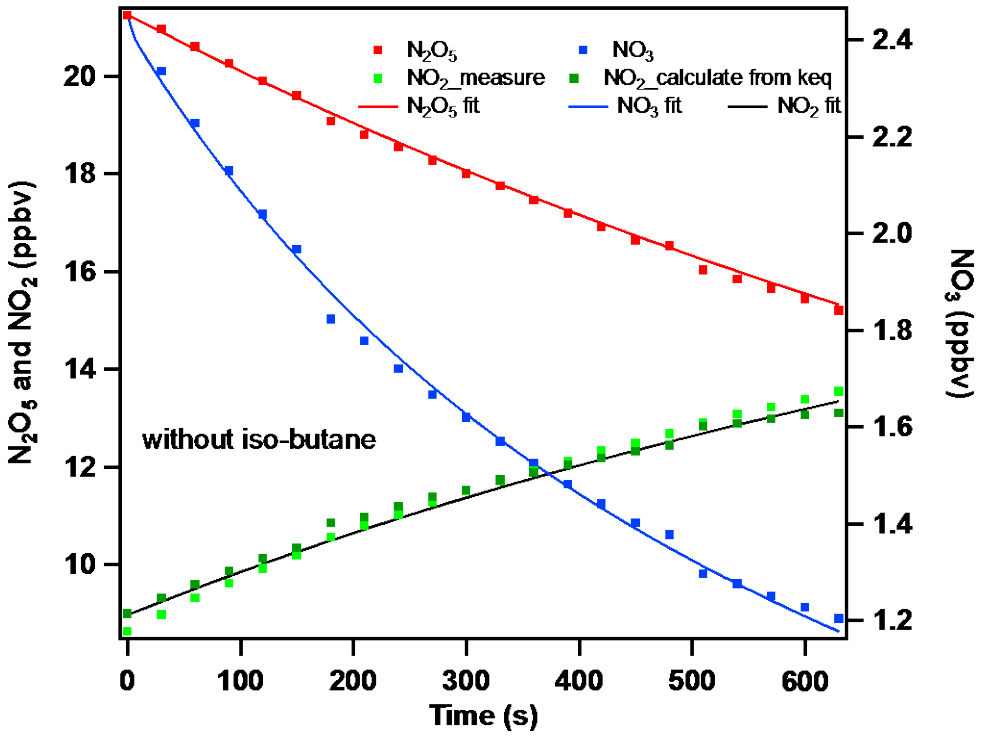

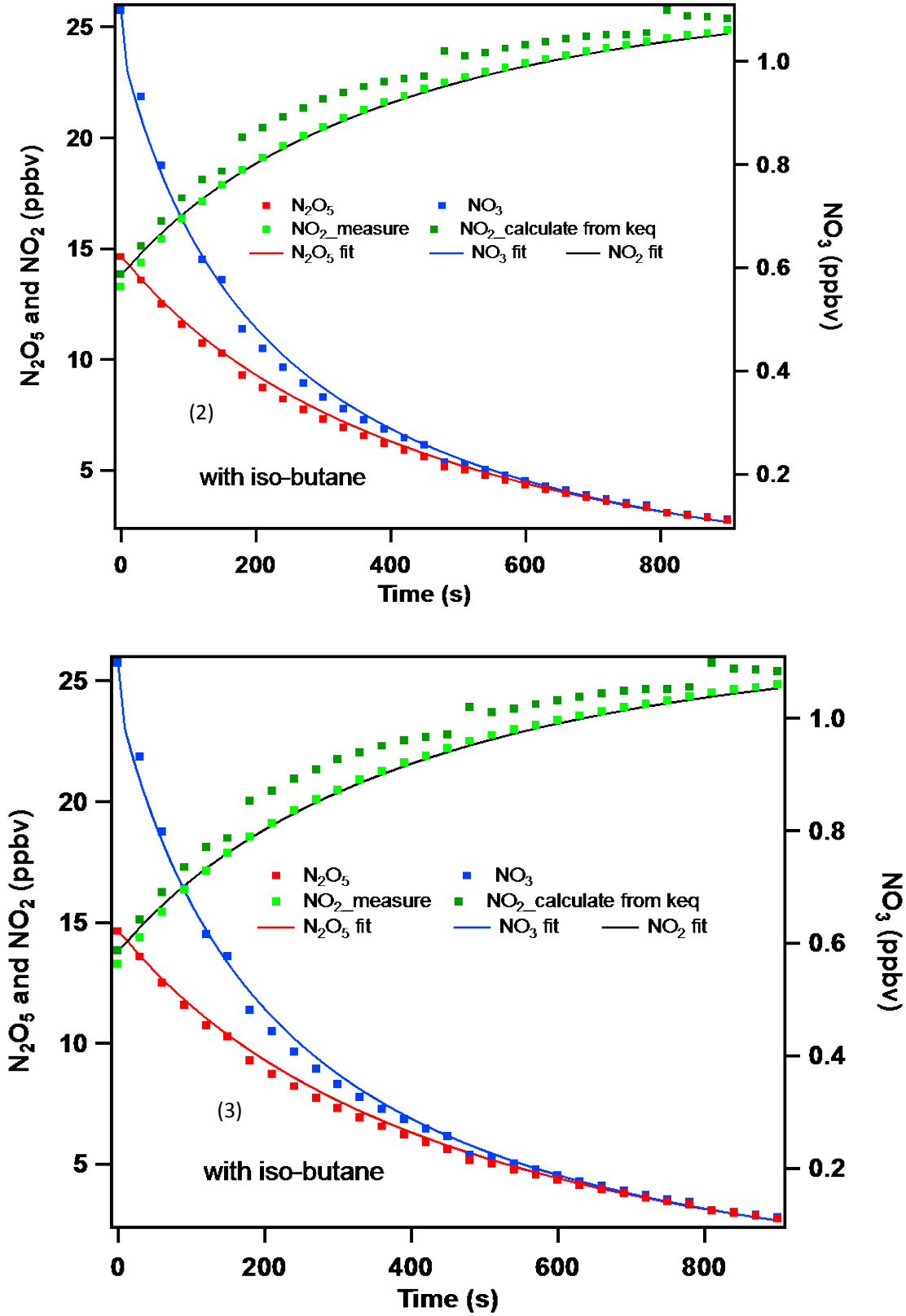

Figure 4S-9 Experimental and simulated results for NO_3, N_2O_5 and NO_2 profiles from chamber experiments. The observed NO_3, N_2O_5 and NO_2 mixing ratios (circles and triangles) and their simulated temporal profiles (lines) are fit in two conditions (1)

without iso-butane (2) the mixing ratios of iso-butane was 10.26 ppmv. Reaction schemes were R1, R2, R3, R4 and R5. The fits yield a value of $k_{VOC} = 1.40 \times 10^{-16}$ molecule^{-1} cm^{3} s^{-1} (3) the mixing ratios of iso-butane was 10.26 ppmv. Reaction schemes were R1, R2, R3, R4, R5, R7, R8, R9 and R10.The fits yield a value of $k_{VOC} = 7.90 \times 10^{-17}$

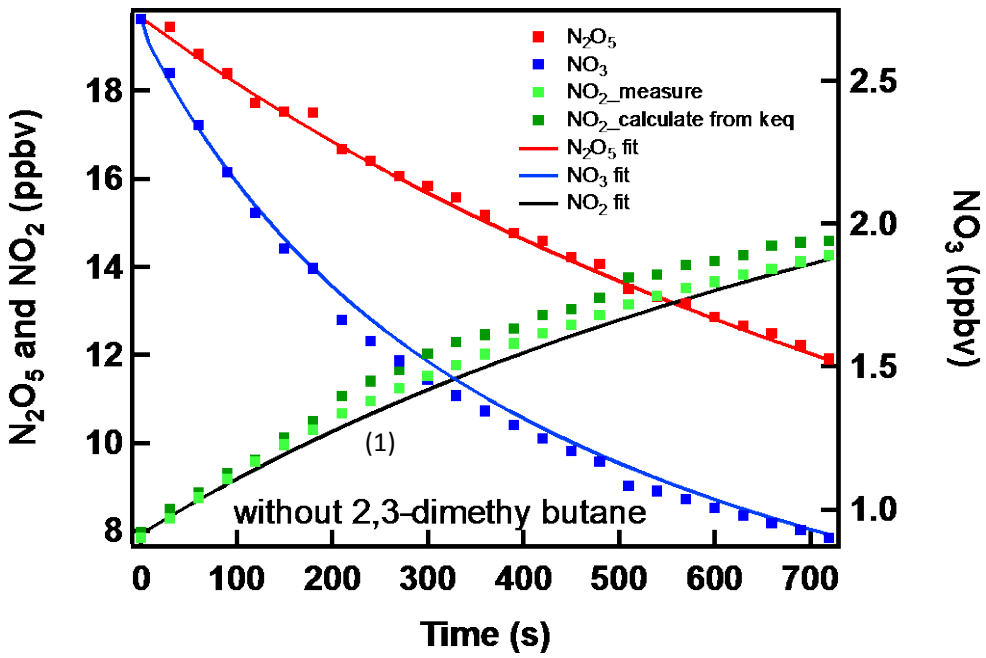

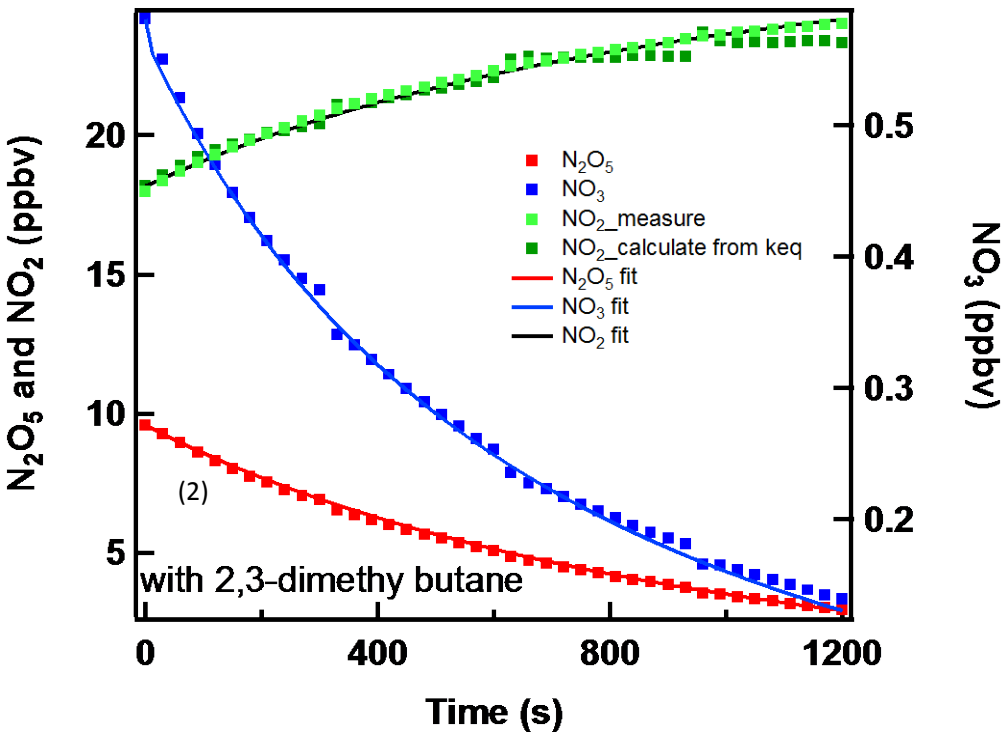

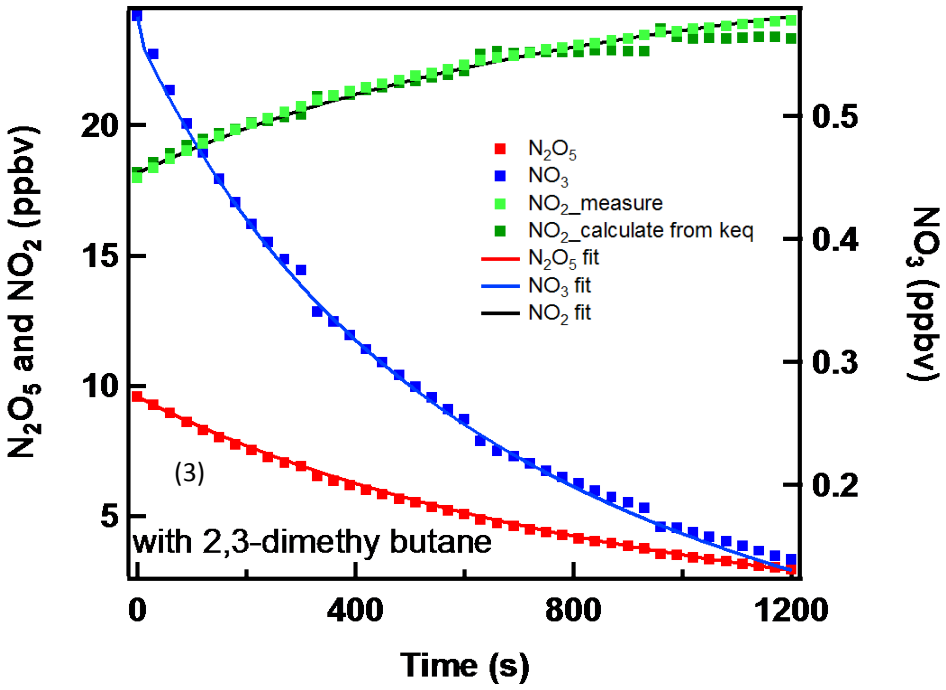

Figure 4S-10 Experimental and simulated results for NO_3, N_2O_5 and NO_2 profiles from chamber experiments. The observed NO_3, N_2O_5 and NO_2 mixing ratios (circles and triangles) and their simulated temporal profiles (lines) are fit in two conditions (1) without methane (2) the mixing ratios of methane was 0.38 ppmv. Reaction schemes were R1, R2, R3, R4 and R5. The fits yield a value of $k_{VOC} = 1.25 \times 10^{-15}$

molecule^{-1} cm^{3} s^{-1} (3) the mixing ratios of methane was 0.38 ppmv. Reaction schemes were R1, R2, R3, R4, R5, R7, R8, R9 and R10.The fits yield a value of $k_{VOC} = 6.50 \times 10^{-16}$ molecule^{-1} cm^{3} s^{-1}

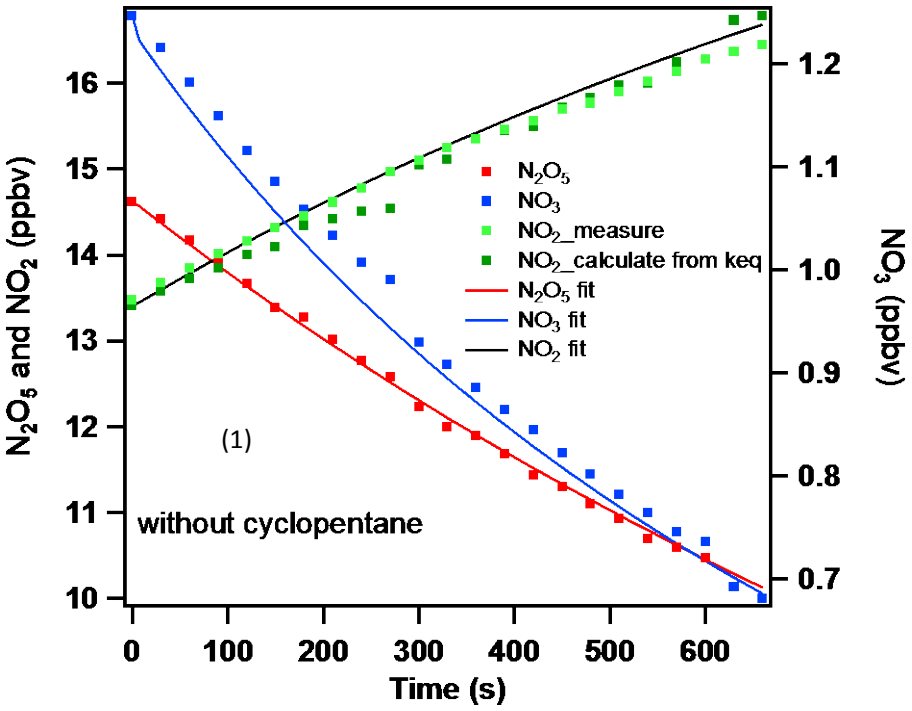

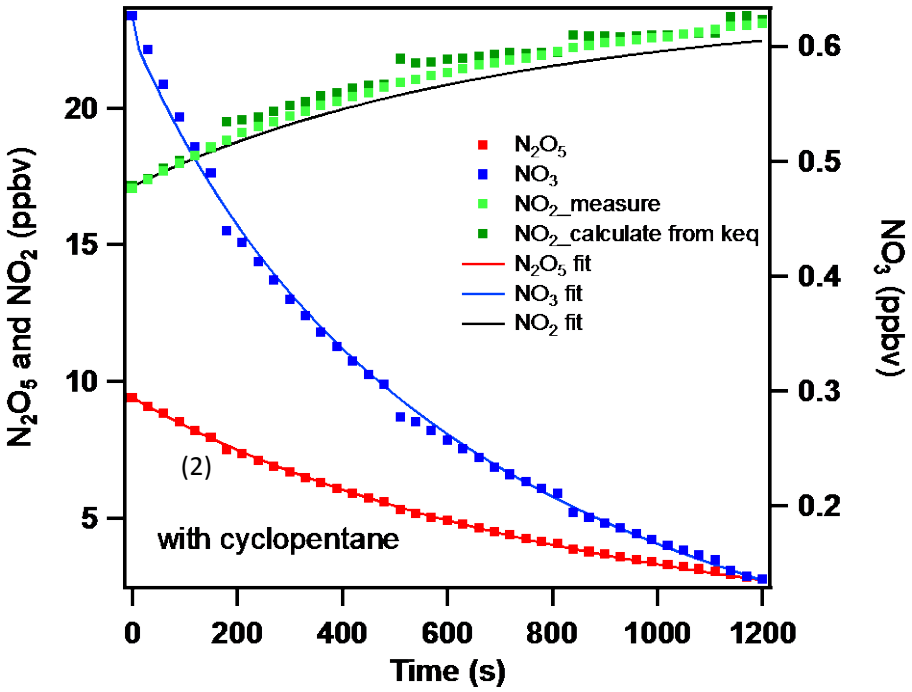

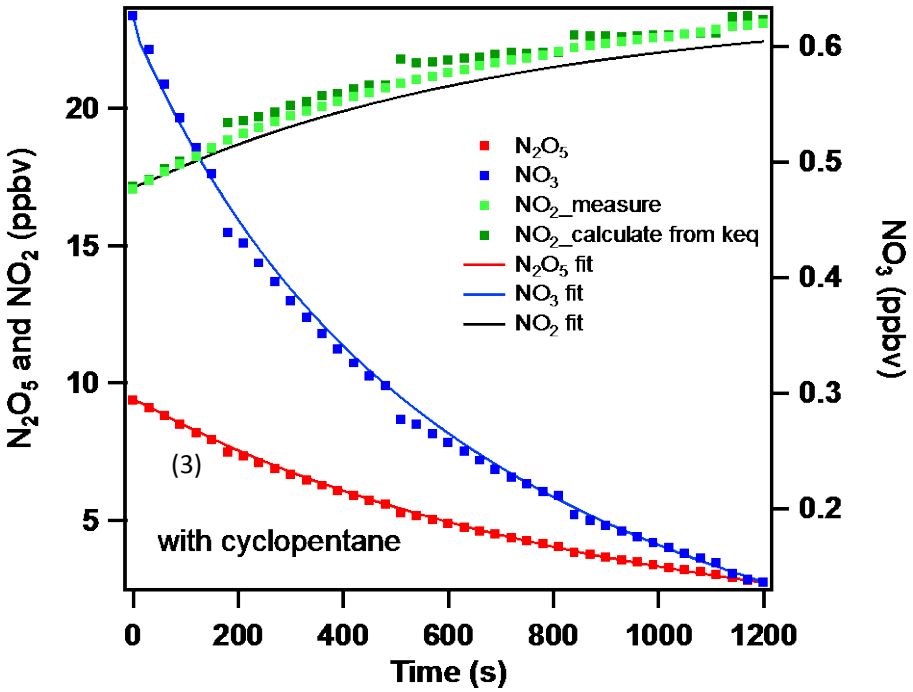

Figure 4S-11 Experimental and simulated results for NO_3, N_2O_5 and NO_2 profiles from chamber experiments. The observed NO_3, N_2O_5 and NO_2 mixing ratios (circles and triangles) and their simulated temporal profiles (lines) are fit in two conditions (1) without cyclopentane (2) the mixing ratios of cyclopentane was 0.63ppmv. Reaction schemes were R1, R2, R3, R4 and R5. The fits yield a value of $k_{VOC} = 2.61 \times 10^{-16}$ molecule^{-1} cm^3 s^{-1} (3) the mixing ratios of cyclopentane was 0.63 ppmv. Reaction schemes were R1, R2, R3, R4, R5', R7, R8, R9 and R10. The fits yield a value of $k_{VOC} = 1.31 \times 10^{-16}$ molecule^{-1} cm^3 s^{-1}

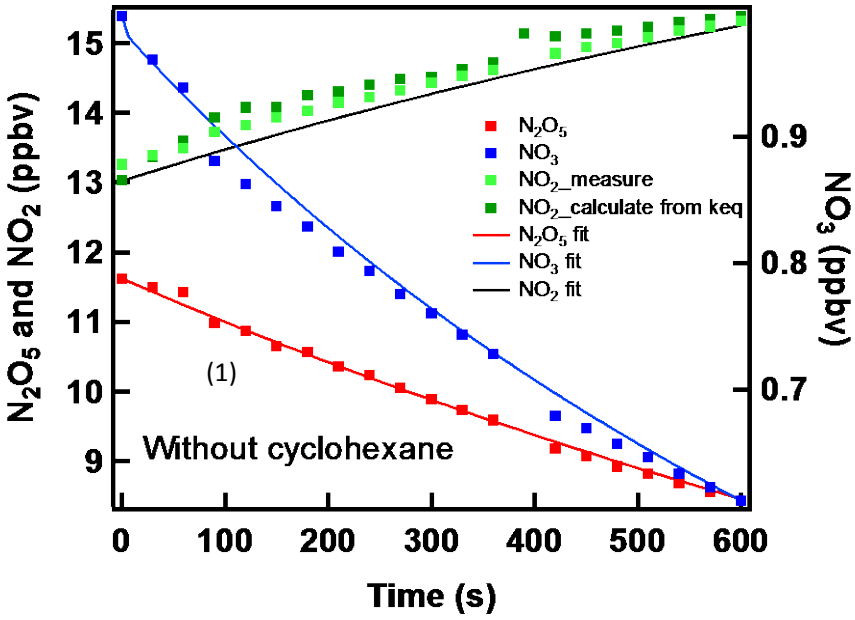
N2O5 and NO2 (ppbv)
NO3 (ppbv)
Time (s)
N2O5
NO3
NO2_measure
NO2_calculate from keq
N2O5 fit
NO3 fit
NO2 fit
(1)
Without cyclohexane

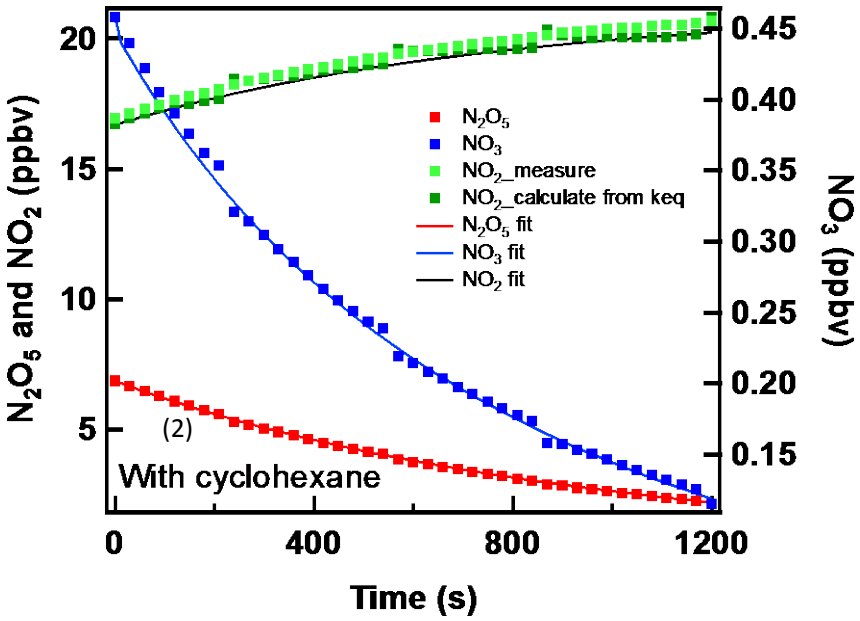
N2O5 and NO2 (ppbv)
NO3 (ppbv)
Time (s)
N2O5
NO3
NO2_measure
NO2_calculate from keq
N2O5 fit
NO3 fit
NO2 fit
(2)
With cyclohexane

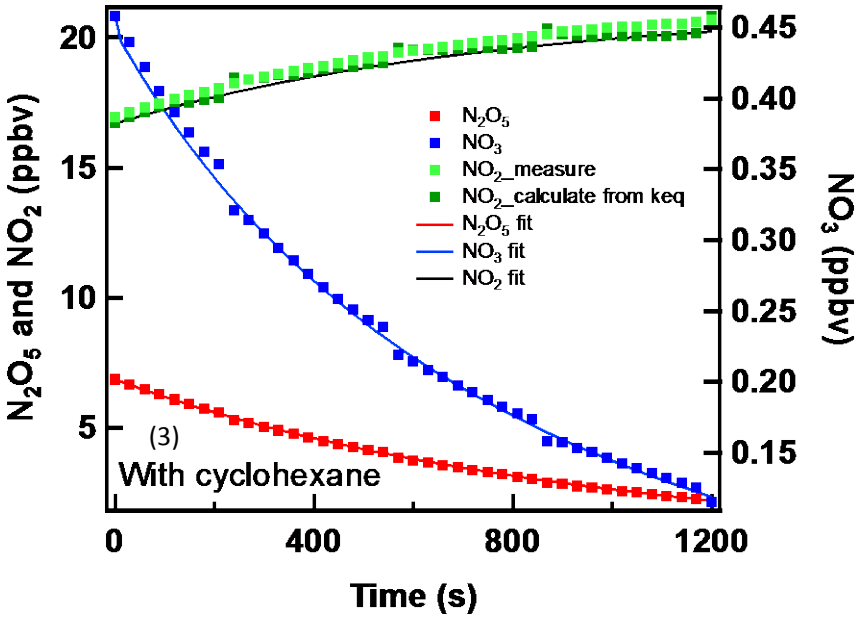

Figure 4S-12 Experimental and simulated results for NO_3, N_2O_5 and NO_2 profiles from chamber experiments. The observed NO_3, N_2O_5 and NO_2 mixing ratios (circles and triangles) and their simulated temporal profiles (lines) are fit in two conditions (1) without methane (2) the mixing ratios of methane was 1.54 ppmv. Reaction schemes were R1, R2, R3, R4 and R5. The fits yield a value of $k_{VOC} = 2.50 \times 10^{-16}$ molecule^{-1} cm^3 s^{-1} (3) the mixing ratios of methane was 1.54 ppmv. Reaction schemes were R1, R2, R3, R4, R5, R7, R8, R9 and R10. The fits yield a value of $k_{VOC} = 1.32 \times 10^{-16}$ molecule^{-1} cm^3 s^{-1}

Table 4-1S: Reactions of the products of the NO_3 reaction with alkanes in the presence of O_2 and nitrogen oxides those were included in simulating the temporal profiles of NO_3 and N_2O_5.

	Reaction	Rate coefficients at 298 K and 1 bar of air	ref
	Alkyl radical + O_2 → RO_2	10^{-11} cm^3 $molecule^{-1}s^{-1}$	Atkinson et al. 2004
R7	***RO_2 +NO_3 → RO + NO_2+O_2***	(C>2)2.3×$10^{-12}$$cm^3$$molecule^{-1}s^{-1}$	MCM
	CH_3O_2+NO_3	1.2×10^{-12} cm^3 $molecule^{-1}s^{-1}$	Daele et al. 1995
	$C_2H_5O_2$+NO_3	2.3×10^{-12} cm^3 $molecule^{-1}s^{-1}$	Ray et al. 1996, Vaughan et al. 2006
R8-R10	***2RO_2 →2RO (0.6)*** ***→ 2ROH (0.2)*** ***→ 2R_1CHO (0.2)***		Atkinson et al. 2006 IUPAC
	CH_3O_2 →CH_3O or CH_3OH or HCHO	3.5×10^{-13} cm^3 $molecule^{-1}s^{-1}$	Atkinson et al. 2006
	$C_2H_5O_2$ →C_2H_5O or C_2H_5OH or CH_3CHO	7.6×10^{-14} cm^3 $molecule^{-1}s^{-1}$	Atkinson et al. 2006
	n-$C_3H_7O_2$→n-C_3H_7O or C_2H_5CHO or n-C_3H_7OH	3×10^{-13} cm^3 $molecule^{-1}s^{-1}$	Atkinson et al. 2006
	i-$C_3H_7O_2$ → i-C_3H_7OH or $CH_3C(O)CH_3$ or i-C_3H_7O	1×10^{-15} cm^3 $molecule^{-1}s^{-1}$	Atkinson et al. 2006
	s-$C_4H_9O_2$ → s-C_4H_9O or s-C_4H_9OH	2.5×10^{-13} cm^3 $molecule^{-1}s^{-1}$	MCM
	t-$C_4H_9O_2$ → t-C_4H_9O or t-C_4H_9OH	6.7×10^{-15} cm^3 $molecule^{-1}s^{-1}$	MCM
	CHEXO2→ CHEXO or CHEXOL or CHEXONE	2.5×10^{-13} cm^3 $molecule^{-1}s^{-1}$	MCM
R11-R12	***RO_2+NO_2→ RO_2NO_2***		Atkinson et al. 2004
	RO_2NO_2→RO_2+NO_2		Atkinson et al. 2004
	CH_3O_2+NO_2 → $CH_3O_2NO_2$	4.0×10^{-12} cm^3 $molecule^{-1}s^{-1}$	Atkinson et al. 2004
	$CH_3O_2NO_2$→ CH_3O_2+NO_2	1.5 s^{-1}	Atkinson et al. 2004
	$C_2H_5O_2$+NO_2 → $C_2H_5O_2NO_2$	5.1×10^{-12} cm^3 $molecule^{-1}s^{-1}$	Atkinson et al. 2004
	$C_2H_5O_2NO_2$→ $C_2H_5O_2$+NO_2	3.4 s^{-1}	Atkinson et al. 2004
R13-R14	***RO+O_2→ R_1CHO+HO_2***	7.14×10^{-14} cm^3 $molecule^{-1}s^{-1}$	
	RO_2+HO_2→ROOH+O_2		
	CH_3O_2+HO_2 → CH_3OOH	5.2×10^{-12} cm^3 $molecule^{-1}s^{-1}$	IUPAC

	$C_2H_5O_2+HO_2 \rightarrow C_2H_5OOH$	7.97×10^{-12} cm^3 $molecule^{-1}s^{-1}$	MCM
	$i\text{-}C_3H_7O_2+HO_2 \rightarrow i\text{-}C_3H_7OOH$	1.19×10^{-11} cm^3 $molecule^{-1}s^{-1}$	MCM
	$s\text{-}C_4H_9O_2+HO_2 \rightarrow s\text{-}C_4H_9OOH$	1.43×10^{-11} cm^3 $molecule^{-1}s^{-1}$	MCM
	$t\text{-}C_4H_9O_2+HO_2 \rightarrow t\text{-}C_4H_9OOH$	1.43×10^{-11} cm^3 $molecule^{-1}s^{-1}$	MCM
	M23C43O2+HO2	1.76×10^{-11} cm^3 $molecule^{-1}s^{-1}$	MCM
	CHEXO2+HO2	1.76×10^{-11} cm^3 $molecule^{-1}s^{-1}$	MCM
R15	$R_3CHO+NO_3 \rightarrow R_3COOO+HNO_3$		
	$HCHO+NO_3$	5.5×10^{-16} cm^3 $molecule^{-1}s^{-1}$	IUPAC
	$CH_3CHO+NO_3$	2.7×10^{-15} cm^3 $molecule^{-1}s^{-1}$	IUPAC
	CH3COCH3+NO3	$<3\times10^{-17}$ cm^3 $molecule^{-1}s^{-1}$	
R16	$HO_2+NO_3 \rightarrow OH+NO_2+O_2$	4×10^{-12} cm^3 $molecule^{-1}s^{-1}$	IUPAC
R17	$OH+NO_3 \rightarrow HO_2+NO_2$	2×10^{-11} cm^3 $molecule^{-1}s^{-1}$	IUPAC
R18	$NO_2+OH \rightarrow HONO_2/HOONO$	6.5×10^{-11} cm^3 $molecule^{-1}s^{-1}$	IUPAC
R19-R27	Related to the impurities		

M23C43O2 is the RO2 from 2,3-dimethybutane.

CHEXO2 is the RO2 from cyclohexane.

References

Atkinson, R. (2003) Kinetics of the gas-phase reactions of OH radicals with alkanes and cycloalkanes. *Atmospheric Chemistry and Physics,* 3**,** 2233-2307.

Atkinson, R., S. M. Aschmann & J. N. Pitts Jr (1988) Rate constants for the gas-phase reactions of the nitrate radical with a series of organic compounds at 296.+-. 2 K. *The Journal of Physical Chemistry,* 92**,** 3454-3457.

Atkinson, R., D. L. Baulch, R. A. Cox, J. N. Crowley, R. F. Hampson, R. G. Hynes, M. E. Jenkin, M. J. Rossi & J. Troe (2004) Evaluated kinetic and photochemical data for atmospheric chemistry: Volume I - gas phase reactions of Ox, HOx, NOx and SOx species. *Atmospheric Chemistry and Physics,* 4**,** 1461-1738.

Atkinson, R., D. L. Baulch, R. A. Cox, J. N. Crowley, R. F. Hampson, R. G. Hynes, M. E. Jenkin, M. J. Rossi, J. Troe & I. Subcommittee (2006) Evaluated kinetic and photochemical data for atmospheric chemistry: Volume II – gas phase reactions of organic species. *Atmospheric Chemistry and Physics (Print),* 6**,** 3625-4055.

Atkinson, R., C. N. Plum, W. P. Carter, A. M. Winer & J. N. Pitts Jr (1984) Kinetics of the gas-phase reactions of nitrate (NO_3) radicals with a series of alkanes at 296.+-. 2 K. *The Journal of Physical Chemistry,* 88**,** 2361-2364.

Bagley, J. A., C. Canosa-Mas, M. R. Little, A. D. Parr, S. J. Smith, S. J. Waygood & R. P. Wayne (1990) Temperature dependence of reactions of the nitrate radical with alkanes. *Journal of the Chemical Society, Faraday Transactions,* 86**,** 2109-2114.

Baldwin, R. R., G. R. Drewery & R. W. Walker (1984) Decomposition of 2, 3-dimethylbutane in the presence of oxygen. Part 2.—Elementary reactions involved in the formation of products. *Journal of the Chemical Society, Faraday Transactions 1: Physical Chemistry in Condensed Phases,* 80**,** 3195-3207.

Beichert, P., L. Wingen, J. Lee, R. Vogt, M. J. Ezell, M. Ragains, R. Neavyn & B. J.

Finlaysonpitts (1995) Rate constants for the reactions of chlorine atoms with some simple alkanes at 298 k - measurement of a self-consistent set using both absolute and relative rate methods. *Journal of Physical Chemistry,* 99**,** 13156-13162.

Boyd, A. A., C. E. Canosa-Mas, A. D. King, R. P. Wayne & M. R. Wilson (1991) Use of a stopped-flow technique to measure the rate constants at room temperature for reactions between the nitrate radical and various organic species. *Journal of the Chemical Society, Faraday Transactions,* 87**,** 2913-2919.

Brown, S. S. (2003) Absorption spectroscopy in high-finesse cavities for atmospheric studies. *Chemical Reviews,* 103**,** 5219-5238.

Brown, S. S., W. P. Dubé, J. Peischl, T. B. Ryerson, E. Atlas, C. Warneke, J. A. de Gouw, S. te Lintel Hekkert, C. A. Brock, F. Flocke, M. Trainer, D. D. Parrish, F. C. Feshenfeld & A. R. Ravishankara (2011) Budgets for nocturnal VOC oxidation by nitrate radicals aloft during the 2006 Texas Air Quality Study. *Journal of Geophysical Research: Atmospheres,* 116**,** n/a-n/a.

Brown, S. S., H. Stark, S. J. Ciciora, R. J. McLaughlin & A. R. Ravishankara (2002a) Simultaneous in situ detection of atmospheric NO_3 and N_2O_5 via cavity ring-down spectroscopy. *Review of Scientific Instruments,* 73**,** 3291-3301.

Brown, S. S., H. Stark & A. R. Ravishankara (2002b) Cavity ring-down spectroscopy for atmospheric trace gas detection: application to the nitrate radical (NO_3). *Applied Physics B-Lasers and Optics,* 75**,** 173-182.

Burrows, J. P., G. S. Tyndall & G. K. Moortgat (1985) Absorption spectrum of NO3 and kinetics of the reactions of NO_3 with NO_2, Cl, and several stable atmospheric species at 298 K. *The Journal of Physical Chemistry,* 89**,** 4848-4856.

Cantrell, C. A., J. A. Davidson, R. E. Shetter, B. A. Anderson & J. G. Calvert (1987) Reactions of nitrate radical and nitrogen oxide (N_2O_5) with molecular species of possible atmospheric interest. *The Journal of Physical Chemistry,* 91**,** 6017-6021.

Castelhano, A. L. & D. Griller (1982) Heats of formation of some simple alkyl radicals. *Journal of the American Chemical Society,* 104**,** 3655-3659.

Daele, V., G. Laverdet, G. Le Bras & G. Poulet (1995) Kinetics of the Reactions CH_3O + NO, CH_3O + NO_3, and CH_3O_2 + NO_3. *The Journal of Physical Chemistry,* 99**,** 1470-1477.

Davidson, J. A., A. A. Viggiano, C. J. Howard, I. Dotan, F. C. Fehsenfeld, D. L. Albritton & E. E. Ferguson (1978) Rate constants for reactions OF O_2^+, NO_2^+, NO^+, H_3O^+, CO_3^-, NO_2^-, and halide ions with N_2O_5 at 300 K. *Journal of Chemical Physics,* 68**,** 2085-2087.

Dorn, H. P., R. L. Apodaca, S. M. Ball, T. Brauers, S. S. Brown, J. N. Crowley, W. P. Dube, H. Fuchs, R. Haeseler, U. Heitmann, R. L. Jones, A. Kiendler-Scharr, I. Labazan, J. M. Langridge, J. Meinen, T. F. Mentel, U. Platt, D. Poehler, F. Rohrer, A. A. Ruth, E. Schlosser, G. Schuster, A. J. L. Shillings, W. R. Simpson, J. Thieser, R. Tillmann, R. Varma, D. S. Venables & A. Wahner (2013) Intercomparison of NO_3 radical detection instruments in the atmosphere simulation chamber SAPHIR. *Atmospheric Measurement Techniques,* 6**,** 1111-1140.

Dube, W. P., S. S. Brown, H. D. Osthoff, M. R. Nunley, S. J. Ciciora, M. W. Paris, R. J. McLaughlin & A. R. Ravishankara (2006) Aircraft instrument for simultaneous, in situ measurement of NO3 and N2O5 via pulsed cavity ring-down spectroscopy. *Review of Scientific Instruments,* 77.

Fuchs, H., W. P. Dube, S. J. Cicioira & S. S. Brown (2008) Determination of inlet transmission and conversion efficiencies for in situ measurements of the nocturnal nitrogen oxides, NO_3, N_2O_5 and NO_2, via pulsed cavity ring-down spectroscopy. *Analytical Chemistry,* 80**,** 6010-6017.

Fuchs, H., W. R. Simpson, R. L. Apodaca, T. Brauers, R. C. Cohen, J. N. Crowley, H. P. Dorn, W. P. Dubé, J. L. Fry, R. Häseler, Y. Kajii, A. Kiendler-Scharr, I. Labazan, J. Matsumoto, T. F. Mentel, Y. Nakashima, F. Rohrer, A. W. Rollins, G. Schuster, R. Tillmann, A. Wahner, P. J. Wooldridge & S. S. Brown (2012)

Comparison of N_2O_5 mixing ratios during NO3Comp 2007 in SAPHIR. *Atmospheric Measurement Techniques,* 5**,** 2763-2777.

Hooshiyar, P. A. & H. Niki (1995) Rate constants for the gas-phase reactions of Cl-atoms with C2-C8 alkanes at T = 296 ± 2 K. *International Journal of Chemical Kinetics,* 27**,** 1197-1206.

J. B. Burkholder, S. P. S., J. P. D. Abbatt,J. R. Barker,R. E. Huie,C. E. Kolb,M. J. Kurylo,V. L. Orkin,D. M. Wilmouth,P. H. Wine (2015) Chemical Kinetics and Photochemical Data for Use in Atmospheric Studies.

Kebabian, P. L., E. C. Wood, S. C. Herndon & A. Freedman (2008) A Practical Alternative to Chemiluminescence-Based Detection of Nitrogen Dioxide: Cavity Attenuated Phase Shift Spectroscopy. *Environmental Science & Technology,* 42**,** 6040-6045.

Qian, H. B., D. Turton, P. W. Seakins & M. J. Pilling (2001) A laser flash photolysis/IR diode laser absorption study of the reaction of chlorine atoms with selected alkanes. *International Journal of Chemical Kinetics,* 34**,** 86-94.

Ray, A., V. Daële, I. Vassalli, G. Poulet & G. Le Bras (1996) Kinetic Study of the Reactions of C_2H_5O and $C_2H_5O_2$ with NO_3 at 298 K. *The Journal of Physical Chemistry,* 100**,** 5737-5744.

Rowley, D. M., R. Lesclaux, P. D. Lightfoot, B. Noziere, T. J. Wallington & M. D. Hurley (1992) Kinetic and mechanistic studies of the reactions of cyclopentylperoxy and cyclohexylperoxy radicals with HO_2. *Journal of Physical Chemistry,* 96**,** 4889-4894.

Vaughan, S., C. E. Canosa-Mas, C. Pfrang, D. E. Shallcross, L. Watson & R. P. Wayne (2006) Kinetic studies of reactions of the nitrate radical (NO_3) with peroxy radicals (RO_2): an indirect source of OH at night? *Physical Chemistry Chemical Physics,* 8**,** 3749-3760.

Wagner, N. L., W. P. Dube, R. A. Washenfelder, C. J. Young, I. B. Pollack, T. B. Ryerson & S. S. Brown (2011) Diode laser-based cavity ring-down instrument for NO_3, N_2O_5, NO, NO_2 and O_3 from aircraft. *Atmospheric Measurement*

Techniques, 4**,** 1227-1240.

Wallington, T. J., R. Atkinson, A. M. Winer & J. N. Pitts (1986) Absolute rate constants for the gas-phase reaction of the nitrate radical with dimethyl sulfide, nitrogen dioxide, carbon monoxide and a series of alkanes at 298 .+-. 2 K. *The Journal of Physical Chemistry,* 90**,** 4640-4644.

Wild, R. J., P. M. Edwards, T. S. Bates, R. C. Cohen, J. A. de Gouw, W. P. Dubé, J. B. Gilman, J. Holloway, J. Kercher, A. R. Koss, L. Lee, B. M. Lerner, R. McLaren, P. K. Quinn, J. M. Roberts, J. Stutz, J. A. Thornton, P. R. Veres, C. Warneke, E. Williams, C. J. Young, B. Yuan, K. J. Zarzana & S. S. Brown (2016) Reactive nitrogen partitioning and its relationship to winter ozone events in Utah. *Atmospheric Chemistry and Physics,* 16**,** 573-583.

Chapitre V Exploration des voies mineures d'élimination atmosphérique du N_2O, du CO et du SO_2: réactions avec le NO_3

La méthode absolue a été utilisée pour déterminer les constantes de vitesse pour les réactions des radicaux NO_3 avec l'oxyde nitreux (N_2O), le monoxyde de carbone (CO) et le dioxyde de soufre (SO_2). Les études ont été réalisées dans une chambre de 7300 L en Téflon.

Les limites supérieures à pression atmosphérique (1000 ± 5 hPa) et à température ambiante (298 ± 1.5 K) sont $\leqslant 4.0 \times 10^{-20}$ pour N_2O, $\leqslant 4.9 \times 10^{-20}$ pour CO et $<3.6 \times 10^{-20}$ pour SO_2 (cm^3 $molécule^{-1}$ s^{-1}).

Ces résultats sont ensuite comparés à ceux trouvés dans la littérature et discutés. Les limites supérieures de ces réactions ont été dépassées d'au moins deux ordres de grandeur.

En conclusion, l'impact atmosphérique des réactions de NO_3 avec ces composés inorganiques est exposé.

Chapter V Exploration of minor pathways for the atmospheric removal of N_2O, CO and SO_2: Reactions with NO_3

Abstract

The absolute method was used to determine the rate coefficients for the reactions of NO_3 radicals with nitrous oxide (N_2O), carbon monoxide (CO) and sulfur dioxide (SO_2). The upper limits of these reactions were pushed at least two orders of magnitude. The upper limits in the units of cm^3 $molecule^{-1}$ s^{-1} at atmosphere pressure (1000±5 hPa) and room temperature (298±1.5 K) are ≤4. 0 ×10^{-20} for N_2O, ≤4. 9 ×10^{-20} for CO and ≤3. 6 ×10^{-20} for SO_2. It indicated reactions with NO_3 radicals were minor pathways for the atmospheric removal of N_2O, CO and SO_2.

1 Introduction

Nitrous oxide (N_2O) is a minor component of Earth's atmosphere, currently with a concentration of about 0.330 ppm (Pendolovska et al. 2013). Most of the N_2O emitted into the atmosphere, from natural and anthropogenic sources, is produced by microorganisms such as bacteria and fungi in soils and oceans. Soils under natural vegetation are an important source of nitrous oxide, accounting for 60% of all naturally produced emissions. Other natural sources include the oceans (35%) and atmospheric chemical reactions (5%) (Menon et al. 2007). Among industrial emissions, the production of nitric acid and adipic acid are the largest sources of nitrous oxide emissions. The adipic acid emissions specifically arise from the degradation of the nitrolic acid intermediate derived from nitration of cyclohexanone (Reimer et al. 1994, Shimizu, Tanaka and Fujimori 2000). Nitrous oxide occurs in small amounts in the atmosphere, but recently has been found to be a major scavenger of stratospheric ozone, with an impact comparable to that of CFCs. It is estimated that 30% of the N_2O in the atmosphere is the result of human activity, chiefly agriculture. (Ravishankara, Daniel and Portmann 2009)

Carbon monoxide is present in small amounts in the atmosphere, chiefly as a product of volcanic activity but also from natural and man-made fires. CO is a ubiquitous atmospheric gas and it is produced from the partial oxidation of carbon-containing compounds; it forms when there is not enough oxygen to produce carbon dioxide (CO_2). Worldwide, the largest source of carbon monoxide is natural in origin, due to photochemical reactions in the troposphere that generate about 5×10^{12} kilograms per year (Weinstock and Niki 1972). Other natural sources of CO include volcanoes, forest fires, and other forms of combustion. Carbon monoxide is a short-lived greenhouse gas and also has an indirect radiative forcing effect by elevating concentrations of methane and tropospheric ozone through chemical reactions with other atmospheric constituents (e.g., the hydroxyl radical, OH.). Through natural processes in the atmosphere, it is eventually oxidized to carbon

dioxide. Carbon monoxide is a temporary atmospheric pollutant in some urban areas, chiefly from the exhaust of internal combustion engines (including vehicles, portable and back-up generators, lawn mowers, power washers, etc.), but also from incomplete combustion of various other fuels (including wood, coal, charcoal, oil, paraffin, propane, natural gas, and trash), and large CO pollution events can be observed from space over cities (Pommier, McLinden and Deeter 2013). Due to its long lifetime in the mid-troposphere, carbon monoxide is also used as tracer of transport for pollutant plumes (Pommier et al. 2010).

SO_2 is a component of great concern and is used as the indicator for the larger group of gaseous sulfur oxides (SO_x). The largest source of SO_2 in the atmosphere is the burning of fossil fuels by power plants and other industrial facilities. Smaller sources of SO_2 emissions include: industrial processes such as extracting metal from ore; natural sources such as volcanoes; and locomotives, ships and other vehicles and heavy equipment that burn fuel with high sulfur content. SO_2 can affect both health and the environment. Short-term exposures to SO_2 can harm the human respiratory system and make breathing difficult. Children, the elderly, and those who suffer from asthma are particularly sensitive to effects of SO_2. SO_2 and other sulfur oxides can contribute to acid rain which can harm sensitive ecosystems. At high concentrations, gaseous SO_x can harm trees and plants by damaging foliage and decreasing growth. SO_2 and other sulfur oxides can also react with other compounds in the atmosphere to form fine particles that reduce visibility (haze).

Due to the high importance of these inorganic compounds in the atmosphere, their loss processes have to be determined. Among them, reactions with NO_3 are treated as minor pathways for the atmospheric removal of N_2O, CO and SO_2.

NO_3 may react with N_2O according to $NO_3+N_2O \rightarrow N_2+O_2$ or $N_2 + NO_2 + O_2$. In Cantrell et al's experiments, they did not observe loss of N_2O and determined an upper limit for the rate constant of the reaction $NO_3 + N_2O \rightarrow$ products of 2×10^{-17} cm^3 molecule s^{-1} (Cantrell et al. 1987).

A slow oxidation of CO to CO_2 in the presence of N_2O_5 was reported by Audley

et al. (Audley et al. 1980), attributed by the authors to the action of the NO_3 radicals generated from the thermal decomposition of N_2O_5. They found that NO_3 might react with CO in an exothermic process. Molecular modulation spectroscopy was applied by Burrows, Tyndall and Moortgat (Burrows, Tyndall and Moortgat 1985) to the study the reaction NO_3 + CO with NO_3 radicals generated by photolysis of a mixture of F_2 and HNO_3. The kinetics of loss of NO_3, measured by absorption in the visible, was followed in the presence of an excess of CO. No reaction was detected and an upper limit for the rate constant at 298 K of 4.0×10^{-16} cm^3 $molecule^{-1}$ s^{-1} was determined. Wallington et al. (Wallington et al. 1986) studied this reaction by a flash photolysis-flow tube technique using three different systems to generate the NO_3 radicals: pure $ClONO_2$, a mixture of Cl_2 + $ClONO_2$, and a mixture of F_2 + HNO_3. In this case, also, visible absorption spectroscopy was employed for the measurement of NO_3. No reaction was observed when CO was added, and an upper limit for this reaction at 298 ± 2 K of 3×10^{-18} cm^3 $molecule^{-1}$ s^{-1} was calculated. A 1.5 m^3 Teflon bag was used as reaction chamber by Hjorth et al. (Hjorth, Ottobrini and Restelli 1986) to follow the decay of the CO concentration when mixed with N_2O_5 and O_3. No evidence was obtained for a reaction between CO and NO_3 at (295 ± 2) K, leading to a calculated upper limit of 4×10^{-19} cm^3 $molecule^{-1}$ s^{-1}.

The kinetic of the reaction between NO_3 and SO_2 has been investigated by Burrows et al., using the same experimental system as described for the study of the reaction of NO_3 with CO (Burrows et al. 1985). They did not observe loss of SO_2 and determined an upper limit for the rate constant of the reaction 4×10^{-16} cm^3 $molecule^{-1}$ s^{-1}. Dlugokencky and Howard also studies the reaction between NO_3 radical and some atmospheric sulfur compounds (Dlugokencky and Howard 1988) and they determined an upper limit for the rate constant of the reaction 1.0×10^{-15} cm^3 $molecule^{-1}$ s^{-1}

Up to now, for N_2O, CO and SO_2, only upper limits to the room temperature rate coefficients have been determined. It would be useful to either push these limits or determine if there is a slow but measurable reaction there. In this work, an absolute

method was used to determine the rate coefficients for the reactions of NO_3 radicals with nitrous oxide (N_2O), carbon monoxide (CO) and sulfur dioxide (SO_2) at atmosphere pressure (1000±5 hPa) and room temperature (298±1.5 K). These kinetic explorations will help to understand the minor pathways for the atmospheric removal of N_2O, CO and SO_2 with NO_3. The kinetic parameters obtained will be useful to chemical modelers of the lower troposphere and assist understanding of the urban night-time troposphere chemistry.

2 Experimental section

2.1 Methods for determining rate coefficients

The kinetic studies of NO_3 reactions with N_2O, CO and SO_2 were conducted at room temperature (298.0±1.5K) in the ICARE-7300L Teflon chamber and at atmospheric pressure (1000±5hPa), similarly to our previous works. This chamber reactor and related gas handling system has been described in detail in previous chapter. During kinetics studies, a small flow (about 10 L/min) of purified air was added to compensate the continuous withdrawal of gas from the chamber for analysis and maintaining the pressure in the chamber slightly above atmosphere pressure. The dilution rate and mixing time of the system were measured by injecting a sample of SF_6 (>99.99%, Alpha Gaz) into the chamber and measuring the temporal profile of SF_6 using the in situ FTIR spectrometer as described in previous studies. The dilution rate expressed as a first-order rate coefficient is around 2.3×10^{-5} s^{-1} in these experiments. The key analytical instruments used in this study are the commercial Nicolet 5700 Magna FT-IR spectrometer (FTIR) and the two-channel Cavity Ring Down Spectrometer (CRDS).

The FTIR spectrometer was coupled to a white-type multiple-reflection mirror system and the base length of this white type mirrors was around 2 meters and was operated at 70 traverses, giving a total optical path length of 140 m. The IR spectra were recorded by co-adding 16 scans with a spectral resolution of 1 cm^{-1}. The N_2O, CO,

SO_2 and SF_6 were monitored at the following infrared absorption wavenumbers: N_2O (2620 cm^{-1}-2410 cm^{-1}), CO (2268 cm^{-1}-1976 cm^{-1}), SO_2 (2539 cm^{-1}-2440 cm^{-1}), and SF_6 (934 cm^{-1} - 954 cm^{-1}).

The peak areas were used for calibration and monitoring the concentrations of the N_2O, CO and SO_2. The detection sensitivities for these compounds were derived from the slopes of the calibrations plots of the peak areas versus the mixing ratio of these compounds (ppmv) in the following Figures (Figure 5-1 to Figure 5-3). When the concentration used in the studies were too high, the peak areas of all the characteristic peaks were partially saturated within the concentrations used in the experiments, the concentration used for each experiment would be calculated from the pressure of gas handle system directly.

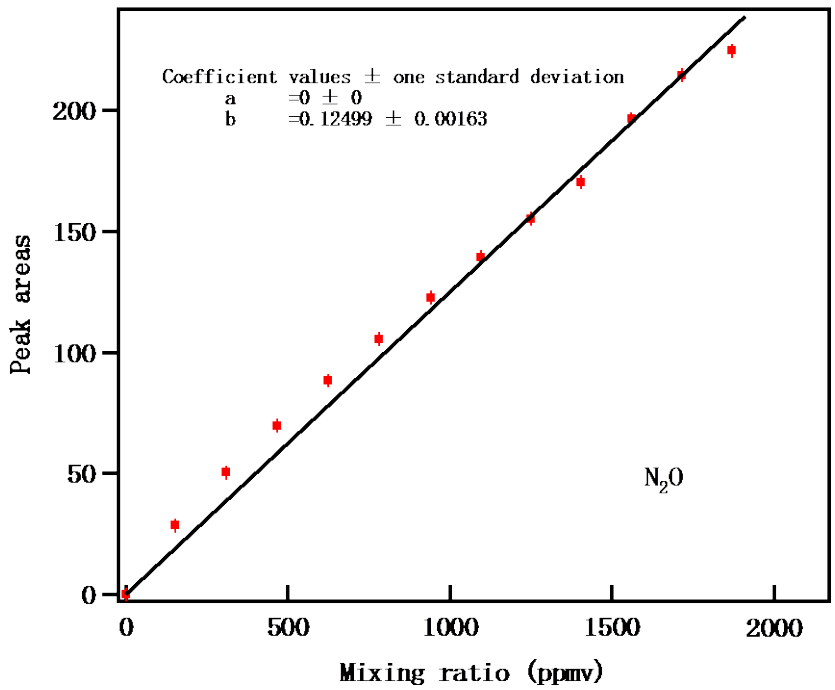

Figure 5-1 Calibration of N_2O using FTIR system.

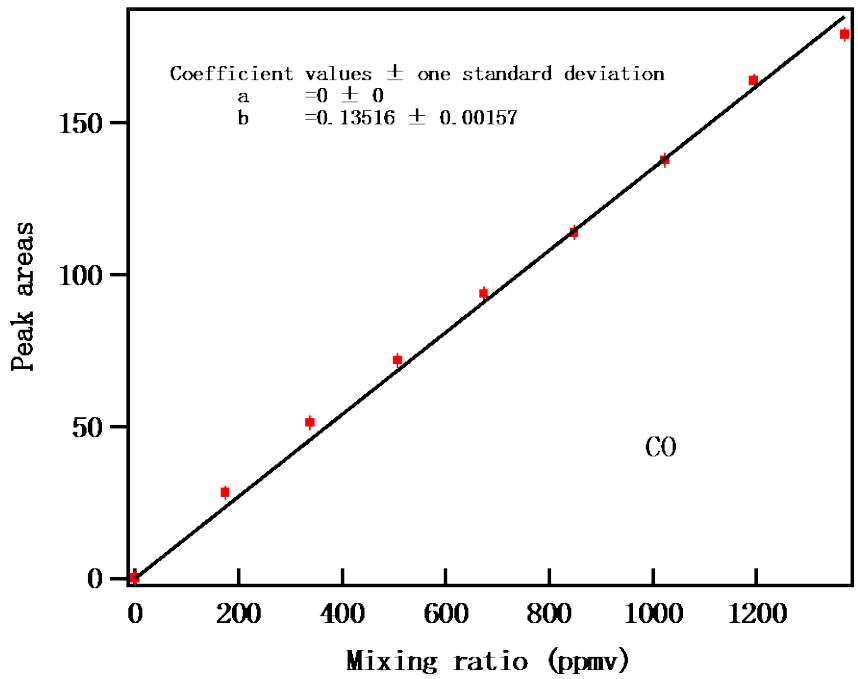

Figure 5-2 Calibration of CO using FTIR system.

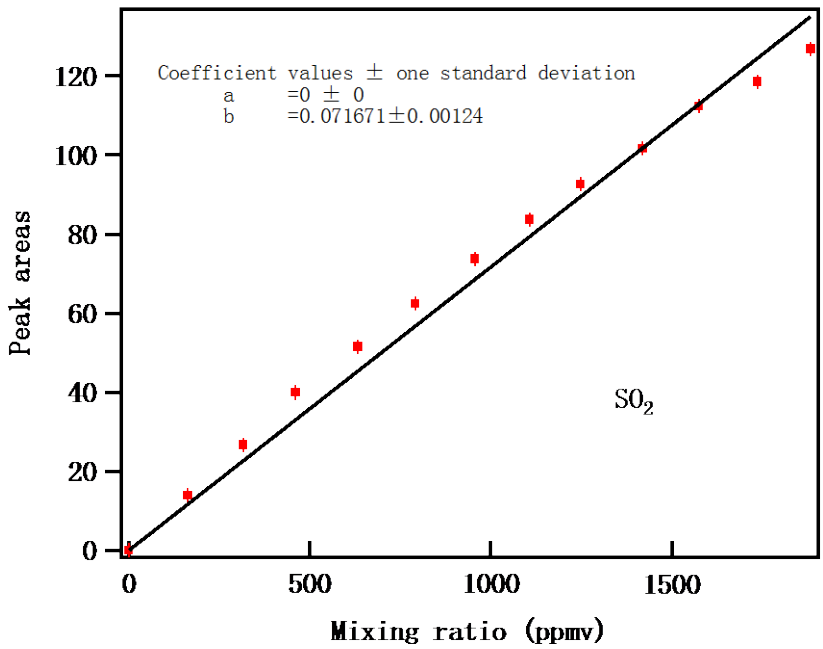

Figure 5-3 Calibration of SO_2 using FTIR system.

The two-channel cavity ring down spectrometer operating at 662 nm was used to measure the concentrations of NO_3 (in one channel) and N_2O_5 + NO_3 (in another channel) simultaneously. The detection principle and operating characteristics of this

instrument have been described in detail in chapter II. The time resolution of the instrument was 1s with detection sensitivities between 0.4 and 2 ppt for NO_3 and N_2O_5 for 1 second integration, as described in detail by Fuchs et al. (Fuchs et al. 2008). The air sample entering the CRDS system was passed through a filter to remove aerosols, which scatter the 662 nm light and degrade the instrument sensitivity for gas phase measurement. The combined loss of NO_3 and N_2O_5 to the walls of the instrument and the filter located upstream of the device have been estimated (Fuchs et al. 2008, Dube et al. 2006, Fuchs et al. 2012, Dorn et al. 2013) to be less than 20% and 4%, respectively, for NO_3 and N_2O_5; these losses are accounted for in calculating the concentrations. The uncertainties in the absorption cross section of NO_3 radical at 662 nm and the ratio of the cavity length to the length over which NO_3 and N_2O_5 are present add to the estimated uncertainties. Based on these factors, the overall accuracy of the NO_3 and N_2O_5 measurements, respectively, are estimated (Wagner et al. 2011) to be -8% to +11% and from −9% to +12%.

The rate coefficients for the reactions of NO_3 radicals with these inorganic compounds were measured by following the temporal profiles of NO_3 and N_2O_5 in an excess of reactants. During this process, NO_3, N_2O_5 and NO_2 are nearly in equilibrium, the rate coefficients can be obtained by attempting to fit the temporal profiles of each compounds.

When N_2O_5 was injected into the middle of the chamber, it decomposed immediately to give NO_3 and NO_2 and set up equilibrium between and among these species. The initial mixing ratios of N_2O_5 were between 8 and 25 ppbv and the initial mixing ratios of NO_3 were between 0.5 and 2.5 ppbv. The concentrations of NO_3 and N_2O_5 decreased with time as N_2O_5 and NO_3 were lost in the chamber due to wall loss and reaction with reactants or impurities. The temporal variations of NO_3 and N_2O_5 in the chamber were continuously measured by CRDS. The measured temporal profiles were fit by using a simple box model that integrated the set of reactions occurring in the chamber to derive the time dependence of NO_3, N_2O_5 and NO_2. The fitting was achieved by minimizing the sum of least-squares for both NO_3 and N_2O_5 profiles by

changing the input parameters.

For these reactants, we fitted the observed profiles to the following set of reactions that occur in the chamber:

$$N_2O_5 \xrightarrow{k_{dc}} NO_3 + NO_2 \quad \text{(R1)}$$

$$NO_3 + NO_2 \xrightarrow{k_f} N_2O_5 \quad \text{(R2)}$$

$$NO_3 \xrightarrow{k_1} \text{loss} \quad \text{(R3)}$$

$$N_2O_5 \xrightarrow{k_2} \text{loss} \quad \text{(R4)}$$

$$\text{reactant} + NO_3 \xrightarrow{kr} R_1O_2NO_2 \quad \text{(R5)}$$

The input parameters include the initial concentrations of each reactant and reaction rate coefficients of each reaction. First, the data in the absence of these organic gases were fit to the reaction scheme with the concentration set to zero with the known values of the rate coefficients for the equilibrium reactions among NO_3, N_2O_5 and NO_2. The equilibrium constant, $k_{eq} = [N_2O_5]/[NO_3][NO_2] = k_f/k_{dc}$, and value of k_{dc}, k_{eq} and k_f at different temperature were taken from NASA/JPL recommendation (Burkholder et al. 2015). The values of the wall loss rate of NO_3 and N_2O_5 (k_1 s^{-1} and k_2 s^{-1}) were derived from the fit.

After about 10 min, the equilibrium was set up, the wall loss rates of N_2O_5 and NO_3 were derived from curve fitting, known concentration of the reactants were introduced into the chamber and their concentrations were measured by using FTIR.

The concentration of the reactants was always much greater than those of N_2O_5 and NO_3 in the chamber. The temporal profiles of N_2O_5, NO_3 and NO_2 measured after injecting the reactants were again fit to minimize the sum of least-squares for NO_3 and N_2O_5 decays in the reaction scheme with only the rate coefficient for the reaction of reactants with NO_3 being the variable.

2.2 Chemicals

The following chemicals, with purities as stated by the supplier, were used without further purification: nitrous oxide (N_2O > 99.998%, Air Liquid), carbon monoxide

(CO, > 99.997%, Air Liquid), sulfur dioxide (SO_2, > 99.9%, Air Liquid). The specifications of each reactant are shown in Table 5-1. In this study, the NO_3 radicals were produced by the thermal decomposition of N_2O_5 injected into the chamber. Pure N_2O_5 was synthesized by mixing NO with O_3 in a slow flow and collecting N_2O_5 in a trap at -80℃, followed by purification, as described by Davidson et al. (Davidson et al. 1978).

Table 5-1 The specification of each reactant (provided by the supplier)

	N_2 (ppm)	O_2 (ppm)	H_2O (ppm)	H_2 (ppm)	CO_2 (ppm)	CO (ppm)	NO_x (ppm)	Ar (ppm)	C_nH_m (ppm)
N_2O (>99.998%)	<10	<2	<3	<0.1	<2	<1	<1		<1
CO (>99.997%)	<10	<5	<3	<1	<1				<2
SO_2 (>99.9%)			<50						

3 Results and discussion

3.1 Experimental results

Figure 5-4 shows the measured temporal profiles of NO_3 and N_2O_5 mixing ratios in the chamber in the absence (up to the gray bar) and presence of N_2O (after the gray bar). The gray bar indicates the time period at which N_2O was injected into the chamber. Figure 5-5 shows the fits of the profiles to the reaction schemes (R1-R5) with and without N_2O. With the known values of the rate coefficients for reactions R1, R2 and initial concentrations of NO_3, N_2O_5 and NO_2 (The initial concentration of NO_2 were derived from k_{eq}), the values of k_1, k_2, were derived from the fit of profiles (1) and (2): loss of NO_3 and N_2O_5 without N_2O. Using the loss rate values of k_1 and k_2, the rate coefficients were obtained from the fit of profiles (3) and (4): loss

of NO_3 and N_2O_5 with N_2O.

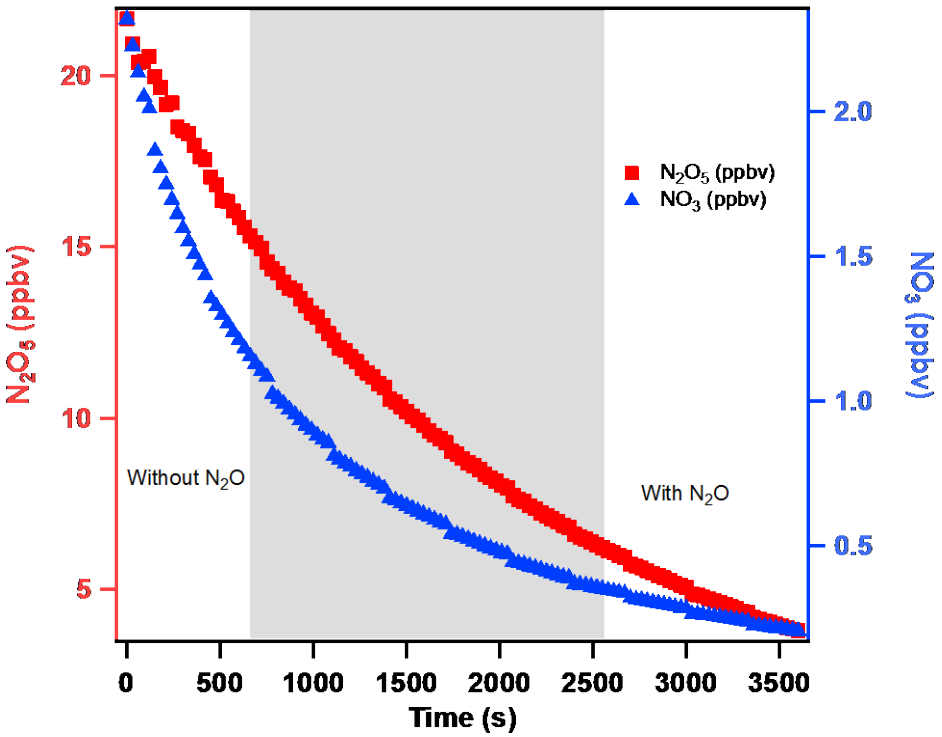

Figure 5-4 Measured temporal profiles of NO_3 and N_2O_5 mixing ratios in the chamber in the absence (up to the vertical gray bar) and presence of N_2O (after the gray bar). The gray bar indicates the time period at which N_2O were injected into the chamber.

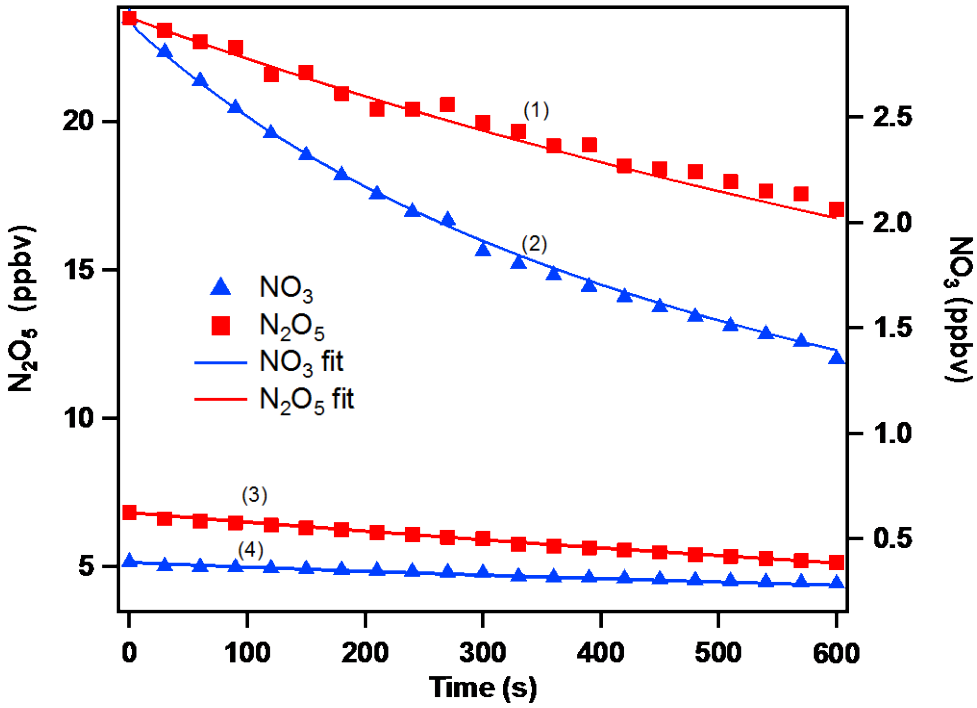

Figure 5-5. Observed NO_3 and N_2O_5 mixing ratios (circles and triangles) and their simulated temporal profiles (lines) after the injection of N_2O into the chamber where NO_3 and N_2O_5 were present at equilibrium. Profile 1: loss of N_2O_5 without N_2O. Profile 2: loss of NO_3 without N_2O. Profile 3: loss of N_2O_5 with N_2O. Profile 4: loss of NO_3 with N_2O. The concentration of N_2O was 5.28×10^{13} molecules cm^{-3}. The fits yield a value of $k_r = 2.30 \times 10^{-20}$ cm^3 $molecule^{-1}$ s^{-1}.

Multiple experiments were carried out with N_2O, CO and SO_2 and initial concentrations of each reactant. The uncertainty in the obtained values of k_r due to fitting was very small, often much less than 5%. The uncertainty in the precision of our measured rate coefficient were obtained by the standard deviation of the mean of multiple measurements and including the Student t value for the limited number of measurements. The results of our measurements for N_2O, CO and SO_2 are given in Table 5-2.

Table 5-2. Summary of the experimental conditions and rate constants for reaction of NO_3 with N_2O, CO and SO_2 at 298.0±1.5K. The k_r measured values shown are those derived from fitting the observed profiles of NO_3 and N_2O_5 to a least squares algorithm.

Compound	T (K)	Initial mixing ratio				k_r	k_r incl. systematic errors
		(ppmv)	NO_3 (ppbv)	N_2O_5 (ppbv)	NO_2 (ppbv)	$\times10^{-20}cm^3$ $molecule^{-1}s^{-1}$	
N_2O	298.5	819	0.52	10.47	25.17	5.50	
	299.1	2148	0.39	6.81	22.27	2.12	
	299.3	2040	0.59	11.55	25.08	1.70	
	299.3	2707	0.39	7.46	21.96	1.08	
	298.5	2439	0.39	8.05	24.02	1.10	
	298.5	2277	0.11	3.24	18.62	2.62	
	293.7	2214	0.49	14.84	19.83	1.01	
	293.7	3201	0.12	4.04	22.64	3.78	
	293.7	2386	0.17	4.54	18.21	3.45	
	294.1	2320	0.34	9.85	19.55	2.97	
						2.76±1.07	2.76±1.56
CO	297.7	1734	0.35	8.09	24.43	4.00	
	297.7	1707	0.27	6.62	25.95	4.00	
	299.7	1906	0.45	6.89	20.44	2.80	
	299.7	1870	0.61	10.89	23.82	2.50	
						3.33±1.58	3.33±1.66
SO_2	296.3	2446	0.39	7.60	17.58	3.20	
	296.3	2346	0.71	15.35	19.66	2.50	
	296.0	2557	0.33	5.87	15.41	2.70	

	296.0	2457	0.59	11.84	17.05	2.30	
						2.68±0.77	2.68±0.87

[a] The k_r values shown are those derived from fitting the observed profiles of NO_3 and N_2O_5 to a least squares algorithm. The quoted error is at the 95% confidence level and is a measure of the precision of our measurements. It includes the Student t-distribution contribution due to the limited number of measurements.

[b] The quoted errors include estimated systematic errors as described in the text.

The errors in determining the rate coefficients by monitoring the temporal profiles of NO_3 and N_2O_5 arise from (1) the precision in the measurements of NO_3, N_2O_5 and NO_2; (2) the uncertainty in the concentration of the reactants in our study; (3) the uncertainty of the rate coefficients used in the reaction schemes of the box model; (4) the precision of the measurements of k by curve fitting; (5) the presence of reactive impurities in the sample of the reactants.

In the present study, the systematic errors in measurements of NO_3 and N_2O_5 using the CRDS system employed here have been assessed to be −8/+11% for NO_3 and −9/+12% for N_2O_5, as noted earlier. Systematic errors in the measured concentration of the reactants are estimated for each compound by using the uncertainty of the slope in the calibration plots (<5%) and the uncertainty in measuring reactants concentration for the calibration (5%); all at 95% confidence level. We just added these two errors to get the estimated uncertainty in the concentration of reactants in the chamber. Then, the overall estimated error was calculated by adding in quadrature the fitting error, estimated contribution of absolute concentrations of NO_3 and N_2O_5, the precision of the measurements of k_r, and the estimated uncertainty in the concentration of the reactants. Table 5-2 lists the uncertainties in the measured values of the rate constants along with the estimated systematic errors. The uncertainty in the fitting, as noted above, is better than 5%. The uncertainty of the rate coefficients used in the reaction scheme of the box model to fit the curves (the uncertainty of K_{eq}) is around 10 % (Burkholder et al. 2015).

Another potential source of error in the rate coefficient measured by using the

absolute method is the presence of reactive impurities in the sample of the reactants. The reactants used in the study were the purest we could obtain from commercial vendors. For N_2O and CO, the impurities are less than 0.003% (30 ppmv) and the main impurities are nonvalent to NO_3 such as, N_2, O_2, and CO_2 et al. We do not believe that our reported values were greatly affected by the presence of these impurities. However, the presence of other reactive species towards NO_3 is not fully excluded. Hence, our reported values can be treated as the upper limits of the rate coefficients of NO_3 radicals react with these inorganic gases and we recommend the following upper limits rate coefficients values at T = 298 ± 2 and P = (1000±5 hPa) of air:

$$k(NO_3+N_2O) \leq 4.3\times10^{-20}\ cm^3\ molecule^{-1}s^{-1}$$

$$k(NO_3+CO) \leq 4.9\times10^{-20}\ cm^3\ molecule^{-1}s^{-1}$$

$$k(NO_3+SO_2) \leq 3.6\times10^{-20}\ cm^3\ molecule^{-1}s^{-1}$$

3.2 Comparison with literature

The available literature data along with the obtained results in this work are summarized in Table 5-3.

- Reaction NO_3 + N_2O:

This reaction has been subject to only one investigation. Cantrell et al.'s studies were performed in a 450-L Pyrex cell at room temperature by using an absolute method. They did not observe loss of N_2O through NO_3 reaction and determined an upper limit for the rate coefficient of 2 $\times10^{-17}$ cm^3 $molecule^{-1}$ s^{-1} (Cantrell et al. 1987).

- Reaction NO_3 + CO:

This reaction was investigated by three different groups. Burrows, Tyndall and Moortgat applied molecular modulation spectroscopy to study the reaction NO_3 + CO with NO_3 radicals generated by photolysis of a mixture of F_2 and HNO_3. The kinetics of loss of NO_3, measured by absorption in the visible, was followed in the

excess of CO. No reaction was observed and an upper limit for the rate constant at 298 K of 4.0 × 10^{-16} cm^3 $molecule^{-1}$ s^{-1} was determined (Burrows et al. 1985). Wallington et al. (Wallington et al. 1986) studied this reaction by a flash photolysis-flow tube technique using three different systems to generate the NO_3 radicals: pure $ClONO_2$, a mixture of Cl_2 + $ClONO_2$, and a mixture of F_2 + HNO_3. In this case, also, visible absorption spectroscopy was employed for the measurement of NO_3. No reaction was observed when CO was added, and an upper limit for this reaction at 298 ± 2 K of 3 ×10^{-18} cm^3 $molecule^{-1}$ s^{-1} was calculated. A Teflon bag (volume = 1.5 m^3) was used as reaction chamber by Hjorth, Ottobrini and Restelli (Hjorth et al. 1986) to follow the decay of the CO concentration when mixed with N_2O_5 and O_3. No evidence was obtained for a reaction between CO and NO_3 at (295 ± 2) K, leading to a calculated upper limit of 4 × 10^{-19} cm^3 $molecule^{-1}$ s^{-1}.The kinetics of the reaction between NO_3 and SO_2 has been also studied by Burrows, Tyndall and Moortgat, using the same experimental system as described for the study of the reaction of NO_3 with CO (Burrows et al. 1985).

- Reaction NO_3 + SO_2:

Using the same experimental system as described above, Burrows et al. (Burrows et al. 1985) did not observe any loss of SO_2 and determined an upper limit for the rate constant of the reaction 4 × 10^{-16} cm^3 $molecule^{-1}$ s^{-1}. Dlugokencky and Howard also studied the reaction between NO_3 radical and some atmospheric sulfur compounds. They determined an upper limit for the rate constant $k(NO_3+SO_2) < 1.0 \times 10^{-15}$ cm^3 $molecule^{-1}$ s^{-1}.

Table 5-3 Summary of the rate coefficients upper limits of NO_3 radicals with N_2O, CO and SO_2 measured by different groups.

Reactant	k_{VOC} cm^3 $molecule^{-1}$ s^{-1}	Reference
N_2O	$< 2 \times 10^{-17}$	Cantrell et al. 1987
	$\leq 4.0 \times 10^{-20}$	This work
CO	$< 4 \times 10^{-16}$	Burrows et al. 1985

	$< 3 \times 10^{-18}$	Wallington et al. 1986
	$< 4 \times 10^{-19}$	Hjorth et al. 1986
	$\leq 4.9 \times 10^{-20}$	This work
SO_2	$< 4 \times 10^{-16}$	Burrows et al. 1985
	$< 1 \times 10^{-15}$	Dlugokencky and Howard 1988
	$\leq 3.6 \times 10^{-20}$	This work

As can be seen in the table, measuring very small reaction rate coefficients are very difficult. comparing with the previously reported values, the upper limits of the rate coefficients derived in our method are much improved and decreased by at least two orders of magnitude.

4 Conclusions and atmospheric implication

Our atmosphere contains many inorganic pollutants, some of which are very long-lived. Three examples of such pollutants are nitrous oxide (N_2O), carbon monoxide (CO), and sulfur dioxide (SO_2); each of these is involved in many important atmospheric issues. Several previous studies have attempted to measure the rate coefficients for their reaction with the NO_3 radical. However, there were major differences in the reported rate coefficients, mostly upper limits for their values. Therefore, the absolute method was used to determine the rate coefficients for the reactions of NO_3 radicals with nitrous oxide (N_2O), carbon monoxide (CO) and sulfur dioxide (SO_2) at room temperature and atmospheric pressure in order to ensure these values, and the kinetic data are reported as upper limits for gas-phase reaction. The upper limits of these reactions were decreased by at least two orders of magnitude. The upper limits in the units of cm^3 $molecule^{-1}$ s^{-1} at 298 K are $<4.3 \times 10^{-20}$ for N_2O, $<4.9 \times 10^{-20}$ for CO and $<3.6 \times 10^{-20}$ for SO_2. A comparison of N_2O, CO and SO_2 atmospheric lifetime with estimated atmospheric lifetimes respect to reactions with NO_3 is listed in Table 5-4. These values indicated reactions with NO_3

radicals are, at most, minor pathways for the atmospheric removal of N_2O, CO and SO_2. In particular, it helps us better constrain the atmospheric lifetime of N_2O and hence improve the ozone depletion potential and global warming potential of N_2O.

Table 5-4 Comparison of N_2O, CO and SO_2 atmospheric lifetime and estimated atmospheric lifetimes respect to reactions with NO_3.

	Atmospheric lifetime	Estimated atmospheric lifetimes respect to reactions with NO_3
N_2O	~110 years	~ 10,000 years
CO	~1 month	~ 10,000 years
SO_2	~5 days	~ 10,000 years

Supporting information

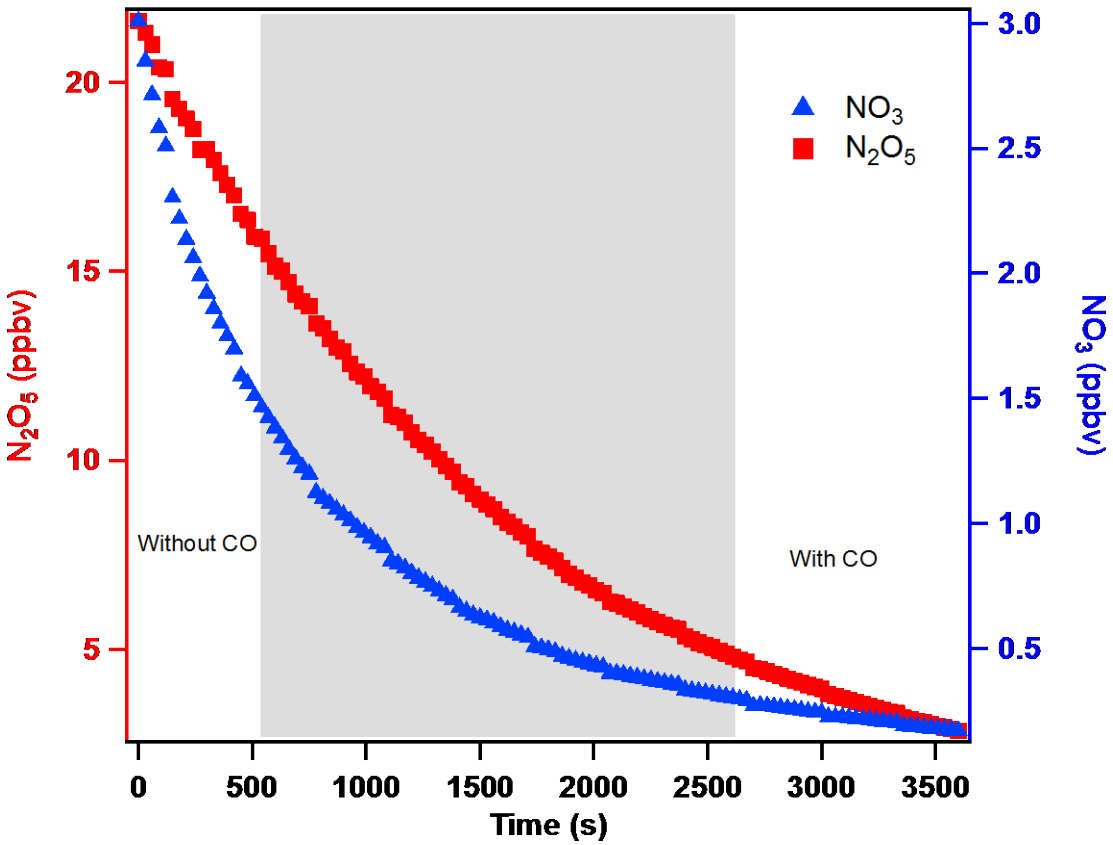

Figure 5S-1 Measured temporal profiles of NO_3 and N_2O_5 mixing ratios in the chamber in the absence (up to the vertical gray bar) and presence of CO (after the gray bar). The gray bar indicates the time period at which CO were injected into the chamber.

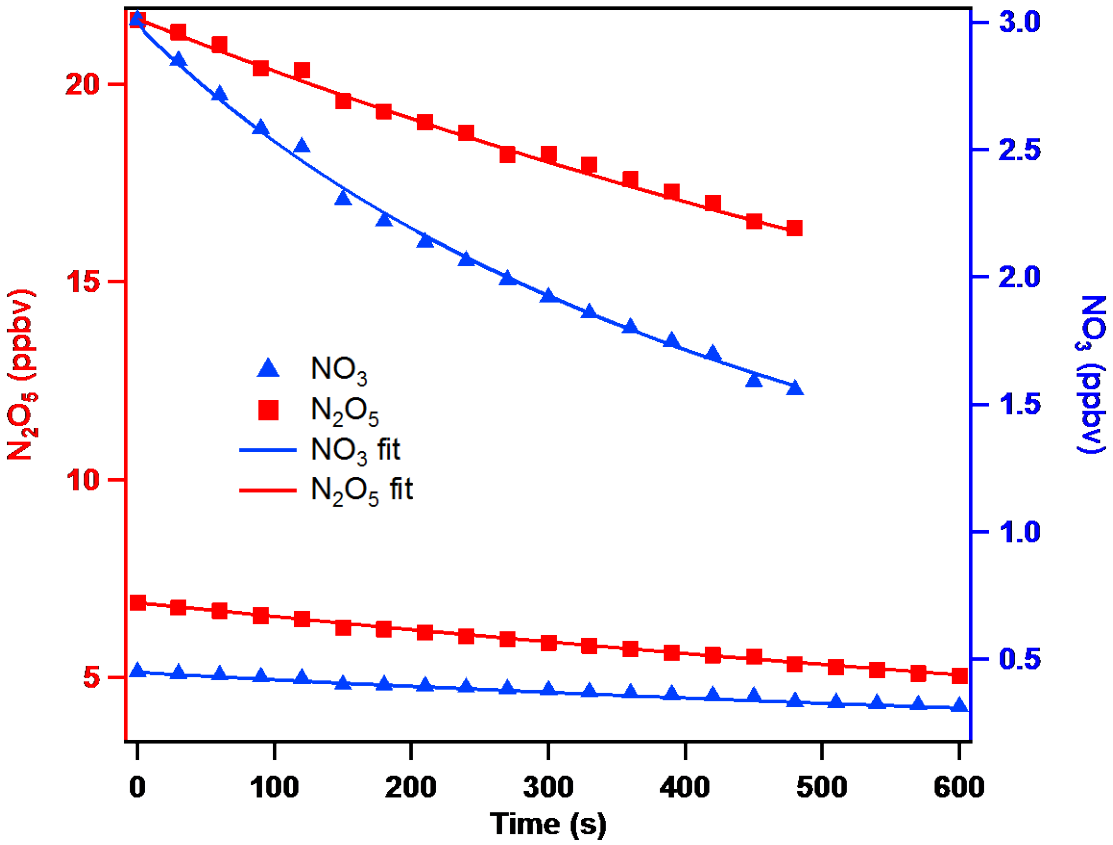

Figure 5S-2. Observed NO_3 and N_2O_5 mixing ratios (circles and triangles) and their simulated temporal profiles (lines) after the injection of CO into the chamber where NO_3 and N_2O_5 were present at equilibrium. Profile 1: loss of N_2O_5 without CO. Profile 2: loss of NO_3 without CO. Profile 3: loss of N_2O_5 with CO. Profile 4: loss of NO_3 with CO. The concentration of N_2O was 4.69×10^{13} molecules cm^{-3}. The fits yield a value of $k_r = 2.80 \times 10^{-20}$ $molecule^{-1}$ cm^3 s^{-1}.

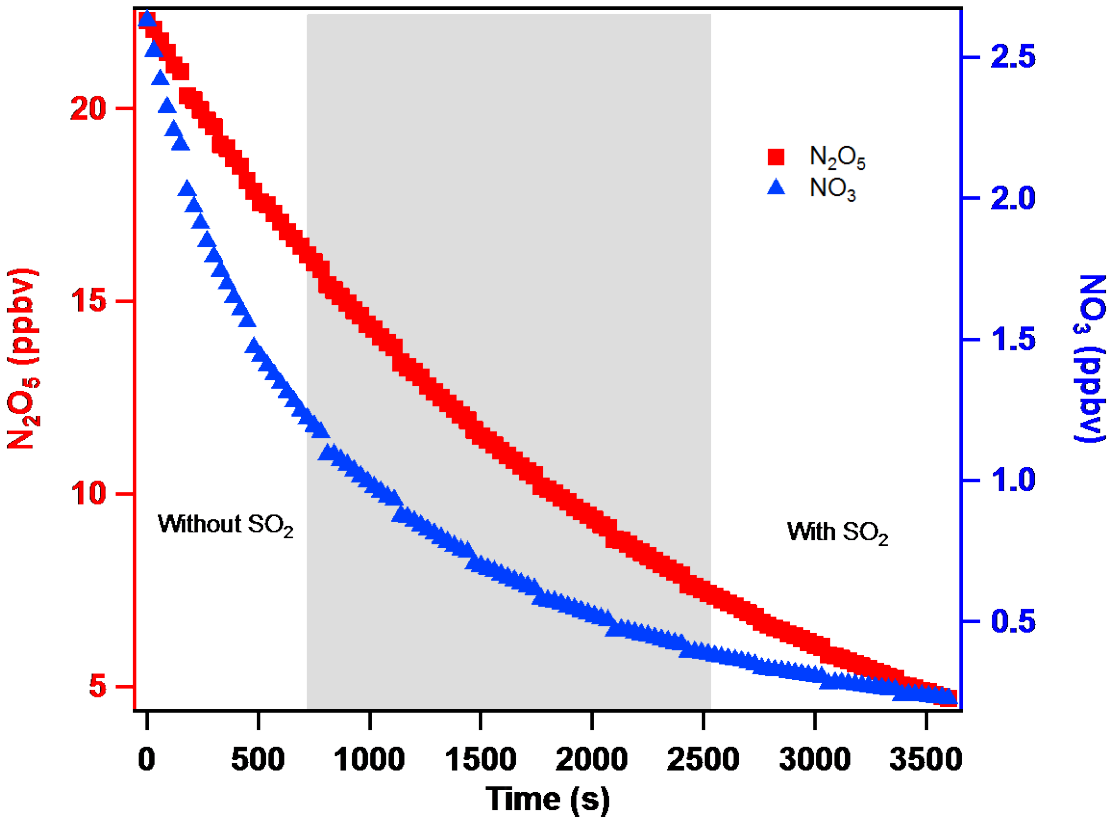

Figure 5S-3 Measured temporal profiles of NO_3 and N_2O_5 mixing ratios in the chamber in the absence (up to the vertical gray bar) and presence of SO_2 (after the gray bar). The gray bar indicates the time period at which SO_2 were injected into the chamber.

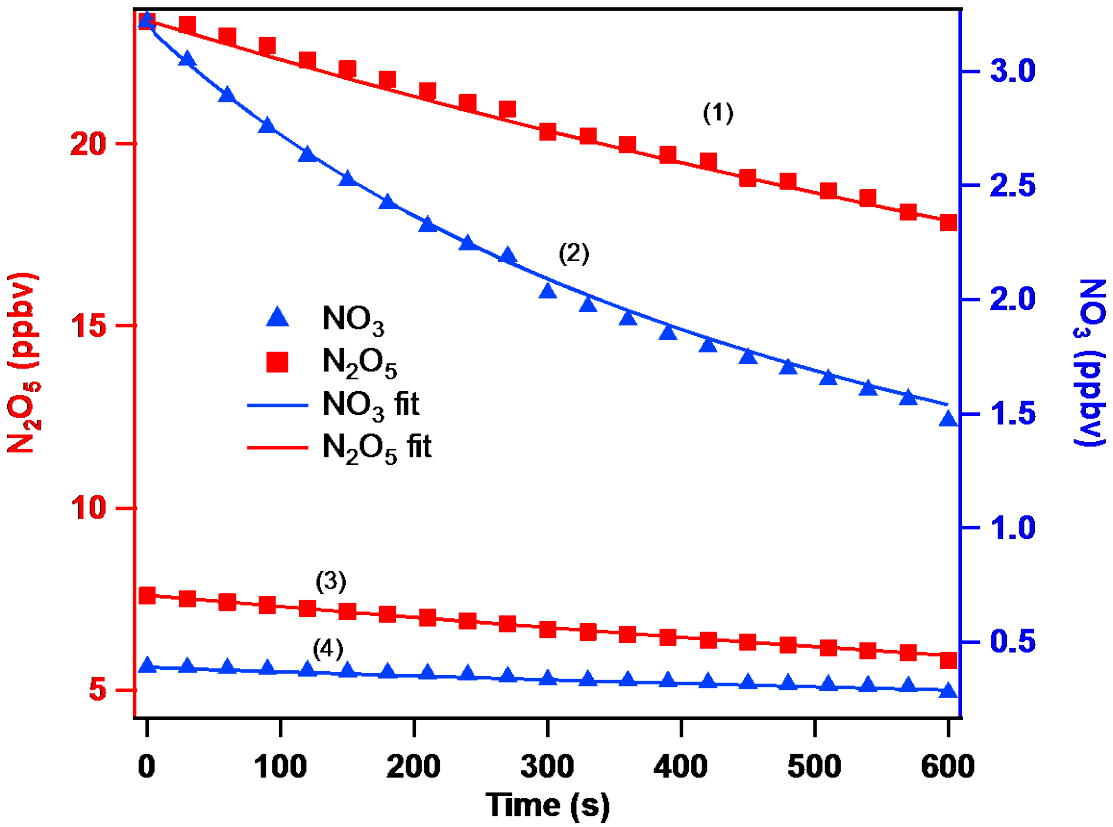

Figure 5S-4. Observed NO_3 and N_2O_5 mixing ratios (circles and triangles) and their simulated temporal profiles (lines) after the injection of N_2O into the chamber where NO_3 and N_2O_5 were present at equilibrium. Profile 1: loss of N_2O_5 without SO_2. Profile 2: loss of NO_3 without SO_2. Profile 3: loss of N_2O_5 with SO_2. Profile 4: loss of NO_3 with SO_2. The concentration of N_2O was 6.02×10^{13} molecules cm^{-3}. The fits yield a value of $k_r = 3.20 \times 10^{-20}$ $molecule^{-1}$ cm^3 s^{-1}.

References

Audley, G. J., D. L. Baulch, I. M. Campbell & L. T. Hamill (1980) Evidence for a new intermediate in N_2O_5 decomposition. *Journal of the Chemical Society, Chemical Communications*, 433-434.

Brown, S. S. (2003) Absorption spectroscopy in high-finesse cavities for atmospheric studies. *Chemical Reviews,* 103, 5219-5238.

Brown, S. S., H. Stark, S. J. Ciciora, R. J. McLaughlin & A. R. Ravishankara (2002a) Simultaneous in situ detection of atmospheric NO_3 and N_2O_5 via cavity ring-down spectroscopy. *Review of Scientific Instruments,* 73, 3291-3301.

Brown, S. S., H. Stark & A. R. Ravishankara (2002b) Cavity ring-down spectroscopy for atmospheric trace gas detection: application to the nitrate radical (NO). *Applied Physics B-Lasers and Optics,* 75, 173-182.

Burkholder J. B., S. P. S., J. P. D. Abbatt,J. R. Barker,R. E. Huie,C. E. Kolb,M. J. Kurylo,V. L. Orkin,D. M. Wilmouth,P. H. Wine (2015) Chemical Kinetics and Photochemical Data for Use in Atmospheric Studies.

Burrows, J. P., G. S. Tyndall & G. K. Moortgat (1985) Absorption spectrum of NO_3 and kinetics of the reactions of NO_3 with NO_2, Cl, and several stable atmospheric species at 298 K. *The Journal of Physical Chemistry,* 89, 4848-4856.

Cantrell, C. A., J. A. Davidson, R. E. Shetter, B. A. Anderson & J. G. Calvert (1987) Reactions of nitrate radical and nitrogen oxide (N_2O_5) with molecular species of possible atmospheric interest. *The Journal of Physical Chemistry,* 91, 6017-6021.

Davidson, J. A., A. A. Viggiano, C. J. Howard, I. Dotan, F. C. Fehsenfeld, D. L. Albritton & E. E. Ferguson (1978) Rate constants for reactions of O_2^+, NO_2^+, NO^+, H_3O^+, CO_3^-, NO_2^-, and halide ions with N2O5 at 300 K. *Journal of Chemical Physics,* 68, 2085-2087.

Dlugokencky, E. J. & C. J. Howard (1988) Laboratory studies of nitrate radical

reactions with some atmospheric sulfur compounds. *The Journal of Physical Chemistry,* 92**,** 1188-1193.

Dorn, H. P., R. L. Apodaca, S. M. Ball, T. Brauers, S. S. Brown, J. N. Crowley, W. P. Dube, H. Fuchs, R. Haeseler, U. Heitmann, R. L. Jones, A. Kiendler-Scharr, I. Labazan, J. M. Langridge, J. Meinen, T. F. Mentel, U. Platt, D. Poehler, F. Rohrer, A. A. Ruth, E. Schlosser, G. Schuster, A. J. L. Shillings, W. R. Simpson, J. Thieser, R. Tillmann, R. Varma, D. S. Venables & A. Wahner (2013) Intercomparison of NO3 radical detection instruments in the atmosphere simulation chamber SAPHIR. *Atmospheric Measurement Techniques,* 6**,** 1111-1140.

Dube, W. P., S. S. Brown, H. D. Osthoff, M. R. Nunley, S. J. Ciciora, M. W. Paris, R. J. McLaughlin & A. R. Ravishankara (2006) Aircraft instrument for simultaneous, in situ measurement of NO_3 and N_2O_5 via pulsed cavity ring-down spectroscopy. *Review of Scientific Instruments,* 77.

Fuchs, H., W. P. Dube, S. J. Cicioira & S. S. Brown (2008) Determination of inlet transmission and conversion efficiencies for in situ measurements of the nocturnal nitrogen oxides, NO_3, N_2O_5 and NO_2, via pulsed cavity ring-down spectroscopy. *Analytical Chemistry,* 80**,** 6010-6017.

Fuchs, H., W. R. Simpson, R. L. Apodaca, T. Brauers, R. C. Cohen, J. N. Crowley, H. P. Dorn, W. P. Dubé, J. L. Fry, R. Häseler, Y. Kajii, A. Kiendler-Scharr, I. Labazan, J. Matsumoto, T. F. Mentel, Y. Nakashima, F. Rohrer, A. W. Rollins, G. Schuster, R. Tillmann, A. Wahner, P. J. Wooldridge & S. S. Brown (2012) Comparison of N_2O_5 mixing ratios during NO3Comp 2007 in SAPHIR. *Atmos. Meas. Tech.,* 5**,** 2763-2777.

Hjorth, J., G. Ottobrini & G. Restelli (1986) Reaction of the NO3 radical with CO: Determination of an upper limit for the rate constant using FTIR spectroscopy. *International journal of chemical kinetics,* 18**,** 819-827.

Menon, S., K. L. Denman, G. Brasseur, A. Chidthaisong, P. Ciais, P. M. Cox, R. E. Dickinson, D. Hauglustaine, C. Heinze & E. Holland. 2007. Couplings

between changes in the climate system and biogeochemistry. Ernest Orlando Lawrence Berkeley National Laboratory, Berkeley, CA (US).

Pendolovska, V., R. Fernandez, N. Mandl, B. Gugele & M. Ritter (2013) Annual European Union Greenhouse Gas Inventory 1990–2011 and Inventory Report 2013. Copenhagen: European Environment Agency.

Pommier, M., K. S. Law, C. Clerbaux, S. Turquety, D. Hurtmans, J. Hadji-Lazaro, P.-F. Coheur, H. Schlager, G. Ancellet, J.-D. Paris, P. Nédélec, G. S. Diskin, J. R. Podolske, J. S. Holloway & P. Bernath (2010) IASI carbon monoxide validation over the Arctic during POLARCAT spring and summer campaigns. *Atmospheric Chemistry and Physics,* 10**,** 10655-10678.

Pommier, M., C. A. McLinden & M. Deeter (2013) Relative changes in CO emissions over megacities based on observations from space. *Geophysical Research Letters,* 40**,** 3766-3771.

Ravishankara, A. R., J. S. Daniel & R. W. Portmann (2009) Nitrous Oxide (N_2O): The Dominant Ozone-Depleting Substance Emitted in the 21st Century. *Science,* 326**,** 123-125.

Reimer, R. A., C. S. Slaten, M. Seapan, M. W. Lower & P. E. Tomlinson (1994) Abatement of N2O emissions produced in the adipic acid industry. *Environmental Progress,* 13**,** 134-137.

Shimizu, A., K. Tanaka & M. Fujimori (2000) Abatement technologies for N_2O emissions in the adipic acid industry. *Chemosphere - Global Change Science,* 2**,** 425-434.

Wagner, N. L., W. P. Dube, R. A. Washenfelder, C. J. Young, I. B. Pollack, T. B. Ryerson & S. S. Brown (2011) Diode laser-based cavity ring-down instrument for NO_3, N_2O_5, NO, NO_2 and O_3 from aircraft. *Atmospheric Measurement Techniques,* 4**,** 1227-1240.

Wallington, T. J., R. Atkinson, A. M. Winer & J. N. Pitts (1986) Absolute rate constants for the gas-phase reaction of the nitrate radical with dimethyl sulfide, nitrogen dioxide, carbon monoxide and a series of alkanes at 298 .+-. 2 K. *The*

Journal of Physical Chemistry, 90**,** 4640-4644.

Weinstock, B. & H. Niki (1972) Carbon monoxide balance in nature. *Science,* 176**,** 290-292.

Chapter VI Conclusions

The nitrate radical, NO_3, is a key intermediate in the chemistry of the Earth's atmosphere. Since it photolyzes rapidly during the daytime and reacts with NO rapidly, its importance is mostly confined to the night-time atmosphere. It has been observed to be present in both stratosphere and troposphere. It is the atmospheric source of N_2O_5, a labile compound that can decompose easily to NO_3 and NO_2. Under favorable conditions, it can transport NOx from one region to another. The heterogeneous removal of N_2O_5 can be a sink for NOx in the troposphere or can even activate chlorine via heterogeneous/multiphase reactions. NO_3 radical can react with a number of VOCs initiating their night time degradation and providing a sink for NO_3, and hence NOx. Reactions of NO_3 and N_2O_5 can lead to the formation of particulate nitrate, one of the most common PMs in the troposphere. Because of these reasons, a fuller understanding of the reactions of NO_3 is vital to our ability to predict and influence the earth's atmosphere.

The NO_3 radicals, however, are not very reactive towards many species present in the atmosphere. Yet, the larger abundances of NO_3 radicals compared to the ubiquitous OH radical or Cl atoms make even slower reactions important. It is important to characterize these slower reactions to determine their influence on atmospheric lifetimes or production of other species. Even a small reaction rate coefficient can significantly alter the lifetimes of long-lived chemicals. For example, the currently published upper limit for the reaction of NO_3 with N_2O could reduce the calculated atmospheric lifetime of N_2O by tens of years with major implication to the transport of N_2O to the stratosphere and the budget of N_2O. Therefore, quantification of slow reactions of NO_3 is important.

Measuring very small reaction rate coefficients are very difficult. The common direct technique such as discharge flow and pulsed photolysis kinetics methods are limited because the reaction times are limited to millisecond or less. The relative rate techniques are very useful, but again the extent of reactant loss will be limited for

slow reactions and necessary references molecules are identified with difficulty.

In our laboratory, we have devised a method where the temporal profiles of NO_3 can be measured for thousands of seconds in a very large chamber where wall loss rates are minimized. This "perturbation" method, where the reactant can be added and mixed rapidly compared to the times for reactions, affords a way to measure very small rate coefficients. We showed in this work that it is possible to measure rate coefficients as slow as 10^{-20} cm^3 $molecule^{-1}$ s^{-1}. Of course, the usual problems of reactive impurities and secondary reactions (common to all direct methods) have to be addressed.

In this thesis, the kinetics of NO_3 with different kinds of compounds were studied at room temperature (298 ± 2 K) and atmospheric pressure (1000 ± 5 hPa) in the ICARE-7300L Teflon chamber with a series of analytical tools including Fourier Transform Infrared Spectroscopy (FTIR), Proton Transfer Reaction-Time of Flight-Mass Spectrometer (PTR-ToF-MS), and Cavity Ring Down Spectrometer (CRDS). The measured rate coefficients varied from 1×10^{-20} to almost 1×10^{-14} cm^3 $molecule^{-1}$ s^{-1}. In some cases, we could use the same system to carry out relative rate studies. These studies fall into 3 categories (each described in a separate chapter): (1) Reasonably rapid reaction of methacralate esters; (2) Much slower reactions of alkanes; and (3) the extremely slow reactions with N_2O, CO, and SO_2, three abundant atmospheric stable chemicals.

Methacrylate esters are important unsaturated oxygenated volatile organic compounds (OVOCs) used in the production of polymers. We report the room temperature rate coefficients for the reactions of NO_3 radical with six of the methacrylate esters (shown below): methyl methacrylate (MMA), k1; ethyl methacrylate (EMA), k2; propyl methacrylate (PMA), k3; isopropyl methacrylate (IPMA), k4; butyl methacrylate (BMA), k5; and isobutyl methacrylate (IBMA), k6.[3] These rate coefficients were derived by using both relative and absolute rate methods. The rate coefficients from these two methods (weighted averages) in the units of 10^{-15}

[3] The reaction numbers in this chapter are not necessarily not those in the previous chapters.

cm^3 $molecule^{-1}$ s^{-1} at 298 K are k1 = 2.98 ± 0.35, k2 =4.67 ± 0.49, k3 = 5.23 ± 0.60, k4 = 7.91 ± 1.00, k5 = 5.91 ± 0.58, k6 = 6.24 ±0.66. The quoted uncertainties are at the 2σ level and include estimated systematic errors. In addition, the rate coefficient k7 for the reaction of NO_3 radical with deuterated methyl methacrylate (MMA-d8) was measured by using the relative rate method to be essentially the same as k1. The trends in the measured rate coefficient with the length and nature of the alkyl group, along with the equivalence of k1 and k7 (k1≈k7), strongly suggest that the reaction of NO_3 with the methacrylate esters proceeds via addition to the double bond on the methacrylate group. Based on these measurements, we were able to estimate the influence of NO_3 reactions on the lifetimes of these esters. We conclude that they can be important in polluted areas close to the emission sources.

Since many urban and oil/gas extraction areas contain relatively high concentrations of a wide variety of alkanes and the huge difference in NO_3 reactivity towards alkanes in field measurements, the reaction rate coefficients of different kinds of alkanes with NO_3 radicals deserve more attention. Therefore, our absolute method was used to determine the rate coefficients for the reactions of NO_3 radicals with methane (CH_4), ethane (C_2H_6), propane (C_3H_8), n-butane (C_4H_{10}), iso-butane (C_4H_{10}), 2,3-dimethybutane (C_6H_{14}), cyclopentane (C_5H_{10}) and cyclohexane (C_6H_{12}) at atmosphere pressure (1000±5 hPa) and room temperature (298±1.5 K). The upper limits of the rate coefficients for methane (CH_4) and ethane (C_2H_6), in the units of cm^3 $molecule^{-1}$ s^{-1} are < 4×10^{-20}, < 8×10^{-19}, respectively. And the rate coefficients for propane (C_3H_8), n-butane (C_4H_{10}), iso-butane (C_4H_{10}), 2,3-dimethybutane (C_6H_{14}), cyclopentane (C_5H_{10}) and cyclohexane (C_6H_{12}) in the units of cm^3 $molecule^{-1}$ s^{-1} are (9.67±5.80) $\times10^{-18}$, (1.57±0.94) $\times10^{-17}$, (8.2±4.9) $\times10^{-17}$, (6.3±3.8) $\times10^{-16}$, (1.27±0.76) $\times10^{-16}$, (1.24±0.74) $\times10^{-16}$, respectively. The quoted uncertainties are at the 2σ level and include estimated systematic errors. Because of the uncertainties of the rate coefficients used in the reaction scheme of the box model to fit the curves are large, the uncertainties for the reported rate coefficients are also large. It will be useful to study these ractions where the ratio of alkane to NO_3 is

much larger and the impurities are better quantified. It will also be useful in the future to carry out relative rate studies for reactions of larger alkanes, which are amenable to such studies. In addition, we showed that the rate coefficients of cyclopentane and cyclohexane with NO_3 radicals are similar. It would be interesting to see if the reactivity of C-H bond in different cycle structure is similar or depending on the number of carbon atoms in the follow-on work. It will be instructive to extend this study to cyclopropane, a highly constrained cyclic compound. These rate constants that have been measured for saturated alkanes suggest that the reaction proceeds via H atom abstraction from the weakest C-H bond. Indeed the correlation of the measured rate coefficients with the exothermicity of the reaction is strikingly good. From our studies, it is clear that the measurement of the temperature dependence of NO_3-alkane reactions would be very instructive. We conclude that the contribution of NO_3 to the loss of alkanes would be small but the influence of large concentrations of alkanes on NO_3 loss rates can be significant and they can now be quantified.

In addition to the organic volatile compounds, our atmosphere contains many inorganic pollutants, some of which are very long-lived. Three examples of such pollutants are nitrous oxide (N_2O), carbon monoxide (CO), and sulfur dioxide (SO_2); each of these is involved in many important atmospheric issues such that, respectively, ozone layer depletion and global warming, tropospheric ozone formation, and sulfate aerosol formation. Several previous studies have attempted to measure the rate coefficients for their reaction with the NO_3 radical. However, there were major differences in the reported rate coefficients, being mostly upper limits. Therefore, the absolute method was used to determine the rate coefficients for the reactions of NO_3 radicals with nitrous oxide (N_2O), carbon monoxide (CO) and sulfur dioxide (SO_2) in order to ensure these values. The upper limits of these reactions were decreased by at least two orders of magnitude. The upper limits in the units of cm^3 $molecule^{-1}$ s^{-1} at 298 K are $<4 \times 10^{-20}$ for N_2O, $<4.9 \times 10^{-20}$ for CO and $<3.6 \times 10^{-20}$ for SO_2. These values indicated that reactions with NO_3 radicals are, at

most, minor pathways for the atmospheric removal of N_2O, CO and SO_2. In particular, it helps us to better constrain the atmospheric lifetime of N_2O and hence improve the ozone depletion potential and global warming potential of N_2O.

Overall, using a new experimental technique, we have opened the horizon for studies of very slow reactions. Such studies will improve our fundamental understanding of chemical kinetics. Furthermore, they will enable better quantification of potentially important atmospheric processes. Specifically, data from our studies enhances the available database on NO_3 reactions, useful to atmospheric modelers of the lower troposphere, and assist understanding of the urban night-time troposphere.

Appendix

1 Student's Distribution Table

Student's t Distribution Table

For example, the t value for 18 degrees of freedom is 2.101 for 95% confidence interval (**2-Tail** $\alpha = 0.05$).

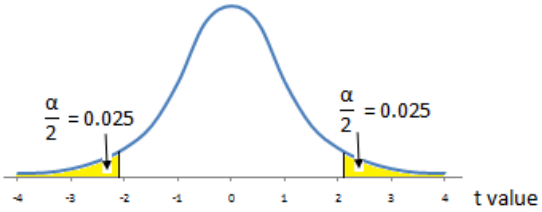

	90%	95%	97.5%	99%	99.5%	99.95%	1-Tail Confidence Level
	80%	90%	95%	98%	99%	99.9%	2-Tail Confidence Level
	0.100	0.050	0.025	0.010	0.005	0.0005	1-Tail Alpha
df	0.20	0.10	0.05	0.02	0.01	0.001	2-Tail Alpha
1	3.0777	6.3138	12.7062	31.8205	63.6567	636.6192	
2	1.8856	2.9200	4.3027	6.9646	9.9248	31.5991	
3	1.6377	2.3534	3.1824	4.5407	5.8409	12.9240	
4	1.5332	2.1318	2.7764	3.7469	4.6041	8.6103	
5	1.4759	2.0150	2.5706	3.3649	4.0321	6.8688	
6	1.4398	1.9432	2.4469	3.1427	3.7074	5.9588	
7	1.4149	1.8946	2.3646	2.9980	3.4995	5.4079	
8	1.3968	1.8595	2.3060	2.8965	3.3554	5.0413	
9	1.3830	1.8331	2.2622	2.8214	3.2498	4.7809	
10	1.3722	1.8125	2.2281	2.7638	3.1693	4.5869	

2 Macro Codes used in the box model

- Macro Code “Mechanism_Setup” for setting up the mechanism schemes of the reactions happened in the smog chamber
- Macro Code “Mechanism_compile” for compiling the initial concentrations of each reactant and rate coefficients of each reactions.
- Macro Code “Run_Model” for running the model depending on the input parameters
- Macro Code “Fleastsquare” for minimizing the error between the fitting value and the experimental results.

Macro Mechanism_Setup(Ncal)

```
Variable Ncal=80
Make/O/T/N=100 Reactant1, Reactant2, Product1, Product2, Product3, Names
Reactant1 = ""
Reactant2 = ""
Product1 = ""
Product2 = ""
Product3 = ""
Names = ""
Make/O/N=100 RateCoefficients
RateCoefficients=0
Make/O/N=(Ncal) CalTime
CalTime=0
```

Edit/W=(5.25,42.5,1122,236) reactant1,reactant2,product1,product2, product3, RateCoefficients

```
    DoWindow/K ReactionMechanism
    DoWindow/C/T ReactionMechanism,"Reaction Mechanism"
    ModifyTable    size=11,width=90
    ModifyTable width(ratecoefficients)=100
    Variable /G dilution = 0
    IncludeChemKineticFuncs() // load subroutines for reaction mechanism from experiment folder
end
```

Macro Mechanism_compile(N_C, fctname)

```
Variable N_C
String fctname = "ChemKinetic"
Prompt fctname, "Select Kinetic Function", popup FunctionList("ChemKinetic*",";","KIND:2")
String/G CurrChemKineticFct = fctname
Variable Rnumber, SpeciesNumber, SpeciesDiff
Variable flag,n,m, nn, position, position2
Variable na,nb,nc,nd, ne
Variable TotalLen, breakpos
String temp, temp1, temp2, temp3, temp4, temp5
String    TotalTemp, totaltemp1, totaltemp2, totaltemp3, totaltemp4,    totaltemp5
String dilutiontemp
String sa,sb,sc,sd, se
String s0,s1,s2,s3,s4,s5,s6,s7,s8,s9,s10
String Plus, Equal
String MyList, tempNote, tempNote2
String/G dydtstr = "" // string to be passed to ChemKineticsFuncs
    Silent 1
    PauseUpdate
    Plus = "+"
    Equal = "="
```

```
s0 = ""
s1 = " "
s2 = S1 + " "
s3 = s2 + " "
s4 = s3 + " "
s5 = s4 + " "
s6 = s5 + " "
s7 = s6 + " "
s8 = s7 + " "
s9 = s8 + " "
s10 = s9 + " "
n=0
//printf "\r\t\t\t\tReaction Mechanism \t\t\t\t\t\t\t\t\t\t Rate Coefficient\r"

Do
    temp = Reactant1[n] + Reactant2[n] + Product1[n] + Product2[n] + Product3[n]
    if (stringmatch(temp,"")) //Empty line in rxn. mechanism means jump to the end of the
loop
        Rnumber = n    // This is the number of reactions
        n += 500
    else                        //There is at least one reactant or product
            na = 10 - strlen(Reactant1[n])
            temp = "s" + num2str(na)
            sa =($temp) + Reactant1[n] + plus
            if(strlen(Reactant2[n]) == 0)
                sa =($temp) + Reactant1[n]
            endif
            if (strlen(Reactant1[n]) == 0)
```

```
            sa = "                                    "
        endif

    nb = 10 - strlen(Reactant2[n])
        temp = "s" + num2str(nb)
        sb =($temp) + Reactant2[n] + equal
        if (strlen(Reactant2[n]) == 0)
            sb = "                                    " + equal
        endif
        nc = 10 - strlen(Product1[n])
        temp = "s" + num2str(nc)
        sc =($temp) + Product1[n]
        if (strlen(Product1[n]) == 0)
            sc = "                                    "
        endif
        nd = 10 - strlen(Product2[n])
        temp = "s" + num2str(nd)
        sd = plus + ($temp) + Product2[n]
        if (strlen(Product2[n]) == 0)
            sd = "                                    "
        endif
    ne = 10 - strlen(Product3[n])
        temp = "s" + num2str(ne)
        se = plus + ($temp) + Product3[n]
        if (strlen(Product3[n]) == 0)
            sd = "                                    "
        endif

    //print "\t\t\t\t" + sa    + sb + sc + sd+ se + "\t\t\t\t\t" + num2str(ratecoefficients[n])
```

```
            endif
            n += 1
        while (n < N_C)
  //print "\r\r"
  //Print " ODEs in Compound Format"


//    Transfer Rate Coefficient Data to KK wave
            Make/O/N=(Rnumber) KK
//                        n = 0
//                        Do
//                        kk[n] = RateCoefficients[n]
//                        n +=1
//                        while(n < Rnumber)
            KK = RateCoefficients[p]
// Capture species names and write to Names[n] wave
                        n = 0
                        Make/O/N=600/T Names = ""
                        Do
                              nn = n*5
                              Names[nn] = Reactant1[n]
                  Names[nn+1] = Reactant2[n]
                  Names[nn+2] = Product1[n]
                  Names[nn+3] = Product2[n]
                  Names[nn+4] = Product3[n]
                  n += 1
                        while (n < rnumber)
//    Remove Blanks from Names List, changed to start at the end, since double empty names
were not properly removed before
                        n=numpnts(Names)-1 // last point in Names
```

```
            Do
        if(strlen(Names[n]) == 0)
            DeletePoints n,1,Names
        endif
        n -=1
            while(n > -1)


//  Remove Duplicate Names from Names List
    Silent 1
    Do
        flag=0
                n=0
            Do
            m=n+1
                Do
                    If(stringmatch(Names[m], Names[n]))
                        DeletePoints m,1,Names
                        flag=1
                    else
                        m += 1
                    endif
                while(m < numpnts(Names))
                    n += 1
                while(n< numpnts(Names) - 1)
            while (flag==1)
//  Determine number of Species in Reaction Names List
            n=0
            Do
                if(stringmatch(Names[n],""))
```

```
                    SpeciesNumber = n
            n = 500
                endif
                n += 1
            while (n < N_C)
            SpeciesNumber = numpnts(Names)
            Make/O/N=(SpeciesNumber) InitialConcentrations
//  Make Output waves for Species with wave Names from Names[n]
            n =0
            Do
                Make/O/D/N=(N_C) $Names[n] = 0
                n +=1
            while (n < SpeciesNumber)
            DoWindow ReactionMechanism
            AppendToTable KK
            AppendToTable Names
            AppendToTable InitialConcentrations
            AppendToTable CalTime
            ModifyTable size(Names)=14, width(Names)=100
            ModifyTable size(KK)=14,rgb(KK)=(65535,0,0), width(KK) = 100
            ModifyTable size(initialconcentrations)=14,
rgb(InitialConcentrations)=(65535,0,0), width(initialconcentrations)=150
            ModifyTable size(CalTime)=14, rgb(CalTime)=(65535,0,0)

// Print  ODEs  for Reaction Mechanism in Chemical Format

n = 0
Do
    m=0
```

```
Totaltemp = ""
Totaltemp1 = ""
Totaltemp2 = ""
Totaltemp3 = ""
Totaltemp4 = ""
Totaltemp5 = ""
Do // Find Reactant 1 in Names
        temp1 = ""
        If(stringmatch(Names[n], Reactant1[m]))
            temp1 = "-" + num2str(ratecoefficients[m]) + " * [" + Reactant1[m] + "] *
["+Reactant2[m] + "]"
            if(strlen(Reactant1[m]) == 0)
                temp1 = "-" + num2str(ratecoefficients[m]) + " * " +    "["+Reactant2[m]
+ "]"
            endif
            if(strlen(Reactant2[m]) == 0)
                temp1 = "-" + num2str(ratecoefficients[m]) + " * [" + Reactant1[m] +
"]"
            endif
        endif
                    Totaltemp1 += temp1
        m += 1
    While(m <rnumber)
m = 0
Do// Find Reactant 2 in Names
    temp2 = ""
    If(stringmatch(Names[n], Reactant2[m]))
        temp2 = "-" + num2str(ratecoefficients[m]) + " * [" + Reactant1[m] + "] *
["+Reactant2[m] + "]"
```

```
                if(strlen(Reactant1[m]) == 0)
                    temp2 = "-" + num2str(ratecoefficients[m]) + " * " +   "["+Reactant2[m] +
"]"
                endif

                if(strlen(Reactant2[m]) == 0)
                    temp2 = "-" + num2str(ratecoefficients[m]) + " * [" + Reactant1[m] + "]"
                endif

            endif

            Totaltemp2 += temp2

            m += 1
        While(m <rnumber)

        m = 0
        Do   // Find Product 1 in Names
            temp3 = ""
            If(stringmatch(Names[n], Product1[m]))
                temp3 = "+" + num2str(ratecoefficients[m]) + " * [" + Reactant1[m] + "] *
["+Reactant2[m] + "]"
                if(strlen(Reactant1[m]) == 0)
                    temp3 = "+" + num2str(ratecoefficients[m]) + " * " +   "["+Reactant2[m] +
"]"
                endif

                if(strlen(Reactant2[m]) == 0)
```

```
                    temp3 = "+" + num2str(ratecoefficients[m]) + " * [" + Reactant1[m] + "]"
                endif
            endif
            Totaltemp3 += temp3
            m += 1
        While(m <rnumber)
        m = 0
        Do          // Find Product 2 in Names
            temp4 = ""
            If(stringmatch(Names[n], Product2[m]))
            temp4 = "+" + num2str(ratecoefficients[m]) + " * [" + Reactant1[m] + "] *
["+Reactant2[m] + "]"

            if(strlen(Reactant1[m]) == 0)
                temp4 = "+" + num2str(ratecoefficients[m]) + " * " +    "["+Reactant2[m] + "]"
            endif
            if(strlen(Reactant2[m]) == 0)
                temp4 = "+" + num2str(ratecoefficients[m]) + " * [" + Reactant1[m] + "]"
            endif
        endif
        Totaltemp4 += temp4
        m += 1
        While(m <rnumber)
        m = 0
        Do          // Find Product 3 in Names
            temp5 = ""
            If(stringmatch(Names[n], Product3[m]))
            temp5 = "+" + num2str(ratecoefficients[m]) + " * [" + Reactant1[m] + "] *
["+Reactant2[m] + "]"
```

```
            if(strlen(Reactant1[m]) == 0)
                temp5 = "+" + num2str(ratecoefficients[m]) + " * " +    "["+Reactant2[m] + "]"
            endif
            if(strlen(Reactant2[m]) == 0)
                temp5 = "+" + num2str(ratecoefficients[m]) + " * [" + Reactant1[m] + "]"
            endif
        endif
        Totaltemp5 += temp5
        m += 1
        While(m <rnumber)

        Totaltemp = totaltemp1 + totaltemp2 + totaltemp3 + totaltemp4 + totaltemp5 // combine all
instances where the name was found
        if(stringmatch(totaltemp, ""))
        else
            //Print "d["+Names[n] + "]/dt = " + Totaltemp
        endif

            n +=1
while (n < speciesnumber)
// Print    ODEs    for Reaction Mechanism in ChemKinetic (integrateODE) Format
//*****************************************
//    Make Notebook to contain ODEs to be Cut and Pasted
//                                    Mylist = WinList("ReactionCopy",";","WIN:16")
//                                    if (strlen(MyList) == 0)
//                                            else
//                                            DoWindow/K ReactionCopy
//                                    endif
```

```
//
NewNotebook/N=ReactionCopy/F=1/V=1/K=0/W=(5,42,505,337)
//                                                    Notebook ReactionCopy defaultTab=36,
statusWidth=238, backRGB=(65535,0,0), pageMargins={72,72,72,72}
//                                                    Notebook ReactionCopy showRuler=1,
rulerUnits=1, updating={1, 60}
//                                                    Notebook ReactionCopy newRuler=Normal,
justification=0,          margins={0,0,468},          spacing={0,0,0},          tabs={},
rulerDefaults={"Times",20,0,(0,0,0)}
//
//                                                    Notebook ReactionCopy ruler=Normal, text
= " Cut and Paste these ODEs into ChemKinetic Function\r\r"
//************************************************
n = 0
Do
    m=0
    Totaltemp = ""
    Totaltemp1 = ""
    Totaltemp2 = ""
    Totaltemp3 = ""
    Totaltemp4 = ""
    Totaltemp5 = ""
        Do
            temp1 = ""
            If(stringmatch(Names[n], Reactant1[m]))
                nn = 0
                position = 0
                Do
                    if(stringmatch(Names[nn],Reactant1[m]))
```

```
                    position = nn
                    nn = 500
                endif
                nn +=1
            while(nn < rnumber*4)

            nn = 0
            position2 = 0
            Do
                if(stringmatch(Names[nn],Reactant2[m]))
                    position2 = nn
                    nn = 500
                endif
                nn +=1
            while(nn < rnumber*4)
            temp1 = "-" + "pw[" + num2str(m) + "]*" + "yw["+ num2str(position) + "]*"
+ "yw["+ num2str(position2) + "]"

            if(strlen(Reactant1[m]) == 0)
                temp1 = "-" + "pw[" + num2str(m) + "]*" +
"yw["+num2str(position2) + "]"
            endif
            if(strlen(Reactant2[m]) == 0)
                temp1 = "-" + "pw[" + num2str(m)+ " ]*" + "yw[" +
num2str(position) + "]"
            endif
        endif
        Totaltemp1 = Totaltemp1 + temp1
        m += 1
```

```
While(m <rnumber)
        m = 0
        Do
                temp2 = ""
                If(stringmatch(Names[n], Reactant2[m]))
                nn = 0
                position = 0
                Do
                if(stringmatch(Names[nn],Reactant1[m]))
                position = nn
                nn = 500
                endif
                nn +=1
                while(nn < rnumber*4)
                nn = 0
                position2 = 0
                Do
                if(stringmatch(Names[nn],Reactant2[m]))
                position2 = nn
                nn = 500
                endif
                nn +=1
                while(nn < rnumber*4)

                temp2 = "-" + "pw[" + num2str(m) + "]*" + "yw["+
num2str(position) + "]*" + "yw["+ num2str(position2) + "]"
                if(strlen(Reactant1[m]) == 0)
                temp2 = "-" + "pw[" + num2str(m) + "]*" +
"yw["+num2str(position2) + "]"
```

```
                    endif
                    if(strlen(Reactant2[m]) == 0)
                    temp2 = "-" + "pw[" + num2str(m)+ " ]*" + "yw[" +
num2str(position) + "]"
                    endif

          else
          endif
                    Totaltemp2 = Totaltemp2 + temp2
     m += 1
     While(m <rnumber)

          m = 0
          Do
                    temp3 = ""
                    If(stringmatch(Names[n], Product1[m]))
                    nn = 0
                    position = 0
                    Do
                    if(stringmatch(Names[nn],Reactant1[m]))
                    position = nn
                    nn = 500
                    endif
                    nn +=1
                    while(nn < rnumber*4)
                    nn = 0
                    position2 = 0
                    Do
                    if(stringmatch(Names[nn],Reactant2[m]))
```

```
                    position2 = nn
                    nn = 500
                    endif
                    nn +=1
                    while(nn < rnumber*4)

                    temp3 = "+" + "pw[" + num2str(m) + "]*" + "yw["+
num2str(position) + "]*" + "yw["+ num2str(position2) + "]"
                    if(strlen(Reactant1[m]) == 0)
                    temp3 = "+" + "pw[" + num2str(m) + "]*" +
"yw["+num2str(position2) + "]"
                    endif
                    if(strlen(Reactant2[m]) == 0)
                    temp3 = "+" + "pw[" + num2str(m)+ " ]*" + "yw[" +
num2str(position) + "]"
                    endif

          else
          endif
                    Totaltemp3 = Totaltemp3 + temp3
     m += 1
     While(m <rnumber)
          m = 0
  Do
                    temp4 = ""
          If(stringmatch(Names[n], Product2[m]))
                    nn = 0
                    position = 0
                    Do
```

```
                    if(stringmatch(Names[nn],Reactant1[m]))
                    position = nn
                    nn = 500
                    endif
                    nn +=1
                    while(nn < rnumber*4)
                    nn = 0
                    position2 = 0
                    Do
                    if(stringmatch(Names[nn],Reactant2[m]))
                    position2 = nn
                    nn = 500
                    endif
                    nn +=1
                    while(nn < rnumber*4)

                    temp4 = "+" + "pw[" + num2str(m) + "]*" + "yw["+
num2str(position) + "]*" + "yw["+ num2str(position2) + "]"
                    if(strlen(Reactant1[m]) == 0)
                    temp4 = "+" + "pw[" + num2str(m) + "]*" +
"yw["+num2str(position2) + "]"
                    endif
                    if(strlen(Reactant2[m]) == 0)
                    temp4 = "+" + "pw[" + num2str(m)+ " ]*" + "yw[" +
num2str(position) + "]"
                    endif
          else
          endif
                    Totaltemp4 = Totaltemp4 + temp4
```

```
m += 1
While(m <rnumber)
m = 0
Do
temp5 = ""
If(stringmatch(Names[n], Product3[m]))
nn = 0
position = 0
Do
if(stringmatch(Names[nn],Reactant1[m]))
position = nn
nn = 500
endif
nn +=1
while(nn < rnumber*4)
nn = 0
position2 = 0
Do
if(stringmatch(Names[nn],Reactant2[m]))
position2 = nn
nn = 500
endif
nn +=1
while(nn < rnumber*4)

temp5 = "+" + "pw[" + num2str(m) + "]*" + "yw["+ num2str(position) + "]*" + "yw["+ num2str(position2) + "]"
if(strlen(Reactant1[m]) == 0)
temp5 = "+" + "pw[" + num2str(m) + "]*" +
```

```
"yw["+num2str(position2) + "]"
                                endif
                                if(strlen(Reactant2[m]) == 0)
                                temp5 = "+" + "pw[" + num2str(m)+ " ]*" + "yw[" +
num2str(position) + "]"
                                endif
                        else
                        endif
                                Totaltemp5 = Totaltemp5 + temp5
            m += 1
            While(m <rnumber)



            Totaltemp = totaltemp1 + totaltemp2 + totaltemp3 + totaltemp4 + totaltemp5
// include dilution
            if (exists("dilution"))
                dilutiontemp = "-d*yw["+ num2str(n) + "]"
                Totaltemp += dilutiontemp
            endif
            TotalLen = StrLen(Totaltemp)
            if (TotalLen>0)

                if (TotalLen>390) // string too long for one line in function
                    breakpos = StrSearch(Totaltemp, "+", 300) // find first "+" past 300 chars
                    if (breakpos<0 || breakpos> 390)
                        breakpos = StrSearch(Totaltemp, "-", 300)) // Check if there's maybe a
"-"
                    endif
                    if (breakpos>300)
```

```
                    //Print "dydt["+ num2str(n) + "]=" + Totaltemp[0,breakpos-1]
                    //Print "dydt["+ num2str(n) + "]+=" + Totaltemp[breakpos,
StrLen(Totaltemp)-1]
                    dydtstr += "dydt["+ num2str(n) + "]="+Totaltemp[0,breakpos-1] + "\r"
                    dydtstr += "dydt["+ num2str(n) + "]+="+ Totaltemp[breakpos,
StrLen(Totaltemp)-1] + "\r"
                else
                    //print Totaltemp
                    abort "something is strange with this string"
                endif

            else
                //Print "dydt["+ num2str(n) + "]=" + Totaltemp
                dydtstr += "dydt["+ num2str(n) + "]=" + Totaltemp+ "\r"
            endif

                endif
        n +=1
while (n < speciesnumber)
    RemoveChemKineticFuncs()
    Execute/Q /P "EditChemKineticFuncs()"
    IncludeChemKineticFuncs()
end
```

Macro Run_Model()

```
    If (!exists("CurrChemKineticFct"))
        Abort "Must compile ODE first!"
    Endif
    String cmd, SpeciesList, CurrSpecies
    Variable n, speciesnumber
    Variable npnts
```

```
	SetDataFolder root:
	Silent 1
	PauseUpdate
	Variable starttime = DateTime
	n=0
	SpeciesList = ""
	SpeciesNumber = numpnts(Names)
	Do
		if(n == 0)
			SpeciesList += Names[n]
		else
			SpeciesList = SpeciesList + "," + Names[n]
		endif
		n += 1
	while (n < numpnts(Names))

	n=0
	Do
		CurrSpecies = Names[n]
		$CurrSpecies[0] = InitialConcentrations[n] // restart: initialize to original values
		n += 1
	while(n < SpeciesNumber)
	cmd= "IntegrateODE/U=1000/X=CalTime "+CurrChemKineticFct+" KK, {"+ SpeciesList
+ "}"
	Execute cmd
end
Function IncludeChemKineticFuncs() // adds include statement to procedure window
                                   // note that ChemKineticsFuncs.ipf must be present in
experiment folder
```

```
                                        // if not present, a blank one will be generated
    // check if experiment was saved
    Pathinfo home
    if (StrLen(S_Path)<1)
        abort "Save experiment first!"
    endif
    String SelectStr=S_Path + "ChemKineticFuncs.ipf"
    String homepath = S_Path
    // check if ChemKineticFuncs.ipf exists in same folder
    GetFileFolderInfo/Z/Q SelectStr
    if (( V_Flag != 0) || (V_isFile==0)) // ChemKineticFuncs.ipf doesn't exist
        DoAlert 1, "ChemKineticFuncs.ipf does not exist, should I generate a blank one?"
        if (V_flag==1) // Yes clicked
            MakeChemKineticFuncs()
        else
            abort "could not include ChemKineticFuncs.ipf"
        endif
    endif
    String cmd = "INSERTINCLUDE "+"\""+homepath+"ChemKineticFuncs\""
    Execute /P cmd
    Execute /P "COMPILEPROCEDURES "
End Function
Function RemoveChemKineticFuncs() // removes include statement from procedure window
                                        // also removes ChemKineticsFuncs.ipf from experiment

    Pathinfo home
    String cmd = "DELETEINCLUDE "+"\""+S_path+"ChemKineticFuncs\""
    Execute /P cmd
    Execute /P "COMPILEPROCEDURES "
```

```
End Function
Function EditChemKineticFuncs()
	if (!exists("dydtstr"))
		abort "could not find dydtstr, try running Mechanism_ODE"
	endif
	SVAR newcode = dydtstr // dynamic code stored in global variable
	if (!exists("CurrChemKineticFct"))
		abort "can't find mechanism name, try running Mechanism_ODE"
	endif
	SVAR mechname = CurrChemKineticFct // mechanism name stored in global variable
	Pathinfo home
	// load ChemKineticFuncs as text into notebook
	String noteBookName = "ChemKineticsFuncsText"
	OpenNotebook /P=home /N=$noteBookName "ChemKineticFuncs.ipf"

	// edit the notebook
	// find dynamic code start
	Notebook $notebookName selection = {startOfFile, startOfFile}, findText={mechname, 0}
	Notebook $notebookName selection={endOfParagraph,endOfParagraph},
findText={"begin dynamic code", 0}
	if (V_Flag ==1)
		NoteBook $notebookName selection={endOfParagraph,endOfParagraph}
//position at return after text found
		GetSelection notebook, $notebookName, 1
	endif
	Variable begin_dyn = V_startParagraph

	// find dynamic code end
	Notebook $notebookName selection = {startOfFile, startOfFile}, findText={mechname, 0}
```

```
	Notebook $notebookName selection={endOfParagraph,endOfParagraph}, findText={"end dynamic code", 0}
	if (V_Flag ==1)
		NoteBook $notebookName selection={endOfParagraph,endOfParagraph} //position at return after text found
		GetSelection notebook, $notebookName, 1
	endif
	Variable end_dyn = V_startParagraph-1

	if (V_Flag ==1)
		NoteBook $notebookName selection={(begin_dyn,0),(end_dyn,0)} //select dynamic code
		NoteBook $notebookName text = newcode+"\r" // replace dynamic code with new code

		// Save the notebook
		SaveNotebook/O /P=home $noteBookName as "ChemKineticFuncs.ipf"
	else
		print "text not found, nothing replaced"
	endif
	// Kill the notebook
	doWindow/K $noteBookName
End Function
Function MakeChemKineticFuncs() // makes new ChemKineticFuncs.ipf in experiment folder
	String noteBookName = "ChemKineticsFuncsText"
	// make notebook
	NewNotebook /F=0 /N=$noteBookName as "ChemKineticFuncs.ipf"
	// add hard-coded text into notebook
	NoteBook $notebookName text = "Function ChemKinetic(pw, tt, yw, dydt)"+"\r"
```

```
NoteBook $notebookName text = "\tWave pw // rate coefficients"+"\r"
NoteBook $notebookName text = "\tVariable tt // time value at which to calculate derivatives"+"\r"
NoteBook $notebookName text = "\tWave yw // containing concentrations of species"+"\r"
NoteBook $notebookName text = "\tWave dydt // wave to receive dA/dt, dB/dt etc. (output)"+"\r"
NoteBook $notebookName text = ""+"\r"
NoteBook $notebookName text = ""+"\tif (exists(\"dilution\"))\r"
NoteBook $notebookName text = ""+"\t\tNVAR d = dilution\r"
NoteBook $notebookName text = ""+"\tendif\r"
NoteBook $notebookName text = "// begin dynamic code, don't modify this line!"+"\r"
NoteBook $notebookName text = ""+"\r"
NoteBook $notebookName text = "// end dynamic code, don't modify this line!"+"\r"
NoteBook $notebookName text = ""+"\r"
NoteBook $notebookName text = "End"+"\r"
// Save the notebook
SaveNotebook/O /P=home $noteBookName as "ChemKineticFuncs.ipf"
// Kill the notebook
doWindow/K $noteBookName
End Function
```

Macro Fleastsquare(Ncal,ac,rc) //Ncal is the number of points in the experiment, and ac is the accuracy of kvoc

```
Variable Ncal = 81,ac = 0.05, rc=10
Make/O/N=(Ncal) dNO3S=0,dN2O5S=0,fNO3S=0, fN2O5S=0 //dNO3S is the square of (NO3_cal-NO3_measure),fNO3S is the square of [(NO3_cal-NO3_measure)/NO3_measure]
Make/O/N=50 SdNO3S=0, SdN2O5S=0, SfNO3S=0, SfN2O5S=0, sf=0
variable k1_0,k1_1,k1_2,k1_3
k1_3=(k1_1+k1_2)/2
```

```
variable n=0,p=1
variable m=0
k1_0 = RateCoefficients[3]

k1_1=k1_0*(1+ ac)
n=0
RateCoefficients[3]=k1_1
KK[3]=k1_1
Mechanism_compile(Ncal,"ChemKinetic")
Run_Model()
dNO3S = (NO3_ppb-NO3_30s)*(NO3_ppb-NO3_30s)
dN2O5S = (N2O5_ppb-N2O5_30s)*(N2O5_ppb-N2O5_30s)
fNO3S = dNO3S/NO3_30s/NO3_30s
fN2O5S = dN2O5S/N2O5_30s/N2O5_30s
do
    SdNO3S[p]+= dNO3S[n]
    SdN2O5S[p]+= dN2O5S[n]
    SfNO3S[p]+= fNO3S[n]
    SfN2O5S[p]+= fN2O5S[n]
    sf[1]= SfNO3S[1]+SfN2O5S[1]
     n+=1
while (n<Ncal)
print "acNO3","acN2O5",k1_1, SfNO3S[p], SfN2O5S[p], sf[p]
p+=1

k1_2=k1_0*(1-ac)
n=0
RateCoefficients[3]=k1_2
KK[3]=k1_2
```

```
Mechanism_compile(Ncal,"ChemKinetic")
Run_Model()
dNO3S = (NO3_ppb-NO3_30s)*(NO3_ppb-NO3_30s)
dN2O5S = (N2O5_ppb-N2O5_30s)*(N2O5_ppb-N2O5_30s)
fNO3S = dNO3S/NO3_30s/NO3_30s
fN2O5S = dN2O5S/N2O5_30s/N2O5_30s
do
    SdNO3S[p]+= dNO3S[n]
    SdN2O5S[p]+= dN2O5S[n]
    SfNO3S[p]+= fNO3S[n]
    SfN2O5S[p]+= fN2O5S[n]
    sf[p]= SfNO3S[p]+SfN2O5S[p]
     n+=1
while (n<Ncal)
print "acNO3","acSN2O5",k1_2, SfNO3S[p], SfN2O5S[p], sf[p]



do
     if (sf[1]>sf[2])
      p+=1
      k1_3=(k1_1+k1_2)/2
      k1_1=k1_3
      n=0
      RateCoefficients[3]=k1_1
      KK[3]=k1_1
      Mechanism_compile(Ncal,"ChemKinetic")
      Run_Model()
      dNO3S = (NO3_ppb-NO3_30s)*(NO3_ppb-NO3_30s)
      dN2O5S = (N2O5_ppb-N2O5_30s)*(N2O5_ppb-N2O5_30s)
```

```
  fNO3S = dNO3S/NO3_30s/NO3_30s
  fN2O5S = dN2O5S/N2O5_30s/N2O5_30s
     do
       SdNO3S[p]+= dNO3S[n]
       SdN2O5S[p]+= dN2O5S[n]
       SfNO3S[p]+= fNO3S[n]
       SfN2O5S[p]+= fN2O5S[n]
       sf[p]= SfNO3S[p]+SfN2O5S[p]
       n+=1
    while (n<Ncal)
  sf[1]=sf[p]
print "acNO3","acN2O5",k1_1, SfNO3S[p], SfN2O5S[p], sf[p]



else
  p+=1
    k1_3=(k1_1+k1_2)/2
    k1_2=k1_3
    n=0
    RateCoefficients[3]=k1_2
    kk[3]=k1_2
    Mechanism_compile(Ncal,"ChemKinetic")
    Run_Model()
    dNO3S = (NO3_ppb-NO3_30s)*(NO3_ppb-NO3_30s)
    dN2O5S = (N2O5_ppb-N2O5_30s)*(N2O5_ppb-N2O5_30s)
    fNO3S = dNO3S/NO3_30s/NO3_30s
    fN2O5S = dN2O5S/N2O5_30s/N2O5_30s
       do
          SdNO3S[p]+= dNO3S[n]
```

```
                SdN2O5S[p]+= dN2O5S[n]
                SfNO3S[p]+= fNO3S[n]
                SfN2O5S[p]+= fN2O5S[n]
                  sf[p]= SfNO3S[p]+SfN2O5S[p]
                  n+=1
              while (n<Ncal)
          print "acNO3","acN2O5",k1_2, SfNO3S[p], SfN2O5S[p], sf[p]
             sf[2]=sf[p]
          endif

    m+=1

     while (m<rc)
End
```

Li ZHOU

Chimie atmosphérique de NO_3: réactions avec une série de composés organiques et inorganiques

Résumé :

Le radical nitrate NO_3 est un intermédiaire clé dans la chimie atmosphérique nocturne. Il peut réagir avec un certain nombre de composés organiques volatils (COV) initiant leur dégradation pendant la nuit. Dans cette thèse, la cinétique de NO_3 avec plusieurs de ces composés a été étudiée à température ambiante (298 ± 2 K) et à pression atmosphérique (1000 ± 5 hpa) dans une chambre de simulation atmosphérique en Téflon (ICARE-7300L) couplée à des outils analytiques tels que : FTIR, PTR-ToF-MS and CRDS etc. Nous avons déterminé les constantes de vitesse pour les réactions du radical NO_3 avec sept esters de méthacrylate à température ambiante: méthacrylate de méthyle, méthacrylate d'éthyle, méthacrylate de propyle, méthacrylate d'isopropyle, méthacrylate de butyle, méthacrylate d'isobutyle, méthacrylate de méthyle deutéré. Les résultats obtenus, suggèrent que la réaction de NO_3 avec les esters de méthacrylate procède par addition sur la double liaison du groupe méthacrylate. Ensuite, une méthode absolue a été utilisée pour déterminer les constantes de vitesse de réaction de NO_3 avec une série d'alcanes et de gaz inorganiques importants dans les processus atmosphériques : le méthane, l'éthane, le pentane, le n-butane, l'isobutane, le 2, 3-diméthylbutane, le cyclopentane, le cyclohexane, l'oxyde nitreux, le monoxyde de carbone et le dioxyde de soufre. Avec l'ensemble des données cinétiques obtenues, les durées de vie atmosphériques de ces composés vis à vis des radicaux NO_3 ont été calculées et comparées à celles déterminées pour d'autres oxydants de l'atmosphère. Ces résultats améliorent également les connaissances de base sur les réactions impliquant le radical NO_3.

Mots clés : Chimie atmosphérique, radicaux NO_3, composés organiques volatils, constantes de vitesse, cinétiques de réaction.

Atmospheric chemistry of NO_3: reactions with a series of organic and inorganic compounds

Abstract :

NO_3 is a key intermediate in the chemistry of the night-time atmosphere. NO_3 radical can react with a number of VOCs initiating their night-time degradation. In this thesis, the kinetics of NO_3 with different kinds of compounds was studied at room temperature (298 ± 2 K) and atmospheric pressure (1000 ± 5 hpa) in a Teflon simulation atmospheric chamber (ICARE-7300L) coupled to analytical tools including Fourier Transform Infrared Spectroscopy, Proton Transfer Reaction-Time of Flight-Mass Spectrometer and Cavity Ring Down Spectrometer etc. The rate coefficients for the reactions of NO_3 radical with seven methacrylate esters are firstly reported: methyl methacrylate; ethyl methacrylate; propyl methacrylate; isopropyl methacrylate, butyl methacrylate, isobutyl methacrylate, and deuterated methyl methacrylate. The trends in the measured rate coefficient with the length and nature of the alkyl group strongly suggest that the reaction proceeds via addition to the double bond on the methacrylate group. Then, an absolute method was used to determine the upper limits or rate coefficients for the reactions of NO_3 radicals with a series of alkanes and some important inorganic gases: methane, ethane, pentane, n-butane, iso-butane, 2,3-dimethybutane, cyclopentane, cyclohexane, nitrous oxide, carbon monoxideand and sulfur dioxide. With the obtained kinetics data, the atmospheric lifetimes of these compounds toward NO_3 radicals were calculated and compared with those due to loss via reactions with the other major atmospheric oxidants. The kinetics results also enhance the available database on NO_3 reactions.

Keywords : Atmospheric chemistry, NO_3 radicals, volatile organic compounds, rate coefficients, kinetic

ICARE-CNRS Orléans
1C, Avenue de la recherche scientifique
CS 50060
45071 Orléans cedex 02
France